Universitat Politècnica de Catalunya

Theses and Dissertation

Mining Engineering and Natural Resources

MULTIPLE SIMULATION EXPERIMENTAL STUDIES OF GAS EMISSION, DISTRIBUTION AND MIGRATION RULES IN MINE VENTILATION SYSTEM AND GOAF AREA

Haoran Zhang

haoranbasketball@gmail.com

MULTIPLE SIMULATION EXPERIMENTAL STUDIES OF GAS EMISSION, DISTRIBUTION AND MIGRATION RULES IN MINE VENTILATION SYSTEM AND GOAF AREA

DISSERTATION

A dissertation submitted in partial fulfillment of the
Requirements for the degree of Doctor of Philosophy in the
Department of Mining Engineering and Natural Resources
At the Universitat Politècnica de Catalunya

By

Haoran Zhang

Manresa, Barcelona, Spain

Director: Dr. Lluis Sanmiquel Pera, Professor of Mining Engineering and Natural Resources
Manresa, Barcelona, Spain

Abstract

MULTIPLE SIMULATION EXPERIMENTAL STUDIES OF GAS EMISSION, DISTRIBUTION AND MIGRATION RULES IN MINE VENTILATION SYSTEM AND GOAF AREA

Gas problems have created severe difficulties for the mining industry around the world, leading to high expenditures and intensity research efforts, and determined attempts to enhance the various ventilation and gas drainage techniques. Meanwhile, gas research is thriving in recent years, and gas drainage technology will continue to be a growing industry over the coming decades in many mining countries

Safety mining technologies including field investigation, numerical simulation and laboratorial experiments have been improved to develop a better understanding of the causes of mine gas-related disasters over the last two decades. Moreover, new and multiple gas control strategies and technologies have been developed, including optimizing the ventilation system constantly, preventing goaf spontaneous combustion timely, enhancing gas risk management effectively, determining the gas emission zone exactly, and implementing a reasonable gas drainage plan correctly.

The first part of this dissertation introduces a multiple gas disaster prevention, control and reduction strategy. Firsly, the basic theories of gas emission, distribution and migration are

discussed. Then a numerical prediction model based on a specific coal mine is established to predict its gas emission. The prediction result shows that the error of the gas emission prediction in the working face is less then 10%, and it also indicates that the prediction measurement of gas emission in the working face is quite close to the actual measurement and owns high accuracy.

The second part of this dissertation offers the establishment of the numerical simulation model (CFD) and laboratorial experimental model for the purpose of discussing the gas distribution and migration rule and determining the most effective gas drainage zones in the working face and goaf. The numerical and laboratorial simulation experiments based on U-type ventilation system and U+L-type ventilation system are performed respectively, and both of two types of simulation experimental results indicate that the over-limit of gas concentration in the working face can be effectively resolved by changing from U-type ventilation system to U+L-type ventilation system. Specifically, in the case of the U-type ventilation system, a large amount of high concentrated gas constantly flows into the upper corner due to the goaf air leakage and the different pressures between air inlet and air outlet. By contrast, U+L-type ventilation system is made up of two air inlets and one air outlet, which accelerates the gas emission, diffusion and flow, balances the air pressure of the upper corner, restrains the gas discharge of the upper corner, and compels the high concentrated gas to flow into the air outlet.

Both of the numerical simulation results and laboratorial experimental results also demonstrate that the most effective gas drainage spot constantly varies with the area where mining activities are performed. In the case of numerical simulation experimental results, it is mainly located in the area of 40m-250m (between working face and deep goaf), 30m-40m from the working face floor (between the working face floor to the roof), and approximately 60m-170m (between air inlet and air outlet). In the case of laboratorial simulation experimental results, it mainly locates in coal seam and rock stratum separation area of 27cm-243cm (between working face and deep goaf), 28cm-42cm (between the working face floor to the roof) and 78cm-182cm (between air inlet and air outlet).

The last part of this dissertation provides a field study in order to obtain the gas distribution and migration rule in the working face and goaf. 25 measuring points are selected and measured in both of production shift and maintenance shift. The field measured results are similar with the results of numerical simulation and laboratorial simulation experiments. Moreover, one entire gas

drainage system is established based on obtained results (numerical simulation, laboratorial experiments and field measurement), and the gas drainage rate is also measured. The field measured results show the average gas drainage rate increased to approximately 48.9 $m^3 \cdot min^{-1}$ (U+L-type ventilation system) from 39.6 $m^3 \cdot min^{-1}$ (U-type ventilation system) while the gas concentration of the special drainage tunnel, upper corner and air outlet decreased to 1.69%, 0.75% and 0.55% (U+L-type ventilation system) from 1.88%, 0.85% and 0.61% (U-type ventilation system) respectively. These results indicate the layout of the gas drainage boreholes is rational and effective; the gas drainage volume is reliable. Therefore, it is feasible and reliable to arrange the layout of gas drainage tunnels based on the experimental results of numerical simulations and laboratorial tests.

KEYWORDS: gas disaster; mining safety; environmental protection; mine ventilation system; goaf area; numerical simulations; laboratorial experiments; field investigation; gas drainage

Haoran Zhang

Ph.D candidate's Signature

01/04/2015

Date

Acknowledgements

I would like thank the following for their assistance, participation and patience:

Dr. Lluis Sanmiquel Pera, Professor of Mining Engineering and Natural Resources, my supervisor for his assistance with initiating the project, bringing the project to a conclusion and his wisdom as the work proceeded.

Universitat Politècnica de Catalunya, Department of Mining Engineering and Natural Resources for the financial support scholarship provided for the period of study without which I would not have been able to proceed.

Iberpotash, SA for the technical support provided for my research work.

China Scholarship Council for the financial support scholarship provided for the period of study without which I would not have been able to proceed.

Dr. Yaojiang Zhao, Professor of Mining Engineering, my former supervisor in China for his assistance with supporting my research, bringing my project to a conclusion and his wisdom as the work proceeded.

Taiyuan University of Technology, College of Mining Engineering, Department of Safety Engineering the technical support provided for my research work.

China University of Mining Technology for the technical support provided for the period of my study.

Dr. Shengrong Xie, Professor of China University of Mining and Technology, my friend and teacher for his important help with supporting my research, experiments and dissertation.

My colleague for Marc Bascompta Massanés for his assistance proofreading the manuscript and friend Dan Zhao for her support of translation and great contribution through the times I was writing this dissertation.

Finally the academic and support staff at Technical College of Manresa for their assistance and for making my stay at UPC enjoyable and productive.

Table of content

List of figure

List of table

List of acronyms and abbreviations

CBM	Coalbed Methane
CDM	Clean Development Mechanism
CERs	Certified Emission Reductions
CFRR	Catalytic Flow Reversal Reactors
CH_4	Methane
CMM	Coal Mine Methane
CMR	Catalytic Monolith Reactor
CNG	Compressed Natural Gas
CO_2	Carbon Dioxide
CO_2e	Carbon Dioxide Equivalent
ERPA	Emission Reduction Purchase Agreement
ERUs	Emission Reduction Units
ESMAP	Energy Sector Management Assistance Program
GHG	Greenhouse Gas
GWP	Global Warming Potential
IBRD	International Bank for Reconstruction and Development
IC	Internal Combustion
I&M	Inspection and Maintenance
JI	Joint Implementation
kWh	Kilowatt-hour
LNG	Liquefied Natural Gas
l/s	Liters per Second
m	Meter
m/s	Meters per Second
m^3/d	Cubic Meters per Day
m^3/s	Cubic Meters per Second
mD	Millidarcy (in common usage, equivalent to approximately 10^{-3} $(\mu m)^2$)

MRD	Medium Radius Drilling
MSA	Molecular Sieve Adsorption
Mt	Million (10^6) tonnes
Mtpa	Million Tonnes per Annum
MW_e	Megawatt of Electricity Capacity
Nm^3	Normal Cubic Meters
PSA	Pressure Swing Adsorption
scfm	Standard Cubic Feet per Minute
t	Tonne (metric)
t/d	Tonnes per Day
TFRR	Thermal Flow Reversal Reactor
TRD	Tight Radius Drilling
UNECE	United Nations Economic Commission for Europe
UNFCCC	United Nations Framework Convention on Climate Change
VAM	Ventilation Air Methane
VERs	Verified Emission Reductions
USBM	United States Bureau of Mines

List of glossary of terms

Within the coal and mine gas industry, there is still confusion over terms and abbreviations used within and across different jurisdictions. In addition to the terms listed here, the UNECE has prepared a Glossary of Coal Mine Methane Terms and Definitions that is more comprehensive and highlights how terminology is used in different regions.

Air lock - an arrangement of doors that allows passage from one part of a mine ventilation circuit to another without causing a short-circuit.

Auxiliary ventilation - proportion of main ventilating current directed to the face of a blind heading (i.e., entry) by means of an auxiliary fan and ducting.

Back-return - a temporary ventilation arrangement formed at the return end of a U-ventilated longwall to divert a proportion of the air behind the face to allow access for gas drainage drilling and prevent high concentration goaf gases encroaching on the face end.

Bleeder shaft - a vertical shaft through which gas-laden air from working districts is discharged.

Blind heading - a development roadway with a single entry that requires auxiliary ventilation.

Bord-and-pillar (room-and-pillar) - a method of mining in which coal is extracted from a series of headings, which are then interlinked leaving un-mined coal pillars to support the roof.

Capture (drainage) efficiency - the proportion of methane (by volume) captured in a methane drainage system relative to the total quantity of gas liberated. Gas liberated comprises the sum of drained gas plus gas emitted into the mine ventilation air. Usually expressed as a percentage, capture (or drainage) efficiency can be determined for a single longwall panel or for a whole mine.

Coal front gas - gas released from the working seam coalface by the action of the coal-cutting machine.

Coalbed methane (CBM) - a generic term for the methane rich gas naturally occurring in coal seams typically comprising 80% to 95% methane with lower proportions of ethane, propane, nitrogen, and carbon dioxide. In common international use, this term refers to methane recovered from un-mined coal seams using surface boreholes.

Coal mine methane (CMM) - gas captured at a working coal mine by underground methane drainage techniques. The gas consists of a mixture of methane and other hydrocarbons and water vapor. It is often diluted with air and associated oxidation products due to unavoidable leakage of

air into the gas drainage boreholes or galleries through mining induced fractures and also due to air leakage at imperfect joints in underground pipeline systems. Any gas captured underground, whether drained in advance of or after mining, and any gas drained from surface goaf wells is included in this definition. Pre-mining drained CMM can be of high purity.

Extraneous gas - gas emissions other than coal front gas.

Firedamp - alternative term for CMM.

Gas drainage - methods for capturing the naturally occurring gas in coal seams to prevent it entering mine airways. The gas can be removed from coal seams in advance of mining using pre-drainage techniques and from coal seams disturbed by the extraction process using post-drainage techniques. It often referred to as Methane drainage if methane is the main gas component target to be captured.

Goaf (United States: gob) - broken, permeable ground where coal has been extracted by longwall coal mining and the roof has been allowed to collapse, thus fracturing and de - stressing strata above and, to a lesser extent, below the seam being worked. The term gob is generally used in the United States; elsewhere, goaf is generally used.

Methane drainage - Methods for capturing the naturally occurring gas in coal seams to prevent it entering mine airways. The gas can be removed from coal seams in advance of mining using pre-drainage techniques and from coal seams disturbed by the extraction process using post-drainage techniques.

Natural gas - typically refers to gas extracted from geological strata other than coal seams (i.e., from “conventional” gas reserves). The gas could be composed mostly of methane and may have originally migrated from coal seam sources.

Pre-drainage (pre-mine drainage) - extraction of gas from coal ahead of mining.

Post-drainage (post-mine drainage) - extraction of gas released as a consequence of mining.

Respirable dust - microscopic particles of dust which can enter and damage the human lung.

Ventilation air methane (VAM) - methane emitted from coal seams that enters the ventilation air and is exhausted from the ventilation shaft at a low concentration, typically in the range of 0.1% to 1.0% by volume.

1 Introduction

1.1 Historical and contemporary significance of mining problem

Researchers, scholars and miners have struggled with threaten of methane liberated into the workings of both coal mines and non-coal mine for a long time. In November 1776, methane was first scientifically identified by Italian physicist Alessandro Volta in the marshes of Lake Maggiore straddling Italy and Switzerland, having been inspired to search for the substance after reading a paper written by Benjamin Franklin about "flammable air" (Volta, 1777). Volta captured the gas rising from the marsh, and by 1778 had isolated the pure gas. He also demonstrated means to ignite the gas with an electric spark.

It is well-known that coal has been an important source of global primary energy production for the past two centuries, and the world will continue to depend on coal as an energy source for the foreseeable future. Methane (CH_4) released during coal mining creates unsafe working conditions in many underground mines around the world, with human fatalities an unacceptable consequence of many gas-related accidents. Early accounts discuss the dangers of firedamp, as it is known in 19^{th} century English coal mines. But people failed to comprehend the dangerous nature of methane buildup which becomes explosive in air when the concentration falls between five and fifteen percent. As a result, the mining industry, and especially coal mining, has endured a tragic history and maintains a reputation for being a dangerous profession.

High concentrated gas (mixture of methane and other hazardous gases) in deep goaf and mining adjacent layers continuously pours into working as the air pressure in different parts of underground mine is imbalanced (Noack, 1998). Strata gas problems have created severe difficulties for the mining industry all over the world, leading to high expenditures and intensity research efforts, and determined attempts to enhance the various ventilation and gas drainage techniques (Leszek and Lunarzewski, 1998; Sander & Connell, 2012). Meanwhile, gas research is thriving in recent years, and gas drainage technology will continue to be a growing industry over the coming decades in many countries (María & González, 2007).

Modern mining techniques, with well-designed ventilation systems and permissible electrical equipment, greatly reduce the potential for methane explosions. The improvements are evident in

the industry statistics, where fires and explosions attributable to gas in underground coal mines have not been the leading cause of injury and fatality.

Encounters with powered haulage, mobile equipment, or rock falls are leading hazards in the mining environment. Coal mine fatality statistics can be seen in Figure 1.1.1 (United States) and Table 1.1.1 (China), comparing methane with powered haulage and other sources of hazard.

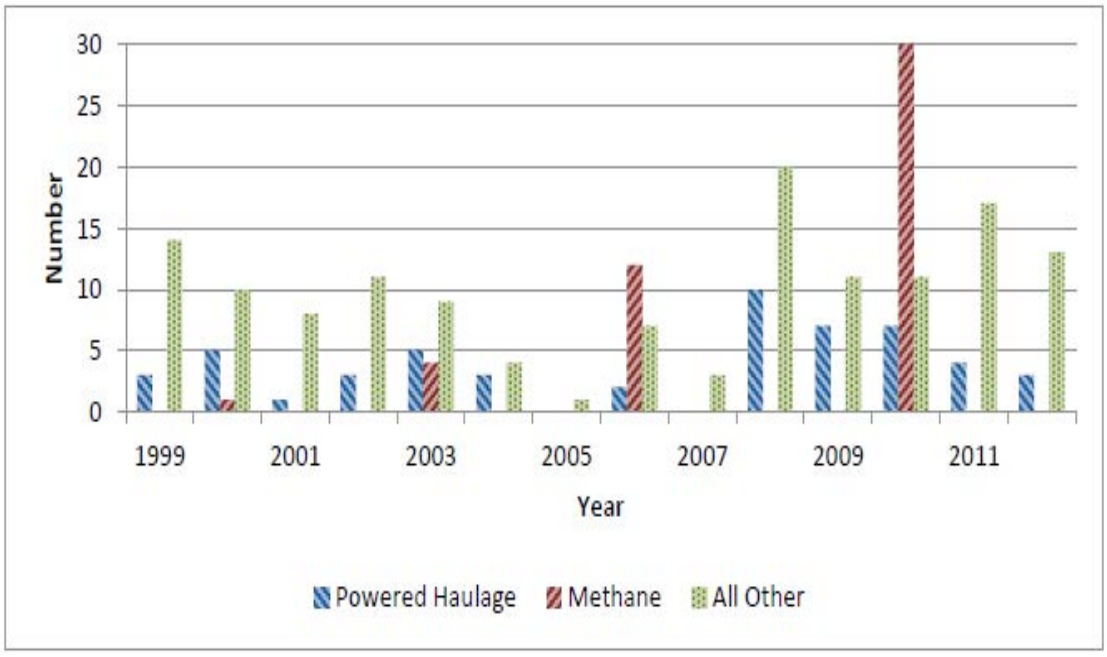

Figure 1.1.1 United States coal mine fatality statistics by type since 1999 (source: MSHA Fatality Statistics 2012)

Gas explosions remain a serious concern because they still occur at irregular intervals. When they occur, they usually cause multiple fatalities and are devastating to the community and the company responsible for the safety of its workers.

Table 1.1.1 Statistics of China coal mine gas explosion accidents in recent 10 years

Year	Frequency of gas explosion accident	Occurrence rate of gas explosion accident occurrence	Death toll of gas explosion accident	Death rate per million tons (DRPMT)
2001	667	3082	5670	5.070
2002	592	3112	6528	4.942

2003	596	4143	6424	3.711
2004	405	3639	6027	3.081
2005	405	3341	5986	2.811
2006	327	2945	4746	2.041
2007	272	2421	3786	1.501
2008	182	1901	3218	1.182
2009	154	1616	2631	0.892
2010	135	1403	2433	0.783
2011	108	1117	1937	0.623

On the one hand, working areas in underground mines have become further and deeper from several inlets and exhaust shafts while mining activities are performed (Widodo et al., 2008). A reasonable ventilation system exerts a long-term effect on mine safety and economic benefits. On the other hand, the zone of deformation, known as the “gas emission zone” of a longwall mine, hosts the sources of longwall gas providing gas to the boreholes, leads to in-mine emissions (Noack, 1998), and interferes with the stability of boreholes. Therefore, determination of the size of the gas emission zone, the locations of gas sources within, and especially the amount of gas retained in those zones is one of the most crucial steps for designing a successful gas control strategy and an efficient ventilation system in longwall coal mining (Karacan et al., 2012).

Safety mining technologies including field investigation, numerical simulation and laboratory experiments have also been improved over the past decade. However, even if the size (height) of the gas emission zone can be estimated globally using various methods or assumptions, it is not uncommon that gas emission predictions may be under- estimated or over-estimated due to the lack of sufficient spatial information defining the quantity and location of the gas sources in the overlying strata (Kurnia, et al., 2014).

Gas explosions remain a serious concern because they still occur at irregular intervals. When they occur, they usually cause multiple fatalities and are devastating to the community and the company responsible for the safety of its workers.

There have been dramatic examples of coal mine explosions o accidents in recent history.

(1) 19th-century severe mining disasters

1872: Pelsall Hall Colliery disaster in Pelsall, West Midlands. 23 people died. 1899: Sumitomo Besshi bronze mine area, landslide with debris flow disaster, Niihama, Shikoku, Japan, 512 died.

(2) 20th-century severe mining disasters

March 10, 1906: Courrières mine disaster in Courrières, France. 1,099 workers died, including children, in the worst mine accident in Europe. December 1, 1907: Naomi Mine Explosion in Fayette City, PA. 34 workers died. December 6, 1907: Monongah Mining Disaster in Monongah, WV. Official death toll is 362, but due to inadequate record keeping, the true death toll could be around 500 (McAteer, 2007). Victims were mostly Italian immigrants, including children. It can be considered the worst coal mining accident in American history. December 19, 1907: Darr Mine Disaster in Rostraver Township, PA. 239 workers died, including children. November 13, 1909: Cherry Mine Disaster in Cherry, IL. 259 workers, some as young as eleven, died. The worst mine fire by deaths in America. October 14, 1913: Senghenydd Colliery Disaster, the worst Mining accident in the United Kingdom, 439 workers died. October 22, 1913: Dawson Stag Mountain Mine Disaster, near Dawson, New Mexico, where 263 workers were killed due to illegal use of dynamite. 1927–1932: Hawks Nest Tunnel Disaster, near Gauley Bridge, West Virginia, United States. Over several years, 476 workers died from silicosis. April 26, 1942: Benxihu Colliery disaster in Benxi, Liaoning, China. 1,549 workers died, in the worst coal mine accident ever in the world. August 8, 1956: Bois du Cazier disaster in Marcinelle, Belgium. A fire in the mines resulted in 262 casualties; of the 274 people working in Bois du Cazieron that morning, only twelve survived. 138 of the victims were Italian migrant workers. 1960: Coalbrook, South Africa, 437 died. 9 May 1960: Laobaidong colliery coal dust explosion Datong, China, 682 died. 9 November 1963: Mitsui Miike Coal Mine disaster Mitsui Miike, Ōmuta, Fukuoka, Japan, 458 died (Kawabata, 2011). May 28, 1965: Dhanbad coal mine disaster took place in Jharkhand, India, killing over 300 miners. October 21, 1966: Aberfan disaster was a catastrophic collapse of a colliery spoil-tip that occurred in the Welsh village of Aberfan, killing 116 children and 28 adults. November 20, 1968: Farmington Mine Disaster in Farmington, WV. 78 workers died. As a result of the disaster, the U.S. Congress passed the Federal Coal Mine Health and Safety Act of 1969. 1972: Wankie coal

mine disaster Wankie, Rhodesia/Zimbabwe, 426 fatalities. 21 March 1973: Lofthouse Colliery disaster, West Yorkshire, England, seven fatalities. 27 December 1975: Chasnala mining disaster, Dhanbad, Jharkhand, India, 372 miners died and another 130 contract workers are claimed to have died when water from adjacent mine gusted after the wall in between collapsed. July 19, 1985: Val di Stava dam collapse took place in the village of Stava, near Tesero, Italy, when two tailings dams used for sedimenting the mud from the nearby Prestavel mine, failed. It resulted in one of Italy's worst disasters, killing 268 people, destroying 63 buildings and demolishing eight bridges. May 9, 1993: Nambija mine disaster, Nambija, Ecuador. Approximately 300 people were killed in a land slide

(3) 21st-century severe mining disasters

January 30, 2000: Baia Mare cyanide spill took place in Baia Mare, Romania. The accident, called the worst environmental disaster in Europe since Chernobyl, was a release of 100,000 tons of cyanide contaminated water by an Aurul mining company due to reservoir broke into the rivers Someş, Tisza and Danube. Although no human fatalities were reported, the leak killed up to 80% of aquatic life of some of the affected rivers. April 5, 2010: Upper Big Branch Mine disaster, West Virginia, United States. An explosion occurred in Massey Energy's Upper Big Branch coal. Twenty-nine out of thirty-one miners at the site were killed (Urbina, 2010). November 19, 2010: Pike River Mine disaster in New Zealand. At 3:45pm, the coal mine exploded. Twenty-nine men underground died immediately, or shortly afterwards, from the blast or from the toxic atmosphere. Two men in the stone drift, some distance from the mine workings, managed to escape. (Extract from Royal Commission of Enquiry Report on Pike River.) May 13, 2014: Soma mine disaster took place in Soma, Turkey. The accident, called the worst mining accident ever in Turkey, and it is the worst mining accident in 21st century so far. 301 people died.

There have been dramatic examples of coal mine explosions o accidents all over the world.

(1) United States

The Monongah Mining Disaster was the worst mining accident of American history; 362 workers were killed in an underground explosion on December 6, 1907 in Monongah, West Virginia. From 1880 to 1910, mine accidents claimed thousands of fatalities. Where annual mining deaths had numbered more than 1,000 a year during the early part of the 20th century, they decreased to an average of about 500 during the late 1950s, and to 93 during the 1990s (Historical

Data on Mine Disasters in the United States U.S). In addition to deaths, many thousands more are injured (an average of 21,351 injuries per year between 1991 and 1999), but overall there has been a downward trend of deaths and injuries. In 1959, the Knox Mine Disaster occurred in Port Griffith, Pennsylvania. The swelling Susquehanna river collapsed into a mine under it and resulted in 12 deaths. In Plymouth, Pennsylvania, the Avondale Mine Disaster of 1869 resulted in the deaths of 108 miners and two rescue workers after a fire in the only shaft eliminated the oxygen in the mine. Federal laws for mining safety resulted from this disaster. Pennsylvania suffered another disaster in 2002 at Quecreek, 9 miners were trapped underground and subsequently rescued after 78 hours. During 2006, 72 miners lost their lives at work, 47 by coal mining. The majority of these fatalities occurred in Kentucky and West Virginia, including the Sago Mine Disaster (All Mining Fatalities by State U.S, 2007; Coal Fatalities By State U.S, 2007). On April 5, 2010, in the Upper Big Branch Mine disaster an underground explosion caused the deaths of 29 miners. The U.S. Bureau of Mines was created in 1910 to investigate accidents, advice industry, conduct production and safety research, and teach courses in accident prevention, first aid, and mine rescue. The Federal Coal Mine Health and Safety Acts of 1969 and 1977 set further safety standards for the mining.

(2) China

According to one source, in 2003 China accounted for the largest number of coal-mining fatalities, accounting for about 80% of the world's total, although it produced only 35% of the world's coal (Zhao et al., 2004). Between January 2001 and October 2004, there were 188 accidents that had a death toll of more than 10, about one such accident every 7.4 days (Zhao et al., 2004).. After the 2005 Sunjiawan mine disaster, which killed at least 210 miners, a meeting of the State Council was convened to work on measures to improve work safety in coal mines. The meeting's statement indicated serious problems such as violation of safety standards and overproduction in some coal mines. Three billion Yuan (360 million US dollars) were dedicated for technological renovation on work safety, gas management in particular, at state-owned major coal mines. The government also promised to send safety supervision teams to 45 coal mines with serious gas problems and invite colliery safety experts to evaluate safety situations in coal mines and formulate prevention measures (Embassy of the People's Republic of China in the U.S.A., 2005). In 2006, according to the State Work Safety Supervision Administration, 4,749 Chinese

coal miners were killed in thousands of blasts, floods, and other accidents. For example, a gas explosion at the Nanshan Colliery killed 24 people on November 13, 2006; the mine was operating without any safety license and the Xinhua News Agency claimed the cause was incorrect usage of explosives. However, the 2006 rate was 20.1% less than 2005 despite an 8.1% increase in production (Reuters, 2007). The New York Times reported that China's lack of a free press, independent trade unions, citizen watchdog groups and other checks of official power has made cover-ups of mining accidents more possible, even in the Internet age. As a result, Chinese bureaucrats habitually hide scandals (such as mine disasters, chemical spills, the 2003 SARS epidemic, and tainted milk powder) for fear of being held accountable by the ruling Communist Party or exposing their own illicit deals with companies involved. Under China's authoritarian system, superiors reward subordinates for strict compliance with goals established by authorities, like reducing mine disasters. Indeed, should a mining accident occur, the incentive to hide it is often stronger than the reward for managing it well, as any disaster is almost surely considered a liability (Lafraniere, 2009). In November 2009, a mining accident in Heilongjiang killed at least 104 people. It is thought to have been caused by a methane explosion followed by a coal dust explosion. Three top officials involved with the mining company were promptly dismissed. On August 30, 2012 an explosion killed 45 people at the Xiaojiawan coal mine in Sichuan province (The Guardian (London), 2012; Xinhuanet news, 2012). A few days later on September 3, 2012 14 miners were killed at Gaokeng Coal Mine in Jiangxi province (The Independent (London), 2012). On March 29, 2013, a landslide trapped 83 people in the Gyama Mine in Tibet (BBC News, 2013). On 4 January 2014 The Chinese Government stated that 1,049 people died in the year 2013, down 24 percent from 2012 (ABC News, 2013).

(3) Europe

Belgium, on March 4, 1887, 120 miners died in a coal mine in La Boule, Borinage due to a methane explosion. On the morning of August 8, 1956, a fire in the mine Bois du Cazier in Marcinelle caused 262 victims, with only 12 survivors. A mining cart on an elevator cage hit an oil pipe and electricity lines, with the resulting fire trapping the miners. Most of the victims were immigrants (136 Italians, 8 Poles, 6 Greeks, 5 Germans, 5 Frenchmen, 3 Hungarians, 1 Englishman, 1 Dutchman, 1 Russian and 1 Ukrainian.)

France, the Courrières mine disaster was the worst ever pit mine disaster in Europe. It caused

the death of 1,099 miners (including many children) in Northern France on 10 March 1906. It seems that this disaster was surpassed only by the Benxihu Colliery accident in China on April 26, 1942, which killed 1,549 miners. A dust explosion, the cause of which is not known with certainty, devastated a coal mine operated by the Compagnie des mines de houille de Courrières (founded in 1852) between the villages of Méricourt (404 killed), Sallaumines (304 killed), Billy-Montigny (114 killed), and Noyelles-sous-Lens (102 killed) about two kilometers (one mile) to the east of Lens, in the Pas-de-Calais department (about 220 km, or 140 miles, north of Paris). A large explosion was heard shortly after 06:30 on the morning of Saturday 10 March 1906. An elevator cage at Shaft 3 was thrown to the surface, damaging pit-head workings; windows and roofs were blown out on the surface at Shaft 4; an elevator cage raised at Shaft 2 contained only dead and unconscious miners.

Netherlands, the twelve mines in the Netherlands, four of which were state owned, were considered among the safest in the world, with only three larger accidents occurring during 70 years of mining: On 13 July 1928 a methane gas explosion killed 13 miners in the state-owned mine Hendrik in Brunssum; On 24 March 1947 13 miners from Staatsmijn Hendrik were killed in a fire caused by an overheated conveyor belt; On 3 March 1958 7 miners lost their lives when a cave-in occurred at Staatsmijn Maurits in Geleen.

Poland, on November 25, 2006, the worst mining disaster occurred in modern Polish history, 23 miners lost their lives at Halemba Coal Mine, a colliery in the town of Ruda Slaska in the southern industrial province of Silesia. A methane explosion at a depth of 1,030 meters caused the November 21 tragedy. The miners were attempting to retrieve €17 million ($US22 million) worth of equipment from a tunnel when a blast caused the shaft to collapse. The tunnel was supposed to have been closed in March due to dangerously high methane concentrations, but was kept active because of the value of the equipment left behind.

United Kingdom, in England, The Oaks explosion remains the worst mining accident, claiming 388 lives on 12 December 1866 near Barnsley in Yorkshire. The Hulton Colliery explosion at West Houghton, Lancashire, in 1910 claimed the lives of 344 miners. An explosion in 1878, at the Wood Pit, Haydock, Lancashire, killed over 200 workers, although only 189 were included in the 'official list'. Another disaster that killed many miners was the Hartley Colliery Disaster, which occurred in January 1862 when the beam of the main steam winding

engine broke suddenly and fell into the single shaft serving the pit. It blocked the shaft, and entombed hundreds of miners. The final death toll was 204, most of who were suffocated by the lack of oxygen in the mine atmosphere. In the metalliferous mines of Cornwall, some of the worst accidents were at East Wheal Rose in 1846, where 39 workers were killed by a sudden flood; at Levant mine in 1919, where 31 were killed and many injured in a failure of the man engine; (Corin, 1992) 12 killed at Wheal Agar in 1883 when a cage fell down a shaft; (Vivian, 1970) and seven killed at Dolcoath mine in 1893 when a large stull collapsed (Vivian, 1970).

1.2 Research objectives and contents

Multiple researches and experiments are needed to develop a better understanding of the causes of mine gas-related disasters. More gas control strategies and technologies (both numerical simulation and laboratorial experiments) should be developed, including optimizing the ventilation system constantly, preventing goaf spontaneous combustion, enhancing gas risk management, determining the gas emission zone, and implementing a reasonable gas drainage plan. The research roadmap can be seen in Figure 1.2.1.

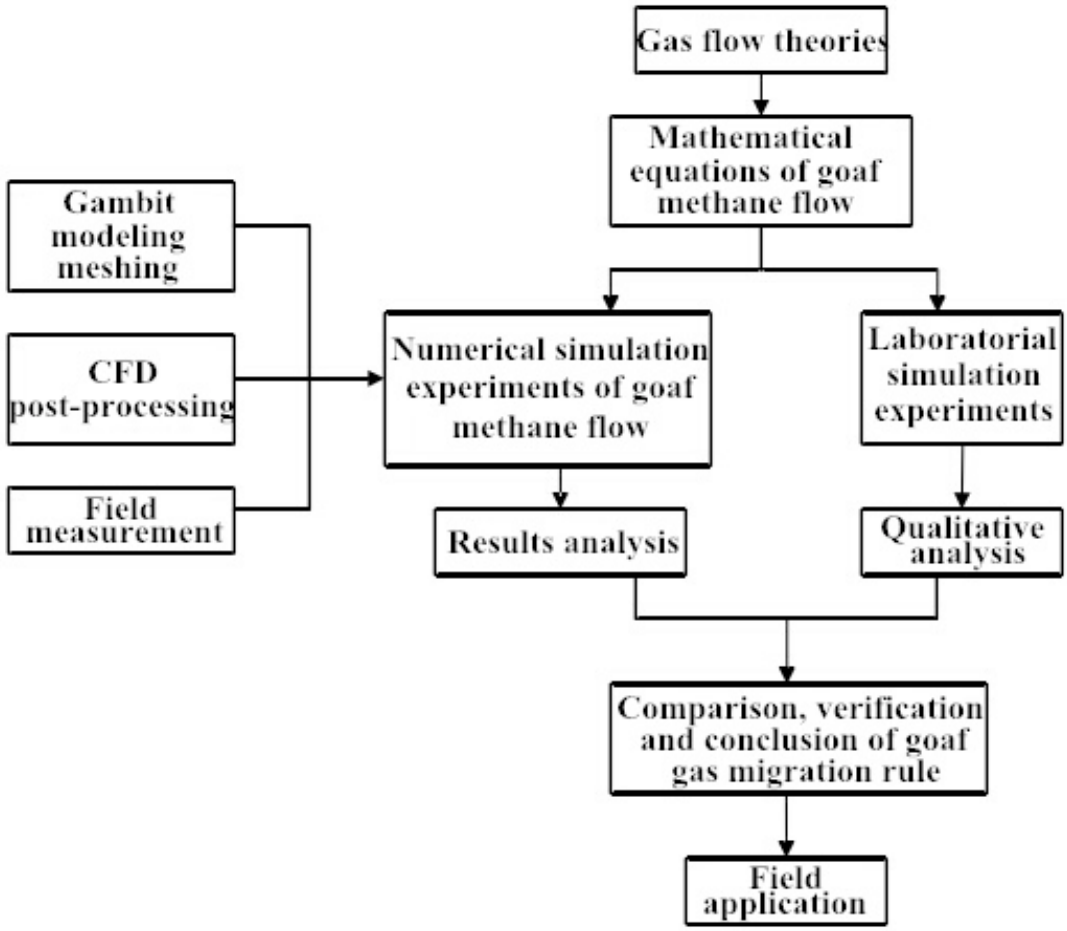

Figure 1.2.1 Research road map

Computational fluid dynamics, as a numerical simulation tool to improve safety in mining, has progressed rapidly, but the challenges of modeling the mine environment are not insubstantial. Ren and Balusu discussed this topic in 2005. Common areas of research include the control of gas and spontaneous heating in the goaf area, goaf inertisation strategies, and dust and method control at the working face (Ren & Balusu, 2005). The quality of this work has been improved by adopting a multi-scale approach from other disciplines. This numerical simulation approach allows one to include the entire mine network within the computational domain, with reduced complexity at areas removed from the immediate area of interest.

Laboratorial simulation model of mine ventilation system and goaf, as an experimental method to ensure and improve safety and environment in mining industrial has developed rapidly, but the challenges of the model design and development are not insubstantial. Wang, Cheng and Xie researched this topic in 2012. Their research results showed that the gas concentration was low intake airflow roadway along goaf towards direction. The goaf gas concentration in air outlet

was far higher than air inlet. There was not combustion phenomenon during the test in the goaf of the coal mining. Meanwhile, the results also confirmed mining extraction process source of gas accumulation in face corner, also can be used for providing the basis of enacting fire prevention measures in the goaf and gas management measures for face corner (Wang et al., 2012). The quality of the work has been improved by adopting flow similarity theory and approach from other disciplines.

The multiple approaches to CFD modeling and laboratory modeling provide a practical means to include the entire mine ventilation system (MVS) and the goaf region in both computational domain and laboratory. This leads to improved understanding of the goaf environment and its influence on mine workings, specifically under transient conditions. The research was broken down into two parts and many key tasks for the development of the numerical and laboratorial models of the entire system. A brief description of these tasks follows.

1.2.1 Numerical simulation model

Gas flow behavior in working face and goaf is a complicated process since numerous factors are involved. Combined with the specific condition of working field, experiences of other numerical models and multiple factors of the mine, the numerical model of gas flow distribution in goaf was established. The establishment of numerical modeling work consists of several basic steps. The first step is to go to working field to collect the basic information, such as geometries, relevant parameters, rate of gas flow, goaf dropping characteristic etc. The second is to establish the 3D finite element model of the mine face, goaf, and tunnel and drainage borehole. The third is to set up gas flow models and boundary conditions through User-Defined Functions. The fourth is to simulate the condition of working face and goaf. The fifth is to calibrate and validate the simulation model by using working field measured data. The last step is to conduct extensive parametric researches and technique evolution by optimizing the numerical model.

1.2.2 Laboratorial simulation model

Air is the flow medium, and its flow state is regarded as pressure steady flows during experiments are performed. The similarity relationship between prototype and model is built

according to the similarity criteria such as geometric and dynamic similarity. The ventilation system model is proportional to the tunnel size of designated coal mine. Taking into consideration the experiment feasibility, the establishment of the ventilation model is simplified.

1.3 Organization of the researches

This research dissertation is composed of seven chapters.

The first chapter describes the subject and its historical and contemporary context. Based on establishing the necessary for this research, it indicates the research approach used to advance the understanding of methane related issues, along with some specific objectives

The second chapter introduces a survey of the literature review concerning mine ventilation system and goaf modeling. The background information and references pertaining to the issue of gas within the coal body and coal seam is presented, including the influence of coal mining activities and subsequent release of methane from adjacent layers and goaf into the mine working face. It then concludes past and present goaf modeling efforts from the researches all over the world. It summarizes with an introduction to the numerical simulation and laboratorial experiments technique which are practiced in other areas of research.

Chapter three is composed of four parts, and it describes contents concerning a numerical prediction model used to establish the mine gas emission of working face 14205. The first part provides a brief introduction of the working face location, roadway layout, mining technology and equipment. The second part offers an analysis of gas emission sources and rules. The next part discusses the establishment of gas emission prediction model of the 14205 working face and goaf. The last part details the gas emission calculation of the 14205 working face and goaf as well as the analysis of the prediction results.

Chapter four is divided into three parts, and it describes contents concerning the numerical modeling used to establish the ventilation system and longwall goaf. The first part provides a brief overview of the application of numerical simulation technique in mineral industry, and analyzes the necessity of numerical simulation. The second part offers an introduction to the theoretical basis of numerical simulation technique and the application of the CFD software. The last part discusses the establishment of the numerical simulation model of the 14205 working face and goaf of Shaqu coal mine as well as the analysis of the experimental findings.

The fifth chapter describes contents concerning the laboratorial modeling used to establish the ventilation system and longwall goaf, and it composed of four parts. The first part provides a brief overview of the application of laboratorial simulation technique in mineral industry, analyzes the necessity of numerical simulation, and describes the research goal and contents. The second part offers an introduction to the theoretical basis of laboratorial simulation technique and similarity theory, similarity criterion and similarity theorem. The next part discusses the establishment of the laboratory simulation model of 14205 working face and goaf of Shaqu coal mine. The last part offers the verification of the simulation model based on non-coal mine ventilation system and mine coal ventilation system as well as the analysis of the experimental findings.

The last chapter describes contents concerning the field gas distribution and migration measurement, gas drainage design and measured results of gas drainage rate in the working field. The first part discusses gas concentration distribution rule of Shaqu coal mine, and provides a measured results of actual gas concentration in 25 different measuring points in the working face. The second part provides an introduction to the gas migration rule of working face and goaf, and analysis the measured results of gas concentration of Shaqu coal mine. The next part offers an analysis of the necessity and feasibility of gas drainage of Shaqu coal mine. The fourth part provides the gas drainage design project, layout and technical parameters based on the simulation results of numerical experiments and laboratorial experiments. The last part offers gas drainage rate of special gas drainage tunnels, the upper corner and the air inlet based on U-type ventilation system and U+L-type ventilation system as well as the analysis of gas drainage rate and results.

2 Literature review

2.1 Overview

The part of literature review has concentrated on five parts. The part one is an overview in the nature and characteristic of coal seam gas. It describes a look at the source of gas, as well as means to quantify the amount of methane emission. The part two discusses gas emission prediction. The third part is talk about the influence of mining activities on the coal seam gas. This identifies the key contributors to the inflow of gas from the mined coal, lost coal, working face, goaf and adjacent layers of the surrounding seam or strata. The third part of literature review discusses the influence of mine ventilation challenge. The next portion discusses the numerical simulation modeling techniques that have been employed to study gas problem, along with a brief introduction to laboratorial simulation modeling approach that was employed in this study. The last part focuses on gas drainage and usage.

2.2 The nature of coal seam gas

Methane gas flows into coal mines under normal, steady-state conditions are generally predictable. Unusual gas emission or gas outburst disasters are not easily predicted. However, the conditions how they can usually occur are reasonably well-known. Detailed approaches for lowing risks under these situations have been studied and should be applied whenever and wherever significant risks are identified. In such circumstances, safety working environment depend on the rigor of implementation and monitoring of methane control and prevent approaches.

The most importance of not only placing underground monitoring devices for the reason of safety mining working environment but also obtaining and applying the numerical simulation data, laboratorial data and field data for safety production cannot be exaggerated.

At present, high-production coal mines encounter increasingly high gas flows when the coal mining efficiency improves and they work deeper and higher gas concentration coal seams. The basic knowledge and reorganization of gas occurrence, emission characteristics, and migration rule from a coal mine as a functionality of the mining production efficiency is significant.

2.2.1 Occurrence of gas in coal beds and seams

The naturally-occurring gas found in coal beds and seams consists mainly of methane (typically 80% to 95%) with lower proportions of heavier hydrocarbon gases, nitrogen, and carbon dioxide (Stéphane et al., 2014). The mixtures of methane, water vapor, air, and associated oxidation products that are encountered in coal mines are often collectively termed "mine gas" (Karacan & Okandan, 2000). Coal bed methane is one of the names given to the gas associated with a seam of coal. It has been referred to by a number of different names, such as coal seam gas, coal seam methane, etc. For our purposes, these are the same. It is not exclusively methane, but rather a mixture of methane, carbon dioxide, and possibly smaller fractions of methane, nitrogen, hydrogen sulfide, and other gases (Rice, 1993). The predominant gas is methane, CH_4, whose hazard within the mining environment is now widely known.

Methane was formed in coal seams as a result of the chemical reactions taking place as the coal was buried at depth. Plant debris such as that found in modern swamps will slowly change from wet, organic detritus to coal, if the material becomes buried at a sufficient depth and remains covered for a length of time through a process known as coalification (Jana et al., 2009). The greater the temperature, pressure, and duration of coal burial, the higher the coal maturity (i.e., rank) and the greater the amount of gas produced. Much more gas was produced during this coalification process than is now found in the seams (Romeo, 2014). The gas lost during the coalification process has been emitted at ancient land surfaces, removed in solution by ground water passing through, or has migrated and been trapped in the pore spaces and structures in surrounding rocks. This gas may have accumulated in adjacent porous strata such as sandstones or may have been adsorbed by organic shale. These reservoir rocks can become significant sources of gas flows into the mine if these gas-bearing layers are sealed by surrounding impermeable strata and remain undisturbed until mining takes place. Methane occurs in much higher concentrations in coal compared to any other rock type because of the adsorption process, which enables methane molecules to be packed into the coal substance to a density almost resembling that of a liquid. In a vertical sequence of coal seams, methane content often increases systematically with depth and rank. Gas content-depth gradients vary from coalfield to coalfield and reflect the geologic history of the basin in which the coal formed. In some coal basins,

methane contents increase with depth, finally reach a maximum and then decrease below this level.

H.F. Coward wrote about the dangers of methane accumulation behind stopping in 1929. In this paper, he presented what came to be known as the Coward Triangle, which is a graphical representation of the explosive range of methane when mixed with air. A version of it can be seen in Figure 2.2.1.

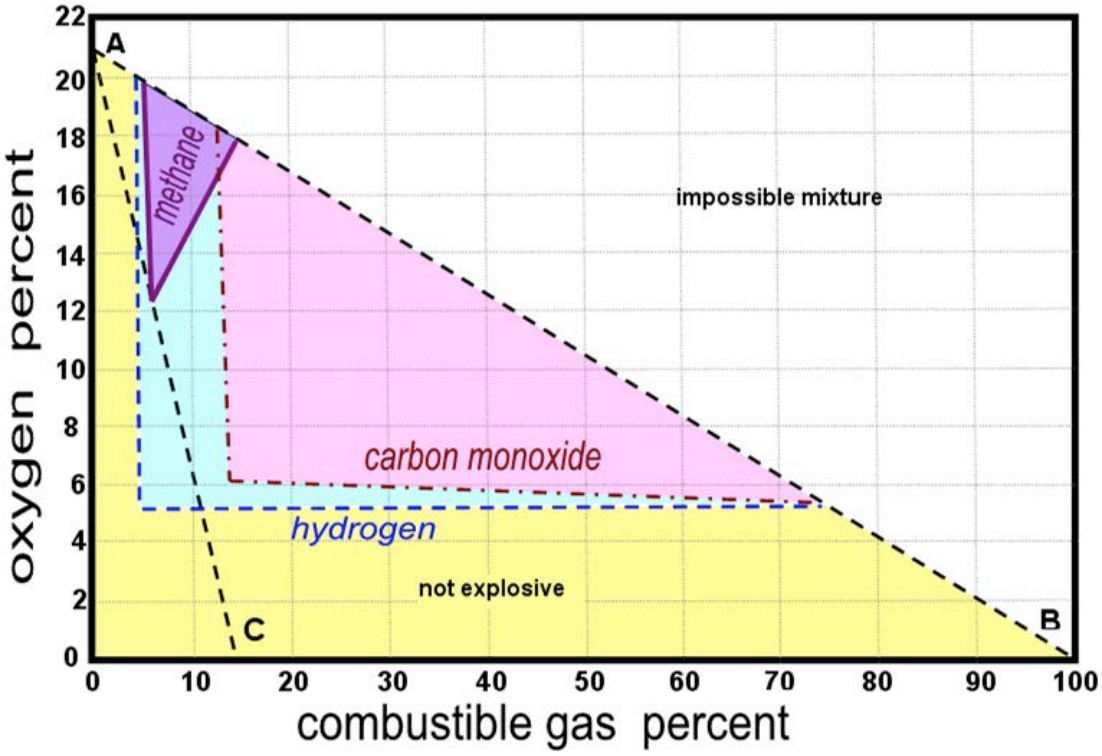

Figure 2.2.1 Coward triangle for methane, carbon monoxide, and hydrogen (Adapted: Malcolm, 2008)

Methane can be found at a high concentration within the coal, sometimes approaching 100%. Methane, in concentrations between 5% and 15% when mixed with air, is explosive. The most energetic mixture is one that is stoichiometrically balanced, or 9.8% methane in air. During the process of dilution, the air and methane mixture must pass through this explosive range to the low levels prescribed by regulation and engineering prudence as shown in Figure 2.2.2 (Kissell, 2006). It is important that this dilution happens as quickly as possible or is contained to a region that is largely inaccessible to minimize the risk.

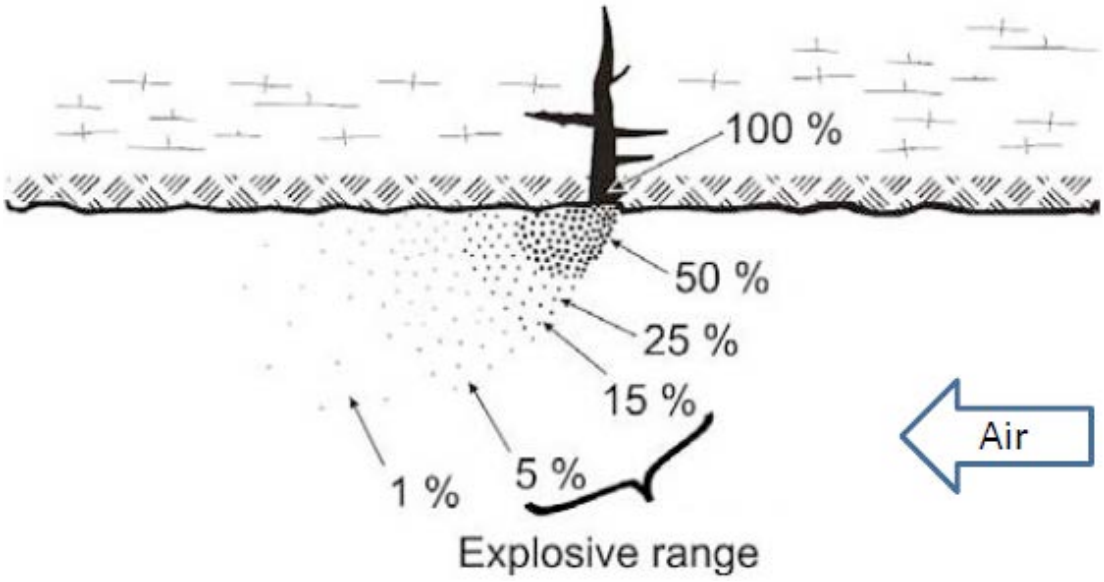

Figure 2.2.2 Diagram of methane inflow from a fracture and the progressive dilution due to airflow in the entry (Adapted: Kissell, 2006)

2.2.2 The source of coal seam methane

Methane within the coal bed is generated during the coalification process (Levine, 1993). This is the process by which plant material is progressively converted to coal. The progression from the early stages of coalification, peat and lignite, to later stages of coalification, anthracite, is due to geophysical and chemical processes in an irreversible process (Levine, 1993; Rice, 1993; Moore, 2012). A visual representation of the coalification process can be seen in Figure 2.2.3.

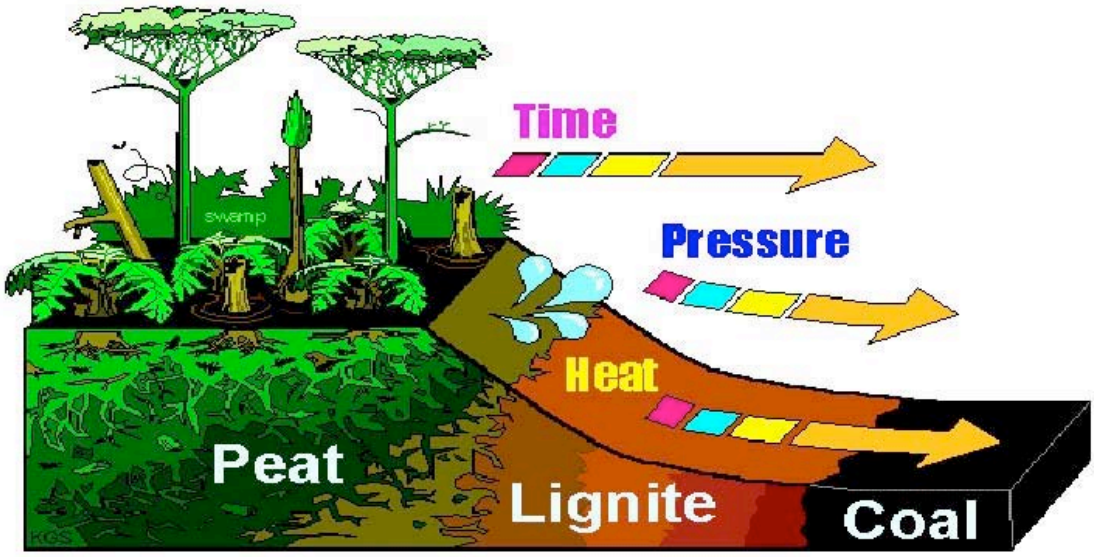

Figure 2.2.3 Coalification process

As organic matter progresses through the coalification process it matures and undergoes both physical and chemical change. The degree of alteration, or metamorphism, which occurs as coal matures, is referred to as the “rank” of the coal. The coal rank classifications used to describe coal, in increasing order of alteration and maturity, with the exception of the highest rank Anthracite, are described in Figure 2.2.4 (Aziz, 2006). Coal rank generally increases in direct correlation to temperature, depth of burial, geothermal gradient, and the length of time the organic material remains in a given regime. Rank is estimated by measuring various rank parameters, which include: carbon content, volatile matter, vitrinite reflectance, moisture content and specific energy (Ward, 1984).

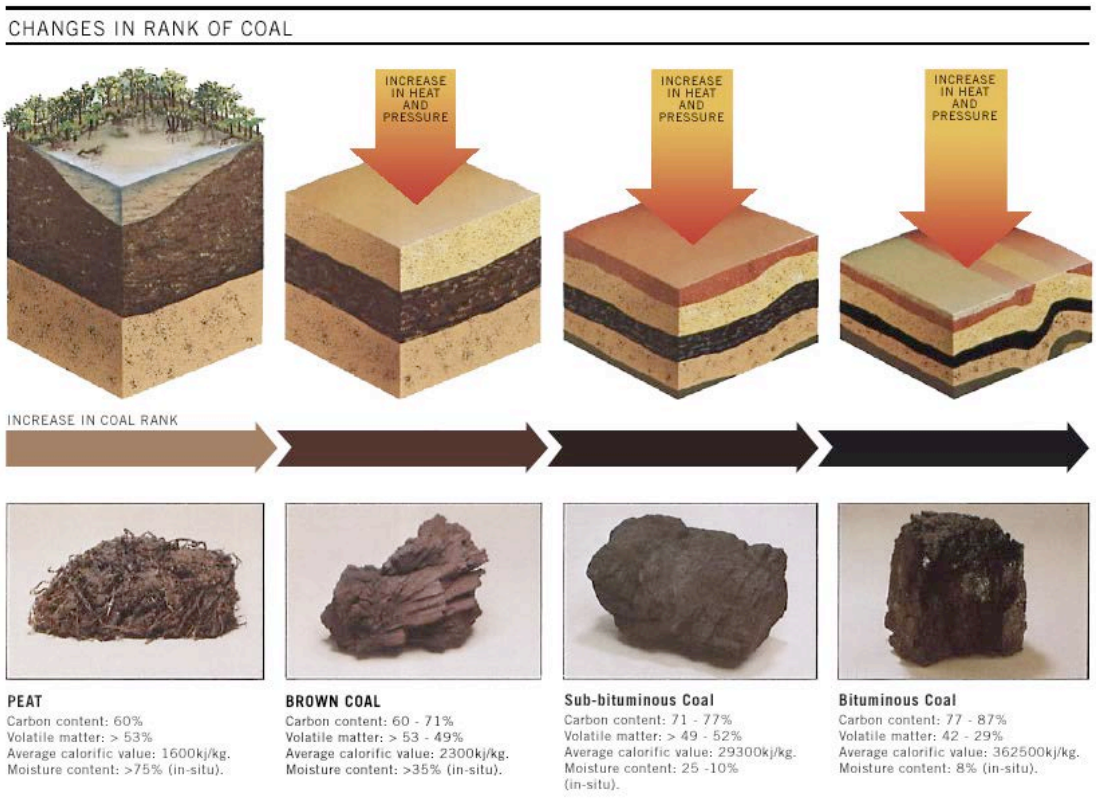

Figure 2.2.4 Changes in coal composition with increasing rank (Aziz, 2006)

Faiz (1993) suggests vitrinite reflectance is the preferred method of determining coal rank as it is not influenced by the presence of mineral matter or moisture and therefore does not require corrections to be made for these factors, which must be made for the other rank parameters. Low rank coals are typically soft and friable with a dull earthy appearance and are characterized by

high moisture and low carbon content. Higher rank coals are typically harder and stronger, with a black vitreous luster and are characterized by reduced moisture levels and increased carbon content. Variation in coal rank is one of the most important factors that govern the gas storage of coal, whilst another important factor is coal type (Faiz, 1993).

At the very starting stages of coalification, almost 99% of the methane generated is biogenic. There are literally thousands of taxa of microorganisms living under the ground, within the coal beds and seams that metabolize methane (Strapoc et al., 2008). These organisms are termed methanogens and are from the bacterial and archaeal domains. These organisms, working in concert, break the low rank coal macromolecules down into simpler components through two main pathways: fermentation and anaerobic oxidation (Green et al., 2008). A generalized process for the production of biogenic methane can be seen in Figure 2.2.5. Gas concentration in low rank coals are rarely above 4 to 6 m^3/ton (Moore, 2012).

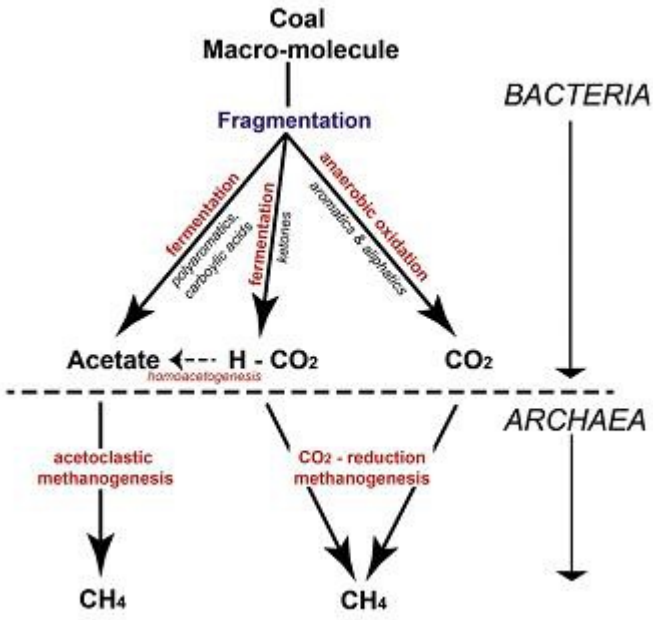

Figure 2.2.5 Generalized biogenic methane production process (Source: Moore, 2012)

Coal serves as both a source and a reservoir for the methane. The methane produced through the biogenic and thermogenic processes is, for the most part, locked away onto the surface of the coal. One of the unique characteristics of coal is its high degree of porosity. Researchers have reported surface areas as high as 115 square meters in a single gram of coal (Şenel et al., 2001). Due to its porosity, coal has an incredible capacity to store methane adsorbed onto the surface area

of its pores (Rice, 1993).

2.3 Coal seam gas and prediction

Peak flows of gas occur in the air outlets of working districts during the coalface cutting cycle and following roof caving as longwall supports are advanced. Statistical studies have shown that these peaks typically rise up to 50% above the mean (Creedy et al, 1997). Gas prediction methods commonly use this relationship in estimating the volume of air that will be necessary in order to meet mandatory gas dilution requirements.

Older empirical methods of predicting gas emissions into coal mines varied from curve fitting procedures to pocket calculators (Creedy et al 1988; CEC, 1988). The continued enhancement of computing power on desk and portable machines has promoted the utilization of sophisticated data processing software. This has resulted in improved reliability of predicting methane emissions from data that are often difficult to correlate (Lunarzewski, 1998). One such procedure utilizes artificial neural networks (Karacan, 2007). This technique seeks patterns and relationships between groups of input data that have appear to have obscure inter-relationships from conventional mathematical or statistical methodologies.

It is a fundamental safety work to calculating the gas content in coal seam and forecasting the gas emission from coal and rock in coal mine (Sander & Connell, 2014). In the 1950s, it has been established some measurement methods and processes of gas content in coal bed, and has been put forward and applied the mine statistical method to calculate and predict mine gas content and emission in coal mines (David et al., 1993). In the 1980s, the method of different-source prediction for gas emission also has been proposed and applied. Since then, the method of analogy method, the gas geology mathematical model, velocity method and other prediction methods for gas emission have been put forward and applied (Karacan et al., 2011). After decades of exploration and study by researcher and scholar, it has been formed the maturity and traditional prediction method and technology for gas emission in coal mines that was suitable the coal seam occurrence conditions (Zofia et al., 2009). All the methods and technologies was offer a scientific basis to design and retrofit for the new and old coal mine. With the expansion of coal mining intensity and production scale, people has deepening understood and grasped the essential feature of mine gas emission system by the development and its application of computer technology and

mathematics method and the nonlinear theory (Yasin & Etem, 2014).

A feature of artificial neural network software is that it can 'learn' as more data is added, so increasing its accuracy of prediction. Nevertheless, we are reminded that the reliability of all empirical models is dependent on the range, quality and detail of the measurements on which the model is based (Li, et al., 2011). Hence, it is the responsibility of the user to ascertain that any given model is applicable to the mine under consideration.

Various methods used to measure or estimate gas content can be mainly grouped into two categories, (i) direct methods, which measure the volume of gas released from a coal sample sealed in a desorption canister, and (ii) indirect methods, which are based on gas sorption characteristics under given temperature and pressure conditions, or empirical correlations between gas content and other coal seam parameters such as coal rank, depth of cover and gas emission rate (Lama & Bartosiewicz, 1982; SAA, 1999).

2.3.1 Direct method of gas measurement

Measurement of the gas content of a coal samples involves three stages: (i) determining the gas lost from the coal sample during core sample recovery (Q_1), (ii) measuring the gas desorbed from the coal sample while sealed in a desorption canister (Q_2), and (iii) measuring the gas released from a coal sub-sample during crushing (Q_3). The gas content measured during each stage is added to give the total measured gas content (Q_m), Equation 3.1.1, which for the purpose of this analysis represents the total volume of gas released per unit mass of coal when the ambient gas partial pressure is maintained at one atmosphere.

$$Q_M = Q_1 + Q_2 + Q_3 \tag{3.1.1}$$

Given the potential for variable temperature and atmospheric pressure conditions during gas content measurement and differences in mineral matter content of the coal samples, the results are typically normalized with QM being reported in NTP (20° C and 101.325 kPa) and 10% non-coal matter (NCM) (Close and Erwin, 1989 and SAA, 1999).

Diamond and Schatzel (1998) list a variety of methods developed to measure gas content subsequent to the introduction of the first method by Bertard et al. in 1970. The techniques include:

Bertard's method; US Bureau of Mines direct method; US Bureau of Mines modified direct method; Smith and Williams method; Decline curve method; Gas Research Institute method; Australian Standard method.

The fast and slow desorption methods used in Australia to directly measure the gas content of coal samples, as described in Australian Standard AS3980: 1999 (SAA, 1999), vary only in the time allowed for gas to desorb from the intact core prior to final crushing. The fast desorption test is typically completed in less than one day whereas slow desorption testing involved a much longer desorption period enabling the rate of gas emission from the intact coal core to be determined. For samples of equivalent Q_m, the $Q_2 : Q_3$ ratio determined from fast desorption testing will be much less than the ratio determined from slow desorption testing. The lost gas volume Q_1 will be the same regardless of the test method.

2.3.1.1 Lost gas component

The lost gas component (Q_1) is the portion of Q_M that escapes from the coal sample during its collection and retrieval, prior to being sealed into a desorption canister. Q_1 can not be directly measured and therefore must be estimated from gas emission data collected subsequent to the sample being sealed into the desorption canister. It is generally accepted that during initial desorption the volume of gas released is proportional to the square root of desorption time. As described in Australian Standard AS3980:1999 (SAA, 1999) and presented in Figure 2.3.1, projecting the line of best fit representing initial gas emission from the time the core was sealed into the gas desorption canister (t_i) to the time midway between the commencement and completion of coring the sample (t_0) gives a measure of the gas volume lost during core sample recovery.

Since Q_1 is an estimated quantity, it is generally accepted to be the least accurate component of Q_M (Mavor *et al.*, 1992; Diamond and Schatzel, 1998 and Williams, 2002). Factors considered to impact the accuracy of the Q_1 measurement include sample recovery time,

integrity of the coal sample, type of drilling fluid, water saturation and the amount of gas stored as free gas (Diamond and Schatzel, 1998). Close and Erwin (1989) refer to an alternative method for determining Q_1, presented by Smith and Williams based on the assumption that methane diffusion in coal is through a bi-disperse pore structure which is contrary to the unimodal pore theory upon which the more commonly used direct method is based. Comparative analysis of gas content measurement of samples from deep coal seams in the western United States indicated potential problems associated with using the Smith and Williams method when compared to other gas content measurement methods (Diamond and Schatzel, 1998).

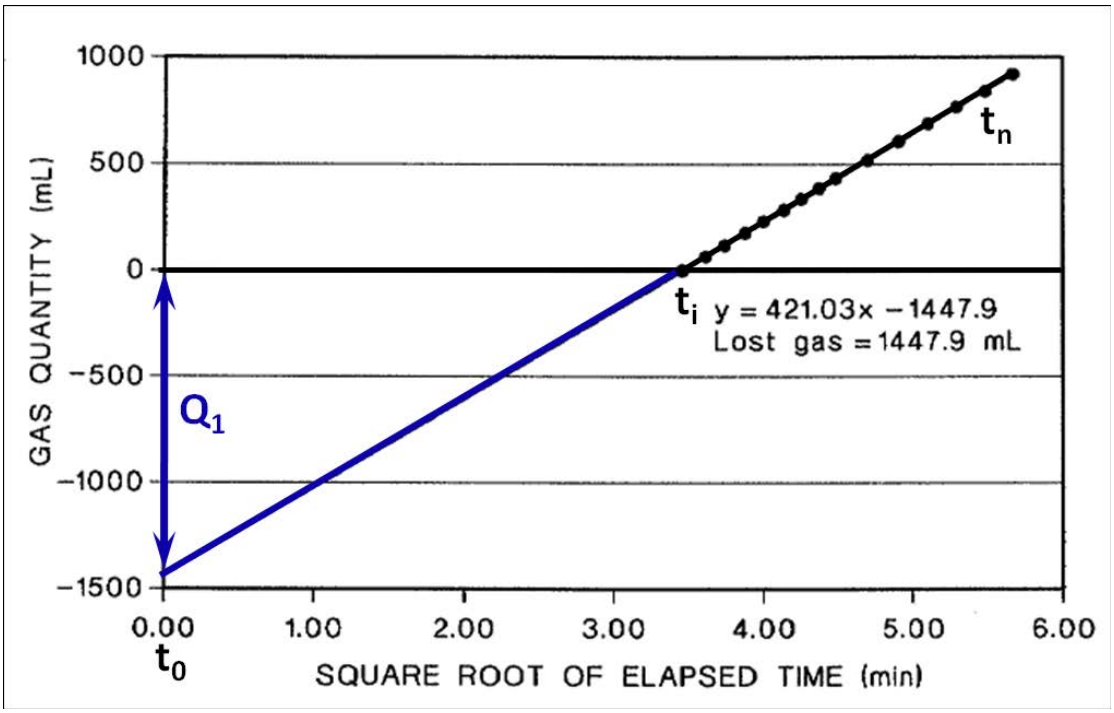

Figure 2.3.1 Q_1 lost gas determination (Source SAA, 1999)

2.3.1.2 Desorbed gas component

The desorbed gas component (Q_2) is a measure of the volume of gas released from a coal sample whilst contained in a desorption canister. The duration of the Q_2 test may be short in the case of a fast desorption method, less than one day, or much longer in the case of slow desorption testing, greater than one month. Typically, gas released from a core sample is measured by water displacement using a graduated glass or plastic measuring flask. As shown in Figure 2.3.2 the

measurement apparatus may be setup such that the gas liberated from the core sample within the desorption canister enters the measuring flask via a tube connected to the bottom or top of the measuring flask. Gas entering the top of the cylinder is preferred as the desorbed gas does not bubble through the water column thereby reducing the risk of gas loss through dissolution, particularly in the case of seam gas containing highly soluble CO_2 (SAA, 1999). Measures used to mitigate CO_2 dissolution in water include the use of acidified water in the measuring flask and a layer of linseed oil as a barrier between the water column and the gas entering the top of the flask (Saghafi *et al.*, 1998). An additional measure to minimize gas loss into solution is the periodic release of gas from the desorption canister which involves opening the valve at the top of the desorption canister, measuring the water displacement and noting other environmental conditions such as temperature and atmospheric pressure, then resealing the desorption canister until the next scheduled gas release (McCulloch *et al.*, 1975; Diamond and Schatzel, 1998 and SAA, 1999).

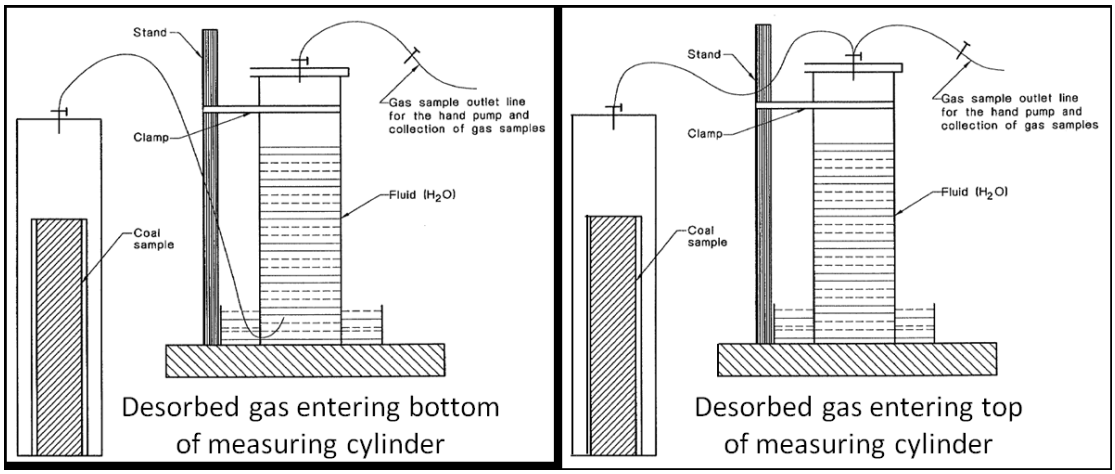

Figure 2.3.2 Desorbed gas volume measurement apparatus (Source SAA, 1999)

2.3.1.3 Crushed gas component

The crushed gas component (Q_3) is a measure of the gas liberated from a coal sample following crushing. Following completion of the desorbed gas test the coal core is removed and a representative sub-sample collected and sealed into a crushing or grinding mill. Following crushing the volume of gas liberated from the coal sample is measured using a water column similar to that used in the desorbed gas measurement.

McCulloch *et al.* (1975) first proposed that coal samples be sealed in a crushing vessel filled

with N2 and crushed to less than 200 µm. Diamond and Levine (1981) proposed crushing a sub-sample of up to 1 000 g for one hour to achieve a -200 µm fine powder and allowing the sample to cool to room temperature prior to measuring the liberated gas by way of water displacement. SAA (1999) recommends testing a minimum of two representative sub-samples of similar mass (±5%) weighing between 15 and 300 g, each sub-sample crushed separately to achieve a minimum of 95% of the material -212 µm.

A comparison of Q_3 testing procedures used by three Australian companies reported by Danell *et al.* (2003) identified differences in sample mass, crushing time and cooling time. Although different, the procedures employed by each laboratory were reported to comply with the guidelines detailed in Australian Standard 3980:1999. An assessment of gas content testing on equivalent reference samples by Danell *et al.* (2003) noted consistent differences in the results reported by each of the laboratories involved, with variability of up to 17%. This result was consistent with the expectation of Australian Standard 3980:1999 (SAA, 1999) which suggest inter-laboratory variability of 15%.

In fast desorption testing, given the short desorption time, Q_3 represent a large percentage of Q_M, whereas in slow desorption testing Q_3 is quite low, representing the residual gas content of the sample. Residual gas content is the volume of gas per unit mass of coal that is naturally retained within the coal and not readily released from an intact sample. The residual gas content also represents the portion of Q_M that will not be liberated into the mine atmosphere from mined or intact coal (Diamond and Schatzel, 1998).

Residual gas content is also an important consideration in the evaluation of coalbed methane gas recovery potential as it represents the portion of QM that will not readily flow to gas drainage boreholes (Diamond and Schatzel, 1998).

2.3.1.4 Fast desorption method

The fast desorption method is the preferred method for gas content measurement used in the Australian underground mining industry due to the relatively short time from core recovery to reporting of gas content and composition. This is particularly important from the point of view of

outburst risk management and control as it decreases response time and reduces the risk of production delays being incurred whilst awaiting the results of gas content measurement.

Past studies by (Saghafi et al., 1998; SAA, 1999; Williams, 2002 and Danell et al., 2003) list potential errors associated with the direct method of gas content testing which include:

• Inaccurate estimation of gas lost during sample recovery, prior to sealing the coal sample into an air tight canister;

• Inaccurate measurement of liberated gas volume, both in the field and laboratory;

• Leakage of gas from desorption canisters;

• Loss of gas due to dissolution when in contact with water;

• Loss of gas during sample transfer between Q_2 and Q_3 testing;

• Inaccurate measurement of temperature and pressure variations during desorption resulting in inaccurate temperature and pressure correction being applied to liberated gas volume; and

• Partial pressure effects within sealed desorption canister impeding the rate of gas desorption.

2.3.1.5 Slow Desorption Method

The slow desorption method for gas content testing is not commonly used in the Australian coal mining industry however is a preferred method in the coalbed methane industry. As the name suggests the desorption test period can take many months and frequent desorbed gas volume measurement is required to achieve an accurate gas emission profile from which sorption time can be determined (Close and Erwin, 1989). Sorption time, considered an important factor in coalbed methane reservoir production modeling, is defined as the time taken for the coal sample to desorbs 63% of Q_M.

Given the partial pressure effect on gas desorption there is a potentially adverse impact on the rate of desorption resulting from sealing the desorption canister between desorption measurements. Although impacted by the frequency and time between desorption measurements the measured gas emission profile is likely to be somewhat lower than would be the case if the sample were allowed to freely desorb. The measuring apparatus described in the US Bureau of Mines modified direct method, referred to by Diamond and Schatzel (1998) and Schatzel and Garcia (1999), has the

potential to address this issue enabling more accurate recording of the rate of gas emission during gas desorption testing.

2.3.2 Indirect method of gas measurement

The most accurate measurement of gas content is achieved through direct measurement from bore core samples (Saghafi et al., 2008). Alternatively gas content may be estimated using an indirect method based on sorption isotherm data (Kim, 1977) or empirical relationships between Q_m and other measurable variables such as coal seam depth and coal rank (Diamond et al., 1976).

Sorption isotherms represent the maximum gas storage capacity of a coal sample at varying pressure and constant temperature. Based on knowledge of the isotherm for a particular coal type and details of the gas pressure, or an estimate of gas pressure based on knowledge of seam depth, the maximum gas content can be determined. However many coal seams are under saturated which, if not accounted for, may result in an over estimate of actual seam gas content (Diamond and Schatzel, 1998), Figure 2.3.3.

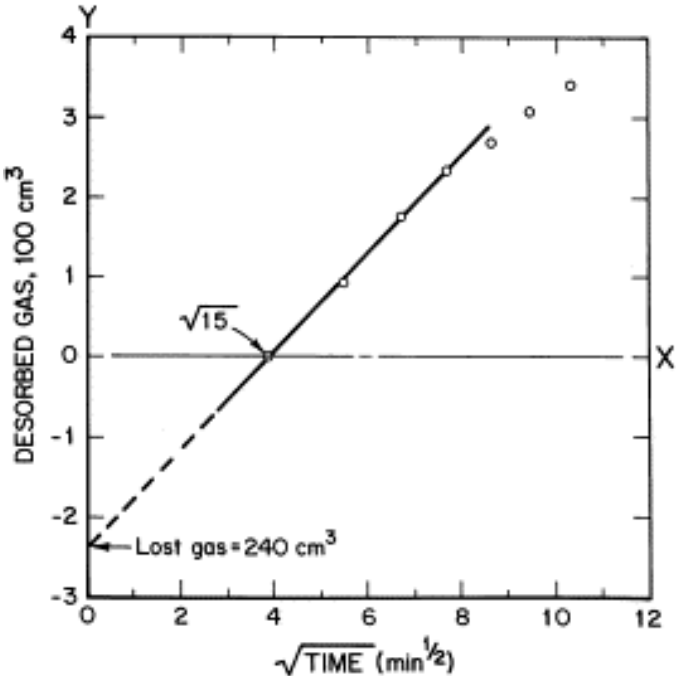

Figure 2.3.3 USBM method of determined the amount of gas lost during retrieval (Source: Diamond and Schatzel 1998)

A variety of potential errors are associated with the use of sorption isotherms to determine

gas content, which include:

• Isotherm data may not be representative of conditions at the sample location due to changes in coal seam gas composition and variable coal characteristics, such as moisture content, temperature, coal rank, and ash content;

• Lack of knowledge relating to degree of gas saturation in the coal seam and changes in gas content occurring naturally and due to the effects of mining and near and far field gas drainage;

• Inaccurate measurement or estimation of seam gas pressure at the sample location.

Gas content may also be estimated using an interpolation technique whereby the gas content value is calculated for the target location based on measured gas content results at neighboring locations (Saghafi et al., 2008).

The use of indirect methods to estimate gas content may be appropriate for use as a preliminary assessment tool for mine planning and gas reservoir assessment, however, given the potential for error, should not be used in detailed planning and economic decision making (Diamond and Schatzel, 1998).

2.4 Influence of mining activities on gas emission and migration

The gas recovered from mining working can be grouped under the term Coal Mine Methane (CMM). Three major drivers for CMM recovery are safety production, environment protection and the possibility to decrease significant quantities of methane emissions arising when coal mining activities are performed. Strong potential to utilize CMM for energy production is also required (Charlee et al., 2014).

Gas emissions in mining working ascend at two major stages. The first one is that gas is emitted as a direct result of the physical process of coal mining process. Currently the coal is mined through longwall mining in many underground coal mines, as with other sub-surface techniques, emits methane previously trapped within the coal beds and seams into the air supply of the mine as layers of the coal mine working face are removed, thus creating a potential safety loophole. The second stage is that gas emissions ascend from the collapse of the surrounding rock strata after a section of the coal seam has been mined and the artificial roof and wall supports are removed as mining process move to other sections. The debris resulting from the collapse is known as goaf and also emits gas (Noim et al., 2015).

Recovery techniques for CMM vary for each of the two stages of emissions. Firstly, gas released from the working face can be diluted and removed by large ventilation systems designed to move vast quantities of air through the mine. These ventilation systems dilute gas within the mine to concentrations below the explosive range of 5-15%, with an aim at gas concentrations under 1%. The ventilation systems move the diluted gas out of the working areas of the mine into shafts leading to the surface. The methane removed from working mines through this technique is known as Ventilation Air Methane (VAM). The VAM is released through the ventilation shafts and can then be destroyed or captured for utilization rather than allowing it to be released directly into the atmosphere, as may have occurred in the past. VAM has the lowest concentration levels of all forms of recoverable gas from coal seams because of its high exposure to air; often displaying levels of 0.05%-0.8%. Secondly, to pre-empt the release of goaf gas from post mining collapse, it is possible for vertical goaf wells to be drilled directly into the coal seam's surrounding strata before mining activities pass through that section. These pre-drilled wells can then remove the goaf gas once the collapse takes place, thus avoiding the release of gas directly into the mine. The goaf gas can then be destroyed or captured for utilization via the wells, rather than allowing it to be released directly into the atmosphere. As goaf gas is exposed to significantly lower volumes of air than VAM, it displays much higher gas concentration levels - typically between 35-75%.

2.4.1 Influence to goaf area

The goaf area resulting from coal mining is a critical area of concern for the mine ventilation system. Strata permeability is a key factor controlling gas emission into the mine working face (Ren and Edwards, 2000), along with production rates, extents of the panel, and the presence of rider coal seams in the surrounding strata (Guo et al., 2008). Two key changes within the goaf area occur as the longwall advances, disturbance to the surrounding strata and the release of overburden pressure (Kissell, 2006).

The first major change is the significant disturbance to the surrounding strata, as seen in Figure 2.4.1 and Figure 2.4.2. Researchers describe this disturbance in terms of four distinct deformation zones in the overburden (Singh and Kendorski, 1981). They are, in order of increasing height above the mined out coal, as follows: The first zone is the caving zone where

rocks from the overlying strata collapse into the void left from the mining activity (Kapp and Williams, 1972). It ranges from 5 to no more than 10 times the mining height; the next is a disturbed zone where sagging rocks exhibit bed separation, fracturing, and joint opening. This extends to a height approximately 15 to 40 times the mining height; above the region with bed separation, there is a zone with minimal disturbance; at the surface, there is a tensile fracture zone that can be up to 20 meters thick (Galvin, 1987).

The actual extent of each of these zones is variable and dependent upon the local geology (Forster and Enever, 1992). The importance of this upheaval is the accompanying increase in permeability. Researchers commonly cite permeability increases up to three orders of magnitude (Reid et al., 1996).

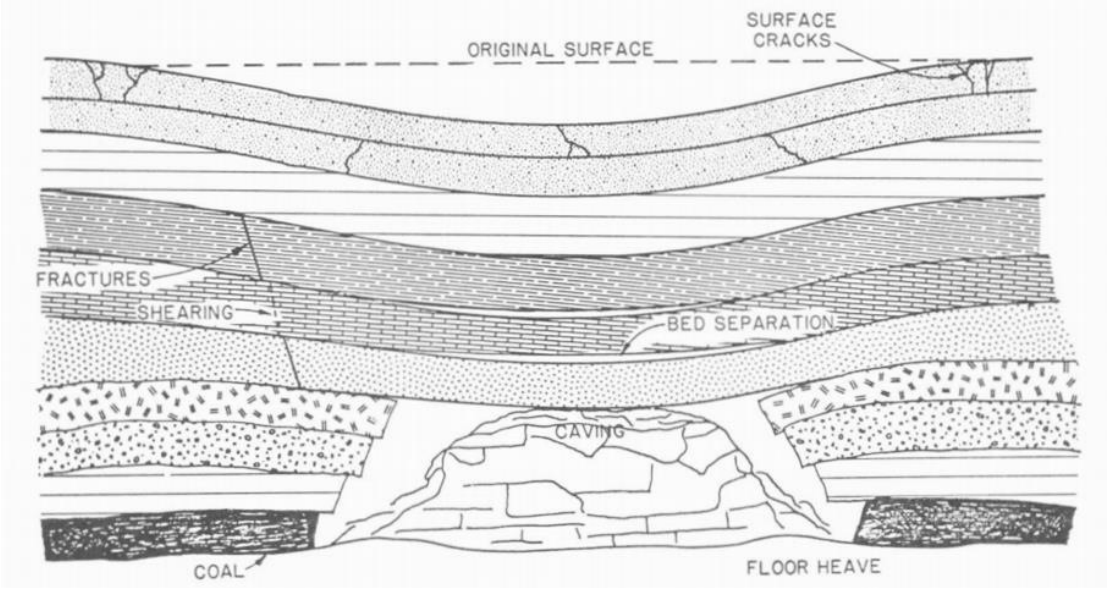

Figure 2.4.1 Expected strata disturbance and subsidence development as a result of coal extraction in a longwall panel (Source: Singh and Kendorski, 1983)

The second major change within the goaf area is the radical change in pore pressure experienced by the strata. The pressure from the overburden is relieved in the caved zone, and significantly lessened in the fractured zone (Zhang, 2005). This is then given a path to communicate with the atmosphere through the mine workings. The gas adsorbed onto the surface of the coal is now free to flow into the mine workings. The change in permeability within the mostly intact strata also comes into play as well as the relatively large fractures open pathways to the mine workings (Esterhuizen and Karacan, 2007). The extent of the area from which the gas emission develops can be seen in Figure 2.4.2. By these estimates, the majority of the gas comes

from within 20 meters of the floor and 60 meters of the roof.

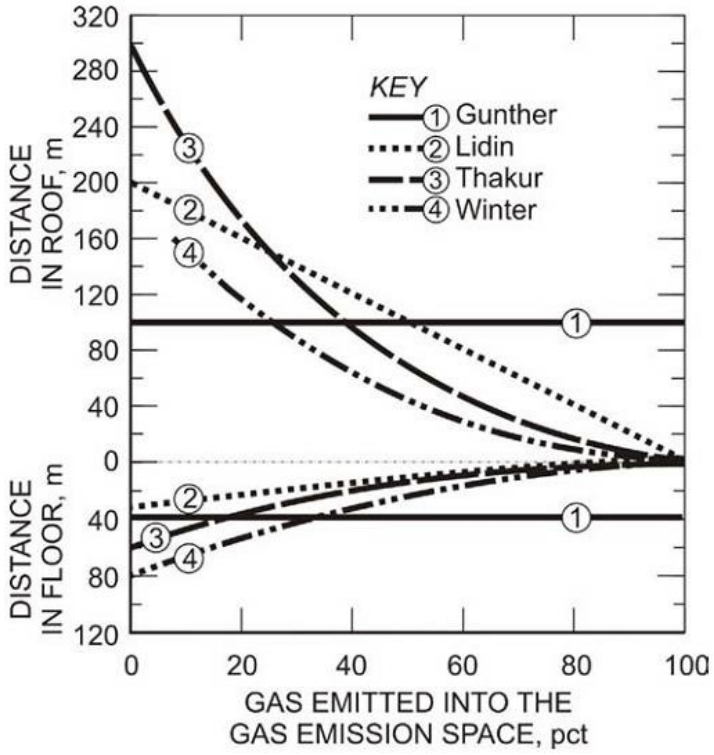

Figure 2.4.2 Extent of gas emission space within the goaf as presented by four different authors: Lidin, 1961; Thakur, 1981; Winter, 1975; and Gunther and Bélin, 1967 (Source: Kissell, 2006)

2.4.2 Influence to adjacent layers

Gas discharge involves various physical factors including the geological conditions, coal occurrence, mining technology and time, etc (Szlązak et al., 2014). The majority sources of coal strata gas, which can be directly discharged into the underground field, are deprived from coal seams (trapped in various surfaces of coal), porous sandstone, fracture networks, joints, faults, and gas pockets (dissociate gas). The amount of gas discharge is greatly influenced by various factors, including the degree of strata destruction, permeability of the coal seam, the scale and method of the mining activities, mine ventilation quantity, etc (Sander and Connell, 2014).

Mining activities disturb existing stress equilibration in the rock mass and create variations to the structural attribute of the affected strata (Wang and Cheng, 2012). The fracture process zones are opened and developed by existing and mining-induced fractures. A mass of gas discharge can be expected from the coal mining and strata of loose floor and roof (Masayuki, et al., 2011). The specific places where coal seam loose occurred are determined by multiple factors including

physical properties of seam system, the geometry of the longwall panel, the volume of the trapped gas sources, and the destructive condition of the relaxed zone (Bartłomiej et al., 2014). Figure 2.4.3 shows the sources of gas emission from different parts of coal mine.

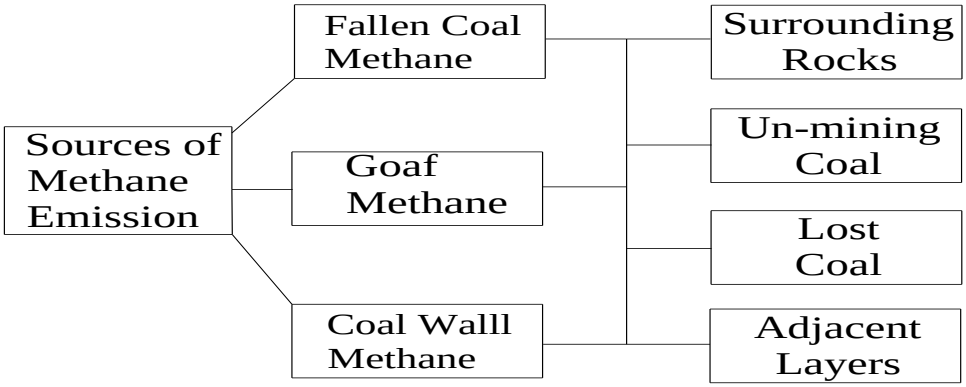

Figure 2.4.3 Sources of gas emission

As a matter of fact, the highest gas emission deprives from working face and goaf since it constantly and alternately destruction and re-compaction. Therefore, the most effective and accurate gas drainage borehole can be expected to pave in this zone (Alireza et al., 2014). Mining strata pressure and movement theory point out that the working face and goaf consists of three parts: coal wall support area, rock separation area and the re-compaction area (Steven et al., 2011).

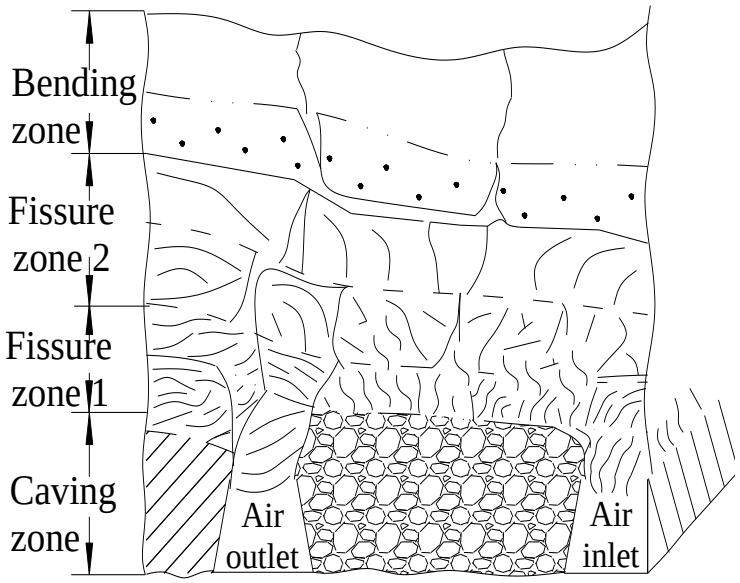

Figure 2.4.4 Gas sources from adjacent layers

The coal wall support area rapidly changes when the mining activities are performed. The re-compaction area has compacted completely; both of them are not in favor of gas drainage (Heather, 2011). Rock separation area where exists an amount of fracture space is the ideal and effective gas drainage zone. Similarly, rock stratum from top to bottom is divided into 3 parts: caving zone, fracture zone and bending subsidence zone (Figure 2.4.4). As a matter of fact, it is extremely difficult to excavate gas drainage borehole in both caving zone and bending subsidence zone. Fracture zone where exists a mass of fissuring area obviously is the more reasonable and effective gas drainage zone (Hao et al., 2012).

2.5 Mine ventilation

Mine ventilation systems are critical components of an overall system to effectively remove methane from mine workings. A mine ventilation system is designed to achieve three objectives. The first one is deliver breathable fresh air to the workers, the second one is control mine air temperature and humidity, and the last one is effectively dilute or removes hazardous gases and airborne reparable dust. Improvements to gas drainage systems can often provide a more rapid and cost-effective solution to mine gas problems than simply increasing the mine's air supply.

2.5.1 History of mine ventilation

Observations of the movements of air in underground passages have a long and fascinating history. Between 4000 and 1200 BC, European miners dug tunnels into chalk deposits searching for flint. Archaeological investigations at Grimes Graves in the south of England have shown that these early flint miners built brushwood fires at the working faces-presumably to weaken the rock. The Laurium silver mines of Greece, operating in 600 BC, have layouts which reveal that the Greek miners were conscious of the need for a connected ventilating circuit. At least two airways served each major section of the mine and there is evidence that divided shafts were used to provide separate air intake and return connections to the surface. Underground mines of the Roman Empire often had twin shafts, and Pliny (AD 23-79) describes how slaves used palm fronds to waft air along tunnels (McPherson, 1993).

Although metal mines were worked in Europe during the first 1500 years anno Domini, there

remain few documented descriptions of their operations. Georgius Agricola (1950) was well aware of the dangers of “blackdamp”, air that has suffered from a reduction in oxygen content-'miners are sometimes killed by the pestilential air that they breathe'-and of the explosive power of 'firedamp', a mixture of methane and air-likened to the fiery blast of a dragon's breath’. De Re Metallica was translated into English in 1912 by Herbert C. Hoover and his wife, Lou.

From the seventeenth century onwards, papers began to be presented to the Royal Society of the United Kingdom on the explosive and poisonous nature of mine atmospheres. The Industrial Revolution brought a rapid increase in the demand for coal. Conditions in many coal mines were quite horrific for the men, women, and children who were employed in them during the eighteenth and nineteenth centuries. Ventilation was induced either by purely natural effects, stagnating when air temperatures on the surface and underground were near equal, or by fire. The first ventilating furnaces of that era were built on surface but it was soon realized that burning coals suspended in a wire basket within the upcast shaft gave improved ventilation (McPherson, 1993).

The years around the turn of the century saw working conditions in mines coming under legislative control. Persons responsible for underground mining operations were required to obtain minimum statutory qualifications. Mine manager's examination papers concentrated heavily on ventilation matters until well into the twentieth century. The 1920s saw further accelerated research in several countries. Improved instrumentation allowed organized ventilation surveys to be carried out to measure airflow and pressure drops for the purposes of ventilation planning, although there was no practical means of predicting airflow in other than simple circuits at that time. Atkinson's theory was confirmed in practice. The first successful axial fans were introduced in about 1930. In 1943, Professor F. B. Hinsley (1967) produced another classical paper advancing understanding of the behavior of airflow by using thermodynamic analyses. Hinsley also supervised the work at Nottingham University that led to the practical use of analogue computers in 1952 to facilitate ventilation planning. This technique was employed widely and successfully for over a decade. The development of ventilation network analysis programs for digital computers in the early 1960s rendered the analogue devices obsolete. Initially, the network programs were written for, and required the power of, mainframe computers. These were employed throughout the 1970s. However, the 1980s saw a shift to desk-top computers and corresponding programs were developed. This is now the dominant method used for ventilation

planning (McPherson, 1993).

2.5.2 Mine ventilation challenges

Ventilation is the primary means of diluting and dispersing hazardous gases in underground mine roadways. Air velocities and quantities are optimized to ensure dilution of gas, dust, and heat. The greater the fresh air quantity supplied to the coalface, the greater the inflow of gas that can be diluted. This dilution process is inherently limited by air availability within the mine and maximum tolerable air velocities (Guang et al., 2015).

Ventilation pressure is proportional to the square of the airflow volume. A modest rise in air quantity therefore requires a significant increase in pressure, which leads to greater leakages across goaf and ventilation doors. Excessive leakage flows across the goaf may also increase spontaneous combustion risks and can impair gas drainage systems. The volume of air required to ventilate the underground workings and the permissible level of pollutants is often mandated by local government agencies (Javier et al., 2015).

A ventilation system that is designed simply to comply with legal minimum airflows or air velocities may be inadequate for the purpose of maintaining a safe and satisfactory environment in an active mine. For this reason, ventilation system design specifications must take into account the expected worst-case pollutant levels.

Methane is considered the principal pollutant and the most hazardous gas for ventilation system specifications. If the selected ventilation system design is capable of removing or satisfactorily controlling the primary pollutant, it is assumed that the lesser pollutants will be adequately controlled or removed at the same time (Ni et al., 2011).

Ventilation requirements are dynamic. Ventilation air demand increases as a mine is developed and the area being ventilated increases, sometimes requiring installation of additional ventilation shafts, upgrading fans, or enlarging existing airways.

Usually ventilation methane is handled in one of two ways. First, they may be allowed to enter the mine air stream where sufficient air is available to dilute the maximum expected gas flows in the airways to safe concentrations (Figure 2.5.1).

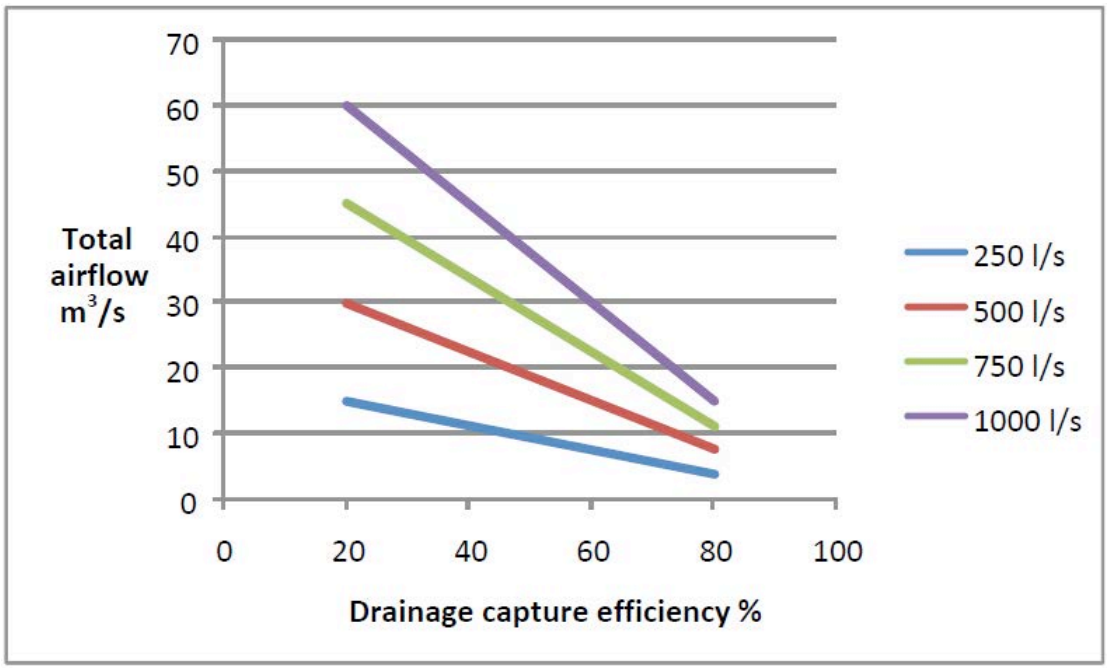

Figure 2.5.1 Airflows required for diluting longwall methane emissions to 2%, allowing for peaks

Secondly, where permitted by local spontaneous combustion propensity or local strata behavior, some portion of the gas may be diverted into a bleeder road behind the face, or across old goaf, to discharge into main returns or at bleeder shafts (Szlązak et al., 2014).

A small change in air volume transported by the mine ventilation system requires a much larger change in power consumption and hence ventilation cost. The ventilation system power requirement, which is one of the most important operating costs at a mine, is proportional to the air volume flow cubed (Figure 2.5.2). Therefore, introducing gas drainage or increasing its effectiveness often represents lower-cost option than increasing ventilation air volumes, which might also involve major infrastructure development in the mine (Arnab et al., 2015).

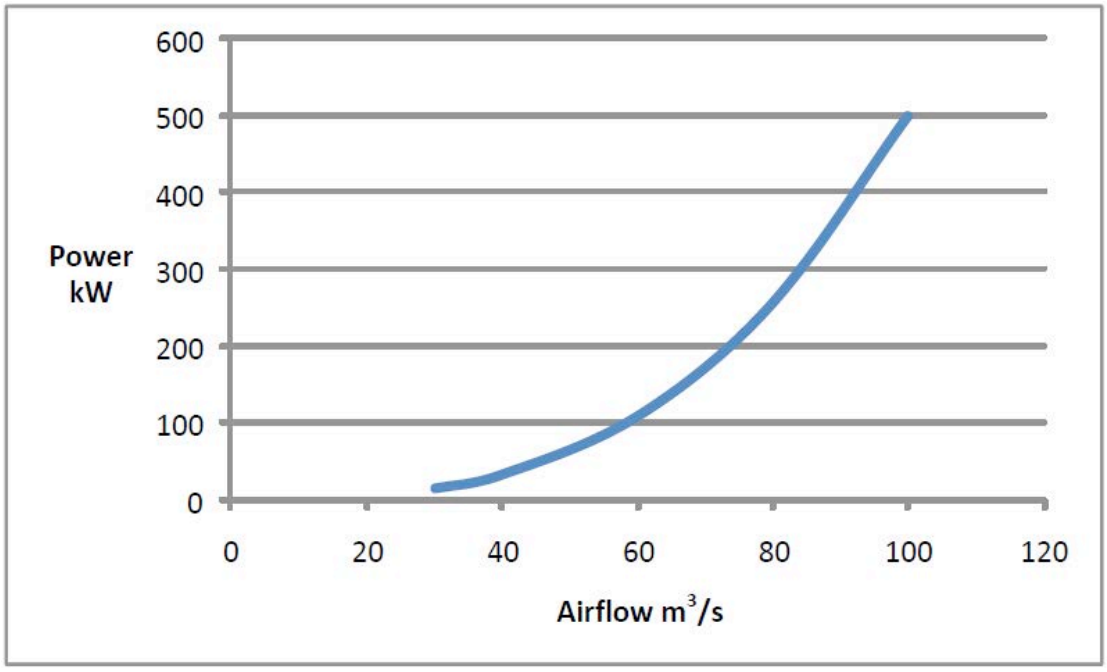

Figure 2.5.2 Example of ventilation air power requirement versus airflow

Distribution control includes redirecting airflow to one location at the expense of other airflows. The relationship between aerodynamic resistance, air pressure, and rate of airflow is well known, and can be used to predict the outcome of airflow redistributions (Hu et al., 2003).

Overall control of the mine ventilation system is directed primarily by the surface fan(s). Increasing the differential surface fan pressure applied at a mine may have only negligible effect on airflows in the most remote parts of the mine. For this reason, increasing surface fan pressure may not solve a problem of shortfall in ventilating airflows in remote working areas. Strata pressures may cause the roof, ribs, and floor converges, which causes increased airflow; therefore, roadways must be maintained to facilitate efficient ventilation as designed (Parra et al., 2006). Continuously controlling and adjusting the main fan is not advisable. A relatively constant airflow underground minimizes the risk of spontaneous combustion and assists in monitoring airflows and pollutant levels. Where a mine is served by a redundantly designed surface fan system (one or more fans running, and one or more fans on standby), using a fan changeover facility is preferable to ensure that mine airflows are not interrupted when the surface fans are stopped for routine maintenance or inspection (Stefopoulos and Damigos, 2007).

2.5.3 Ventilation safety technologies

Grubb (2008) studied the efficacy and cost effectiveness of the technologies and techniques available to mines to reduce the risk of spontaneous combustion in underground coal mines. These preventative measures can be classified in seven groups. The first one is understanding the spontaneous combustion behavior of the coal seam mined; the second one is detection and monitoring systems; the next one is pressure differential management; the fourth one is sealing and inertization, the following one is inhibitors and sealants; the sixth one is extinguishment planning; and the last one is other preventative measures (Grubb, 2008). The measures were analyzed using a financial model based on a western U.S. coal mine; measures that resulted in a mine with negative net present value, and measures that had not demonstrated the ability to reduce risk were eliminated. The final recommendations included the use of real time monitoring of gas concentrations using a tube bundle system, and the progressive sealing and inertization of longwall panels (Grubb, 2008).

There are a variety of mechanisms available for diverting methane found in coal seams before it reaches the ventilation system. This includes horizontal in-seam boreholes, in-mine vertical boreholes, vertical hydro-fracked wells, and vertical small-radius boreholes drilled from the surface (Kissel, 2006). These vertical small-radius boreholes are also referred to as gob vent boreholes (GVBs). Figure 2.5.3 depicts the installation of a goaf vent borehole system, and its interaction with the longwall mine, goaf, and overlying strata (Hartman et al., 1997).

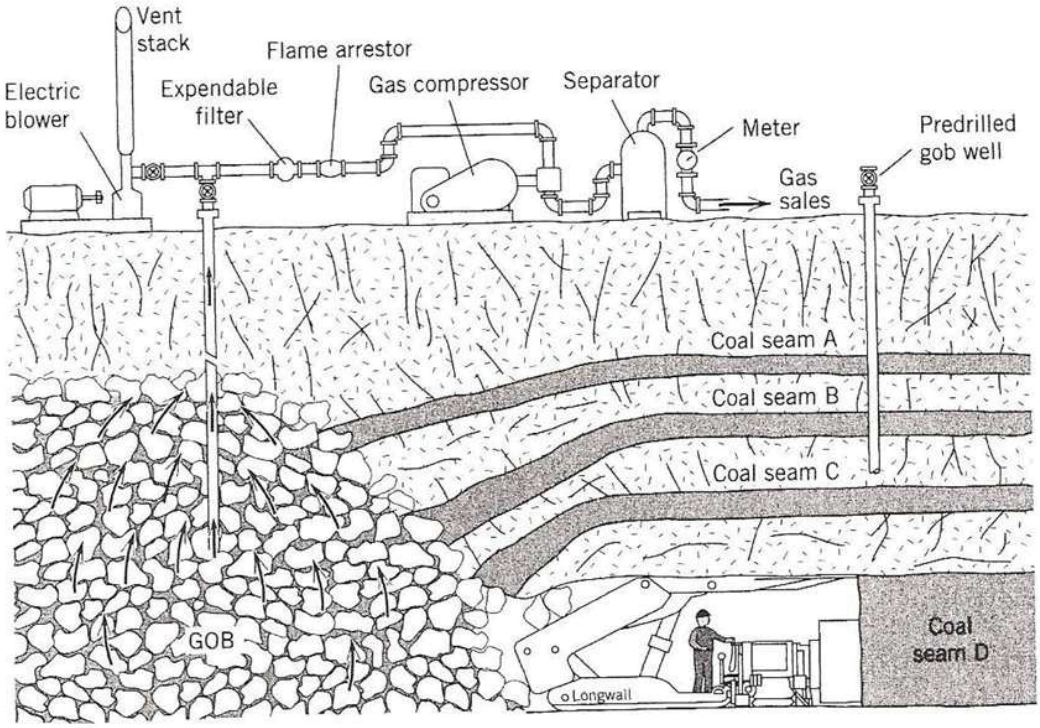

Figure 2.5.3 Cross-sectional diagram of Goaf vent borehole (Hartman et al., 1997)

2.6 Mine gas distribution and migration rule

2.6.1 The significance of mine gas distribution and migration rule study

With the decrease of conventional energy resources, most researches are focused on unconventional ones. Shale gas has been deemed as an important substitute due to its abundant reserves. Hydraulic fractures are the predominant source of porosity and permeability in shale (Mohaghegh, 2013), therefore, multi-fractured horizontal well is an effective technology.

Natural porous media usually have extremely pore structure with pore sizes extended over several orders of magnitude (Cai et al., 2012). Shale gas exists in various forms (free gas, adsorbed gas, dissolved gas) in the nanoscale pores. In the shale with abundant organics, the content of kerogen and organic matter arrives at 40% (Passey et al., 2010). The adsorbed gas coexists with dissolved gas which cannot be neglected in the organics (Chalmers and Bustin, 2007; Ross and Bustin, 2009; Clarkson and Bustin, 2011). Appreciable quantity of gas diffusing from kerogen in shale statistically shows that a significant amount of gas exists in kerogen (Javadpour et al., 2007; Javadpour, 2009). The amount of desorbed gas is close to that of diffused gas from

kerogen (Swami and Settari, 2012). Thus, the gas obtained from canister test probably contains free gas, adsorbed gas, and dissolved gas from kerogen that is in large amount due to the high original formation pressure. However, most present mathematical models of shale gas reservoir are focused on the adsorbed gas on the wall of matrix pores and free gas in the matrix but without considering the dissolved gas diffusion which needs to be added to achieve a more accurate model conforming to actual production.

Porosity and permeability of the consolidated shale matrix are so low that Darcy flow equation is impossible to precisely describe the gas migration law because the gas migration in it contains multiple mechanisms (viscous flow, slip flow, transition flow, Knudsen diffusion and adsorbed gas desorption). The transport of gas follows multi-mechanistic mechanism triggered by pressure and concentration gradients (Thararoop et al., 2012). Javadpour (2009) and Ozkan et al. (2009) demonstrated that slippage effect and Knudsen diffusion are significant in the nano-pore of the shale. Ozkan and Raghavan (2010) presented a dual-porosity and dual permeability model considering the Knudsen diffusion in the nano-pore by modifying the Darcy flow in the natural matrix and fracture system. Nobakht et al. (2013) analyzed type curves of horizontal well with multiple fractures in shale gas reservoir. Zhao and Zhang (2012) and Sang et al. (2014) respectively proposed a percolation mathematical model considering adsorption and desorption of shale gas. Ezulike and Dehghanpour (2014) proposed a model for simultaneous matrix depletion into natural and hydraulic fracture network. Guo et al. (2013) put forward a numerical simulation method applicable to multi-mechanism flow. However, the present percolation models don't fully contain the effects of multi-mechanism migration and dissolved gas diffusion in kerogen, leading to a biased productivity prediction.

2.6.2 Previous studies of mine gas distribution and migration

Outburst of gas is a dynamic phenomenon occurring when gas is suddenly released through fissures and cavities or from tectonic fault zones when uncovered by boreholes or mining works. The outburst of coal and/or sandstone and clay stones and gas includes dynamic phenomena whose source is the elastic energy of coal, rock and gas. Due to the risk of gas outbursts, high emission of coal bed gases is a major problem in coal mining. Dynamic coal gas phenomena such

as the outflow of methane in coal seams, coal and gas gushes and Outburst of gas is a dynamic phenomenon occurring when gas is suddenly released through fissures and cavities or from tectonic fault zones when uncovered by boreholes or mining works. The outburst of coal and/or sandstone and clay stones and gas includes dynamic phenomena whose source is the elastic energy of coal, rock and gas. Due to the risk of gas outbursts, high emission of coal bed gases is a major problem in coal mining. Dynamic coal gas phenomena such as the outflow of methane in coal seams, coal and gas gushes and Coal Mine has an average coal gas mixture of approximately $CO_2 : CH_4 \geq 2:1$(Zavšek, 2004), where a high proportion of carbon dioxide is adsorbed on the lignite structure or is captured in the coal matrix, while methane is mostly present free in coal fractures. The CO_2:CH_4 ratio changes in advance of the working face (Kanduč et al., 2011). When the advance rate of the longwall face is slow (less than 2m/day), better opportunities exist for the slow escape of the gases under high pressure in the virgin coal. However, at the faster rates of advance of the coal face now implemented, less time is available for the equalization of gas pressure and mining-induced stresses. Yet, some doubt still exists as to whether outbursts are actually 'triggered' by gas pressures or by stresses induced in the rock itself during mining operations (Smith and Gould, 1980; Zhang et al., 2007). Gas outbursts are associated not only with methane gas, but also with carbon dioxide, which is the case in the Velenje Basin (Zavšek, 2004). When an outburst occurs, the rock/coal/gas system transforms from a stable to an unstable state, with the release of a significant volume of gas over the duration of the outburst. Outbursts involving CO_2 are more violent, more difficult to control and more dangerous because of the greater sorption capacity for carbon dioxide (Lama and Saghafi, 2002). Previous studies on Velenje lignite showed that fine-detrital gelified varieties are especially critical in the case of outbursts; on the other hand, xylite-rich lignite is more stable and is mostly not liable to the occurrence of gas outbursts. Critical zones are contacts between fine-detrital lignite and xylite-rich lignite where coalbed gas can be emitted easily, a process which is caused by the different amounts of gas in these locations (Zavšek, 2004).

An improved understanding of the geochemical processes that control the occurrence and composition of coalbed gas provides an important contribution not only to remediation of potential environmental or mining hazards, but also for exploration and development strategies for

utilizing coalbed gas as an energy resource (Clayton, 1998). The stable carbon isotopes of coalbed methane are usually applied for the identification of its genesis (Guoyi et al., 2007). There are three main sources of hydrocarbon gases and CO_2 in sedimentary basins: biogenic, microbial and thermogenic (Rice, 1993). In general, thermogenic gases are typically associated with high rank coal, whereas microbial gases are typically associated with low rank coal. It was found that thermal generation of hydrocarbon gases in sedimentary systems such as Western Canadian sedimentary basin show that low temperature thermal generation of non-methane hydrocarbons occurs at temperatures lower than 62 °C and possibly as low as 20 °C (Rowe and Muehlenbachs, 1999). To provide a better characterization of the origin and volume of thermogenic gas generation from coals, hydrous pyrolysis experiments have been conducted at 360 °C for 72 h on Polish coals ranging in rank from lignite (0.3% Rr) to semi anthracite (2.0% Rr) (Kotarba and Lewan, 2004). The thermogenic gases generated in the experiments were considered to be similar to those generated during natural coalification. Kotarba and Lewan, 2004 found that significant quantities of CO_2 are generated from coals during thermal maturation as simulated by hydrous pyrolysis. At a vitrinite reflectance of 1.7% Rr, more than 90% of the maximum potential of a coal to generate CO_2 was expended. Assuming that these quantities of generated CO_2 with a sourcing coal bed as uplift or erosion provide conditions conducive for microbial methanogenesis, the resulting quantities of microbial methane generated by complete CO_2 reduction could exceed the quantities of thermogenic methane generated from same coal bed by a factor of 2-5. The origin of natural gases associated with oil and condensate accumulations within the Middle Cambrian sandstone reservoir of the Polish and Lithuanian Baltic Basin was characterized by means of its molecular composition, the stable carbon isotope composition of methane, ethane, propane butanes, pentanes and carbon dioxide, the stable hydrogen isotopes of methane and stable nitrogen isotopes of gaseous nitrogen (Kotarba and Lewan, 2013). Carbon dioxide of natural gases is generated during thermogenic processes and gaseous nitrogen generally originates during the thermal transformation of organic matter and from NH_4-rich illites of clayey faces of the Lower Palaeozoic strata. In spite of losses due to reactions and solution during migration and entrapment, the $\delta^{13}C$ values of the pyrolysis CO_2 are within the same range as the CO_2 in the natural gases. Abiogenic sources of gas are typically found in deep subsurface (Sherwood Lollar et al., 2006).

Primary thermogenic gases have a methane carbon isotope composition higher than −50‰ (Golding et al., 2013). Because production gases from many CBM and some shale gas fields are relatively dry, the ratio of methane to the sum of ethane and propane ($C_1/C_2 + C_3$)) is widely used to distinguish between microbial and thermogenic gases. Ratios greater than 1000 and less than 100 (wet gases commonly associated with oil tend to show$C_1/ (C_2+C_3) < 50$) are considered to be characteristic of microbial and thermogenic gas, respectively, when used in combination with the methane carbon isotope composition (Flores et al., 2008). Two pathways have been identified for the generation of biogenic gas: carbon dioxide reduction and methyl-type fermentation (Jenden and Kaplan, 1986). A detailed review of coalbed methane was given in Moore, 2012 and the references therein. The stable isotopes of CH_4, CO_2 and H_2O have been used in different studies to distinguish the pathways of microbial methane generation (i.e. acetate fermentation versus CO_2 reduction) (Flores et al., 2008).

Carbonate rock, clastic rock, the coal seam and magmatic rock are the main CO_2 reservoirs; solubility trapping by the formation of water sinks and free-state saving are the dominant forms of CO_2 in the rock layer (Gilfillan et al., 2009). Natural analogue studies of CO_2 occurring in the subsurface have the potential to yield insights into the mechanisms of CO_2 storage over geological time scales and therefore the sources and distribution of gases in lignite represent the basis for understanding coalbed gas behavior. Most CO_2 is adsorbed on the surface of the micro porous coal matrix. The critical point where CO_2 enters the supercritical phase is defined at 31.1 °C and 7.38 MPa, which is within the range of known reservoir conditions and can be achieved at a depth of only 756munder hydrostatic pressure (Li et al., 2013). Sequestration of CO_2 in deep un-mined coal beds is one of the more promising of several methods of geological sequestration that are currently being investigated (Busch et al., 2004). In this respect coal samples from Miocene lignite deposits in Belchatow, Adamow, Konin and Turow (Poland) were analyzed to determine the relationships between coal properties and gas capacity (Macuda et al., 2011). Samples of coals from several coalbeds in Indiana were analyzed for CO_2 and CH4 sorption capacity using a high-pressure adsorption isotherm technique (Mastalerz et al., 2004). Numerical modeling of the processes of CO_2 storage in coal and enhanced coalbed methane (ECBM) production requires information on the kinetics of adsorption and desorption processes. In order to address this issue, the sorption kinetics of CO_2 and CH4 were studied on a high volatile bituminous Pennsylvanian (Upper

Carboniferous) coal (VRr = 0.68%) from the Upper Silesian Basin of Poland in the dry and moisture-equilibrated states (Busch et al., 2004).

2.7 Previous simulation studies

Safety mining technologies including field investigation (Bruneau et al., 2003; Johanna and Maria, 2009; Claus et al., 2010; Ginting et al., 2013; Plante et al., 2014), numerical simulation (René et al., 2001; Molson et al., 2005; Xue et al., 2006; Manoj et al., 2012; Arif et al., 2013) and laboratory experiments (Evangelos et al., 2008; Joaquimet al., 2008; Haoran et al., 2011; Liu et al., 2011; Packham et al., 2012; Zhang et al., 2015) have also been improved over the past decade. However, even if the size (height) of the gas emission zone can be estimated globally using various methods or assumptions, it is not uncommon that gas emission predictions may be under- or over-estimated due to the lack of sufficient spatial information defining the quantity and location of the gas sources in the overlying strata (Jundika, et al., 2014). Therefore, multiple research and experiment of gas control strategies should be developed, including optimizing the ventilation network, preventing goaf spontaneous combustion, enhancing gas risk management, determining the gas emission zone, and implementing a reasonable gas drainage plan.

2.7.1 Previous numerical simulation studies

CFD is commonly accepted as referring to the broad topic embracing mathematics and numerical solution, by computational methods, of the governing equations which describe the motion of fluid flow, the set of the Navier-Stokes equations, continuity and any additional conservation equations, such as energy or species concentrations. Today CFD has grown from a mathematical curiosity to become an essential tool in almost every branch of fluid dynamics, from aerospace propulsion to weather prediction. The availability of robust commercial CFD codes and high speed computing has lead to the increasing use of CFD for the solution of fluid engineering problems across all industrial sectors and the mining industry is no exception.

CFD modeling has been used in the minerals industries in a number of areas. It has been used in the mining and energy environment since the 1990s, including methane and spontaneous heating control (Creedy and Clarke, 1992; Tauziede, Mouilleau and Bouet, 1993; Ren and

Edwards, 2000), dust control (Aziz, Srinivasa and Baafi, 1993; Sullivan and Heerden, 1993), diesel particulate emissions (Currie, 1994), mine fires and explosions (Woodburn and Britter, 1996), methane control (Jazbec et al., 2000), ventilation velocity in tunnel fires (Hwang and Edwards, 2005), methane emissions and goaf gas (Karacan et al, 2007), controlling longwall goaf heating (Ren and Balusu, 2009; Taraba and Michalec, 2011), and gas behaviors in auxiliary ventilation of mining headings (Torno et al, 2013) and mineral processing (Fletcher et al, 1995). Although some of these studies are at their early stages, results from these investigations have shown the potential of CFD as a powerful tool in solving many problems in which gases or fluids move through or around objects in the minerals industries.

Gas flow rule in coal mine is a complicated process due to numerous factors are involved, including ventilation system layout, gas content, emission rate and compositions, working face orientation and dip, gas buoyancy and goaf permeability. Lately, a large number of CFD models have been established to achieve further understanding of gas flow mechanics, characteristic and distribution rules in mine working face and goaf. A commercial CFD code called FLUENT contains broad physical modeling capabilities needed to model flow, turbulence, heat transfer, and reactions for industrial applications ranging from air flow over an aircraft wing to combustion in a furnace, from bubble columns to oil platforms, and from clean room design to waste water treatment plants.

In the past, mine ventilation systems have been successfully modeled using network based flow simulation programs such as MineVent, VentZroby and VnetPC (Karacan, 2009a). Work done using network type simulation by researchers in Poland (Dziurzynski & Wasilewski, 2012). More recently, Computational Fluid Dynamics (CFD) has been used to further study ventilation in underground longwall mines. CFD has the advantage of allowing the user to model a larger range of geometries, and to solve for multiple flow regimes, chemical reactions, and species mixing. Work by Wala et al. (1997) showed that CFD can accurately model the main airways of a ventilation system by comparing computational results with experimental data. Further studies showed that CFD simulations could accurately duplicate experimental results of methane distribution in a longwall panel (Wala et al., 2007).

CFD models have been used to evaluate the mixing of gas with fresh ventilation air at the tailgate corner. This research was able to model the formation of explosive gas mixtures as

methane is released from the tailgate shields. Further analysis yielded the conclusion that caving of the immediate tailgate entry can create 'acute explosion hazard' and that methane sensors located on the shearer body of longwall tailgate drive will not detect these explosive gas mixtures (Brune & Sapko, 2012).

CFD has also been used to model coal spontaneous combustion and heating in longwall goaf (Yuan, 2009; Yuan and Smith, 2008), including modeling the effect of longwall face advance on coal heating (Yuan, 2010). The impact of variable permeability within gobs, in particular the impact of lower permeability zones in the centers of goaf, has also been modeled using CFD (Yuan et al., 2006).

2.7.2 Previous laboratorial experimental studies

In recent years, the rules of gas distribution and movement in goaf area are simulated through both computer software and field trial around the world (Russell et al., 2011). Simulation is the imitation of the operation of a real-world process or system over time (Banks et al., 2001). It can be used when the real system cannot be engaged, because it may not be accessible, or it may be dangerous or unacceptable to engage, such as coal mine ventilation network and goaf area (Sokolowski & Banks., 2009). The act of simulating a ventilation network and goaf area first requires that a model be developed; this model represents the key characteristics, behaviors or functions of the selected physical, abstract system or process. The model represents the system itself, whereas the simulation represents the operation of the system over time. The principles of gas distribution and migration in goaf area can be intuitively observed and understood when the simulation experiments are performed.

There are many studies (Table 2.7.1, Table 2.7.2, Table 2.7.3, Table 2.7.4, Table 2.7.5 and Table 2.7.6) that have taken experimental measurements of gas flow in coal mines, both to establish methane emission rates and to better understand how gas flows in underground coal mines (Ramurthy et al., 2003; Esterhuizen and Karacan 2005; Esterhuizen and Karacan 2007; Karacan, 2009c; Wachel, 2012).

Table 2.7.1 Permeability values of coal seams and overburden study (Ramurthy et al., 2003)

Layer described	Permeability (md)	Permeability (Darcy)	Permeability (m^2)	Resistance ($1/m^2$)
Coal seam	4.5	4.50E-03	4.44E-15	2.25E+14
Pictured cliffs	1.5	1.50E-03	1.48E-15	6.75+14

Table 2.7.2 Permeability values of coal seams and overburden study (Esterhuizen and Karacan 2005)

Layer described	Permeability (md)	Permeability (Darcy)	Permeability (m^2)	Resistance ($1/m^2$)
Working face cleat	4	4.00E-03	3.95E-15	2.53E+14
Coal butt cleat	1	1.00E-03	9.87E-16	1.10E+15
Moderate Shale	1	1.00E-03	9.87E-16	1.10E+15

Table 2.7.3 Permeability values of coal seams and overburden study (Esterhuizen and Karacan 2007)

Layer described	Permeability (md)	Permeability (Darcy)	Permeability (m^2)	Resistance ($1/m^2$)
Max perm	1.00E+06	1.00E+03	9.87E-10	1.01E+09
Max perm	1.00E+05	1.00E+02	9.87E-11	1.01E+10
Max perm	5.00E+05	5.00E+02	4.93E-10	2.03E+09

Table 2.7.4 Permeability values of coal seams and overburden study (Karacan, 2009b)

Layer described	Permeability (md)	Permeability (Darcy)	Permeability (m^2)	Resistance ($1/m^2$)
upper adjacent layer	100	1.00E-01	9.87E-14	1.01E+13
upper adjacent layer	1000	1.00E+00	9.87E-13	1.01E+12

Table 2.7.5 Permeability values of coal seams and overburden study (Wachel, 2012)

Layer described	Permeability	Permeability	Permeability	Resistance ($1/m^2$)

	(md)	(Darcy)	(m^2)	
Coal seam roof	4.907E+01	4.91E-02	4.84E-14	2.07E+13
Fractured zrea	2.937E-01	2.94E-04	2.90E-16	3.45E+15
Goaf area	2.026E+08	2.03E+05	2.00E-07	5.00E+06

Table 2.7.6 Permeability values used in modeling longwall panels

	Goaf permeability (md)		Goaf permeability (m^2)		Goaf resistance ($1/m^2$)	
	High	Low	High	Low	High	Low
(Esterhuizen & Karacan, 2007)	1.00E+06	1.00E+05	9.87E-10	9.87E-11	1.01E+10	1.01E+09
(Lolon, 2008)	4.70E+08	8.00E+06	4.64E-07	7.90E-09	2.16E+06	1.27E+08
Yuan and Simith (2008)	1.25E+05	3.00E+03	1.24E-10	2.96E-12	8.09E+09	3.38E+11
Wachel (2012)	2.03E+10	2.03E+09	2.00E-05	2.00E-07	5.00E+04	5.00E+06

Experimental results for methane flow across the face of an active panel have been made in the Pittsburgh Coalbed (Schatzel et al., 2006). Schatzel et al. (2006) measured the volumetric flow rate of methane at different points along the length of a longwall panel to predict methane emission rates in mines with widening panels. The measurements demonstrated an increase in gas emissions over the width of the panel, but also variation within the location of the mine and between different cutting directions.

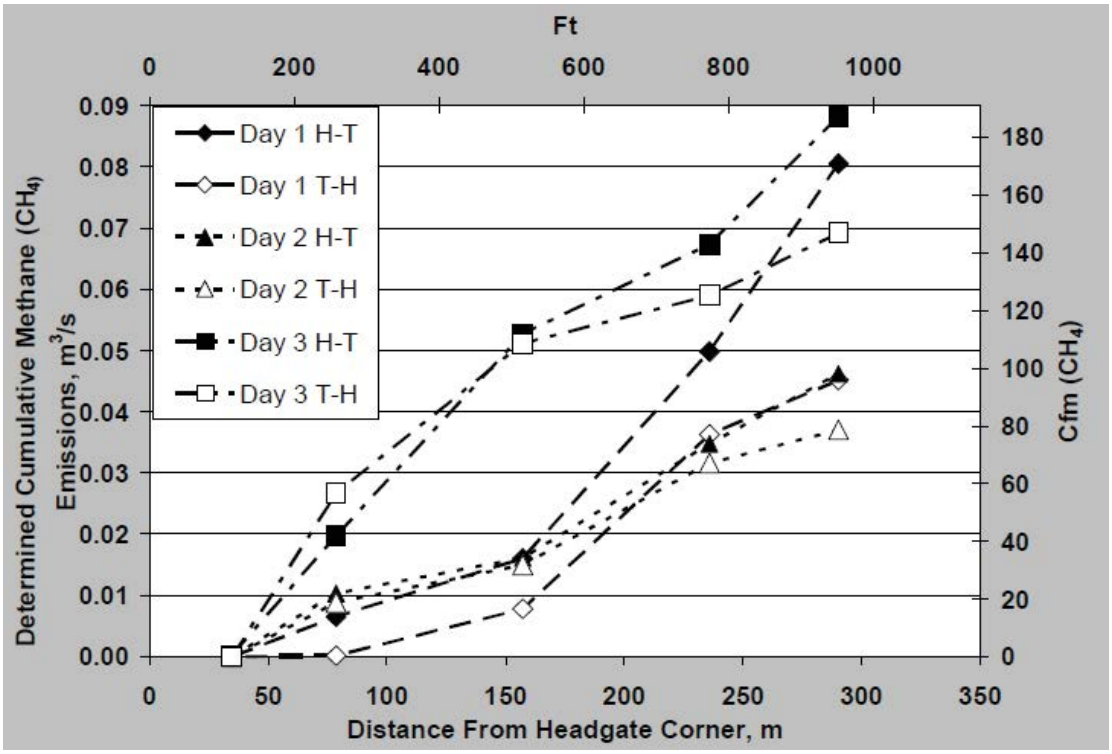

Figure 2.7.1 Cumulative longwall face methane emissions for three days of monitoring, showing the face section end points (Schatzel et al., 2006).

The first observation, demonstrated in Figure 2.7.1 illustrates the importance of modeling Goaf Vent Boreholes (GVBs) and other structural differences within the panel. The locations of the measurements on different days are shown in Figure 2.7.2.

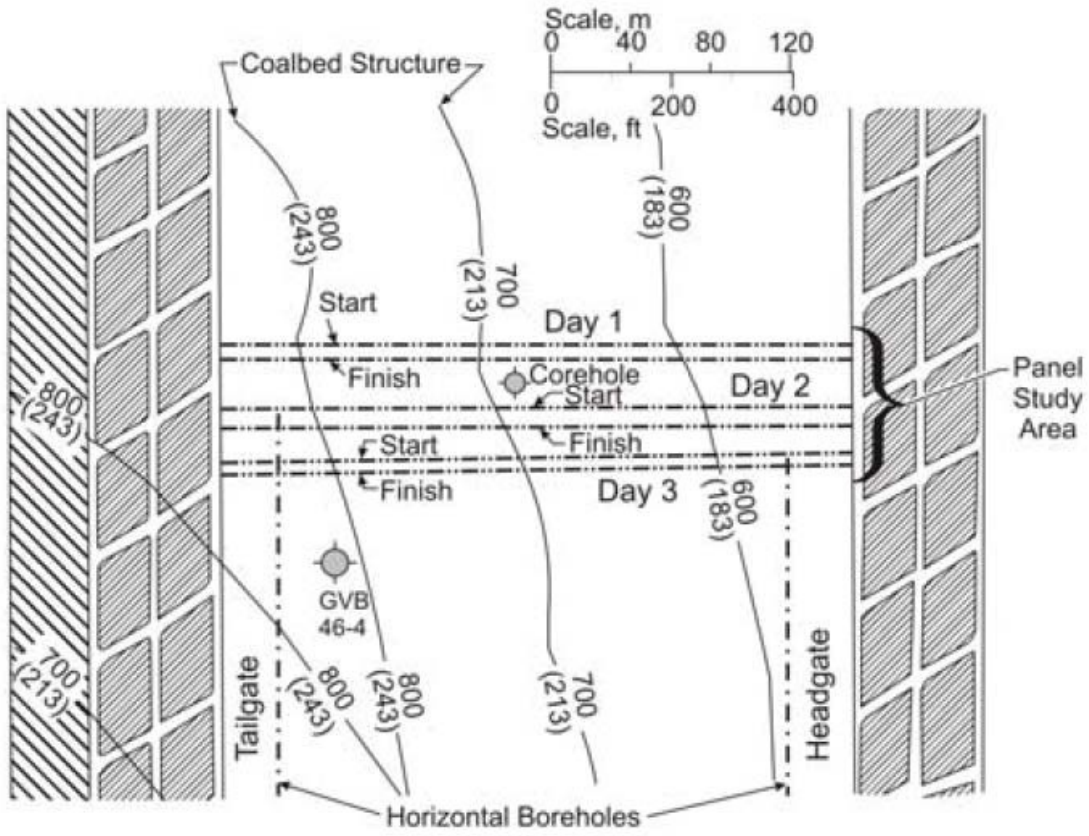

Figure 2.7.2 Location of the three monitoring days (Schatzel et al., 2006)

The second observation that the direction of the cutting method affects the quantity of methane observed at the tailgate can be seen in Figure 2.7.3, could be of great use in validating a model of an active longwall panel. One critical component of this modeling effort will be to establish a source term related to the cutting of fresh coal. Care must be taken, however, as the coal properties in the Pittsburgh Seam are different than the Western coal seams encountered in this research.

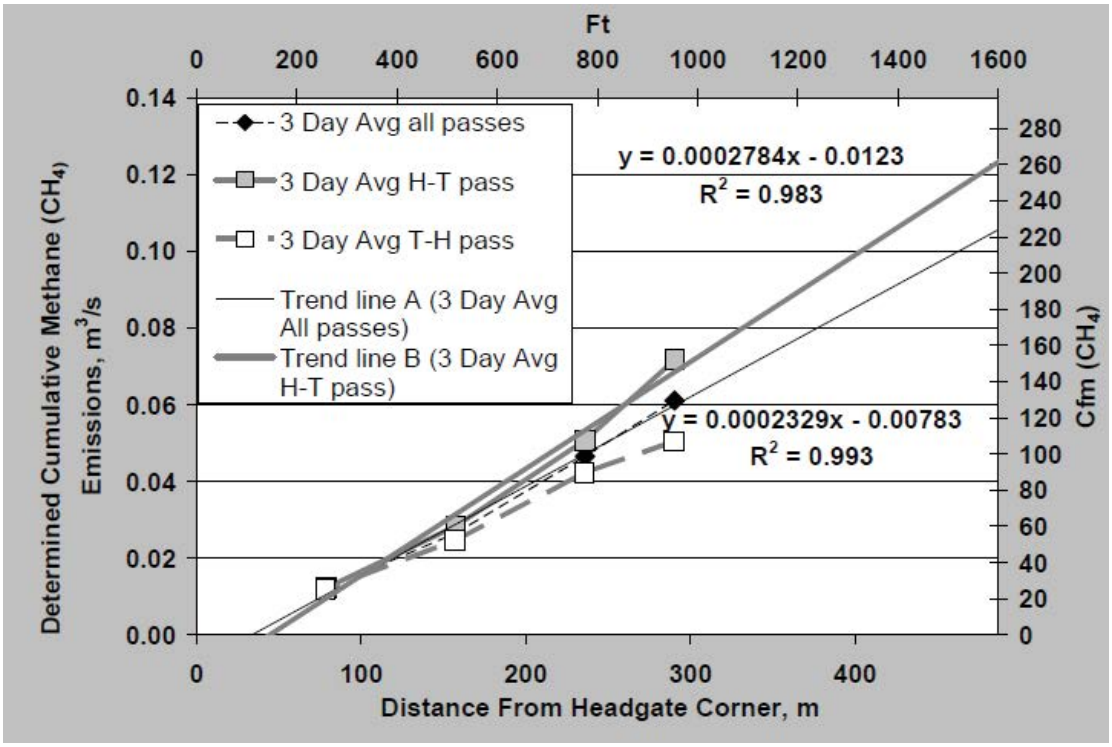

Figure 2.7.3 Gas emissions as a function of distance from head gate corner (Schatzel et al., 2006).

Diamond et al., in their 1999 paper (Diamond et al., 1999) performed a detailed experiment by injecting tracer gas into an inactive Gob Vent Borehole (GVB) in an active coal panel and into the ventilation system directly. It is important to note that this was in an Eastern coal mine and the mine utilized a bleedered ventilation system. One of the more important observations of the study is that tracer gas released directly into the ventilation system stayed almost exclusively in the ventilation system (with a maximum of 0.7% reaching producing GVBs), and that gas released into the gob via an injecting GVB tended to stay in the goaf as long as the producing GVBs stayed active. In addition, the speed in which the tracer gas reached the producing GVBs indicates a relatively high permeability flow path between these two points in the goaf (Figure 2.7.4).

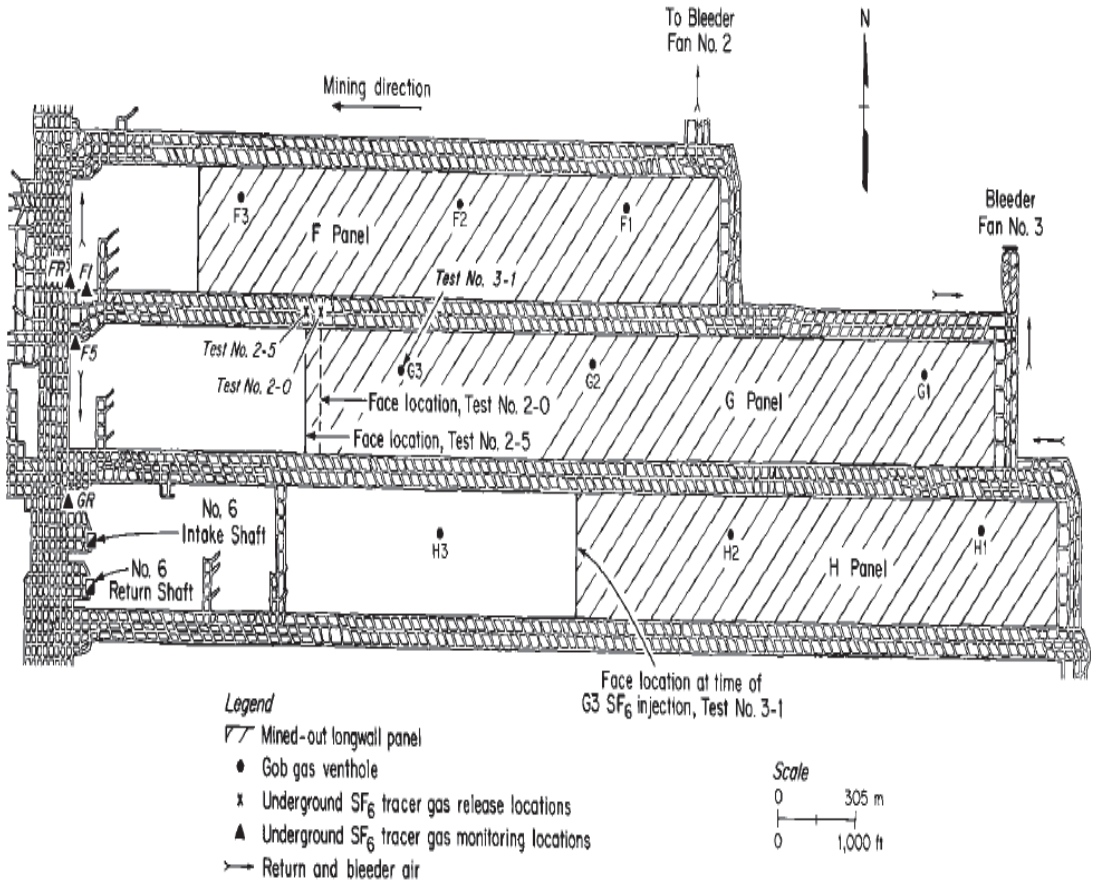

Figure 2.7.4 Location of injection points for goaf tracer gas test (Diamond et al., 1999).

In addition to these observations, the test generated data that could be used in the future for further model validation. Attempts could be made to match the modeled arrival and quantity of tracer gas with the experimental results. This would help further contribute to the understanding of goaf permeability.

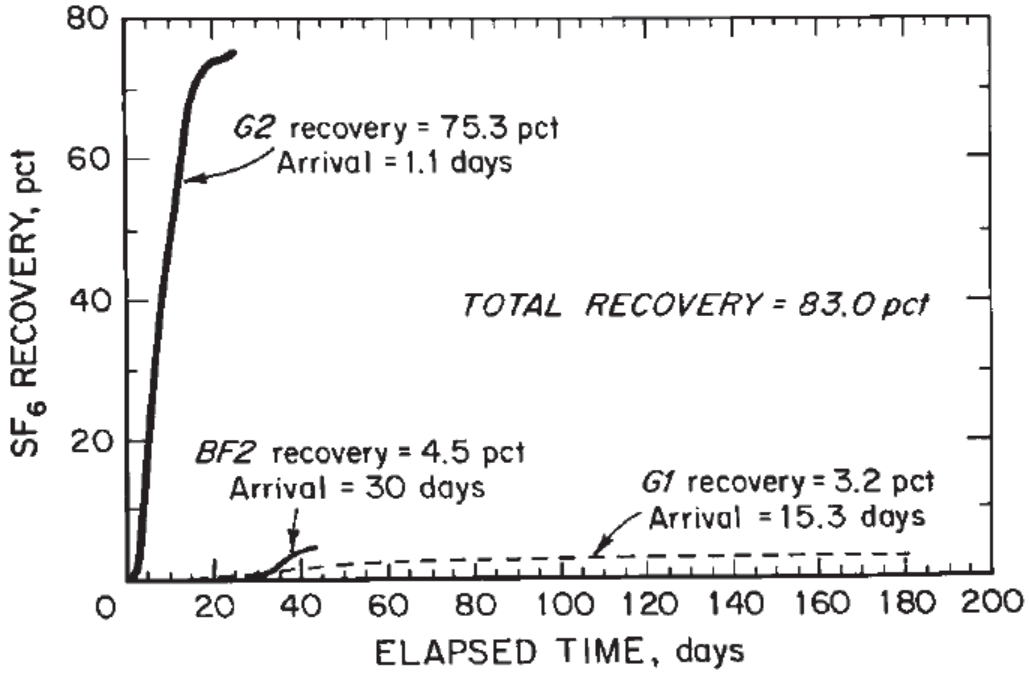

Figure 2.7.5 location of injection points for goaf tracer gas test (Diamond et al., 1999).

Figure 2.7.5 shows the tracer gas recovery over time on the borehole injection test that would serve as a good experimental validation data set for future models. Diamond, Ulery and Kravits (Diamond et al., 1992), published a work “determining the Source of Longwall Goaf Gas: Lower Kittanning Coalbed, Cambria County, PA”. This work established that 91% of gas removed from a coalbed’s overlying strata originally came from the coalbed itself. By using material balance calculations to compare the volume of gas produced from gob vent boreholes and gas removed by the mine’s ventilation system to the original gas in place in the directly overlying 275 ft. of strata, it was established that only 40% of the total gas produced actually came from the strata directly overlying the mine. This indicates the additional gas must have been produced from down dip coal strata as well as adjacent overlying strata. This reinforces the need to consider the larger reservoir as a source of methane within a simulation of flow in mine ventilation systems. It also corroborates the planned modeling at Colorado School of Mines, which treats a higher coal seam as a significant source of gas, in addition to the desire to model gas flow updip from deeper basin coals.

3 Gas emission sources, migration rules and emission prediction

3.1 Overview

This chapter describes contents concerning a numerical gas emission prediction model used to establish the Shaqu coal mine gas emission of working face 14205. The first part provides a brief introduction of basic law of coal seam gas migration, gas concentration distribution and migration law in working face and goaf. The second part provides a brief introduction of the working face location, roadway layout, mining technology and equipment. The third part offers an analysis of gas emission sources and rules. The next part discusses the establishment of gas emission prediction model of the 14205 working face and goaf of Shaqu coal mine. The last part details the gas emission calculation of the 14205 working face and goaf of Shaqu coal mine as well as the analysis of the prediction results.

3.1.1 The necessity of the research of gas emission prediction

It is a fundamental safety work to calculating the gas content in coal seam and forecasting the gas emission from coal and rock in coal mine (Sander & Connell, 2014). In the 1950s, it has been established some measurement methods and processes of gas content in coal bed, and has been put forward and applied the mine statistical method to calculate and predict mine gas content and emission in coal mines (David et al., 1993). In the 1980s, the method of different-source prediction for gas emission also has been proposed and applied. Since then, the method of analogy method, the gas geology mathematical model, velocity method and other prediction methods for gas emission have been put forward and applied (Karacan et al., 2011). After decades of exploration and study by researcher and scholar, it has been formed the maturity and traditional prediction method and technology for gas emission in coal mines that was suitable the coal seam occurrence conditions (Zofia et al., 2009). All the methods and technologies was offer a scientific basis to design and retrofit for the new and old coal mine. With the expansion of coal mining intensity and production scale, people has deepening understood and grasped the essential feature of mine gas emission system by the development and its application of computer technology and mathematics method and the nonlinear theory (Yasin & Etem, 2014). So, many new prediction

methods has been to research and application for coal seam gas emission, For example, based on multivariate linear regression to prediction gas emission (Sanna et al., 2014), based on the grey system theory (Jing et al., 2011), neural network (Zhang & Ian., 2010), support vector machine (SVM) (Chen et al., 2002), evidence theory (Shi et al., 2006), chaos theory (Ding et al., 2011), fractal theory (He et al., 2006), rough set theory (Darshit et al., 2007), and so on methods to prediction gas emission in coal mines. The research and application of these new methods have been to promoting the improvement of the level of research on mine gas emission rule, and improved and raised the level of the coal mine safety production.

3.1.2 The introduction of coal seam gas content measurement and method

Gas concentration is an important factor in relation to mine safety and mine planning, and has become increasingly important in coal bed methane resource assessment and recovery operations (William & Steven, 1998). Gas concentration data may be used in the calculation of gas resources and as input data for reservoir modeling and gas production simulators and to evaluate coal seam gas control options in underground coal mining (Tang et al., 2012). Various methods used to measure or estimate gas content can be grouped into two categories, (i) direct methods, which measure the volume of gas released from a coal sample sealed in a desorption canister, and (ii) indirect methods, which are based on gas sorption characteristics under given temperature and pressure conditions, or empirical correlations between gas content and other coal seam parameters such as coal rank, depth of cover and gas emission rate (Lama & Bartosiewicz, 1982; SAA, 1999).

3.1.2.1 Direct method

Measurement of the gas concentration of a coal samples involves three stages: (i) determining the gas lost from the coal sample during core sample recovery (Q_1), (ii) measuring the gas desorbed from the coal sample while sealed in a desorption canister (Q_2), and (iii) measuring the gas released from a coal sub-sample during crushing (Q_3). The gas content measured during each stage is added to give the total measured gas content (Q_m), Equation 3-1-1, which for the purpose of this analysis represents the total volume of gas released per unit mass of

coal when the ambient gas partial pressure is maintained at one atmosphere.

$$Q_M = Q_1 + Q_2 + Q_3 \quad (3\text{-}1\text{-}1)$$

Given the potential for variable temperature and atmospheric pressure conditions during gas content measurement and differences in mineral matter content of the coal samples, the results are typically normalized with QM being reported in NTP (20° C and 101.325 kPa) and 10% non-coal matter (NCM) (Close and Erwin, 1989 and SAA, 1999).

Diamond and Schatzel (1998) list a variety of methods developed to measure gas content subsequent to the introduction of the first method by Bertard et al. in 1970. The techniques include:

- Bertard's method;
- US Bureau of Mines direct method;
- US Bureau of Mines modified direct method;
- Smith and Williams method;
- Decline curve method;
- Gas Research Institute method; and
- Australian Standard method.

The fast and slow desorption methods used in Australia to directly measure the gas content of coal samples, as described in Australian Standard AS3980: 1999 (SAA, 1999), vary only in the time allowed for gas to desorb from the intact core prior to final crushing. The fast desorption test is typically completed in less than one day whereas slow desorption testing involved a much longer desorption period enabling the rate of gas emission from the intact coal core to be determined. For samples of equivalent Q_m, the $Q_2 : Q_3$ ratio determined from fast desorption testing will be much less than the ratio determined from slow desorption testing. The lost gas volume Q_1 will be the same regardless of the test method.

3.1.2.2 Indirect method

The most accurate measurement of gas content is achieved through direct measurement from bore core samples (Saghafi et al., 2008). Alternatively gas content may be estimated using an

indirect method based on sorption isotherm data (Kim, 1977) or empirical relationships between Q_m and other measurable variables such as coal seam depth and coal rank (Diamond et al., 1976).

Sorption isotherms represent the maximum gas storage capacity of a coal sample at varying pressure and constant temperature. Based on knowledge of the isotherm for a particular coal type and details of the gas pressure, or an estimate of gas pressure based on knowledge of seam depth, the maximum gas content can be determined. However many coal seams are under saturated which, if not accounted for, may result in an over estimate of actual seam gas content (Diamond and Schatzel, 1998). A variety of potential errors are associated with the use of sorption isotherms to determine gas content, which include:

• Isotherm data may not be representative of conditions at the sample location due to changes in coal seam gas composition and variable coal characteristics, such as moisture content, temperature, coal rank, and ash content;

• Lack of knowledge relating to degree of gas saturation in the coal seam and changes in gas content occurring naturally and due to the effects of mining and near and far field gas drainage;

• Inaccurate measurement or estimation of seam gas pressure at the sample location.

Gas content may also be estimated using an interpolation technique whereby the gas content value is calculated for the target location based on measured gas content results at neighboring locations (Saghafi et al., 2008).

The use of indirect methods to estimate gas content may be appropriate for use as a preliminary assessment tool for mine planning and gas reservoir assessment, however, given the potential for error, should not be used in detailed planning and economic decision making (Diamond and Schatzel, 1998).

3.2 Laws of gas migration in the coal seam

3.2.1 Basic law of gas migration in the coal seam

3.2.1.1 Gas migration and movement in the coal seam

It is commonly known that the existence of gas is accompanied by the formation of the coal seam. From a macro point of view, it is mainly adsorbed and free in the coal seam, of which free

gas is in the gas pores and cracks of the coal seam gas molecules, and absorbed gas is the solid state attached to the surface of coal and coal internal structure. Usually in coal seams, there is the dynamic equilibrium where free gas and adsorbed gas molecules continuously keep exchanging, which results in the complication of the gas migration state in the coal seam. It is currently believed the diameter of the gas molecule is approximately 0.414nm and it is able to migrate between coal pores and fractures. According to the current study it is concluded that when the crack width is greater than 10^{-7}m, the gas migration in the coal seam is in the form of laminar motion which also changes non-stop.

This is because the transport channel itself is bent and the cross section is always changing. What is more, the pore size of the coal, and shape and expend degree of the fractures are all depends on the impact of crustal stress, which leads to the fact that the gas migration status is always in slow laminar motion and turbulent flow.

In general, when the crack width is less than 10^{-7}m, gas molecules is not in free motion, thus coal gas migration is in diffusive motion and does not normally depend on the pressure difference but on the concentration difference. Therefore, it is generally believed that gas migration in coal is in the form of surface diffusion and solid diffusion.

3.2.1.2 Basic law of gas flow in the coal seam

Gas flow in the coal seam is a complex activity that is closely related to the structure of the medium and gas formation. As coal is a fractured porous medium, gas flow in coal seams can be seen as the gas flow in porous medium. Generally in the fracture system, gas flow of coal seams is mostly laminar flow movement, and in the pore structure, it is in diffusive motion. Thereby, based on the fracture system in coal seams and pore distribution in coal, it is considered that the gas flow in the coal seams is mainly diffusion movement and laminar flow penetration movement.

(1) Diffusion movement.

Diffusion is the concentration equilibrium process of free movement of molecules moving from high concentration system to low concentration system. Diffusion is also the association of the speed of the diffusive flow and its concentration gradient. Coal is a porous medium, and according to the studies of domestic and foreign researchers, when the pore diameter of the gas

flow is small (generally considered <1μm), the gas molecules can not move freely, and the mass flow of the gas is proportional to gas density gradient, which is in line with the diffusion law, namely Fick law:

$$J = -D\frac{\partial X}{\partial n} \tag{3-2-1}$$

Where: J ——speed of diffusion, $m^3/(m^2 \cdot d)$;

X ——gas content in coal, m^3/m^3;

D ——diffusion coefficient of gas in coal, m^2/d.

According to the gas emission granularity laboratory findings of Coal Research Institute Fushun Branch (China), when the coal size is less than a certain value that is mainly composed of the pore structure the gas flow follows the diffusion law, as is shown in Figure 3.2.1.

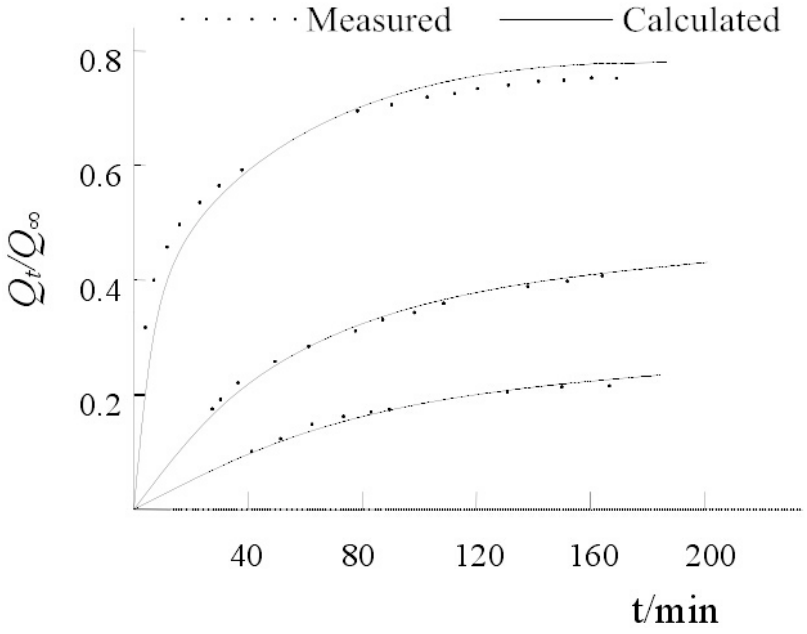

Figure 3.2.1 Diffusion curve of gas in coal

The gas diffusion rate of small pores is generally smaller than gas permeation rate of the large holes and cracks; however, the major part of controlling gas diffusion in coal blocks lies in the gas diffusion movement in small pores. The larger the proportion of the small pores in coal body is, the more gas diffusion movement is in accordance with the diffusion law. Hypothetically the coals seams is composed by the extreme coal of Fick law, according to law of conservation of mass and Fick law, the differential equation of the coal diffusion movement is:

$$\frac{\partial X}{\partial t} = D\left(\frac{\partial^2 X}{\partial r^2} + \frac{2}{r}\frac{\partial X}{\partial r}\right) \tag{3-2-2}$$

where: r ——radius of any point within the coal particle, m;

t ——time, s.

Refer to the meaning of other symbols above.

In fact, in the coal seam pore - fracture structural system, the volume of pore unit is quite small, and the fracture system of coal seam is well developed, especially for the highly intense and dangerous seam. Therefore, gas flow in the coal seam is mainly laminar movement.

(2) Laminar movement.

There are two possible forms of gas migration in pores and fractures with holes bigger than 1μm: laminar and turbulent flow. Laminar flow is generally divided into linear and nonlinear permeation.

(2.1) Darcy law

When the gas flow in coal seams is linear permeation that is when the gas flow rate is proportional to coal seam gas pressure gradient; it is in line with the linear law and Darcy law:

$$V = -\frac{K}{\mu}\mathrm{g}\frac{\partial p}{\partial n} \tag{3-2-3}$$

where: K ——permeation rate of the coal seam, m^2(1D=9.869×10-13m^2);

V ——gas flow rate, m/s;

μ ——gas absolute viscosity, $Pa \cdot s$;

$\frac{\partial p}{\partial n}$ ——gas pressure gradient, Pa/m.

Formula of gas flow volume can be calculated based on (3-1-3):

$$q = -\lambda \frac{\partial P}{\partial n} \tag{3-2-4}$$

where: q ——gas flow volume, m^3 /(m^2·d);

λ ——coal seam permeability coefficient, m^2 /(MPa^2·d);

P ——gas pressure squared, $P = p^2$, MPa^2.

Many researchers test the gas permeation using samples of artificially suppressed pulverized coal and the laboratory findings suggest that the gas flow in coal samples with pores of large diameter is in complete compliance with Darcy law, which is shown in Figure 3.2.2 (latm=101325 Pa).

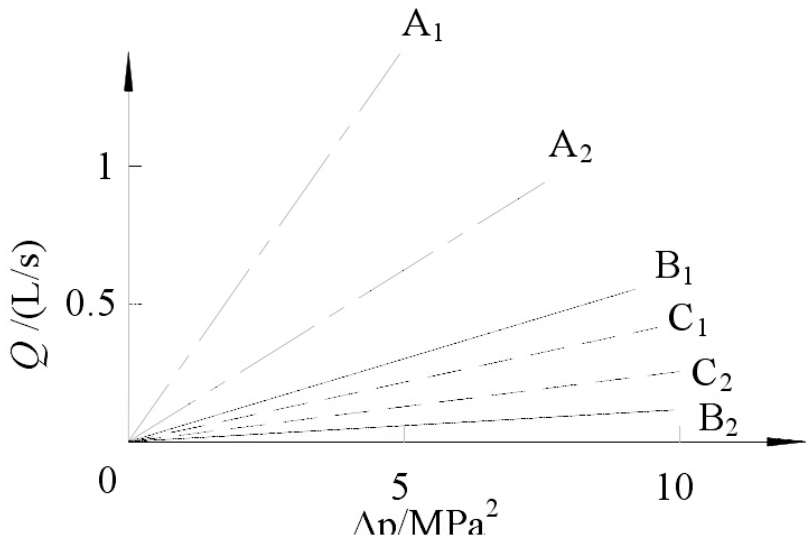

Figure 3.2.2 Relation between gas flow volume and difference of squares of both ends of the coal sample

Seen from Figure 3.2.2, due to the large gap between the artificial samples of coal particles, the gas flow in the coal samples follows the rules of linear permeation, but its permeability coefficient reduces with the increase of the ring pressure. Previously it was believed that Darcy law is merely applicable of laminar flow, and classified those that deviate from Darcy law as turbulence. After 1940s, many experiments confirmed that not all of the laminar movements of underground fluids follow Darcy law that is when the critical Reynolds number of the fluid is far less than 2000; Darcy law will not apply on the fluid movement. As such, gas flow in coal can be divided into three categories:

Low Reynolds zone, Re<1 ~ 10, viscous forces dominate, linear laminar flow region, in line with Darcy law.

Medium Reynolds zone, the upper limit of Re is 100, nonlinear laminar flow zone, subject to non-linear permeability law.

High Reynolds zone, Re> 100, a turbulent flow, inertial forces dominate, flow resistance is proportional to the square of flow rate.

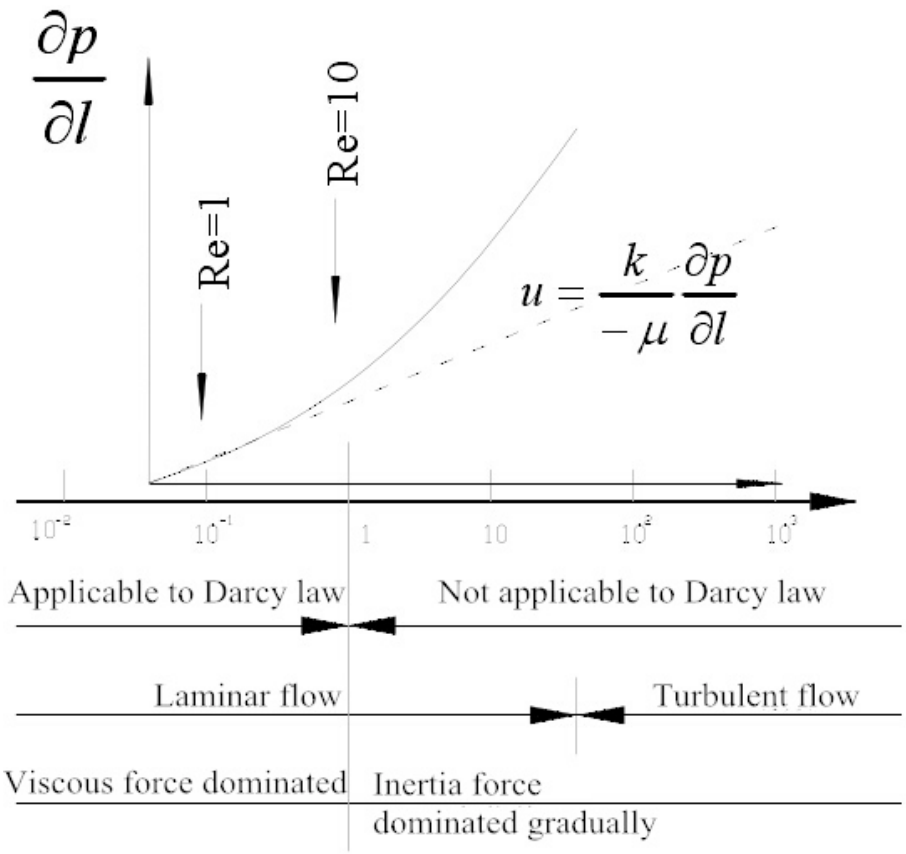

Figure 3.2.3 Variation of flow law in porous medium

Figure 3.2.3 is the variation of the state and law of the fluid flow in porous medium. It shows the range of application of Darcy law is smaller than that of laminar flow. From the laminar flow motion that follows Darcy law to laminar flow motion not following Darcy and to turbulence, its transformation is gradual and there is no clear dividing line. This is because the transport channel the gas flows in is bent and the cross section is always changing.

Each fluid particle moves along the curve with a changeable speed and acceleration; when the pore is small and the particle is slow, the viscous force dominants that is the frictional resistance generated by viscosity dominants. Compared with viscous forces, inertial forces can be ignored, which means Darcy law is being followed. When the pore size and flow speed increase, the inertia force increases as the square of the speed of the flow rate, and when it reaches the order of magnitude, Darcy law is not applicable, which happens prior to the transfer from laminar flow to turbulent. In fact, this is mainly because the size, shape, curvature, pore structure and extension level of the coal is very uneven, combined with impact of the crustal stress, as a result all the factors are unstable and vary within a larger range. Even so, in most cases, the whole gas flow in coal seams still follows Darcy law.

(2.2) Non-linear permeability law

The above findings suggest that when the Reynolds is greater than a certain value, gas flow in the coal body will deviate from Darcy law in the form of non-linear permeability flow; on the condition of non-linear laminar flow and turbulent flow, there is index relation between the flow rate and pressure difference:

$$u_m = -\lambda\left(\frac{dp}{dl}\right)^m \tag{3-2-5}$$

where: u_m——flow speed;

λ——gas permeability coefficient of coal;

m——permeability index，when m=1，$\lambda = \frac{K}{\mu}$, the above formula is Darcy law，experiments testify that $m = 1:\ 2:-\frac{dp}{dl}$——gas pressure gradient.

In fact, it can be considered that binomial theorem seepage is much more reasonable:

$$-\frac{dp}{dl} = AV + BV^2 \tag{3-2-6}$$

The first term on the right-hand side of the above formula reflecting the characteristics of Darcy law is the pressure loss caused by direct friction between the fluid and the porous medium. When velocity V is small, the corresponding Reynolds is small, and the first term dominants, $A = \frac{\mu}{K}$. The second term reflects the pressure loss caused by the shrinkage, expansion and turn of the fluids when they bypass the irregular solid system of porous medium, referring to as the pressure loss of "microscopic local resistance". When the flow velocity and Reynolds is large, the second term dominants, and fluid flow in porous medium is non-linear influent flow.

In the theory of laminar flow based on Darcy law, it was hypothesized that due to the presence of the shear stress, the speed of the fluid on the solid wall is zero. On the contrary, in the gas stream the gas molecules do not have close contact with the solid wall, and the gas on the solid wall may have a certain non-zero speed. Thus, when the size of the gas molecules is getting close to the channel, all the molecules on the interface are in motion, and generate an additional flux. This phenomenon is called molecular slipstream phenomena or Klinkenberg effect. Because of the existence of the effect, airflow in porous medium under low pressure will in many cases deviate

from Darcy's law.

3.2.2 Gas flow in coal seams

As is mentioned above, in the coal seam gas will flow from the high pressure area to low pressure area. When there is unequal distribution of gas pressure in the coal seam, a certain flow range of gas - usually called the flow field - is formed, that is, within the range of the flow field, gas is in flow state and has flow direction, flow rate and gas pressure gradient or concentration gradient.

To facilitate the research on gas flow in coal, the gas flow field in the coal seam is required to be classified. Currently two kinds of classifications are normally adopted: classification based on space and classification based on time (stability).

In the flow field, gas flow can be basically divided into three types by the geometry of space: one-way flow, radial flow and ball flow.

(1) One-way flow - in the x, y, z three-dimensional space, there is only one direction of the flow rate, the flow rate of the other two directions is zero. In coal mines, if the exploitation is along the roadway, the thickness of the coal seam is smaller than the height of the roadway, the roadway all cut open, the gas flow on both sides of the roadway are parallel to each other along the driving direction, and the flow net in the same direction is one-way flow, as is shown in Figure 3.2.4.

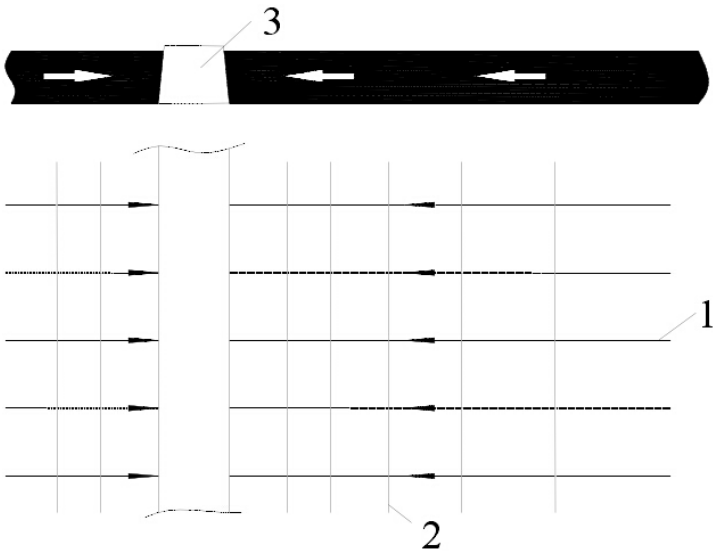

Figure 3.2.4 Diagram of one-way flow

1- flow line; 2- isobaric line; 3- drills

(2) Radial flow - in the x, y, z three-dimensional space, velocity component exists in two directions. The velocity component of the third direction is zero. For example, when the cross-hole, shafts and drill holes penetrate vertically through the coal seams, the gas flow on the coal wall basically belongs to the radial flow field. Usually, the gas pressure line is in parallel line, such as coal was approximately concentric circular wall, as in Figure 3.2.5. As radial flow is generally flat flow, x, y rectangular coordinates is adopted in research work, and polar coordinates can also be used, depending on the requirement of the practical work.

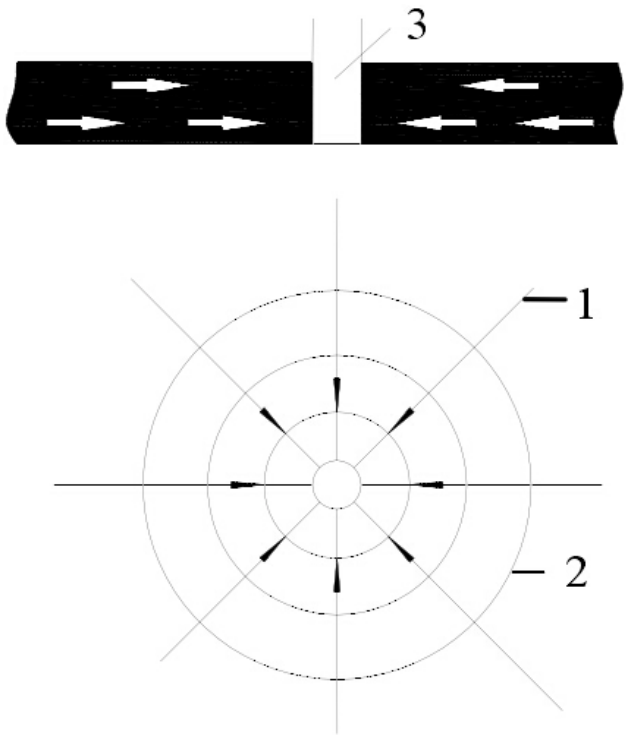

Figure 3.2.5 Diagram of radial flow

1- flow line; 2- isobaric line; 3- drills

(3) Ball flow - in the x, y, z three-dimensional space, there are velocity component in three directions. For example, at the coal wall of the advancing working face in thick coal seams, gas flows from the entrance of drills and cross-hole into coal seams and from fallen coals is all ball flow as in Figure 3.2.6. It is generally believed the characteristic of the ball flow is that it forms isobars of concentric spherical approximation whereas the flow lines are generally net radiation. As ball flow belongs to the three-dimensional flow, x, y, z rectangular coordinates and the spherical polar coordinates can both be employed in practical researches.

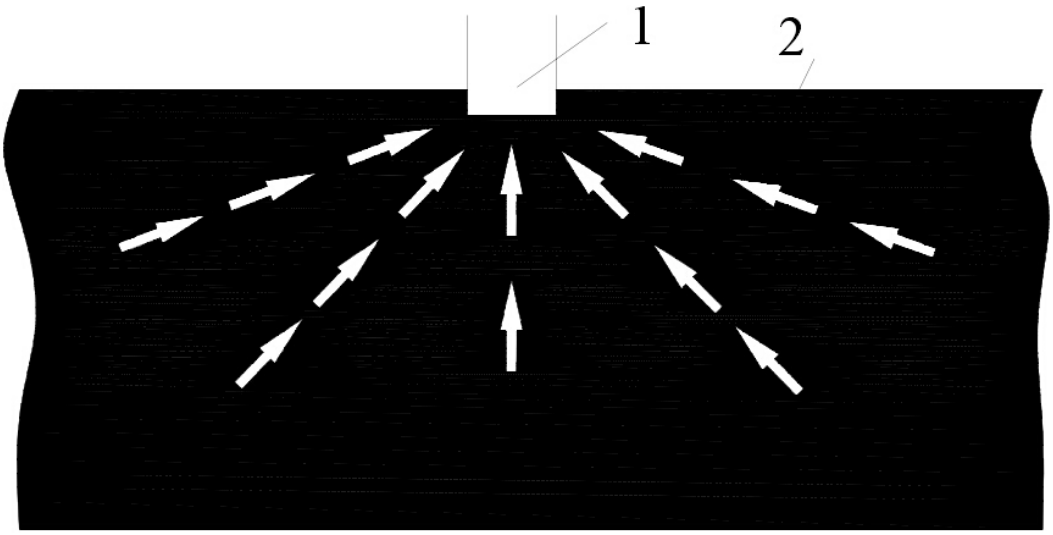

Figure 3.2.6 Diagram of ball flow

1- advancing working face in the coal seam; 2- flow lines

The three flow fields above are the basic forms, but in practical mining. Gas flow field in drills and roadway coal wall is complex and even integrated three flow fields due to the anisotropy of the coal seam, variation in litho logy of coal seam roof and floor and other natural conditions. Thereby, in order to establish a relatively accurate flow model, detailed analysis should be carried out individually in practical experiments.

3.3 Introduction to the measurement of mechanized working face

3.3.1 Working face location and roadway layout

The 14205 mechanized working face of Shaqu Mine is an inclined longwall face. It's the fifth working face in the second south mining area. In its north is the completed 14204 working face, in its south is protection coal pillar of Jiaqiangta village, in its east is the centralized material roadway of South 2, while the west is protection coal pillar of Guantou village. Its face floor elevation is between 380 ~ 440m.

There are altogether 3 gate roads in the 14205 mechanized working face with the length of 895m, of which the orbital gateway (14204 tail roadway) and the belt gateway are inlet airway and tail roadway is the return airway. The belt gateway and tail roadway are connected to cooperate with das drainage borehole to drainage gas and regulate the ventilation air flow, the layout of the roadway can be seen in Figure 3.3.1. The open-off cut of the working face is 200m, minable

length is 855m, and minable area is 0.17km^2.

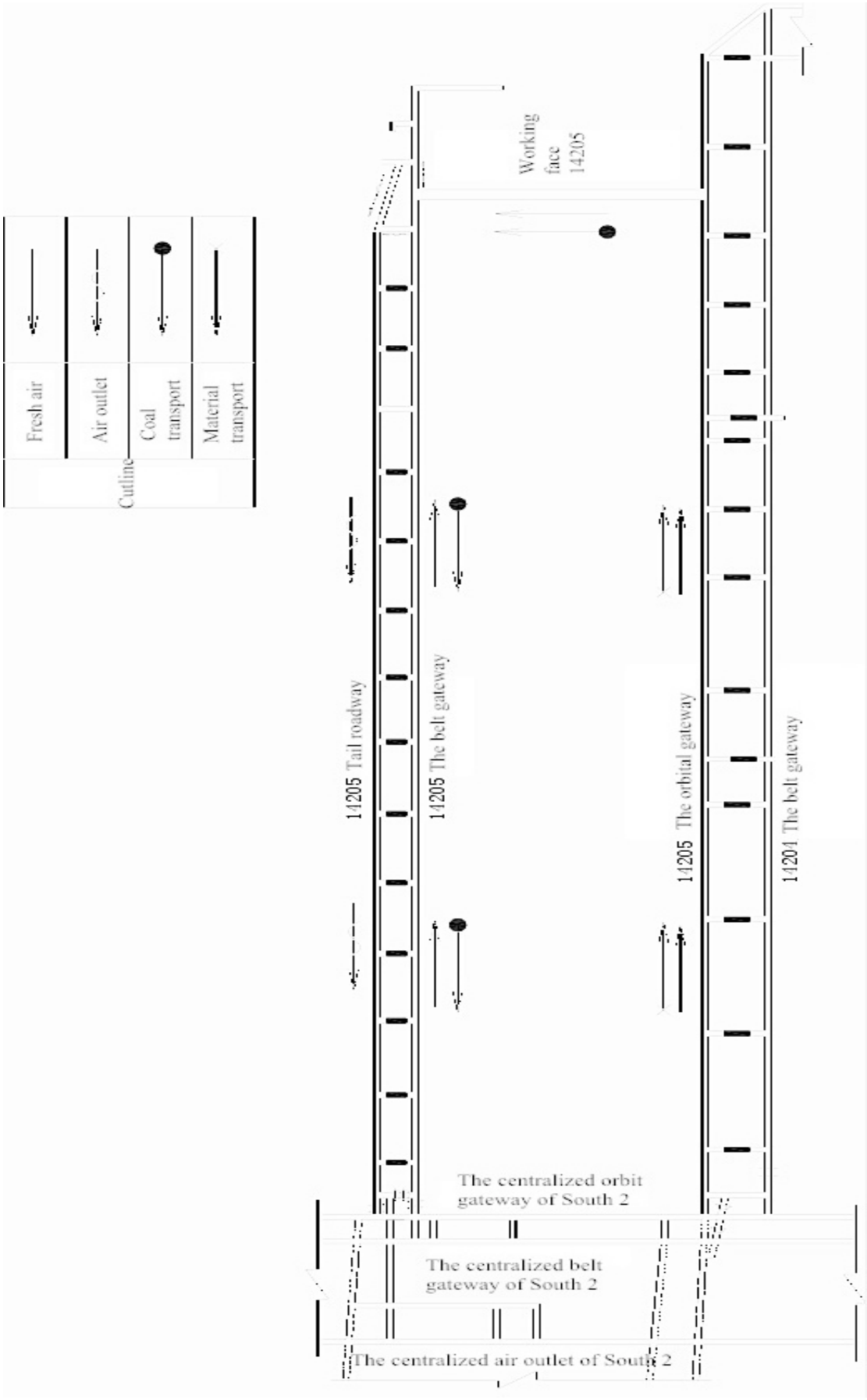

Figure 3.3.1 Layout of lanes of the14205 working face

3.3.2 Coal mining technology

The 14205 working face adopts the mechanized mining methods, and its main production process is as follows:

Advanced Maintenance → back shed → shearer cutting coal and loading → coal transportation → push the slide frame shift → pushes slides → float coal cleaning.

3.3.3 Main equipment of the working face

Table 3.3.1 List of basic equipment in the 14205 mechanized mining face

Serial number	Name	Specifications and models	Unite	Amount
1	Coal cutter	MG250/580w	Piece	1
2	Hydraulic support	ZZ4000-1.6/2.6	Piece	133
3	Drag conveyer	SGZ-764/500	Piece	1
4	Reversed loader	SZB-730/750	Piece	1
5	Belt conveyor	SSJ-1000/2×160	Piece	1

3.3.4 Five systems of the working face

Transportation system: working face scraper conveyor loader → reversed loader → transport trough belt conveyor → panel centralized roadway → transportation roadway → main shaft → ground;

Supporting system: the working face adopts hydraulic support of support protection, and the support strength is 74.40t/m^2;

Ventilation System: the working face adopts the "two air inlets and one air outlet" ventilation system, with the track and tape trough being the inlet airway and lane end being the return airway;

Water supply and drainage systems:

Water supply: purification station → auxiliary shaft → transportation roadway lane → panel

centralized roadway → two gateways (the material gateway and the orbit gateway) and the working face;

Water drainage: two gateways (the material gateway and the orbit gateway) and the working face → panel centralized roadway → transportation roadway lane ditch → well bottom sump → auxiliary shaft → ground;

Security system: anti gas and harmful gases, fire, water and dust.

3.4 Analysis of gas emission sources

The source is where gas emits within the mining area. The mixture layer of coal and rock containing gas is affected by mining operations, and coal seam gas deposit and the surrounding rock conditions are destroyed, resulting in the fact that the gas flows into the working face and forms a part of the gas emission in the working face. The sources of the gas emission in the working face of Shaqu Mine is shown in Figure 3.4.1. It includes the gas emission of the coal wall, mined coal and the goaf. Goaf gas emission contains gas emission of side coal wall and surrounding rocks, loss coal, upper adjacent layers and lower adjacent layers.

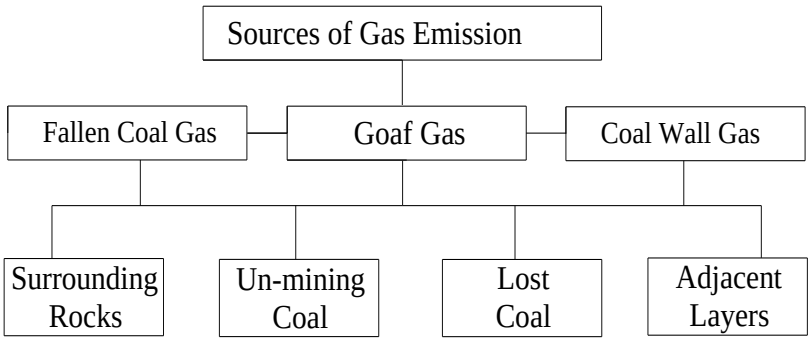

Figure 3.4.1 Source form of gas in the working face of Shaqu coal mine

3.4.1 Coal wall gas emission

When the mining working face constantly moves forward and fresh coal wall continually exposes, under the pressure of the rock, the equilibrium of the coal body ahead of the working face is destroyed and distressed zone with high gas permeability is formed. There is always a certain amount of gas pressure gradient, and a great amount of gas in the coal seam flows along

the fracture into the working face, and the intensity of the gas emission gradually decreases with the increase of the exposure time of the coal wall.

The amount of gas emission from the coal wall depends on the raw coal gas pressure, permeability, advance speed of the working face and other factors.

3.4.2 Fallen coal gas emission

With the advance of the working face, the coal on the wall keeps falling and shipped out, meanwhile the gas it contains is released into the mining area. Fallen coal is in the shape of block, which largely increases the expose coverage of the surface of the coal body, thereby increases the strength and speed of the gas desorption and leads to an increased amount of gas emission.

The gas emission rate of the fallen coal depends on the block size: the smaller the size is, the faster the gas emits; likewise, the larger the size is, the slower gas emits.

The gas emission quantity of the fallen coal mainly depends on the volume of the fallen coal, the original gas pressure, permeability and other factors. As the coal wall, the intensity of the gas emission of fallen coal is also decreased with the increase of the amount of time.

3.4.3 Goaf gas emission

Coal mining goaf is porous media and filled with loss coal and fallen rocks, and the compaction condition in different area of goaf are different, air pressure changes enormously, resulting in the various gas flow rates among different spots in goaf. Gas at the emission sources release the pressure due to the rock deformation and collapse, flows into goaf, get mixed, and under the effect of differential concentration and negative pressure ventilation, rushes to the working face. Studies show that the main source of goaf gas is the pressure release of the adjacent seams. The exploitation of the 4th seam in Shaqu coal mine will cause overburden movement and fracture, and seam #3 locates in the collapse area and releases gas directly to the mined-out area, while the seam #2 gas moves into goaf through the fractures in the overlying rock seam.

With the effect of crustal stress, lower coal strata swells and deforms, greatly increasing the permeability and a great amount of high-concentrated gas in the seam #5 steadily releases to goaf. The maximum distance of the adjacent seams diffuse gas to goaf depends on the nature of the

strata and development of fractures. The scope of gas supply to goaf relies on the nature of the adjacent seams, management of the top layer as well as the shape of the mining area, etc.

3.5 Rules of gas emission at emission source

3.5.1 Rules of gas emission on coal wall

The quantity of gas emission in the mechanized working face mainly depends on the gas emission intensity at emission source, with coal wall gas emission intensity usually being the amount of emitting gas in unit time per square meter, and majorly depending on the gas pressure and fracture structure in the seam, gas adsorption properties and spatial conditions. Under a certain circumstance, the gas emission intensity of coal wall can be indicated by the function of exposure duration. According to coal gas flow theory and analysis of actual measurement, the variation of coal wall gas emission intensity in unit area varies with time, which is gas emission characteristics, complies with the following rules:

$$V_1 = V_0 \cdot (1+t)^{-\beta} \tag{3-5-1}$$

where: V_1——point-in-time of coal wall exposure, gas emission intensity on unit area of coal wall, $m^3/(m^2 \cdot min)$;

V_0——initial time of coal wall exposure, gas emission intensity on unit area of coal wall, $m^3/(m^2 \cdot min)$;

β——attenuation coefficient of coal wall gas emission, min^{-1};

t——coal wall exposure duration, min.

In order to determine the relation between the coal wall gas emission intensity and the cumulative gas emission quantity and coal wall exposure time period, the research conducts field observations in the working face of Shaqu coal mine. The process is to set a number of measuring points in the tunnel at a certain distance (as is shown in Figure. 3.5.1). Non-production time, air flow and gas concentration of each measuring point is regularly measured, then the amount of gas emission per unit time at each measuring point and based on the coal wall exposure area the coal wall gas emission intensity are calculated, finally the average exposure time of each corresponding segment is determined in accordance with the roadway driving speed.

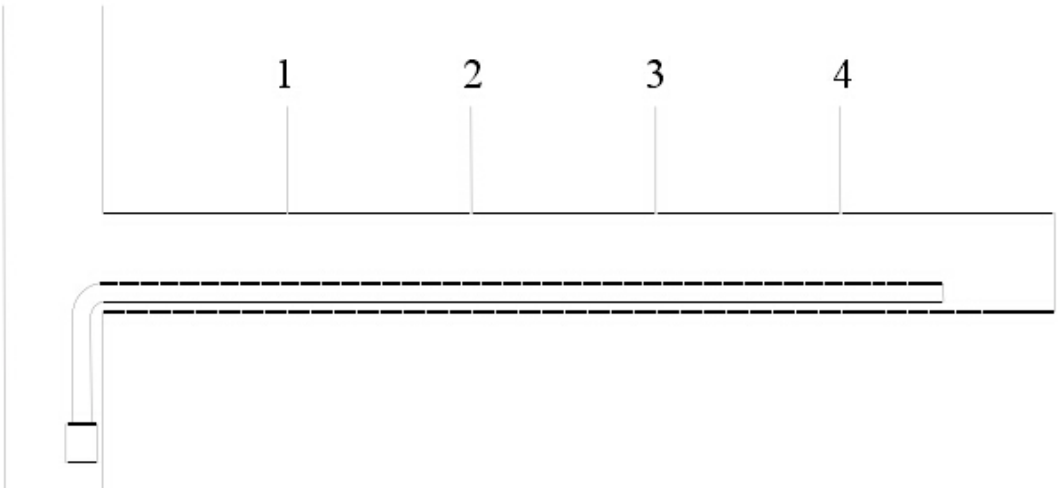

Figure 3.5.1 Tunnel measurement method

Test data can be seen in Table 3.5.1, and the regularity of coal wall gas emission can be obtained by the original measured data. Put all the measured data on complex logarithm coordinate system of $V-t$ relation, and the relation of $V-t$ can be regards as a relation of power function, and the empirical equation of $V-t$ relation can be shown:

$$V_1 = 0.261(1+t)^{-0.203} \tag{3-5-2}$$

Table 3.5.1 Relation between coal wall gas emission intensity and exposed time

Exposed time of coal wall (t/min)	Gas emission intensity of coal wall ($m^3/(m^2 \cdot min)$)	Exposed time of coal wall (t/min)	Gas emission intensity of coal wall ($m^3/(m^2 \cdot min)$)
1	0.225	20	0.140
3	0.212	25	0.137
5	0.177	30	0.130
7	0.168	40	0.125
9	0.163	50	0.123
11	0.155	70	0.111
13	0.153	90	0.105
15	0.149	120	0.090

The variation rule of coal wall gas emission intensity and time period can be seen in Figure 3.5.2 shows

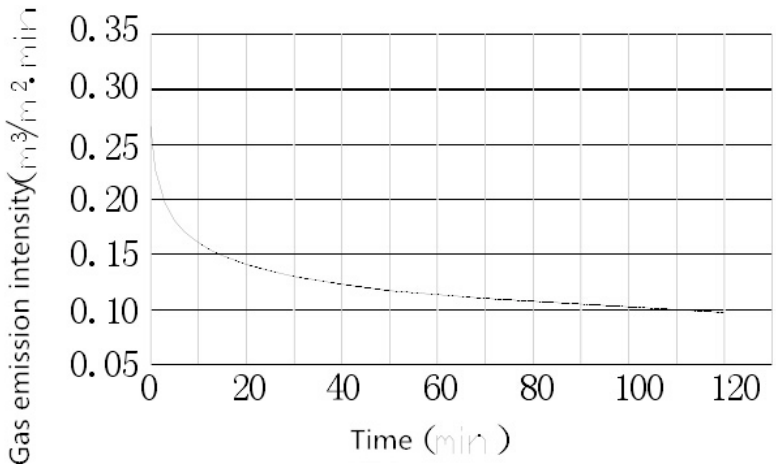

Figure 3.5.2 Variation rule of coal wall gas emission intensity and time period

3.5.2 Rules of gas emission of fallen coal

A part of gas in the working face comes from the fallen coal. The gas emission rate of different particle size of coal are different, the coal particle size smaller, the emission rate faster, and the coal particle size bigger, the emission rate slower. Usually, the particle size of mechanized coal mining is smaller and more even than that of blasting mining, and it can improve the intensity of parsing of coal gas. Similarly, the intensity of parsing of coal gas is decreased with the increasing of time.

The gas come from mined coal continually flow over into the working face and upper corner during the transport of mined coal on the drag conveyer. According to the gas flow theory and the analysis of the measure data, the rules of the gas emission of fallen coal can be obtained:

$$V_2 = V_1 \cdot e^{-nt} \tag{3-5-3}$$

Where: V_2——gas emission intensity of fallen coal staying in the working face for the duration of time t, $m^3/(t \cdot min)$;

V_1——original gas emission intensity of fallen coal, $m^3/(t \cdot min)$;

n——attenuation coefficient of mined coal, min^{-1};

t——duration of time of fallen coal staying in the working face, min.

Residual coal left in the mechanical working face will still continuously release its remaining gas into the working face, and its gas emission rule is in line with Formula (3-5-3).

Coal mining colony on the basic parameters of the amount of gas emission measurement

applications roadway assay was determined. Namely coal roadway driving in normal, every certain distance select two more regular sections AA and BB shown in Figure 3.5.3.

The basic parameters of mined coal gas emission can be determined by the measurement of roadway. In the advancing coal roadway, AA and BB - two relatively structured cross sections with a certain distance - are selected as is shown in Figure 3.5.3.

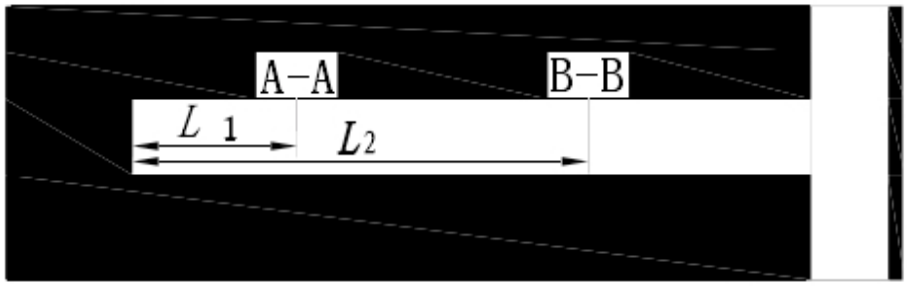

Figure 3.5.3 Layout of gas emission measuring points in roadway

Non-production time, air volume and gas concentration at the two cross sections are measured, and coal wall gas emission of different places (sections) to the working face is obtained, and α and V_0 are able to calculated through the formulas below.

$$\begin{cases} Q_{A-A} = \dfrac{v_0 v_1 U}{2\alpha}\left(1 - e^{-\frac{2\alpha L_1}{v_1}}\right) \\ Q_{B-B} = \dfrac{v_0 v_1 U}{2\alpha}\left(1 - e^{-\frac{2\alpha L_2}{v_1}}\right) \end{cases} \tag{3-5-4}$$

Q_{A-A}——air volume of cross section A, m^3/min;

Q_{B-B}—— air volume of cross section B, m^3/min;

α——attenuation coefficient of coal wall gas, min/1

v_0——the initial coal wall exposure, the absolute gas emission rate on each unit area of roadway, m^3 / (m^2·min);

v_1—— average advancing speed in the roadway, m/min;

U ——the perimeter of fully-mechanized excavating roadway, or the perimeter of fully-mechanized excavating coal wall, m;

L_1——the distance from section A to the heading end, m;

L_2 ——the distance from section B to the heading end, m.

When the above method is adopted, special attentions should be paid that cross sections $A-A$ and $B-B$ should apply the exact same measurement at the same time, in case that the fluctuation of the air volume affects the outcomes. Also, a number of cross sections in the roadway should be selected for the accuracy of the measurement (requirement: $L_2 = 2L_1$). On the condition that the production in the working face and transportation system are both functioning regularly, gas concentration and air volume are measured at the two cross sections, then the absolute gas emission volume at the two sections are calculated. With the obtained α and v_0 above, the gas emission volume of fallen coal at the corresponding section is acquired as follows:

$$Q_2 = \frac{\rho q_0 S v_3}{\beta}\left(1 - e^{-\frac{\beta l}{v_2}}\right) \tag{3-5-5}$$

Q_2——absolute amount of gas emission of fallen coal in the working face, m^3/min;

ρ ——density of coal blocks, t/m^3;

q_0—— the initial relative gas emission of mined coal, $m^3/(t \cdot min)$;

S ——cross section area of the mining roadway, m^2;

v_3——the average excavating speed in the roadway, m/min;

β ——the attenuation coefficient of mined and loss coal gas emission, min^{-1};

v_2——speed of the transport carrier, m/min;

l ——length of transportation routes of fallen coal in the working face, m,

Finally, β and q_0 are obtained through the formula below:

$$Q = \frac{v_0 v_1 U}{2\alpha}\left(1 - e^{\frac{-2\alpha l_1}{v_1}}\right) + \frac{\rho q_0 S v_3}{\beta}\left(1 - e^{\frac{\beta l}{v_2}}\right) \tag{3-5-6}$$

Based on the measured data in Table 3.5.2 - Table 3.5.5, β and q_0 are acquired β =0.084min^{-1}, q =0.189 $m^3/(m^2 \cdot min)$. The $V-t$ relation of the fallen coal can be presented as the formula below:

$$V_2 0.189e^{-0.084t}$$

Table 3.5.2 Distribution of gas concentration in non-working time

20m from heading end				40m from heading end			
Air quantity (m^3/min)	Gas concentration (%)	Section (m^2)	Perimeter (m)	Air quantity (m^3/min)	Gas concentration (%)	Section (m^2)	Perimeter (m)
532	0.25	10.6	13.9	534	0.26	10.5	13.8
531	0.24	10.6	13.9	531	0.27	10.5	13.8
532	0.24	10.6	13.9	533	0.28	10.5	13.8

Table 3.5.3 Distribution of gas concentration in non-working time

30m from heading end				60m from heading end			
Air quantity (m^3/min)	Gas concentration (%)	Section (m^2)	Perimeter (m)	Air quantity (m^3/min)	Gas concentration (%)	Section (m^2)	Perimeter (m)
533	0.21	10.4	13.6	535	0.28	10.5	13.8
528	0.20	10.4	13.6	529	0.30	10.5	13.8
534	0.21	10.4	13.6	534	0.31	10.5	13.8

Table 3.5.4 Distribution of gas concentration in working time

20m from heading end				40m from heading end			
Air quantity (m^3/min)	Gas concentration (%)	Section (m^2)	Perimeter (m)	Air quantity (m^3/min)	Gas concentration (%)	Section (m^2)	Perimeter (m)
533	0.34	10.6	13.9	535	0.33	10.5	13.8
531	0.44	10.6	13.9	540	0.39	10.5	13.8
532	0.56	10.6	13.9	538	0.51	10.5	13.8

Table 3.5.5 Distribution of gas concentration in working time

30m from heading end				60m from heading end			
Air quantity (m^3/min)	Gas concentration (%)	Section (m^2)	Perimeter (m)	Air quantity (m^3/min)	Gas concentration (%)	Section (m^2)	Perimeter (m)
460	0.43	10.4	13.6	465	0.48	10.5	13.8
461	0.42	10.4	13.6	462	0.49	10.5	13.8
463	0.39	10.4	13.6	466	0.42	10.5	13.8

The variation rule of gas emission intensity of fallen coal and duration of time is presented in Figure 3.5.4

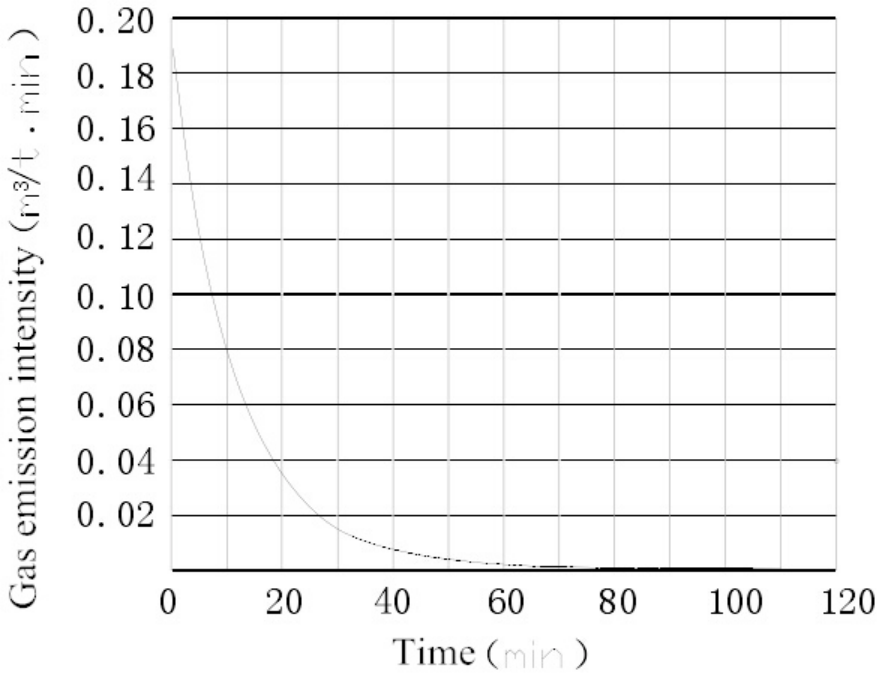

Figure 3.5.4 Variation curve of gas emission intensity of fallen coal and duration of time

3.5.3 Rules of gas emission of upper and lower adjacent layers

Gas emission volume of the adjacent layers mainly depends on the original gas content and gas emission rate of the adjacent layers, distance between the exploitation layer and adjacent

layers, mining speed of the working face, etc. The proportion of gas emission volume of the adjacent layers is quite significant, especially for the combined mining method of multiple seam or layer mining of high seam - when the first coal seam or layer mining, its gas emission volume is usually much higher than that of in-the-seam mining.

(1) With coal mining distance of the working face gradually increases, the release of the upper adjacent layer is gradually getting obvious. As a result, gas pressure decreases and gas emission volume of the working face increases. Therefore, gas emission rules of adjacent layers are considered consistent with the roof release activities.

(2) The length of the mining working face has a significant impact on the release range and gas emission of the adjacent layers. Through a great number of research on data of other mining area, the gas parameter of adjacent layer (length 140m and width 90m) is easy to change, especially in the upper adjacent layer of 59m (Yangquan Coal Mine coal seam #12) , the initial gas pressure decrease to 0.19 MPa and 0.22 MPa from 0.38MPa.

(3) The height of the exploitation layer is closely related to the release range and gas emission of the adjacent layers. In the same geological conditions, the increase of mining height will cause the increase of the range and level of the release of the adjacent rocks, and the rock strata that is unable for the release is forced to release the pressure, thereby the permeability of the rock strata is extended and the gas emission volume of the adjacent layers is increased.

(4) The absolute amount of gas emission will be reduced by speeding up the advance speed in the working face. As the working face is rapidly mining, the roof of the exploitation layer sinks, but the damage it has is relatively insignificant. Therefore, the gas emitted from the upper adjacent layer into the working face and goaf reduces due to the resistance. The slower the mining retrieving is, the huger the damage of the rock strata is, and the more the absolute amount of gas emission is.

Under a certain geological and mining circumstance, the extent of the gas emission of the adjacent layers decreases as the interlayer spacing decreases. At a certain critical distance, gas emission is ignored.

According to the difference between the original gas content in the coal seam and residual gas content, gas emission of adjacent layers with difference interlayer spacing is obtained. Through the regression analysis, based on logarithmic curve, gas emission rate (Kui) decreases as

the interlayer spacing H increases.

3.6 Establishment of prediction model of working face gas emission

According to the analytical research on current and traditional prediction methodology of gas emission volume, difference of the emission rules of gas sources is summarized, characteristics of mechanized mining is analyzed, gas source of the working face is carefully classified, and a prediction model with high accuracy and adaptability and dynamic features is established for the gas emission measurement of the working face, so that gas emission volume of the working face is able to be accurately predicted.

3.6.1 Gas emission volume of coal wall

Assume that one schedule of coal mining cycle is 1 (cut deep of fully mechanized machine, m), the average advancing speed of the working face is n (m/min), time of coal mining cycle schedule is $t_1 = 1/u$ (min), gas emission intensity of unit area of coal wall after t minutes (m^3/(m^2·min)), thus, the total gas emission amount of each unit area of coal wall is

$$q_1 = \int_0^{t_1} V_1 dt \tag{3-6-1}$$

put equation (3-4-1) into equation (3-5-1), then simplify the integrals:

$$q_1 = V_0 \left(\frac{(1+t)^{1-\beta}}{1-\beta} - \frac{1}{1-\beta} \right) \tag{3-6-2}$$

Where: q_1——gas emission intensity of unit area of coal wall after t_1 minutes, m^3/min;

Assume that the effective exposure area of the working face is $S = m(L - 2L_H)$, and then put $t_1 = l/u$ into equation (3-5-2), one schedule of coal mining cycle is $G_1^{'} = \delta mlCL$, and then the absolute gas emission rate of coal wall Q_1 is

$$Q_1^{'} = \frac{V_0 (L - 2L_H)}{\delta CLl} \left(\frac{(1+l/u)^{1-\beta}}{1-\beta} - \frac{1}{1-\beta} \right) \tag{3-6-3}$$

where: Q_1——the relative gas emission rate of working faces, m^3/t;

m——thickness of the coal seam, m;

L ——length of the working face, m;

L_H ——width of gas emission are, m;

β ——attenuation coefficient of coal wall gas emission, min^{-1}.

The absolute gas emission rate of coal wall is

$$Q_1 = \frac{mu\left(L-2L_H\right)V_0}{l}\left(\frac{\left(1+l/u\right)^{1-\beta}}{1-\beta}-\frac{1}{1-\beta}\right) \tag{3-6-4}$$

The calculation of the gas emission of the layer mining of high coal seam or the caving mining can be calculated by equation (3-5-4).

3.6.2 Gas emission volume of fallen coal

Assume that gas emission intensity of unit weight after t minute is V_2, the total absolute gas emission rate of unit weigh is:

$$q_2 = \int_0^{t_2} V_2 dt \tag{3-6-5}$$

put equation (3-5-3) into equation (3-5-5), then simplify the integrals:

$$q_2 = \frac{V_1}{n}\left(1-e^{-nt_2}\right) \tag{3-6-6}$$

where: q_2 ——accumulative gas emission volume of fallen coal, m^3/t;

V_1 ——original gas emission intensity of fallen coal, m^3/ (t·min);

t_2 ——duration of time of fallen coal in excavation roadway, min.

The gas emission volume of fallen coal is:

$$Q_2' = \int_0^{L-2L_H} q_2 \cdot dA \tag{3-6-7}$$

put equation (3-5-6) into equation (3-5-7), and then simplify the integrals:

$$Q_2' = \int_0^{L-2L_H} \frac{V_1}{n}\left(1-e^{-nt_2}\right) dA \tag{3-5-8}$$

where: Q_2 ——accumulative gas emission volume of fallen coal, m^3;

t_2 —— duration of time of fallen coal in the working faces, min;

$t_2 = \left(L-L_{H-X}\right)/v_2$

v_2——the average pulling speed of coal cutter, m/min;

dA—— the weight of loss and fallen coal in the infinitesimal length dx of the direction of traction machine, t;

$$dA = C \cdot \delta \cdot mldx$$

C——retrieving rate of the working face;

δ——density of fallen coal, t/m^3.

Thus Formula (3-6-8) can be presented as follows:

$$Q_2' = \int_0^{L-2L_H} \frac{V_1}{n}\left(1 - e^{-n(L-L_H-x)/v_2}\right) C\delta ml \cdot dx \tag{3-6-9}$$

simplify the integrals of equation (3-6-9), then the relative gas emission rate of mined and fallen coal is:

$$Q_2' = \frac{C\delta mV_1}{n}\left(\left(L-2L_H\right) - \frac{v_2}{n}\left(e^{-nL_H/v_2} - e^{-n(L-L_H)/v_2}\right)\right) \tag{3-6-10}$$

where: Q_2——the relative gas emission rate of mined and fallen coal, m^3/t;

the absolute gas emission rate of mined and fallen coal:

$$Q_2 = \frac{C\delta uV_1}{n}\left(\left(L-2L_H\right) - \frac{v_2}{n}\left(e^{-nL_H/v_2} - e^{-n(L-L_H)/v_2}\right)\right) \tag{3-6-11}$$

3.6.3 Gas emission volume of residual coal in goaf

Hypothetically residual coal is evenly distributed among goaf and the coal wall in the working face, and then on the opposite direction of mining, the absolute gas emission volume of residual coal is:

$$Q_3 = \int_0^{l_1+l_2} V_3 dA \tag{3-6-12}$$

where: Q_3——accumulative gas emission volume of residual coal in goaf, m^3/min;

V_3——gas emission intensity of residual coal in goaf after it stays in the working face for the time of t, m^3/(t·min);

l_1——distance between coal wall of the working face to rear hydraulic support, m;

l_2——width of unstable goaf gas area opposite the mining direction, m;

Assume that the weight of mined and fallen coal of the infinitesimal length dx of opposition of mining direction is dA, and then:

$$dA = (1-C)\cdot \delta m (L-2L_H)dx \tag{3-6-13}$$

put equation (3-6-1) and equation (3-6-13) into equation (3-6-12), then simplify the integrals:

$$Q_3 = \int_0^{l_1+l_2} V_1 e^{-nt_3}\cdot (1-C)\delta m (L-2L_H)dx \tag{3-6-14}$$

where: t ——effective duration of stay of residual coal in goaf, min; $t = xu$

u ——the average mining speed of the working face, in;

Simplify the integrals, and then the absolute gas emission volume of residual coal:

$$Q_3 \frac{\delta V_1 (1-C)(L-2L_H)mu}{n}\left(1-e^{-\frac{l_1+l_2}{u}n}\right) \tag{3-6-15}$$

where: Q_3—— absolute gas emission volume of residual coal, m^3/t;

3.6.4 Gas emission volume of the adjacent layers

With the float tendency of coal mining, gas emission of the adjacent layers is consistent of the exploitation layer. Gas emission volume is proportional to the thickness of the adjacent layers. As a consequence, the gas emission volume of the adjacent layers is shown as follows:

$$Q_4 = Q_1 \cdot \sum m_i \cdot \eta_i / m \tag{3-6-16}$$

where: Q_4—— gas emission volume of the adjacent layers, m^3/min:

Q_1——gas emission volume of the coal wall of the exploitation layer, m^3/min;

$\sum m_i$——total thickness of the upper and lower adjacent layers, m;

η_i——gas emission coefficient of the adjacent layers;

m——thickness of the exploitation layer, m.

In gently inclined coal seams, the emission range of gas in the adjacent layers is about 1/2 of the length of the working face (in the upper half of the exploitation layer), and 1/3 of the length of the working face (in the lower half of the exploitation layer). Within the range the gas emission volume of the adjacent layers is inversely proportional to the interlayer space. As a result, gas emission coefficient of the adjacent layers can be calculated as follows:

upper adjacent layer: $\eta_s = 1 - \frac{h}{0.50B}$

lower adjacent layer: $\eta_x = 1 - \frac{h}{0.33B}$

where: η_s and η_x ——gas emission coefficient of the upper and lower adjacent layers respectively;

h——interlayer space of the exploitation layer and adjacent layers (weighted average) m;

B——length of the working face, m.

When there is shale in the upper and lower adjacent layers, a certain amount of gas will be emitted, the thickness calculation of sandy shale and carbonaceous shale will take one fourth and one third.

3.6.5 Gas emission volume of the working face

As is mentioned above, the gas emission of the working face consists of four parts - gas emission of the coal wall, gas emission of the fallen coal, gas emission of goaf and gas emission of the adjacent layers. Therefore, the gas emission volume of the working face is:

$$Q = Q_1 + Q_2 + Q_3 + Q_4 \tag{3-6-17}$$

where： Q—— gas emission volume of the working face, m^3/t.

3.7 Prediction of gas emission volume of the working face of Shaqu coal mine

3.7.1 Mining conditions of the working face

According to the mining deploy of Shaqu Mine, the mining method is confirmed as the comprehensive mechanization of inclined longwall retrieving with full caving. Therefore, the prediction of the coal mine is mainly based on the working face of a full mining height. Measurement of gas emission volume of the working face is also made. The 14205 working face is taken as an example for the prediction of gas emission volume. Table 3.7.1 and Table 3.7.2 reveal the mining factors of the 14205 working face.

Table 3.7.1 Outcomes of cycle number per day and advance rate per year of the 14205 working face

The length of working face (m)	200
Mining height (m)	2.45
circulation time (min)	160
cycle number per working time	3
Yield of the each work (t)	1148
cycle number per day (t)	6
Yield of the each day (t)	2296
Yield of the each year (Mt)	160
advance rate per year (m)	1296

Table 3.7.2 Mining technical data of Shaqu coal mine

The length of working face (m)	200
Mining height (m)	2.45
Excavate height (m)	2.45
Mining rate (%)	95
Mining speed (m/d)	3.6
Dig depth of coal cutter (m)	0.6
The speed of coal cut (m/min)	5
Density of coal (t/m3)	1.37

3.7.2 Prediction of gas emission volume of the working face

The prediction model of gas emission volume is established for the 14205 working face of Shaqu coal mine. The prediction outcomes are shown in Table 3.7.3.

Table 3.7.3 Prediction of gas emission volume of the working face of Shaqu coal mine

The length of the	Mining height (m)	Gas emission rate (m3/min)				
		Coal wall	Adjacent	Mined coal	Loss coal	Total

working face (m)			layer			
200	2.45	35.72	56.08	9.16	1.85	102.81
Proportion (%)		34.74	54.55	8.91	1.80	100

3.8 Measurement and calculation of gas emission of the working face

3.8.1 Measurement of gas emission volume of the working face

In working time and non-working time under the circumstance of regular production, air speed, and air volume and gas concentration of the tail roadway of gas are repeatedly measured. The measured data of ventilation air methane emission volume and gas drainage volume in working time of the 14205 working face is presented separately in Table 3.8.1 and Table 3.8.2

Table 3.8.1 Measurement of ventilation air methane emission volume of the 14205 working face in working time

Date	Gas emission rate of the belt gateway of air outlet (m^3/min)	Gas emission rate of crossheading No.11 (m^3/min)	Gas emission rate of crossheading No.12 (m^3/min)	Gas emission rate of induced pipe in upper corner (m^3/min)	Gas emission rate of the induced pipe in goaf (m^3/min)
8.24	11.82	18.59	11.75	11.55	1.28
8.25	13.82	19.82	14.33	12.14	1.12
8.26	14.12	20.89	13.57	11.99	1.23
8.27	13.88	20.89	13.57	11.99	1.23
8.28	16.07	20.75	10.64	12.42	1.23
8.29	13.36	20.15	11.05	11.71	1.19
8.30	16.67	21.82	12.58	11.32	1.21
8.31	15.32	19.85	11.79	12.71	1.34
9.10	13.23	19.73	14.25	12.68	1.21
9.20	15.22	22.49	10.43	12.37	1.24

9.30	12.62	20.77	11.22	10.24	1.25
9.40	11.71	17.73	11.93	12.23	1.24
9.50	14.38	19.95	12.69	12.38	1.26
9.60	11.39	21.49	13.26	12.52	1.35

Table 3.8.2 Measurement of gas drainage volume of the 14205 working face in working time

Date	Gas of tail roadway (m^3/min)	Gas drainage volume of high level tunnel (m^3/min)	Gas drainage volume of in seam (m^3/min)	Kilometers gas drainage tunnel (m^3/min)
8.24	21.04	12.67	4.52	0.78
8.25	23.67	15.23	5.13	0.71
8.26	18.42	15.02	3.53	0.89
8.27	18.41	14.57	3.67	0.73
8.28	18.73	13.97	4.72	0.75
8.29	18.89	15.84	4.35	0.64
8.30	16.81	15.86	3.81	0.44
8.31	19.46	15.76	3.92	0.38
9.10	15.46	14.67	4.22	0.77
9.20	17.91	13.97	4.01	0.71
9.30	19.15	14.57	3.68	0.57
9.40	18.17	14.57	3.92	0.68
9.50	17.54	10.96	4.36	0.57
9.60	19.89	14.24	4.64	0.76

By the calculation of the above data, during in working time, the average ventilation gas drainage amount of the 14205 working face of Shaqu coal mine is 59.90 m^3/min, the gas drainage volume is 38.09 m^3/min，and the total amount is 97.99 m^3/min.

The measured data of ventilation air methane emission volume and gas drainage volume in non-working time of the 14205 working face of Shaqu coal mine is presented separately in Table

3.8.3 and Table 3.8.4.

Table 3.8.3 Measurement of ventilation air methane emission volume of the 14205 working face in non-working time

Date	Gas emission rate of the belt gateway of air outlet (m^3/min)	Gas emission rate of crossheading No.11 (m^3/min)	Gas emission rate of crossheading No.12 (m^3/min)	Gas emission rate of induced pipe in upper corner (m^3/min)	Gas emission rate of the induced pipe in goaf (m^3/min)
8.24	8.74	16.48	8.70	5.81	0.89
8.25	7.98	17.23	7.49	6.12	0.92
8.26	9.85	17.30	8.91	7.18	0.94
8.27	11.85	17.28	10.32	7.32	0.88
8.28	12.15	16.68	11.85	7.51	0.92
8.29	11.91	18.36	11.20	7.48	0.93
8.30	12.83	14.92	11.96	7.03	0.91
8.31	13.35	16.35	12.53	6.35	0.87
9.10	11.26	17.42	11.06	6.94	0.96
9.20	14.10	18.02	13.52	6.79	0.80
9.30	11.39	16.38	11.02	7.04	0.98
9.40	14.70	15.96	13.58	7.17	0.96
9.50	13.25	19.02	12.84	7.04	1.02
9.60	10.95	13.26	9.46	7.22	0.79

Table 3.8.4 Measurement of gas drainage volume of the 14205 working face in non-working time

Date	Gas of tail roadway (m^3/min)	Gas drainage volume of high level tunnel (m^3/min)	Gas drainage volume of in seam (m^3/min)	Kilometers gas drainage tunnel (m^3/min)
8.24	17.68	15.33	5.08	0.70
8.25	17.68	14.14	3.55	0.64

8.26	18.16	14.27	3.53	0.83
8.27	19.16	13.54	3.41	0.64
8.28	19.16	13.54	3.52	0.69
8.29	22.94	15.41	4.22	0.58
8.30	17.69	15.43	4.01	0.38
8.31	16.08	14.14	3.98	0.32
9.10	18.73	14.14	3.92	0.64
9.20	14.73	10.53	4.56	0.64
9.30	17.18	12.24	4.64	0.51
9.40	18.42	14.80	4.79	0.52
9.50	17.44	14.59	4.35	0.51
9.60	16.81	13.81	4.11	0.64

By the calculation of the above data, during non-working time, the average the average ventilation gas drainage amount of the 14205 working face of Shaqu Mine is 47.37 m^3/min, the gas drainage volume is 36.69 m^3/min，and the total amount is 84.06 m^3/min.

3.8.2 Calculation of gas emission volume in coal wall and goaf

As gas emission is complicated and goaf is inaccessible, gas emission volume cannot be directly measured, thus an indirect method is adopted for the measurement.

In working time under the circumstance of regular production, the measurement points are evenly arranged between the coal wall of air outlet and support of working face. The measurement method consists of five steps. Firstly, the gas concentration of each point are measured; secondly the lowest point is found; thirdly, the distance between lowest measured point of gas concentration to the coal wall and goaf is measured; fourthly, the data is processed and plotted graph; finally gas emission volume in goaf is calculated by graphing method.

Three sets of measuring points are arranged (20m, 30m and 40m from coal wall to goaf) along the return airway of the working face, of which the arrangement of 1 set of measuring points are shown in Figure 3.8.1. Gas concentration is measured repeatedly as Table 3.8.5, Table 3.8.6

and Table 3.8.7 presents, and Figure 3.8.2 is drawn through data process, based on which the proportion of gas emission from coal wall and goaf in the total amount of gas of the working face is obtained.

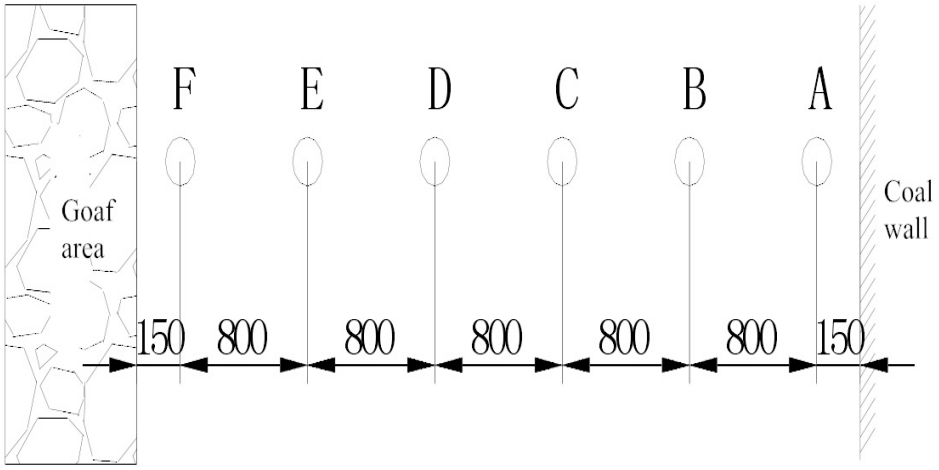

Figure 3.8.1 Layout diagram of measuring points in coal wall and goaf of the working face

Table 3.8.5 Test data of measuring points in coal wall and goaf of the working face (14/08/2012)

Data	Measured point	No.	Point A CH_4%	Point B CH_4%	Point C CH_4%	Point D CH_4%	Point E CH_4%	Point F CH_4%
14/ 08/ 2012	20m from the belt roadway of air outlet	1	0.72	0.58	0.48	0.60	0.84	0.94
		2	0.69	0.60	0.50	0.61	0.80	0.92
		3	0.66	0.62	0.52	0.60	0.76	0.88
	30m from the belt roadway of air outlet	1	0.70	0.64	0.62	0.66	0.70	0.79
		2	0.67	0.65	0.60	0.67	0.70	0.79
		3	0.66	0.65	0.61	0.70	0.70	0.79
	40m from the belt roadway of air outlet	1	0.62	0.54	0.52	0.55	0.60	0.62
		2	0.60	0.53	0.49	0.56	0.61	0.64
		3	0.58	0.49	0.52	0.56	0.60	0.63

Table 3.8.6 Test data of measuring points in coal wall and goaf of the working face (15/08/2012)

Data	Measured point	No.	Point A CH_4%	Point B CH_4%	Point C CH_4%	Point D CH_4%	Point E CH_4%	Point F CH_4%

15/ 08/ 2012	20m from the belt roadway of air outlet	1	0.68	0.64	0.62	0.62	0.66	0.96
		2	0.66	0.62	0.60	0.65	0.69	0.98
		3	0.67	0.60	0.64	0.63	0.67	0.99
	30m from the belt roadway of air outlet	1	0.77	0.73	0.73	0.76	0.80	0.86
		2	0.78	0.73	0.70	0.68	0.76	0.87
		3	0.78	0.74	0.73	0.61	0.70	0.90
	40m from the belt roadway of air outlet	1	0.72	0.66	0.60	0.66	0.66	0.83
		2	0.70	0.68	0.68	0.64	0.72	0.82
		3	0.68	0.65	0.65	0.62	0.78	0.81

Table 3.8.7 Test data of measuring points in coal wall and goaf of the working face (16/08/2012)

Data	Measured point	No.	Point A CH_4%	Point B CH_4%	Point C CH_4%	Point D CH_4%	Point E CH_4%	Point F CH_4%
16/ 08/ 2012	20m from the belt roadway of air outlet	1	0.64	0.62	0.60	0.66	0.68	0.77
		2	0.61	0.61	0.59	0.66	0.67	0.77
		3	0.58	0.59	0.57	0.65	0.66	0.77
	30m from the belt roadway of air outlet	1	0.59	0.59	0.53	0.50	0.65	0.70
		2	0.60	0.58	0.55	0.54	0.62	0.70
		3	0.60	0.57	0.57	0.58	0.62	0.69
	40m from the belt roadway of air outlet	1	0.55	0.52	0.55	0.53	0.50	0.56
		2	0.53	0.52	0.51	0.50	0.53	0.58
		3	0.54	0.52	0.47	0.46	0.56	0.60

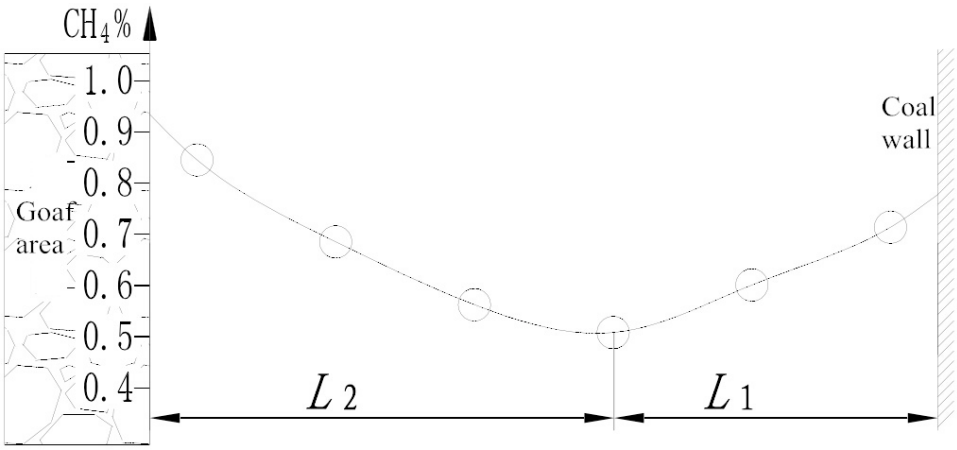

Figure 3.8.2 Distribution diagram of gas concentration at cross section of the working face

It can be clearly seen from the figure that the proportion of gas emission from the goaf to the working face is:

$$K_l = \frac{L_1}{L_1 + L_2} = \frac{2390}{4300} = 59.3\%$$

The proportion of gas emitted from coal wall:

$$K_l = \frac{L_1}{L_1 + L_2} = \frac{1750}{4300} = 40.7\%$$

Based on the ratio above, the gas emission volume of the 14205 working face can be estimated. The average gas emission volume of the 14205 working face during production is 84.06m^3/min, while gas emitted from goaf and from the coal wall are $84.06 \times 59.3\% = 49.85 m^3/\min$ and $84.06 \times 40.7\% = 34.21 m^3/\min$ respectively.

3.8.3 Gas emission calculation from mined and fallen coal in the working face

The gas emission amount of mined and fallen coal is affected by many factors such as the duration in the working face and limitation of working field, and it is difficult to measure the gas emission amount from the mined and fallen coal. Therefore, it could be calculated by the following equation:

$$Q_{fallen} = Q_{\min ed} + Q_{un-\min ed}$$

Q_{fallen}——the gas emission amount of working face fallen coal, m^3/min;

$Q_{\min ed}$ ——total gas emission amount of the working face during the working time, m^3/min;

$Q_{un-\min ed}$ ——total gas emission amount of the working face during the non-working time, m^3/min.

Specifically, Q_{fallen} not only come from the fallen coal, but also from the gas emission difference between new exposure coal wall and the old exposure coal wall, the gas emission difference between working time and non-working time. Actually, the calculated value will more than the actual value, and the actual value is affected by my factors such as time measurement duration in non-working time, the operation condition of coal cutter in working time, measured point and the fault of survey crew. Therefore, the calculated value of Q_{fallen} greatly fluctuate by many factors, and it only can be used as reference value. The calculated gas emission amount of mined and fallen coal is 14.48 m^3/min; it can be seen in Table 3.8.8

Table 3.8.8 Calculation of gas emission volume of fallen coal

Date	The gas emission rate in working time (m^3/min)	The gas drainage rate in working time (m^3/min)	The gas emission rate in non-working time (m^3/min)	The gas drainage rate in non-working time (m^3/min)	The gas emission calculation value (m^3/min)
8.24	54.99	39.01	40.62	38.79	14.59
8.25	61.23	39.74	44.74	36.01	20.22
8.26	61.80	37.86	44.18	36.79	18.69
8.27	58.26	37.38	47.65	36.75	11.24
8.28	61.11	38.17	49.11	36.91	13.26
8.29	57.46	39.72	49.88	36.15	11.15
8.30	63.61	36.92	47.65	37.51	15.37
8.31	61.01	39.52	49.45	34.52	16.56
9.10	61.10	35.12	47.64	37.43	11.15
9.20	61.75	36.60	53.23	30.46	14.66
9.30	56.01	37.97	46.81	34.57	12.69

9.40	53.84	37.34	42.37	38.53	10.28
9.50	60.66	33.43	53.17	30.89	10.03
9.60	60.01	39.53	41.68	35.37	22.49

3.8.4 Calculation of gas emission volume of upper and lower adjacent layers

Coal seams that are affected by the mining activity of the adjacent layers will emit gas into the working face and goaf of the exploiting layer. Based on the location with the exploiting layer, adjacent layers can be divided into upper adjacent layer and lower adjacent layer. The gas emission volume of the adjacent layers depends on the gas content, thickness and number of the adjacent layers, height of the exploiting layer and gas emission rate of the adjacent layers.

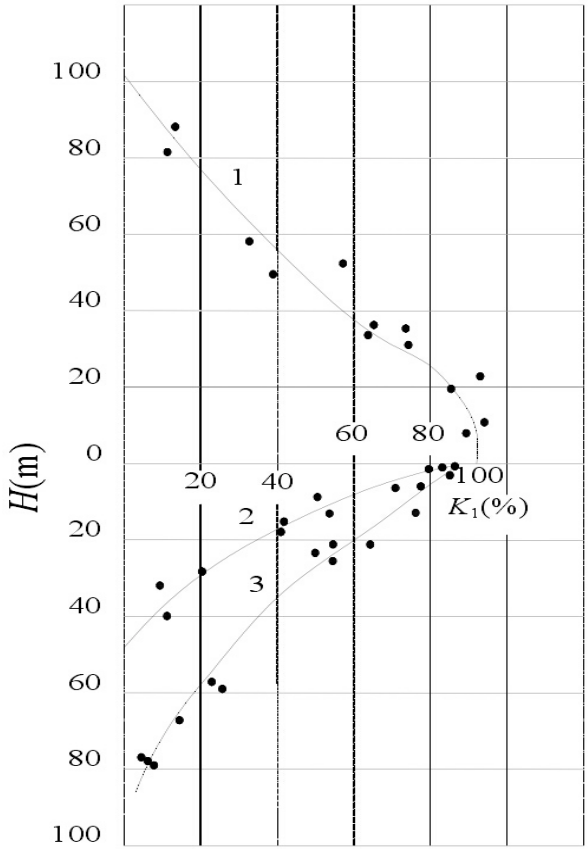

Figure 3.8.3 Curve of gas emission of different space among adjacent layers

1-upper adjacent layer; 2- lower adjacent layer of gently inclined coal seam; 3- lower adjacent layer of steeply inclined coal seam

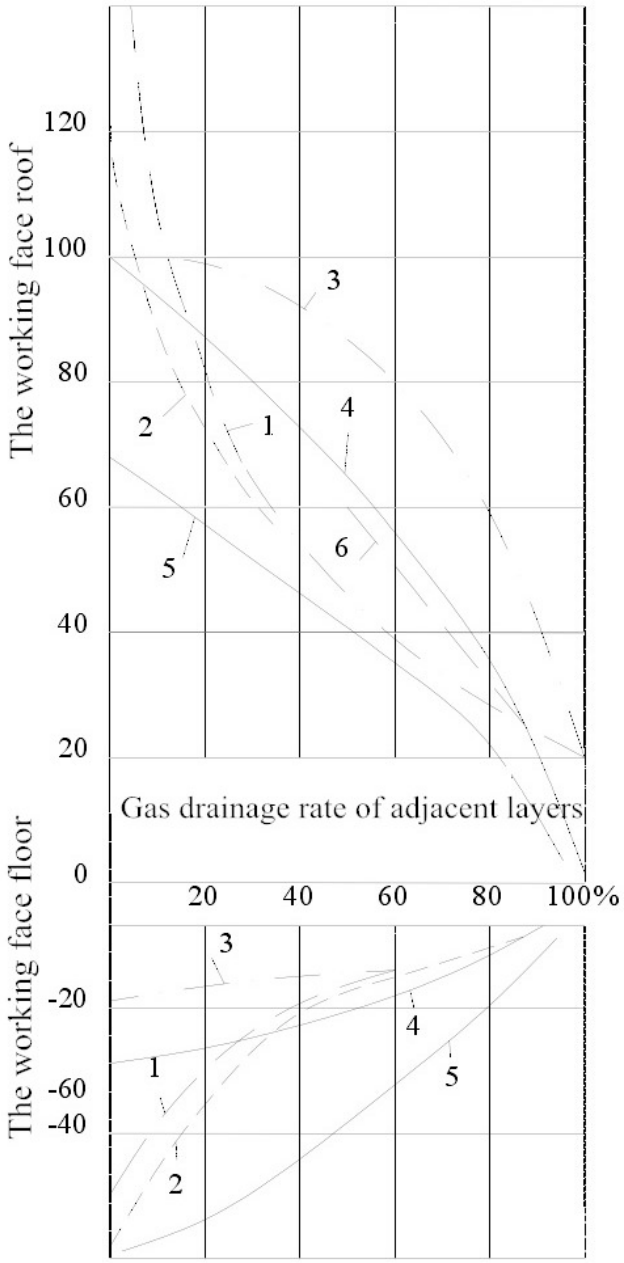

Figure 3.8.4 Relation curve of gas emission rate and interlayer space of adjacent layers

1- Dr Venter curve; 2- Christopher Ken curve; 3- Sue ritz curve; 4- Kim lee curve (horizontal layers); 5- Kim lee curve（inclination 70°; 6- Biqiuke curve (M=1m)

$$q_2 = \sum_{i=1}^{n} \frac{m_i}{M} \cdot k_i \cdot X_{0i} \qquad (3\text{-}8\text{-}1)$$

The formula of gas emission volume of adjacent layers is:

where: q_2—— gas emission volume of adjacent layers, m^3/t;

m_i——thickness of the adjacent layer i, m;

M ——mining height, m;

n ——number of adjacent layers;

X_{0i} ——original gas content of adjacent layer i, m^3/t;

k_i ——gas emission rate of adjacent layers i, %。

Values can be selected through the following method based on the mining thickness.

If the mining height is in the low and middle seam condition (lower than 4.5m), the gas drainage rate of the adjacent layer can be selected based on Figure 3.8.3. This practical and effective figure is obtained by the field measured results of three Chinese large mining areas (Yangquan mining area, Beipiao mining area and Huainan mining area). Similarly, the gas drainage rate of the adjacent layer can also be selected based on other method, such as Figure 3.8.4. If the mining seam height is higher than 4.5m, the upper adjacent layer will be significantly affected by adapted roof coal mining method. Thus, the gas emission amount will be sharply increased because the decompression of the adjacent layer is exacerbated. Taking many research results into account, and computational formula of the high-seam gas drainage rate can be obtained by determining the relation between gas drainage rate k_i and mining height M, length of working face L and interlayer spacing H:

$$k_i = 100 - 0.47\frac{H}{M} - 84.04\frac{H}{L} \tag{3-8-2}$$

When adjacent layers are rich of gas, the gas emission q of the adjacent layers can be obtained through the formula below:

$$q_2 = k_4\left(\sum_{i=1}^{n} Lvm_i\gamma_i X_i k_i + \sum_{i=1}^{n} Q_i\right) \tag{3-8-3}$$

Where: q_2 —— gas emission of adjacent layers that are rich of gas, m^3/t;

k_4 ——influence coefficient of gas drainage in adjacent layers, with drainage k_4=1.2, without drainage k_4=1;

L —— length of the working face, m;

v ——average mining speed per day in the working face, m/d;

m_i ——thickness of adjacent layer i, m;

γ_i ——density of adjacent layer i, t/m^3;

X_i ——gas content of the adjacent layer, m^3/t;

Q_i ——average gas emission of adjacent layers i, m^3/d;

k_i ——gas emission rate of adjacent layers i, %;

A ——daily output in the working face, t

Combined with the actual production conditions of Shaqu Mine, the gas emission of the adjacent layers in the working face of Shaqu Mine is 56.54 m^3/min based on Formula 3-8-3.

3.9 Comparison of prediction and measured data in working face

Prediction values are verified and compared with actual measurement values of gas emission in the working face, and the prediction error is as below:

$$\delta = \frac{q_y - q_s}{q_s} \times 100\% \tag{3-9-1}$$

where: δ ——predicted relative error;

q_y ——prediction value of gas emission;

q_s ——actual measurement values of gas emission.

$$\delta = \frac{102.81 - 97.99}{97.99} \times 100\% = 4.92\%$$

It can be observed from the results that the error of the gas emission prediction in the working face is less then 10%. It shows that the prediction measurement of gas emission in the working face is quite close to the actual measurement and owns high accuracy

Table 3.9.1 Prediction of gas emission and output of the 14205 working face of Shaqu coal mine

Mining height (m)	Schedule of mining (m)	Production of mining (m)	Gas emission rate (m^3/min)				
			Coal wall	Adjacent layer	Mined and fallen coal	Remaining coal	Total
2.45	1296	0.837	35.72	56.08	9.16	1.85	102.81
2.45	1512	0.976	41.65	65.39	10.78	2.06	119.88

2.45	1728	1.117	48.63	77.78	12.41	2.27	141.09
2.45	1944	1.256	53.56	89.09	13.93	2.57	159.15
2.45	2160	1.396	61.53	100.46	15.96	2.78	180.33
2.45	2376	1.535	68.11	110.77	16.78	3.04	197.40
2.45	2592	1.675	74.44	114.66	18.31	3.20	210.40
2.45	2808	1.814	77.37	116.97	19.83	3.50	218.67
2.45	3024	1.954	79.85	119.86	20.36	3.81	223.88

Taking into account the uneven factor of gas emission in the working face always reaches 20%, it is considered that the prediction accuracy can totally meet the design and production requirements, and also indicates that the method is fully credible and feasible for the prediction of gas emission in the working face of Shaqu Mine. Prediction result of gas emission is made under the different circumstances of exploitation as is shown in Figure 3.9.1 and Table 3.9.1.

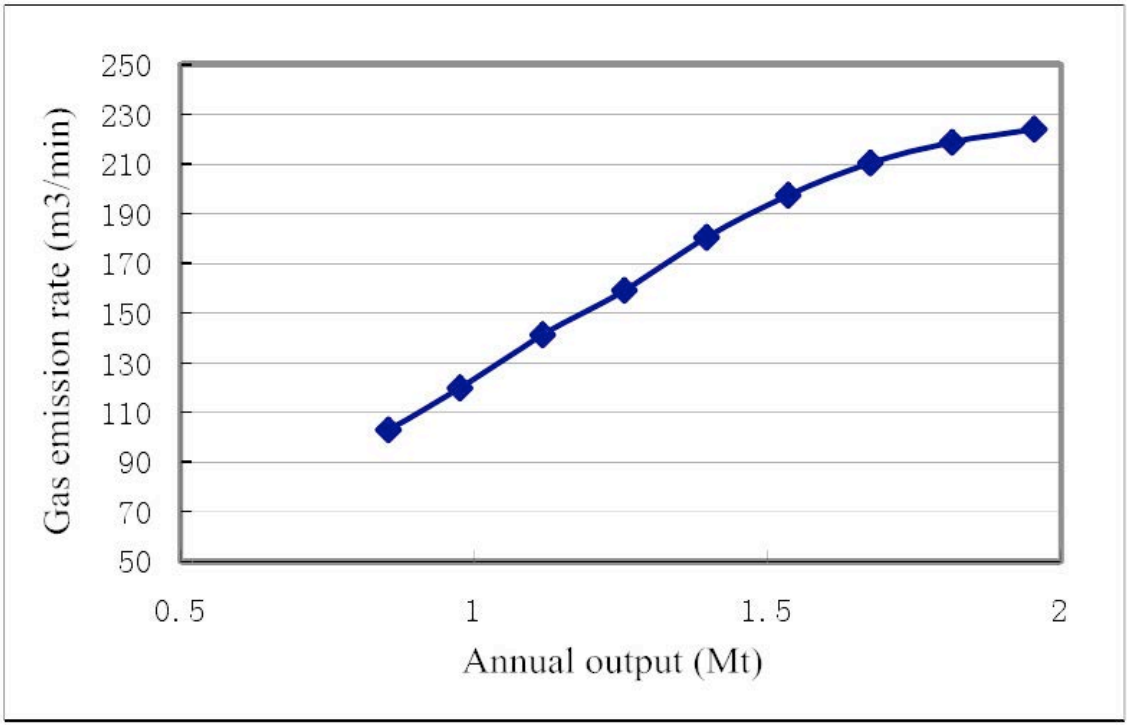

Figure 3.9.1 Prediction curve of gas emission and output of the 14205 working face of Shaqu coal mine

3.10 Chapter conclusion

This chapter identifies the emission sources in the working face of Shaqu Mine, studies the gas emission rules of each emission source, and obtains the prediction model of gas emission in the working face of Shaqu Mine. It also compares the predictive values and measured values of the amount of gas emission, and then comes to the conclusion that this gas prediction method is feasible. Finally, in order to improve the gas management and guidance in the working face, the gas emission rate under different situations (different mining schedule, output, etc.) are predicted by using the gas prediction method mentioned above.

4 Numerical simulation research on ventilation system and gas disaster prevention and control

4.1 Overview

This chapter describes contents concerning the numerical modeling used to establish the ventilation system and longwall goaf. The first part provides a brief overview of the application of numerical simulation technique in mineral industry, and analyzes the necessity of numerical simulation. The second part offers an introduction to the theoretical basis of numerical simulation technique and the application of the CFD software. The last part discusses the establishment of the numerical simulation model of the 14205 working face and goaf of Shaqu coal mine as well as the analysis of the experimental findings.

4.1.1 The necessity of the application of numerical simulation technique in mineral industry

Coal mine gas issues have created severe difficulties in the mining industry and environment protection around the world, and led to high expenditures, intense research efforts and determined attempts to enhance the various ventilation and gas drainage techniques (Leszek and Lunarzewski, 1998). The release of a large number of harmful gases by mine working face and goaf, the worst-hit area of mine strata problems, is the cause of mine safety problems, serious accidents, many casualties and greenhouse effect (Joseph et al., 2011). As a result, safety mining technologies including field investigation, numerical simulation and laboratory test have been improved over the past decades as experts around the world are paying more attention to the rules of gas emission and outburst in mine working faces and goaf (Russell et al, 2011). However, it is still extremely difficult to precisely observe gas movement in ventilation system, upper corner, working face and goaf, and effectively predict process behavior under different situations and constraints in fieldwork (Widodo et al., 2008; Gauti et al., 2012). In order to refine the knowledge and reference of coal mine gas distribution rule, ensure the safety production, and create a chance of high production, a numerical model with a CFD code has been established in the simulation laboratory. This model is based on the practical condition of high gas occurrence characteristics of

working face No.14205 of Shaqu coal mine in Shanxi province, China. By simulating and comparing two different types of ventilation systems (U-type and U+L-type), the gas movement rule in the strata and goaf is determined. Therefore, the results of the experiments offer meaningful and valuable references for the placement selection of gas drainage borehole, as well as providing a feasible solution for the comprehensive treatment of mine safety.

4.1.2 The application of numerical simulation technique in mineral industry

CFD modeling has been used in the mining and energy environment since the 1990s, including gas and spontaneous heating control (Creedy and Clarke, 1992), mine fires and explosions (Woodburn and Britter, 1996), methane control (Jazbec et al., 2000), ventilation velocity in tunnel fires (Hwang and Edwards, 2005), gas emissions and goaf gas (Karacan et al, 2007), controlling longwall goaf heating (Ren and Balusu, 2009; Taraba and Michalec, 2011), and gas behaviors in auxiliary ventilation of mining headings (Torno et al, 2013). Gas flow rule in coal mine is a complicated process due to numerous factors are involved, including ventilation system layout, gas concentration, emission rate and compositions, working face orientation and dip, gas buoyancy and goaf permeability. Lately, a large number of CFD models have been established to achieve further understanding of gas flow mechanics, characteristic and distribution rules in mine working face and goaf. A commercial CFD code called FLUENT contains broad physical modeling capabilities needed to model flow, turbulence, heat transfer, and reactions for industrial applications ranging from air flow over an aircraft wing to combustion in a furnace, from bubble columns to oil platforms, and from clean room design to waste water treatment plants.

4.2 Theoretical basis of computational fluid dynamics (CFD)

The development of computational fluid dynamics (CFD) software took off with the increase in computational power in the latter part of the 20th century (Ohba, 2010). The description of fluid flows with differential equations had been described by the early 19th century, but the nonlinear behavior of these equations meant that solutions for any type of general, compressible flow field was impossible until using finite volume numerical techniques became practical (Talay et al., 2004). This fluid flow description is based on equations describing the conservation of mass,

momentum, species, and energy for fluid flow (Andrei et al., 2013). This theory is well established and FLUENT is one of many software packages that provide tools for solving real problems with discretization of the standard conservation equations (Cao, 2008). The following sections give a brief description of how this process is done. The book Chemically Reacting Flow (Kee et al., 2003) and the Theory Guide published by ANSYS (ANSYS, 2010) were relied on heavily for the following chapter.

4.2.1 Substantial derivative

Before beginning the physical description of fluid flow, it is useful to briefly review the substantial derivative. The substantial derivative of a vector is defined as:

$$\frac{DV}{Dt} = \frac{\partial V}{\partial t} + V \cdot (\nabla V) \tag{4-2-1}$$

For the velocity vector with three components in Cartesian coordinates,

$$V = ue_x + ve_y + we_z \tag{4-2-2}$$

This becomes a series of three equations:

$$\frac{Du}{Dt} = \frac{\partial u}{\partial t} + u\frac{\partial u}{\partial x} + v\frac{\partial u}{\partial y} + w\frac{\partial u}{\partial z} \tag{4-2-3}$$

$$\frac{Dv}{Dt} = \frac{\partial v}{\partial t} + u\frac{\partial v}{\partial x} + v\frac{\partial v}{\partial y} + w\frac{\partial v}{\partial z} \tag{4-2-4}$$

$$\frac{Dw}{Dt} = \frac{\partial w}{\partial t} + u\frac{\partial w}{\partial x} + v\frac{\partial w}{\partial y} + w\frac{\partial w}{\partial z} \tag{4-2-5}$$

4.2.2 Conservation of mass

All fluid flows must obey the law of conservation of mass. If a control volume of fluid is considered, mass must neither be created nor destroyed within this volume, meaning the change in mass of the control volume must be equal to the mass entering or leaving the control volume (Kee et al., 2003).

$$\left(\frac{dm}{dt}\right)_{system} = \int_{CV}\left(\frac{\partial \rho}{\partial T} + \nabla \cdot \rho V\right)dV = 0 \tag{4-2-6}$$

This can be written in differential form, Equation (4-2-7), if the control volume is considered differential; i.e. small enough that the integrand is constant over the volume.

$$\frac{\partial \rho}{\partial t} + \nabla \cdot \rho V = 0 \tag{4-2-7}$$

The $\frac{\partial \rho}{\partial t}$ term corresponds to the change in mass (density) in the control volume over time. The $\nabla \cdot \rho V$ term is related to the mass carried in and out of the control volume by the velocity field. Using the chain rule, Equation (4-2-7) can be written as Equation (4-2-8).

$$\frac{\partial \rho}{\partial t} + \rho \nabla \cdot V + V \cdot \nabla \rho = 0 \tag{4-2-8}$$

For clarity, Equation (4-2-8), when written in terms of Cartesian coordinates with the velocity vector defined as $V = ue_x + ue_y + ue_z$, is shown in long form in Equation (4-2-9).

$$\frac{\partial \rho}{\partial t} + u\frac{\partial \rho}{\partial x} + v\frac{\partial \rho}{\partial y} w\frac{\partial \rho}{\partial z} + \rho\frac{\partial u}{\partial x} + \rho\frac{\partial v}{\partial y} + \rho\frac{\partial w}{\partial z} = 0 \tag{4-2-9}$$

For incompressible flows this can be simplified. However, in this case, with the flow through porous media creating fairly large pressure gradients, the full variable density form of the conservation of mass must be considered.

4.2.3 Navier stokes

The equations of conservation of momentum for fluid flow are better known as Navier-Stokes. The conservation of momentum, states that the change in momentum over time must be equal to the sum of forces on the fluid. The vector P represents the momentum of a system,

$$\frac{dP}{dt} = \sum F \tag{4-2-10}$$

In fluid mechanics, the Reynolds transport theorem must be used to convert the momentum conservation of a system, that is, a fixed amount of mass, to momentum conservation with regards to a control volume fixed in space. Using the substantial derivative to simplify, Equation (4-2-10) can be written as Equation (4-2-11) (Kee et al., 2003).

$$\rho\frac{DV}{Dt} = \sum F_{body} + \sum F_{surfaces} \tag{4-2-11}$$

Here it is useful to separate the body forces and forces acting on the surfaces of the control

volume. In all the models run in this project, gravity has been neglected. The sum of forces on the right hand side of Equation (4-2-11) then becomes:

$$\sum F = -\nabla p + \nabla \cdot T' \tag{4-2-12}$$

where T' is the stress tensor.

$$T' = \begin{pmatrix} \left[2\mu\frac{\partial u}{\partial x} + k\nabla\cdot V\right] & \mu\left(\frac{\partial u}{\partial y} + \frac{\partial v}{\partial x}\right) & \mu\left(\frac{\partial u}{\partial z} + \frac{\partial w}{\partial x}\right) \\ \mu\left(\frac{\partial y}{\partial x} + \frac{\partial u}{\partial y}\right) & \left[2\mu\frac{\partial v}{\partial y} + k\nabla\cdot V\right] & \mu\left(\frac{\partial v}{\partial z} + \frac{\partial w}{\partial y}\right) \\ \mu\left(\frac{\partial w}{\partial x} + \frac{\partial u}{\partial z}\right) & \mu\left(\frac{\partial w}{\partial y} + \frac{\partial v}{\partial z}\right) & \left[2\mu\frac{\partial w}{\partial z} + k\nabla\cdot V\right] \end{pmatrix} \tag{4-2-13}$$

The final results are the three Navier-Stokes equations (for a three dimensional flow field).

$$\rho\left(\frac{\partial u}{\partial t} + u\frac{\partial u}{\partial x} + u\frac{\partial u}{\partial y} + u\frac{\partial u}{\partial z}\right) = \frac{\partial p}{\partial x} + \frac{\partial}{\partial x}\left[2\mu\frac{\partial u}{\partial x} + k\nabla\cdot V\right] + \frac{\partial}{\partial y}\left[\mu\left(\frac{\partial u}{\partial y} + \frac{\partial v}{\partial x}\right)\right] + \frac{\partial}{\partial z}\left[\mu\left(\frac{\partial u}{\partial z} + \frac{\partial w}{\partial x}\right)\right] \tag{4-2-14}$$

$$\rho\left(\frac{\partial v}{\partial t} + u\frac{\partial v}{\partial x} + u\frac{\partial v}{\partial y} + u\frac{\partial v}{\partial z}\right) = \frac{\partial p}{\partial y} + \frac{\partial}{\partial x}\left[\mu\left(\frac{\partial v}{\partial x} + \frac{\partial u}{\partial y}\right)\right] + \frac{\partial}{\partial y}\left[2\mu\frac{\partial v}{\partial y} + k\nabla\cdot V\right] + \frac{\partial}{\partial z}\left[\mu\left(\frac{\partial v}{\partial z} + \frac{\partial w}{\partial y}\right)\right] \tag{4-2-15}$$

$$\rho\left(\frac{\partial u}{\partial t} + u\frac{\partial u}{\partial x} + u\frac{\partial u}{\partial y} + u\frac{\partial u}{\partial z}\right) = \frac{\partial p}{\partial z} + \frac{\partial}{\partial x}\left[\mu\left(\frac{\partial w}{\partial x} + \frac{\partial u}{\partial z}\right)\right] + \frac{\partial}{\partial y}\left[\mu\left(\frac{\partial w}{\partial y} + \frac{\partial v}{\partial z}\right)\right] + \frac{\partial}{\partial z}\left[2\mu\frac{\partial w}{\partial z} + k\nabla\cdot V\right] \tag{4-2-16}$$

4.2.4 Species conservation

Similar to the mass conservation law, molecules of individual species must not be created or destroyed within a control volume. Unlike the conservation of mass, species conservation has an exception; if a chemical reaction is occurring within the control volume, the concentration of different species may change within the volume. If the mole fraction of a species i is described by Y_i, then the conservation of species is described by Equation (4-2-17):

$$\rho\frac{DY_i}{Dt} = -\nabla\cdot J_i + R_i + S_i \tag{4-2-17}$$

where J_i the mass diffusion flux is vector (in units of $\left(\frac{mol}{m^2 \cdot s}\right)$), R_i is the mass rate of creation or destruction, and S_i is the surface adsorption mass rate for the control volume for a given species. Because the sum of all mass fractions must be 1, for N species a total of N—l equations must be solved. When the substantial derivative of Y_i is expanded, Equation (4-2-17) can be written as Equation (4-2-18).

$$\frac{\partial}{\partial t}\left(\rho Y_i\right) + \nabla \cdot \left(\rho V Y_i\right) = -\nabla J_i + R_i + S_i \tag{4-2-18}$$

In the work described in this thesis, chemical reactions are largely ignored. This means that the effects of spontaneous heating of coal within the gob and surrounding pillars are ignored. The description of the mass flux depends on whether flows are laminar or turbulent. For laminar flows,

$$J_i = -\rho D_{i,m} \nabla Y_i - D_{T,i} \frac{\nabla T}{T} \tag{4-2-19}$$

where $D_{i,m}$ is the mass diffusion coefficient, and $D_{T,i}$ is the thermal diffusion coefficient (ANSYS 2010). For turbulent flows, the mass diffusion flux is defined as

$$J_i = -\left(\rho D_{i,m} + \frac{\mu_t}{Sc_t}\right) \nabla Y_i - D_{T,i} \frac{\nabla T}{T} \tag{4-2-20}$$

where μ_t is the turbulent viscosity and Sc_t is the Schmidt number (A NSYS 2010). It is also critical to account for the transport of enthalpy in the mixing flows (ANSYS 2010). This energy transport is shown in Equation (4-2-21), where h_i is the enthalpy of species i.

$$\nabla \cdot \left(\sum_{i=1}^{N} h_i J_i\right) \tag{4-2-21}$$

In Cartesian coordinates, and assuming there are no reactions, the species transport equation can be written as:

$$\begin{aligned} &\frac{\partial\left(\rho k\right)}{\partial t} + \frac{\partial\left(\rho k u\right)}{\partial x} + \frac{\partial\left(\rho k v\right)}{\partial y} + \frac{\partial\left(\rho k w\right)}{\partial z} = \\ &\left[\rho D_{i,m}\left(\frac{\partial Y_i}{\partial x} + \frac{\partial Y_i}{\partial y} + \frac{\partial Y_i}{\partial z}\right) + D_{T,i}\frac{1}{T}\left(\frac{\partial T}{\partial x} + \frac{\partial T}{\partial y} + \frac{\partial T}{\partial z}\right)\right] \end{aligned} \tag{4-2-22}$$

4.2.5 Energy equation

In order to solve for species flow, as well as account for temperature changes caused by expansion and compression of fluids in the domain, the conservation of energy equation must be solved. The first law of thermodynamics states that energy of a system must be conserved. For a fluid flow, this is usually stated as: the change in energy of a system is equal to the heat added to the system plus the work done on or by the system. In equation form, this is written as

$$\frac{d\rho E_t}{dt} = \frac{dQ}{dt} + \frac{dW}{dt} \tag{4-2-23}$$

where E_t is the total energy of the system (usually in joules), Q is the heat added to the system, and W is the work done on the system (Kee et al., 2003). The total energy of the system is described in Equation (4-2-24),

$$E_t = \sum_{i=1}^{N} h_i Y_i - \frac{p}{\rho} + \frac{[V]^2}{2} \tag{4-2-24}$$

where p is the pressure. The relationship between a system and a control volume allows 4-2-23 to be written with the substantial derivative for fluid flows.

$$\rho \frac{DE_t}{Dt} = \frac{dQ}{dt} + \frac{dW}{dt} \tag{4-2-25}$$

FLUENT solves this equation for fluid flow in the form shown in Equation (4-2-26).

$$\frac{\partial}{\partial t}(\rho E_t) + \nabla \cdot (V(\rho E_t + p)) = \nabla \left(k_{eff,c} \nabla T - \sum_{i=1}^{N} h_i J_i + (T \cdot V) \right) + S_h \tag{4-2-26}$$

Here, the S_h term is a volumetric heat source, $k_{eff,c} \nabla T$ corresponds to conduction in the fluid, $\sum_{i=1}^{N} h_i J_i$ corresponds to enthalpy transfer by diffusion, and $T \cdot V$ corresponds to viscous dissipation by the flow field.

4.2.6 Turbulence modeling

Turbulent flow is defined by the highly irregular flow patterns that develop in high energy flows. Turbulent flows are chaotic, typically involve much faster mixing than laminar diffusion would allow, and characterized by rapid dissipation of the kinetic energy of the fluid as the kinetic

energy of the turbulence is converted into internal energy of the fluid (Tobias et al., 2012). In order to fully capture this chaotic behavior numerically would be prohibitively expensive, so a number of methods have been developed to solve for turbulent flows where eddies created by turbulence are treated on an average velocity basis (Jafari et al., 2015).

FLUENT offers a variety of turbulent model options, but the two-equation $k-\varepsilon$ models were used in this research. According to the FLUENT Users Guide (ANSYS, 2010), two-equation models are the most widely used turbulence models in industrial CFD, ANSYS (2010). The $k-\varepsilon$ turbulence models are offered in three variations: standard, RNG, and Realizable. The RNG (from renormalization group theory) $k-\varepsilon$ method provides some significant improvements over the standard $k-\varepsilon$ model, and is more accurate over a wider range of fluid flows than the standard version. The primary differences between the standard and RNG $k-\varepsilon$ models are described by ANSYS (2010):

The RNG model has an additional term in its ε equation that improves the accuracy for rapidly strained flows. The effect of swirl on turbulence is included in the RNG model, enhancing accuracy for swirling flows. The RNG theory provides an analytical formula for turbulent Prandtl numbers, while the standard $k-\varepsilon$ model uses user-specified, constant values. While the standard $k-\varepsilon$ model is a high-Reynolds-number model, the RNG theory provides an analytically derived differential formula for effective viscosity that accounts for low-Reynolds-number effects.

This is significant in the modeling of longwall panels because of the existence of both turbulent flows and laminar flows within the same computational domain (Yuan & Smith, 2008). In comparison runs, the standard $k-\varepsilon$ model gives significantly different results than the RNG solution. Because of the above reasons and the dependence of results on the turbulence model chosen, it is imperative that the RNG turbulence model be used. At this point, realizable $k-\varepsilon$ models have not shown a significant improvement over RNG models (ANSYS, 2010).

4.2.6.1 Description of $k-\varepsilon$ RNG models

All two-equation $k-\varepsilon$ models introduce the two transport equations for the variables k, the turbulent kinetic energy, and ε, the turbulent dissipation. These two values are then used to

calculate a turbulent viscosity, μ_t, that is added to the fluid's laminar viscosity in the Momentum and Energy equations. This adds two additional non-linear variables that must be solved at each iteration. The transport equations for the RNG method are given by:

$$\frac{\partial(\rho k)}{\partial t}+\frac{\partial(\rho k u)}{\partial x}+\frac{\partial(\rho k v)}{\partial y}+\frac{\partial(\rho k w)}{\partial z}= \frac{\partial}{\partial x}\left(\partial_k \mu_{eff}\frac{\partial k}{\partial x}\right)+\frac{\partial}{\partial y}\left(\partial_k \mu_{eff}\frac{\partial k}{\partial y}\right)+\frac{\partial}{\partial z}\left(\partial_k \mu_{eff}\frac{\partial k}{\partial z}\right)+G_K+G_b+\rho\varepsilon-Y_M+S_k \tag{4-2-27}$$

and

$$\frac{\partial(\rho\varepsilon)}{\partial t}+\frac{\partial(\rho\varepsilon u)}{\partial x}+\frac{\partial(\rho\varepsilon v)}{\partial y}+\frac{\partial(\rho\varepsilon w)}{\partial z}=\frac{\partial}{\partial x}\left(\partial_k \mu_{eff}\frac{\partial \varepsilon}{\partial x}\right) +\frac{\partial}{\partial y}\left(\partial_k \mu_{eff}\frac{\partial \varepsilon}{\partial y}\right)+\frac{\partial}{\partial z}\left(\partial_k \mu_{eff}\frac{\partial \varepsilon}{\partial z}\right)+C_{1\varepsilon}\frac{\varepsilon}{k}\left(G_k+C_{3\varepsilon}G_b\right)-C_{2\varepsilon}\rho\frac{\varepsilon^2}{k}-R_\varepsilon+S_\varepsilon \tag{4-2-28}$$

Using the definitions given by (ANSYS 2010), G_k represents the relationship between the turbulence kinetic energy to the mean velocity gradients, and is calculated as $G_k=\mu_t S^2\cdot S$ is the modulus of the shear rate-of-strain tensor, and is defined as $S=\sqrt{2S_{ij}S_{ij}}$ G_b S is the generation of turbulence kinetic energy due to buoyancy, but is zero when gravity is neglected. Y_M represents the contribution of the fluctuating dilation in compressible turbulence to the overall dissipation rate, and is neglected here. Y_M is defined as:

$$Y_M=2\rho\varepsilon M_t^2 \tag{4-2-29}$$

where the turbulent Mach number M_t is:

$$M_t=\sqrt{\frac{k}{a^2}} \tag{4-2-30}$$

where $a\equiv\sqrt{\gamma RT}$ is the speed of sound. In the speed of sound equation, γ is the adiabatic index and is defined as the ratio of specific heats of a gas at constant pressure and constant volume, $\gamma=C_p/C_v$. The values α_k and α_ε are the inverse Prandtl numbers for k and ε. S_k and S_ε are user defined source terms (not used in the efforts in this research project). $C_{1\varepsilon}=1.42$, $C_{2\varepsilon}=1.68$, and $C_v=100$ are constants. The turbulent viscosity ratio, $\hat{\nu}$, is

defined as:

$$\hat{\nu} = \frac{\mu_{eff}}{\mu} \tag{4-2-31}$$

For clarity, $\mu_{eff} = \mu + \mu_t$, where μ_t is the turbulent viscosity. The turbulent viscosity ratio $\hat{\nu}$ is described by the differential equation:

$$d\left(\frac{\rho^2 k}{\sqrt{\varepsilon\mu}}\right) = 1.72 \frac{\hat{\nu}}{\sqrt{\hat{\nu}^3 - 1 + C_\nu}} d\hat{\nu} \tag{4-2-32}$$

This allows for low Reynolds number effects to be taken into account, but using the differential definition of turbulent viscosity ratio requires that the 'Differential Viscosity Model' option is enabled in FLUENT. The term for R_ε is the primary difference between the RNG and standard $k-\varepsilon$ equations. It is given by:

$$R_\varepsilon = \frac{C\mu\rho\eta^3\left(1-\eta/\eta_0\right)}{1+\beta\eta^3}\frac{\varepsilon^2}{k} \tag{4-2-33}$$

where $\eta \equiv Sk/\varepsilon$, $S = \sqrt{2S_{ij}S_{ij}}$, $\eta_0 = 4.38$ and $\beta = 0.012$.

Treatment of friction losses at the walls is accomplished with the default standard wall functions. This is partly to reduce computational and meshing requirements over the very large domain, but also because near wall behaviors are not particularly significant to the results the group is interested in.

4.2.6.2 Turbulence boundary conditions

When using turbulence models, turbulent characteristics of the flow at the boundaries must be defined. The $k-\varepsilon$ models in ANSYS FLUENT allow for turbulent boundary conditions to be defined using one of three methods, each requiring two values to be set. They are:

- k and epsilon (set the $k-\varepsilon$ values directly)
- Turbulent Intensity and Hydraulic Diameter
- Turbulent Intensity and Length Scale

Turbulent Intensity and Hydraulic Diameter are primarily used for fully developed internal

flows, which did not apply here for the methane inlets. It is impossible to know k and ε at the boundaries before solving the flow field. As a result, the boundary conditions were set with Turbulent Intensity, I, and Turbulence Length Scale, l. ANSYS provides the following guidelines for estimating each:

$$I \equiv \frac{u'}{u_{avg}} \approx 0.16 \left(\mathrm{Re}_{D_H}\right)^{-1/8} \tag{4-2-34}$$

and

$$l = 0.07L \tag{4-2-35}$$

where L is the relevant geometric flow length (taken as the hydraulic diameter of the entries), Re_{D_H} is the Reynolds number of the flow for a given $_{D_H}$, the hydraulic diameter, u' is the root mean square of the average turbulent velocity fluctuations, and u_{avg} is the mean flow velocity (ANSYS, 2010).

In general, the solutions developed are relatively independent of the turbulent boundary conditions. This was shown to be true in the simulations done in this research. No difference was seen between simulations using k and ε boundary conditions and Intensity and Length boundary conditions.

4.2.7 Equation of state

For a compressible flow, an equation coupling pressure and density must be used. Because the pressures in all of the simulations done to date do not differ significantly from atmospheric conditions, it was decided that the ideal gas law would be sufficient.

$$p = \frac{nRT}{V} \tag{4-2-36}$$

where V is the volume and R is the ideal gas constant ($8.314 JK^{-1}mol^{-1}$).

4.2.8 List of equations in FLUENT

For simulations performed in this research, the total list of nonlinear conservation equations solved by FLUENT is shown below.

- continuity (of mass), Equation 4-2-9

- x-momentum, Equation 4-2-14
- y-momentum, Equation 4-2-15
- z-momentum, Equation 4-2-16
- energy, Equation 4-2-26
- k, Equation 4-2-27
- epsilon, Equation 4-2-28
- $N-1$ species conservation equations, Equation 4-2-22

4.2.9 Solver settings

FLUENT provides a number of solver options for simulation fluid flow (Taraba & Michalec, 2011). There are two numerical methods, the pressure based solver and the density based solver (Chu et al., 2011). The pressure based approach was initially developed to solve low speed, incompressible flows, and the density based solver high-speed compressible flows (Hao et al., 2011). Currently, both methods are applicable to a wide variety of flows ANSYS (2010), but the pressure based solver was used in this project. In the pressure based solver, the pressure throughout the model is solved using the conservation of mass and momentum equations, and then densities are extracted from the pressure field using the equation of state.

ANSYS FLUENT solves the governing equations using a control volume technique. This begins with spatially dividing the computational domain into discrete control volumes. This requires creating a mesh, created in this case in ANSYS Meshing. The governing equations are then integrated on each individual control volume, resulting in a series of algebraic equations for the flow unknowns (i.e. velocity, pressure, and species mole fraction). This system of algebraic equations is then linearized, and the resulting linear system of equations is solved to provide updated values for each unknown. This is repeated at each iteration until the updated values are relatively unchanged from the previous iteration. If key physical monitors are not changing iteration to iteration, then a solution to the non-linear flow equations is considered to have been found.

4.2.10 Meshing

The use of numerical control volume solution techniques require that the flow domain be divided into discrete volumes. This was accomplished in ANSYS meshing. ANSYS recommends using two main mesh statistics as quality control: the mesh skewness, which should be minimized, and the aspect ratio, which should be maintained below 40. Higher aspect ratios are acceptable in cases of flow aligned mesh cells. Skewness is calculated for each cell as the ratio of the volume of a perfectly regular cell shape (either tetrahedral or hex based shapes are used) minus the volume of the actual mesh cell divided by the regular cell volume. Figure 4.2.1 shows the relative quality of mesh cell skewness values for solving flows in ANSYS FLUENT. Skewness was kept below 0.95 for all cells in all of the meshes used in the modeling efforts described in this document.

Figure 4.2.1 Skewness guidelines (ANSYS, 2010)

4.2.11 Flow in porous media

Fluid flow in porous media was initially described by Darcy's law in the mid 19th century (Preziosi & Farina, 2002). While Darcy's law is a purely empirical definition, modern reservoir engineering uses Darcy's description of flow for describing most reservoir fluid flow behavior (Chevalier et al., 2013). This section discusses how FLUENT implements flow in porous media and how this application compares to Darcy's law.

4.2.11.1 Porous media in FLUENT

The Navier-Stokes momentum equation, taken from (Kee et al. 2003), in general vector form is:

$$\rho \frac{DV}{Dt} = f - \nabla p + \nabla \cdot T \tag{4-2-37}$$

where ρ is the fluid density, V is the velocity vector, f is the set of body forces acting on the fluid, p is the pressure, and T is the stress tensor.

This is derived from Newton's second law, which states that an acceleration must be the result of external forces: $ma = \sum F$. In Equation (4-2-37), the left hand side captures the change in velocity (acceleration) acting on a mass (in this case the density), while the right hand side includes the summation of forces acting on the volumetric body. These include generic body forces f (in units force per unit volume), forces due to the pressure gradient ∇p, and shear forces from the divergence of the stress tensor ∇T. The left hand side of Equation (4-2-37), to better match the momentum equation referenced by FLUENT, can be rewritten as:

$$\rho\left(\frac{\partial V}{\partial t} + V \cdot \nabla V\right) = f - \nabla p + \nabla T \quad (4\text{-}2\text{-}38)$$

In order to account for the loss of energy of fluid flow as it moves through a porous media, FLUENT adds a source term to the right hand side of the momentum equation. For a simple homogeneous porous media, this source term reduces to equation 4-2-22 from the FLUENT manual (ANSYS, 2010), where $i = l - 3$ for the three direction vectors.

$$S_i = -\left(\frac{\mu}{\alpha} v_i + C_2 \frac{1}{2} \rho |v| v_i\right)\alpha \quad (4\text{-}2\text{-}39)$$

where S_i is the momentum source term in the ith direction, α is permeability in FLUENT's terminology, v is the velocity vector, and v_i is the magnitude of velocity in the ith direction. This includes two losses, one for laminar losses and one for additional turbulent losses. The $\frac{\mu}{\alpha}$ term corresponds to the laminar losses, and when included as the only source term in the momentum equation, will reduce to Darcy's law. The C_2 coefficient relates to the additional losses suffered by turbulent flow. C_2 is estimated by the Ergun Equation (4-2-40):

$$C_2 = \frac{3.5}{D_p} \frac{(1-\varepsilon)}{\varepsilon^3} \quad (4\text{-}2\text{-}40)$$

Where D_p is the mean particle diameter and ε is the void fraction, defined as the volume

of voids divided by the volume of the packed bed region. Inserting the permeability source term, Equation (4-2-39), into the momentum Equation (4-2-38) results in:

$$\rho\left(\frac{\partial V}{\partial t}+V\cdot\nabla V\right)=f-\nabla p+\nabla\cdot T+S \tag{4-2-41}$$

$$\rho\left(\frac{\partial V}{\partial t}+V\cdot\nabla V\right)=f-\nabla p+\nabla\cdot T-\left(\frac{\mu}{\alpha}V+C_2\frac{1}{2}\rho|V|\cdot V\right) \tag{4-2-42}$$

This is duplicated in the FLUENT manual (with a porosity correction) in Equation 4-2-31 (ANSYS, 2010).

4.2.11.2 Porous media flow in FLUENT and Darcy's Law

Darcy's Law is a common equation used to describe fluid flow in porous media (Kim et al., 2001). It is a useful exercise to demonstrate how Darcy's Law can be derived from the momentum Equation (4-2-42), what assumptions are made in the presentation of Darcy's Law, and the form of the permeability used in FLUENT and how it is typically reported in the literature. The first form of Darcy's Law is from Reservoir Engineering by (Van Kirk 2010):

$$q=\frac{0.00127kA\left(P_1-P_2\right)}{\mu L} \tag{4-2-43}$$

where q is the flow rate in reservoir barrels, k is the permeability in millidarcies, A is the cross sectional area in square feet, μ is the viscosity in centipoises, L is the length of the flow path in feet, and P_i are pressures in psig.

This form of Darcy's Law refers to flow through a channel of a given cross section. The pressure conditions at either end of the channel are the independent variables, and the flow rate is solved for in volumetric form.

Returning to Equation (4-2-43) and comparing to the momentum Equation (4-2-42) gives:

$$q=\frac{kA\left(P_1-P_2\right)}{\mu L} \tag{4-2-44}$$

$$\rho\left(\frac{\partial V}{\partial t}+V\cdot\nabla V\right)=f-\nabla p+\nabla\cdot T-\left(\frac{\mu}{\alpha}V+C_2\frac{1}{2}\rho|V|\cdot V\right) \tag{4-2-45}$$

In order to reduce Equation (4-2-45) to the standard form of Darcy's Law, the following assumptions must be made. Darcy's Law allows for no reduction in fluid momentum due to inertial losses, so C_2 is treated as 0. In addition, there are no body forces in the simplified version of Darcy's Law, so the f term is also eliminated.

$$\rho\left(\frac{\partial V}{\partial t}+V\cdot\nabla V\right)=-\nabla p+\nabla\cdot T-\left(\frac{\mu}{\alpha}V\right) \quad (4\text{-}2\text{-}46)$$

Darcy's Law also treats the viscosity μ as a constant. There are no velocities in the y or z directions (assuming q is defined in the x direction), so the momentum equation can be rewritten as Equation B.13 on page 767 of Chemically Reacting Flow (Kee et al., 2003). In this case V is now treated as u, or a scalar velocity in the x direction.

$$\rho\left(\frac{\partial u}{\partial t}+u\frac{\partial u}{\partial x}+\frac{\partial u}{\partial y}+\frac{\partial u}{\partial z}\right)=-\frac{\partial p}{\partial x}+\mu\nabla^2 u-\left(\frac{\mu}{\alpha}u\right) \quad (4\text{-}2\text{-}47)$$

We have already stated that v and w are zero, so Equation (4-2-47) simplifies to:

$$\rho\left(\frac{\partial u}{\partial t}+u\frac{\partial u}{\partial x}\right)=-\frac{\partial p}{\partial x}+\mu\nabla^2 u-\left(\frac{\mu}{\alpha}u\right) \quad (4\text{-}2\text{-}48)$$

The final assumption is that u does not vary with time, and does not vary in the x, y, or z directions. That is to say u is constant throughout the channel flow described by Darcy's Law. This assumption causes all of the derivatives of u to vanish resulting in:

$$0=-\frac{\partial p}{\partial x}-\left(\frac{\mu}{\alpha}u\right) \quad (4\text{-}2\text{-}49)$$

which can be rewritten as:

$$\frac{\partial p}{\partial x}=\left(\frac{\mu}{\alpha}u\right) \quad (4\text{-}2\text{-}50)$$

Discretizing the pressure derivative $\frac{\partial p}{\partial x}\partial$ as $\frac{P_2-P_1}{L}$ results in the following:

$$\frac{\mu}{\alpha}u=-\frac{P_2-P_1}{L} \quad (4\text{-}2\text{-}51)$$

The assumptions made earlier require that the cross sectional area remain constant, so the velocity u can be rewritten as $\frac{q}{A}$, where q is a volumetric flow rate and A is the cross sectional area.

$$\frac{\mu}{\alpha}\frac{q}{A}=\frac{P_2-P_1}{L} \tag{4-2-52}$$

Solving for q results in:

$$q=\frac{\alpha A\left(P_2-P_1\right)}{\mu\cdot L} \tag{4-2-53}$$

which matches Equation (3.44), with the exception that k has been renamed α.

$$q=\frac{kA\left(P_2-P_1\right)}{\mu L} \tag{4-2-54}$$

It is important to note that FLUENT requires the permeability of a porous media to be entered as resistance, $\frac{1}{\alpha}$ (or $\frac{1}{k}$), with units of m^{-2}.

4.3 Development of the numerical model

4.3.1 CFD calculation method and stage

Gas flow behavior in working face and goaf is a complicated process since numerous factors are involved. Combined with the specific condition of working field, experiences of other numerical models and multiple factors of the mine, the numerical model of gas flow distribution in goaf was established. The establishment of numerical modeling work consists of several basic steps. The first step is to go to working field to collect the basic information, such as geometries, relevant parameters, rate of gas flow, goaf dropping characteristic etc. The second is to establish the 3D finite element model of the mine face, goaf, and tunnel and drainage borehole. The third is to set up gas flow models and boundary conditions through User-Defined Functions. The fourth is to simulate the condition of working face and goaf. The fifth is to calibrate and validate the simulation model by using working field measured data. The last step is to conduct extensive parametric researches and technique evolution by optimizing the numerical model.

4.3.2 General situation of Shaqu coal mine

Coal seam #4 in Shaqu coal mine with large gas content (approximately reaches up to $30m^3/t$) has created severe difficulties in mine safety and production. The working face length and the strike length of coal seam #4 are 200m and 950m respectively. Extracting method is longwall

retreating extraction with U-shaped ventilation system. It is obtained that gas drainage quantity of 14205 working face of coal seam #4 can approximately reach up to 100 m^3/min (Table 4.3.1). A number of gas drainage methods have been performed by Shaqu coal mine for the purpose of mine safety. However, the results of goaf gas drainage have been far from satisfactory. A great deal of gas fails to extract, but has directly flow into the goaf instead, which constantly leads to the overrunning of gas concentration in upper corner.

Table 4.3.1 Basic gas parameters in Shaqu coal mine

Layer	Gas pressure (MPa)	Gas content (m^3/t)	Emissions (m^3/100m)	Permeability coefficient ($m^2/MPa^2 \cdot d$)	Attenuation coefficient ($100d^{-1}$)
Coal Seam 2#	0.99～1.03	7.92～8.10	4085～4346	1.577～3.999	0.02～0.028
Coal Seam 3#	1.11～1.18	9.70～10.06	4433～5068		0.02～0.025
Coal Seam 4#	1.52～1.57	7.30～17.82	21648～24490		0.01～0.016
Coal Seam 5#	2.20～2.40	10.84～20.15	24350～27180		0.01～0.019

4.3.3 Establishment of numerical simulation model

The rule of gas emission basically depends on variation of crustal stress distribution caused by mining activities as it exerts an enormous influence on the variation of permeability of mined layers and adjacent layers. Permeability of coal strata is the key factor of gas emission control and prevention. The reduction in permeability mainly depends on the fissured development of the fractures in the front layer of the working face and the crustal stress release in the rear area of the working face. Obviously, the coal porosity and mining intensity have a strong influence on coal seam and goaf permeability. The distribution of goaf permeability can be obtained by analyzing crustal stress distribution of goaf and results of extensive previous studies. The variation of different areas may vary from 10^{-4} to 10^{-9} m^2.

4.3.3.1 The basic hypotheses of the goaf

In this CFD simulation experiment, gas movement inside coal body, diffusive motion inside

pore and gas adsorption process follow Darcy's and Hooke's law as well as the Langmuir's equation, while gas desorption process inside coal body is ignored. Mine working face and goaf are regarded as porous medium, gas is regarded as an ideal gas, and porous flow process is regarded as an isothermal process. Therefore, the standard equation of fluid flow combines with momentum source in order to perform the numerical simulation. In laminar flow of porous medium, the pressure is directly proportional to the speed, and the convection acceleration and diffusion are ignored. Numerical simulation based on the fundamental equation of gas flow of mine working face and goaf establishes the numerical model by determining the boundary conditions. Thus, gas flow and distribution rules are obtained. In this research, a standard k-e equation (k is Turbulent Energy and ε is dissipation rating) is used to calculate the turbulent transport through the flow region since it can be used to simulate a large-scale turbulent flow. Besides, the gas flow near the boundaries is simulated by the application of standard wall functions. These simulation models are developed to model the conditions of gas turbulent flow near the mine working face and the situation of gas laminar flow inside the goaf area.

4.3.3.2 The establishment of the geometric model

In accordance with the necessity of the actual situation and numerical simulation of the 14205 working face of Shaqu coal mine, the geometrical model of the goaf and working face is simplified as follows:

(1) Goaf is seen as cuboids. The model takes into consideration the influence of nothing but the working face, the air inlet of transport gateway, the air inlet of the orbital gateway and the special air outlet on the gas movement in goaf.

(2) Based on the factual characteristics of the working face, the goaf model takes into account the adjacent layers. The goaf is divided into caving zone 1, caving zone 2, caving zone 3, fissure zone 1, fissure zone 2, coal seam #2, coal seam #3, coal seam #5, and the working face floor in order to differentiate the porosity.

(3) Length and width are respectively selected as 400m and 210m along the strike in the goaf (the air inlet of transport gateway and the air inlet of the orbital gateway are included, the special air outlet is excluded), and vertical height is selected as 60m. What's more, 3 sets of spots are

arranged along the strike: 20m, 100m and 280m respectively; 7 sets of spots are arranged along the vertical direction: 20m, 3m, 14m, 3m, 10m, 7m and 3m.

(4) The length of the air inlet of transport gateway, the air inlet of the orbital gateway and the special air outlet are all selected as 12m; width and height are both 3m. Length of the working face is selected as 210m, width as 10m and height as 3m.

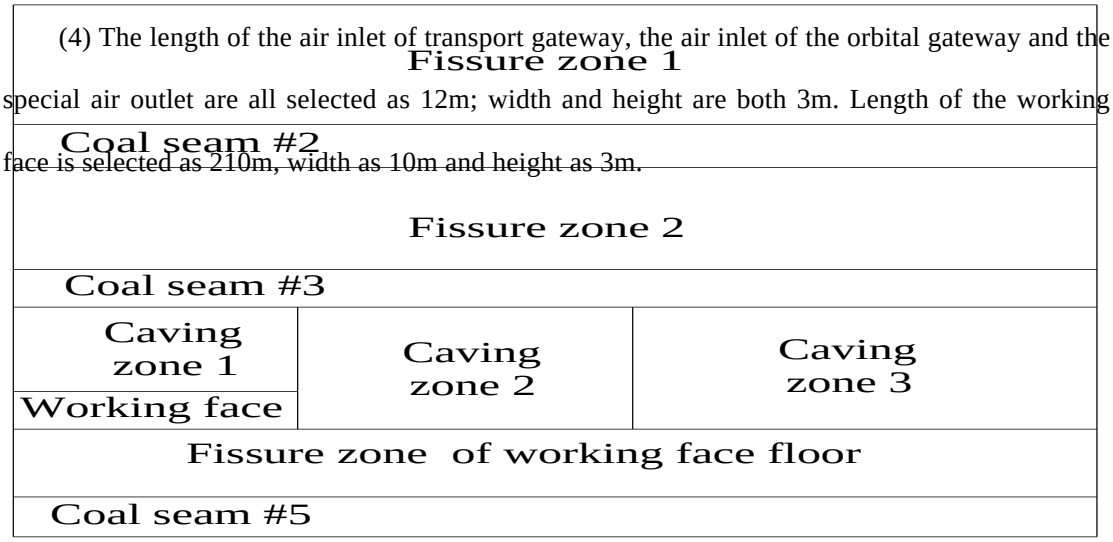

Figure 4.3.1 Numerical simulation model of stereogram in goal

The plan view and sectional view of geometrical model can be seen in Figure 4.3.1 and Figure 4.3.2.

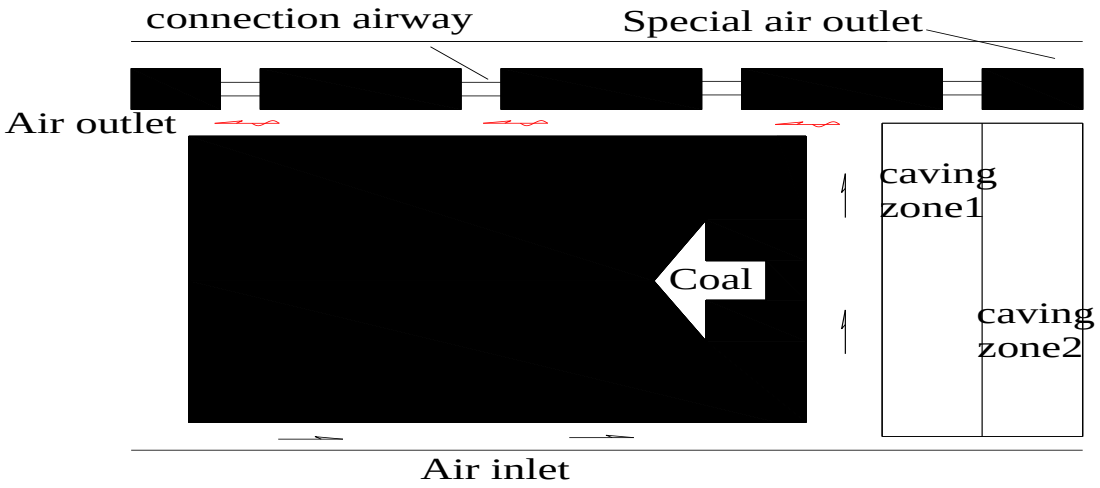

Figure 4.3.2 Numerical simulation model of plan in goal

4.3.3.3 Definition of Boundary Conditions

CFD models can be developed from the real mine layouts and its related parameters are shown in the Table 4.3.1. Air inlet boundary setting: VELOCITY—INLET; Air outlet boundary setting: OUTFLOW; boundary conditions obtained from field. The air velocity of the working face entrance is 1.5 m/s, while the pressure in the exit is 90kPa. Numerical simulation model and its parameters can be seen in Table 4.3.2 and Table 4.3.3

Table 4.3.2 Model of specification in numerical modeling

Model	Define
Solver	Segregated
Viscous model	k -epsilon
Specious model	Methane-air
Energy	On

Table 4.3.3 Numerical simulation parameters of the coal seam

Parameter Name		Values	Parameter Name		Values
Velocity of inlet of workface/(m·s^{-1})		1	Fracture Zone 1	Porosity	0.02
				Viscous Drag Coefficient	10 000
Outlet Pressure/kPa		90		Source	1.1×10^{-7}
Caving Zone 1	Porosity	0.333	Fracture Zone 2	Porosity	0.002
	Viscous Drag Coefficient	1 000		Viscous Drag Coefficient	100 000
	Source	3.56×10^{-8}		Source	1.96×10^{-7}
Caving Zone 2	Porosity	0.231	Floor	Porosity	0.002
	Viscous Drag Coefficient	2 500		Viscous Drag Coefficient	100 000
	Source	6.5×10^{-8}		Source	2.18×10^{-7}
Caving	Porosity	0.167	Coal	Porosity	0.333

Zone 3	Viscous Drag Coefficient	4 000	Seam 3#	Viscous Drag Coefficient	1 000
	Source	1.5×10^{-7}		Source	3.2×10^{-8}
Coal Seam 2#	Porosity	0.02	Coal Seam 5#	Porosity	0.002
	Viscous Drag Coefficient t	10 000		Viscous Drag Coefficient	100 000
	Source	1.83×10^{-7}		Source	2.5×10^{-7}

According to calculation method of the mathematical model, the boundary conditions and distribution of porosity of goaf are two essential requirements. The immateriality of goaf can be shown in the immateriality of mined coal and rocks and the variation of flow field height, and it can be controlled by the hulking coefficient (K_p) of mined coal and rocks. According to the regularity of general mine ground pressure, then

$$K_p = K'_p\left(K_p^{(0)} - K'_p\right)e^{-\alpha x} \tag{4-3-1}$$

where: $K_p^{(0)}$ is the initial hulking coefficient of the caving zone, K'_p is the hulking coefficient of compaction, α is decay rate. The variation of K_p can be seen in Figure 4.3.3, the distribution of the hulking coefficient of goaf chooses the maximum value, and porosity of goaf is $n = 1 - 1/K_p$.

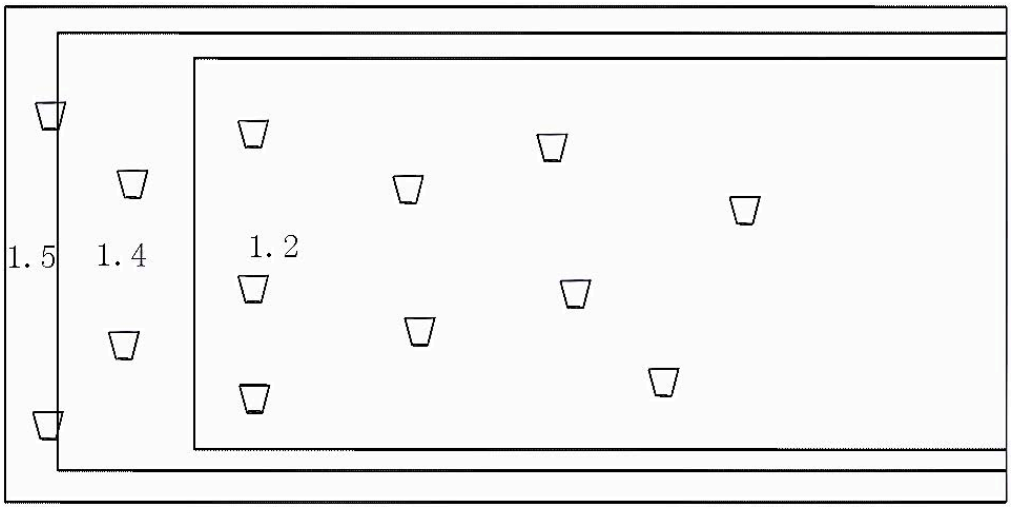

Figure 4.3.3 Distribution of compaction break and expansion ratio

(1) The determination of porosity

With the development in the mining working face, the working face roof is caved continually; the hulking coefficient is gradually decreased along with the compaction of the rocks and mined coal in the deep goaf. The measured data show that the initial hulking coefficient can be reached at 1.5, and then it decreased gradually. The three part of the hulking coefficient in the numerical simulation model are 1.5, 1.3 and 1.2, respectively. Therefore, the porosity can be calculated based on each hulking coefficient of caving zone:

Porosity of caving zone 1: $\frac{1.5-1}{1.5}=0.333$

Porosity of caving zone 2: $\frac{1.3-1}{1.3}=0.231$

Porosity of caving zone 3: $\frac{1.2-1}{1.2}=0.167$

Based on the porosity of caving zones, the porosity of fissure zone 1, fissure zone 2, coal seam #3, coal seam #5, coal seam #2 and the working face floor choose 0.02, 0.002, 0.02, 0.002, 0.002 and 0.002, respectively.

(2) The determination of viscosity coefficient

According to the data of different porosities of different zones and the permeability coefficient of coal seam ($1.577 \sim 3.999 m^2 / MPa^2 \cdot d$), the coefficient of viscosity of caving zone 1, caving zone 2 and caving zone 3 are 10^3, 10^4 and 10^5; the coefficient of viscosity of fissure zone 1 and the fissure zone 2 are 1.3^{e+10} and 1.3^{e+13}; the coefficient of viscosity of fissure of coal seam #3, coal seam #5, coal seam #2 and working face floor are 1.3^{e+10}, 1.3^{e+13}, 1.3^{e+10} and 1.3^{e+10}, respectively.

(3) The determination of the source (gas emission amount of goaf)

The total gas emission amount of working face 14205 is measured by field measurement. Based on knowledge of the formation of gas emission of the working face, it can be known that the gas source of working face mainly come from goaf, coal wall and mined coal. Therefore, the gas emission of goaf is 68.6 m^3/min, and gas emission of coal wall and mined coal is 29.4 m^3/min. The amounts of goaf gas emission are made up of the upper adjacent layers 40% (27.44 m3/min), caving zone 50% (34.3 m3/min), and the lower adjacent layers 10% (6.86 m^3/min). Generally speaking, the fissure zone, coal seam #2 and coal seam #3 are part of the upper adjacent layers;

coal seam #5 and the working face #5 are part of the lower adjacent layers, and the other part of gas emission calculation are:

The gas concentration is 0.7 kg/m^3,

(3.1) Source of each part of caving zone

According to the length of different caving zones and the hulking coefficient, the average hulking coefficient can be calculate by using the method of weighted average:

$$\frac{1.5\times 20+1.3\times 100+1.2\times 280}{20+100+280}=1.24$$

Total source of caving zone: $\frac{34.3}{60\times 210\times 10\times 400}=6.8e^{-7}\ kg/m^3\cdot s$

Source of caving zone 1: $\frac{1.5}{1.24}\times\frac{20}{400}\times 6.8e^{-7}=4.12e^{-8}\ kg/m^3\cdot s$

Source of caving zone 2: $\frac{1.3}{1.24}\times\frac{100}{400}\times 6.8e^{-7}=1.78e^{-8}\ kg/m^3\cdot s$

Source of caving zone 3: $\frac{1.2}{1.24}\times\frac{280}{400}\times 6.8e^{-7}=4.61e^{-8}\ kg/m^3\cdot s$

(3.2) Source of each part of the adjacent layer

The proportion of gas emission amount of caving zone 1 and caving zone 2 is 3:1, and the proportion of gas emission amount of fissure zone 1 and fissure zone 1 is 3:1. Besides, baesed on the original gas emission amount of coal seam #2 and coal seam #3, the gas emission amount of fissure zone 1, fissure zone 2, coal seam #2 and coal seam #3 can be dertermined (12.25 m^3/min, 4.08 m^3/min, 1.44 m^3/min and 9.67 m^3/min), and their source are:

The source of fissure zone 1: $\frac{12.5}{60\times 210\times 14\times 400}=1.37e^{-7}\ kg/m^3\cdot s$

The source of fissure zone 2: $\frac{4.08}{60\times 210\times 20\times 400}=4.05e^{-7}\ kg/m^3\cdot s$

The source of coal seam #3: $\frac{9.67}{60\times 210\times 3\times 400}=6.39e^{-7}\ kg/m^3\cdot s$

The source of coal seam #2: $\frac{1.44}{60\times 210\times 3\times 400}=9.52e^{-7}\ kg/m^3\cdot s$

(3.3) Each source of adjacent layers

The source of coal seam #5: $\frac{4.35}{60\times 210\times 3\times 400}=2.87e^{-7}\ kg/m^3\cdot s$

The source of working face floor: $\frac{2.51}{60\times 210\times 7\times 400}=7.11e^{-7}\ kg/m^3\cdot s$

4.3.4 Introduction of U+L-type ventilation system

Due to the different air pressure between the front goaf and the back goaf, high concentrated gas constantly flows into working face from deep goaf. Moreover, a great deal of high concentrated gas continually flows over into upper corner because of the air leakage of goaf and different pressures between air inlet and outlet. Therefore, a valid ventilation system plays an important role in dealing with difficulties of goaf gas.

The simulation model is based on U+L-type ventilation system (Figure 4.3.5) rather than U-type ventilation system (Figure 4.3.4). U+L-type ventilation system consists of track roadway (air inlet), working face, beltway (air inlet), and air return roadway. The inlet airway, directly opposite to upper corner, balances the pressure of the upper corner, restrains the gas discharge of the upper corner, and compels the high concentrated gas to flow over into outlet airway. U+L-type ventilation system is based on the gas control theory, and it accelerates the gas emission, diffusion and flow, lowering the gas concentration of local areas, which effectively solve the difficulties of gas over-limit concentration in the working face. In addition, the total air volume of the working face has significantly increased as fresh air is constantly offered from two inlet airways.

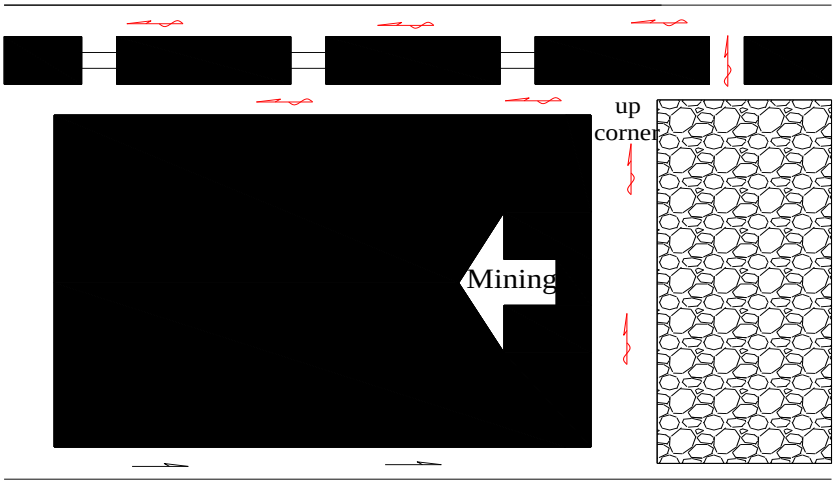

Figure 4.3.4 U-type ventilation network consisting of one air inlet and one outlet

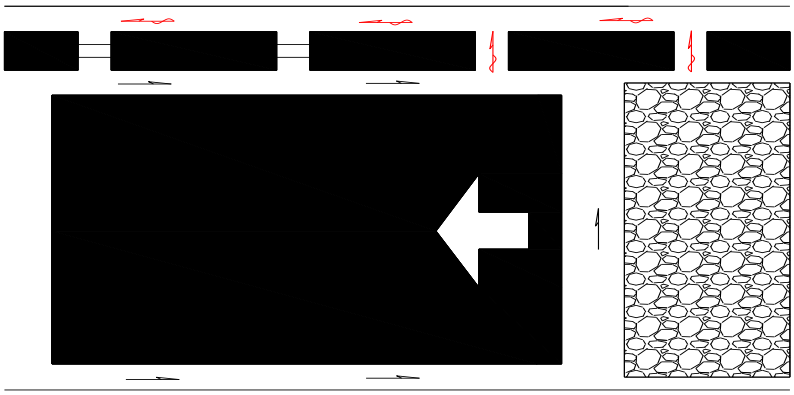

Figure 4.3.5 U+L-type ventilation system including two air inlets and one outlet

4.4 Simulation results

In this experiment, the CFD simulations based on U-type and U+L-type ventilation systems are performed respectively. Particularly, U+L-type ventilation system consists of two track roadways (air inlet), working face, one beltway (air inlet) and tail roadway.

4.4.1 Simulation results of U-type ventilation system

According to the parameters and boundary conditions mentioned above, the simulation experiment based on U-type ventilation system is performed. The air velocity of inlet is 1.5 m/s, and the pressure of outlet is 90kPa. To facilitate the research, figures of different cross-sections of goaf gas concentration distribution are selected with Z=0m (Working face floor) in Figure 4.4.2, Z=7m (Working face roof) in Figure 4.4.3, Z=15m (Caving zone) in Figure 4.4.4, Z=30m (Fracture zone) in Figure 4.4.5 and Z=50m (Bending Subsidence zone) in Figure 4.4.6.

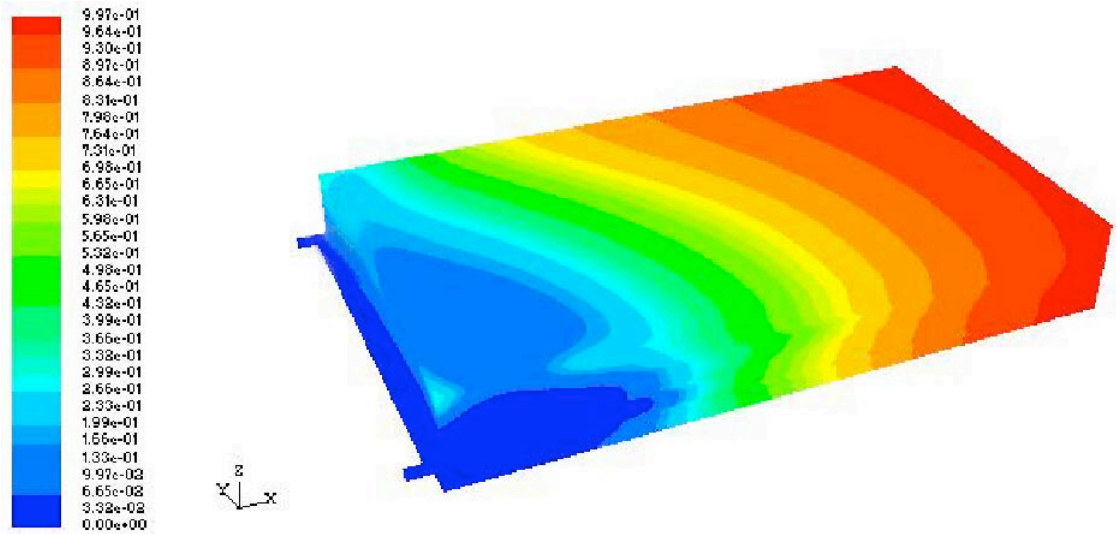

Figure 4.4.1 Goaf gas concentration distribution in three-dimensional map

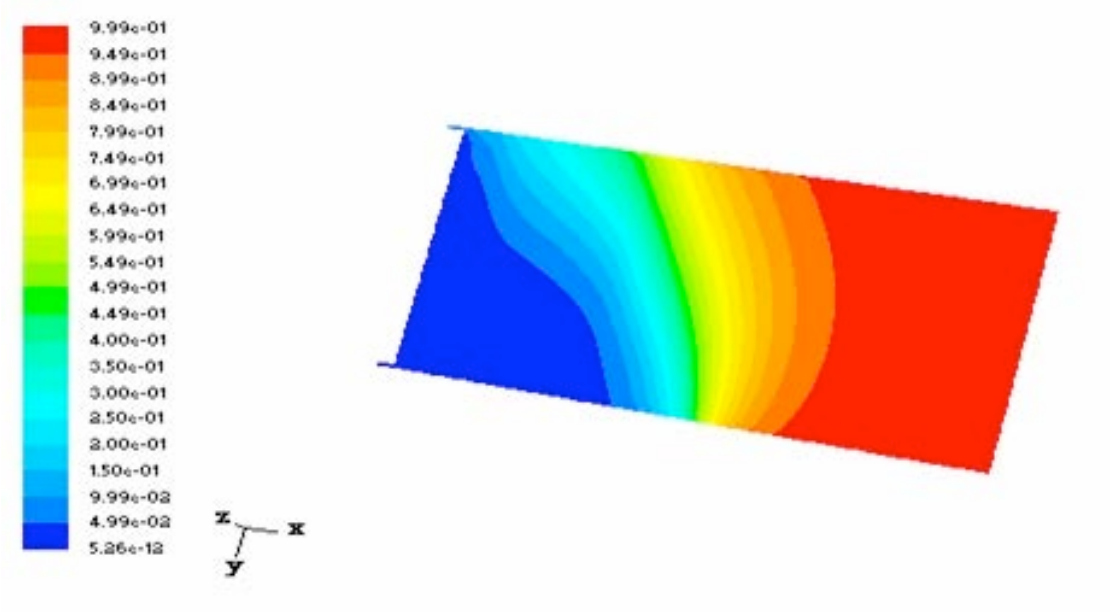

Figure 4.4.2 Cross-section of the gas concentration distribution in the goaf (Working face floor, Z=0m)

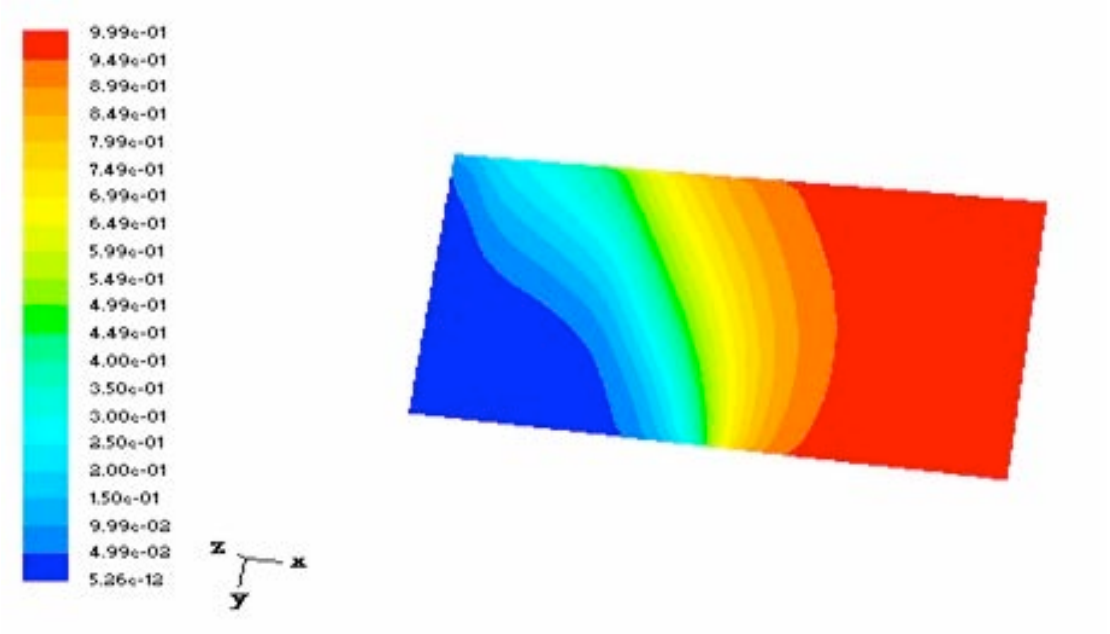

Figure 4.4.3 Cross-section of the gas concentration distribution in the goaf (Working face roof, Z=7m)

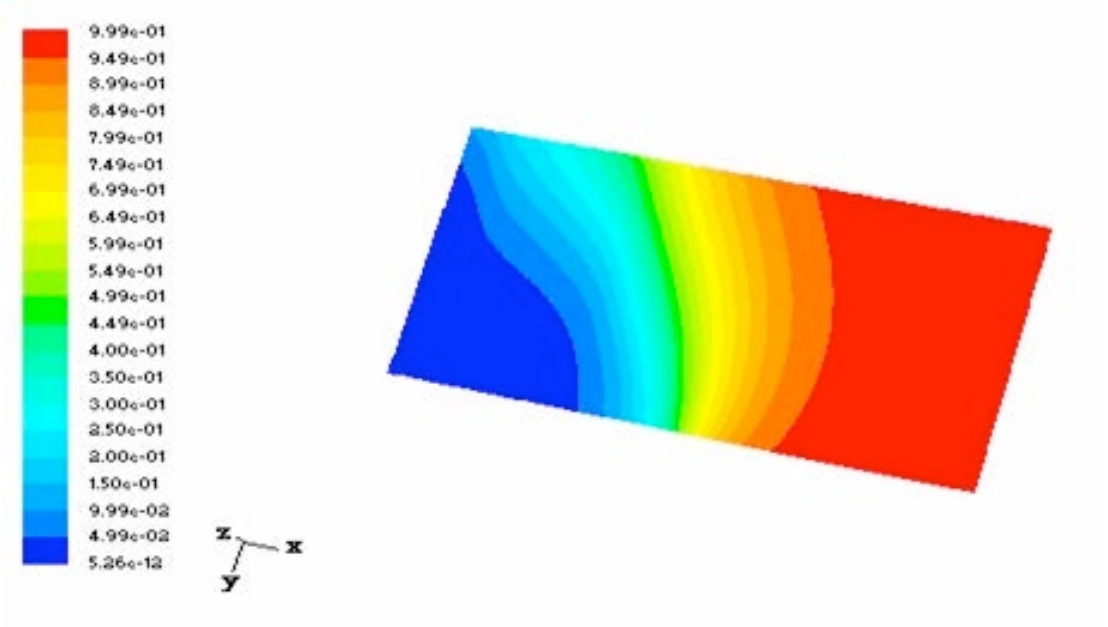

Figure 4.4.4 Cross-section of the gas concentration distribution in the goaf (Caving zone, Z=15m)

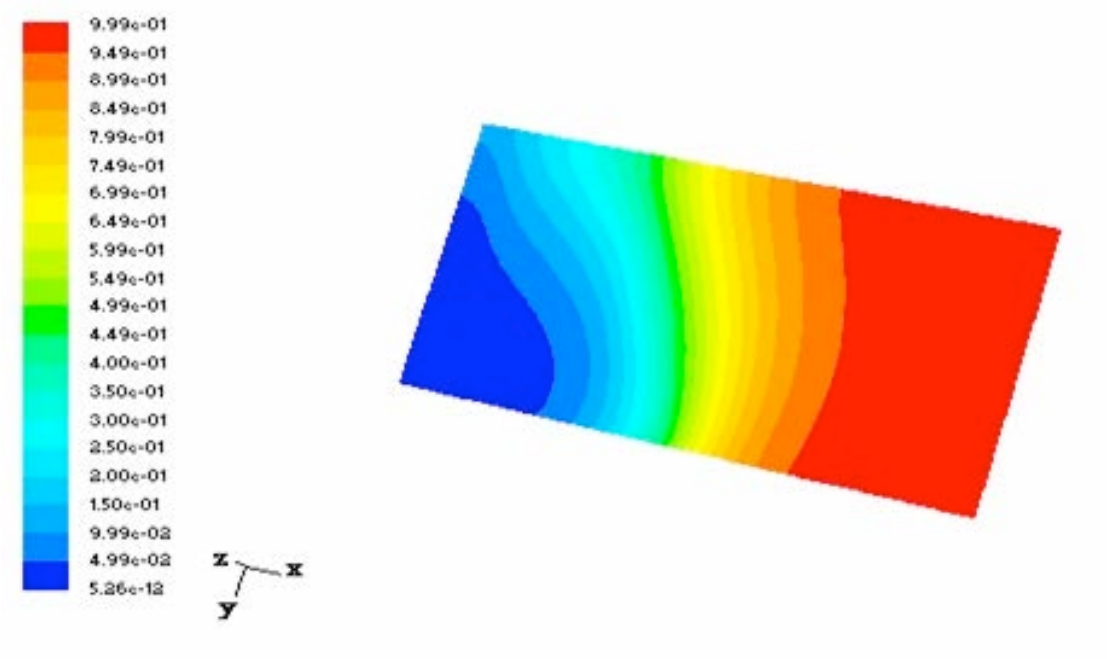

Figure 4.4.5 Cross-section of the gas concentration distribution in the goaf (Fracture zone, Z=30m)

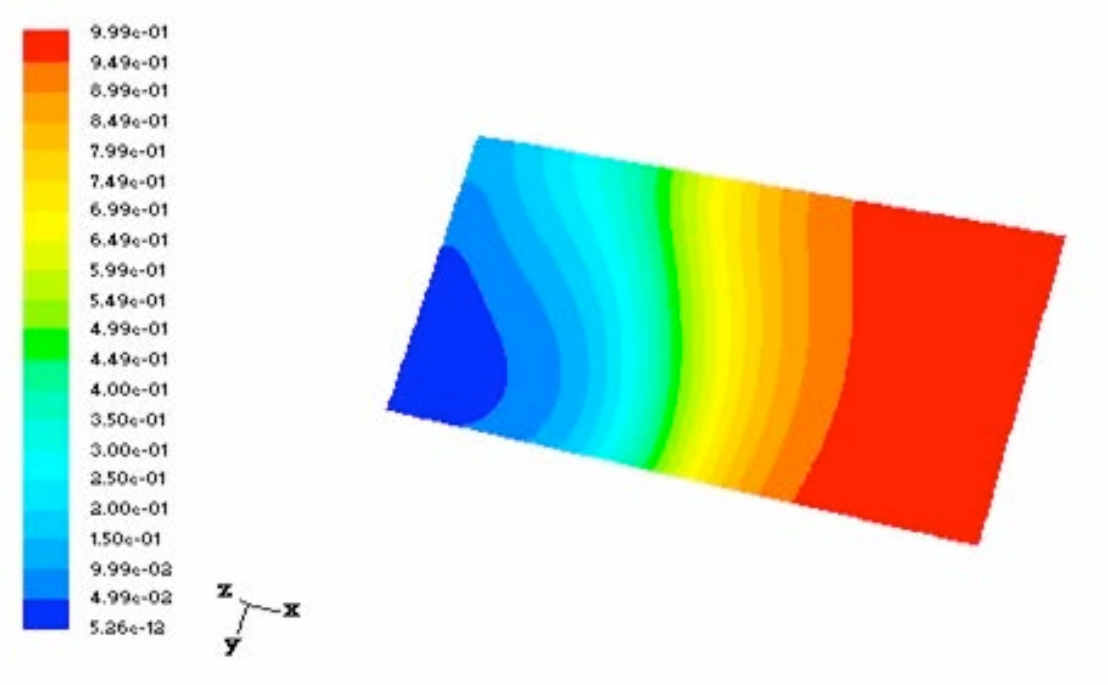

Figure 4.4.6 Cross-section of the gas content distribution of goaf (Bending Subsidence zone, Z=50m)

It can be seen from these figures that the gas is mainly gathered in the upper corner of the working face. Firstly, along the mining direction of the working face, gas concentration gradually increases from the working face to the deeper goaf and then it tends to be steady after a certain distance. Secondly, along the vertical direction of the working face, gas content gradually increases from the floor to the roof and fracture zones as the air volume gradually decreases from the top to the bottom. Lastly, along the width direction of the working face, gas content gradually increases from the air inlet side to the outlet. The air leakages of the goaf and different pressures between air inlet and outlet result in the overflow of plenty of gas concentrated in the upper corner.

Similar simulation experiments have been performed with the same parameters and boundary conditions, but the air velocity of inlet increases to 2.0 m/s. The results show that the goaf gas distribution rule is almost the same as before. Besides, with the increase of air velocity, high gas content slightly moves to the deeper goaf. It indicates that gas content of the upper corner can be effectively reduced by a slightly increase in the air volume for a certain extent. However, the problem of gas in the working face cannot be completely solved by unlimitedly increasing the air volume. Instead, it must be combined with multiple technological methods including the

optimization of the ventilation system and forming special gas extraction systems.

4.4.2 Simulation results of U+L-type ventilation system

The parameters and boundary conditions of the simulation experiment based on U+L-type ventilation system are the same as those of U-type ventilation system. The air velocity of inlet is 1.5 m/s, and the pressure at the outlet is 90kPa. Besides, figures of different cross-sections of the goaf gas content distribution are selected from the simulation experiments with Z=0m (Working face floor) in Figure 4.4.8 goaf methane concentration distribution in three-dimensional map, Z=7m (Working face roof) in Figure 4.4.9, Z=15m (Caving zone) in Figure 4.4.10, Z=30m (Fracture zone) in Figure 4.4.11 and Z=50m (Bending Subsidence zone) in Figure 4.4.12.

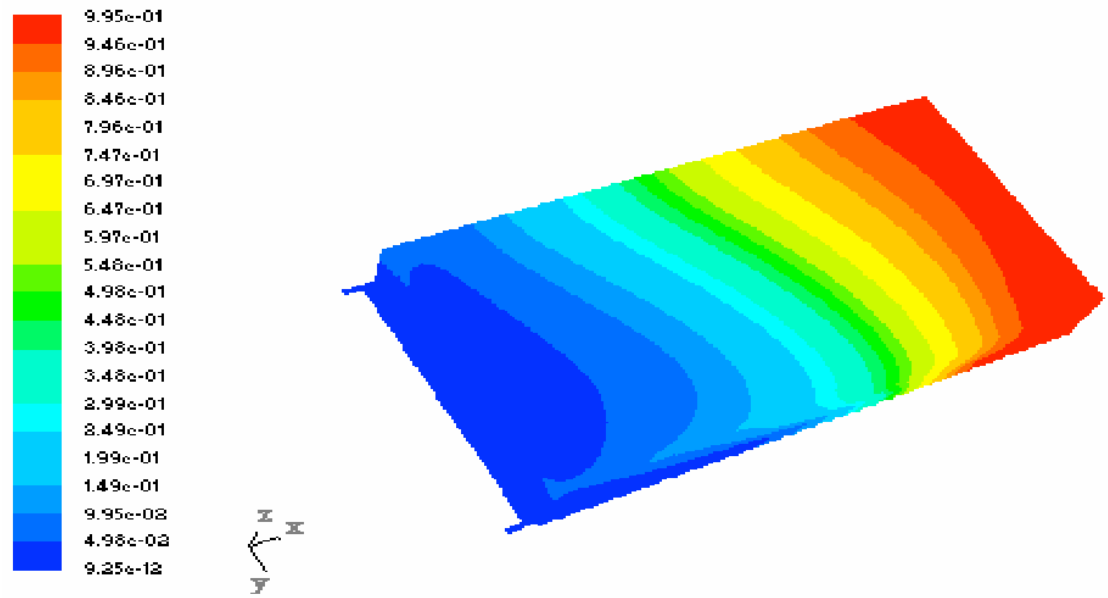

Figure 4.4.7 Goaf gas concentration distribution in three-dimensional map

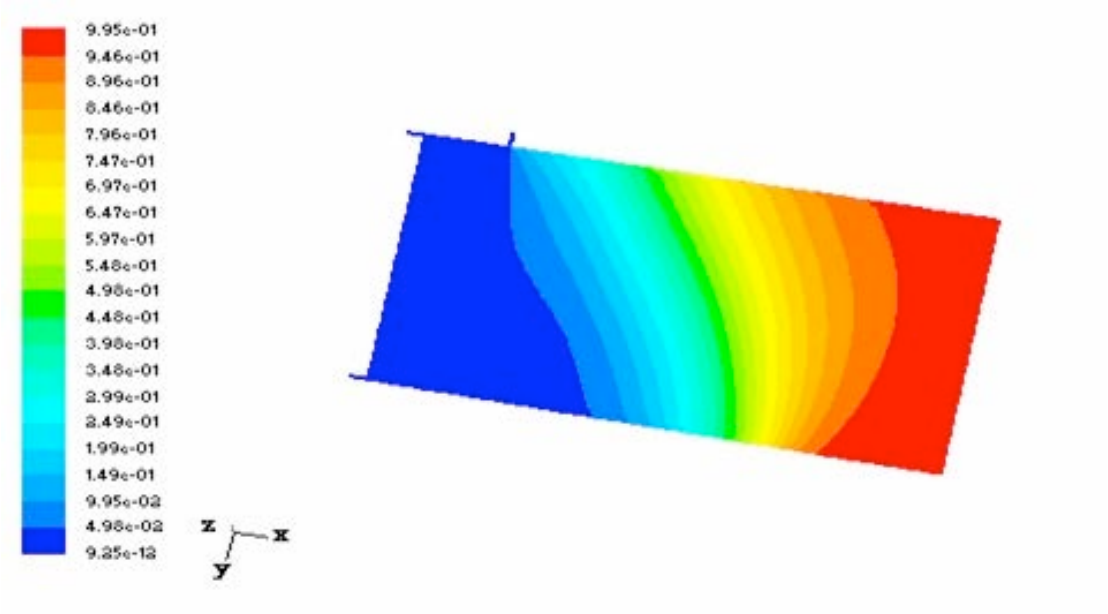

Figure 4.4.8 Cross-section of the gas content distribution in the goaf (Working face floor, Z=0m)

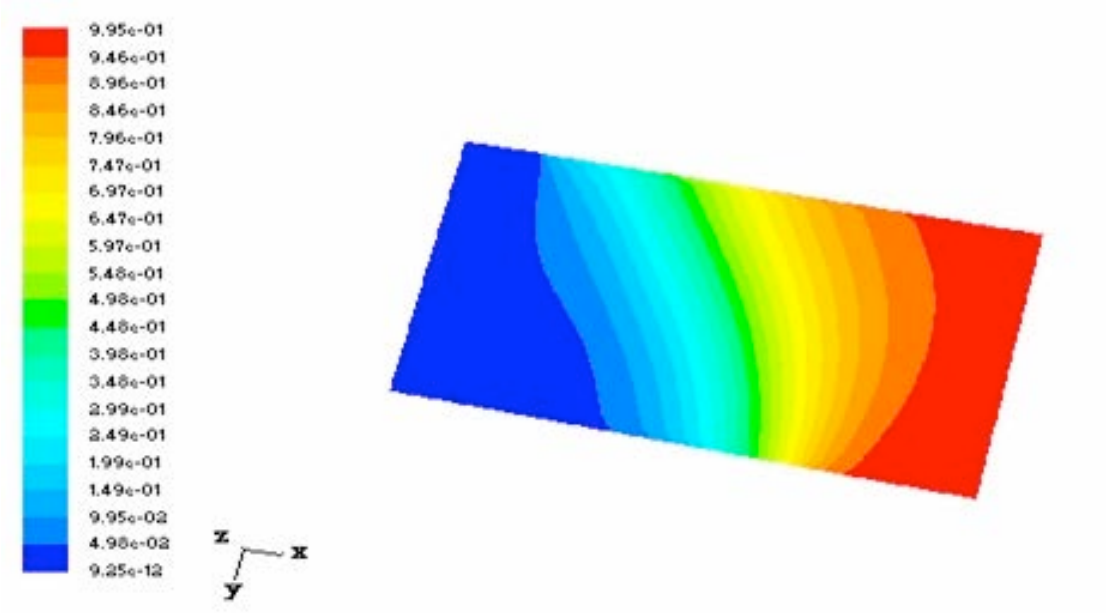

Figure 4.4.9 Cross-section of the gas content distribution in the goaf (Working face roof, Z=7m)

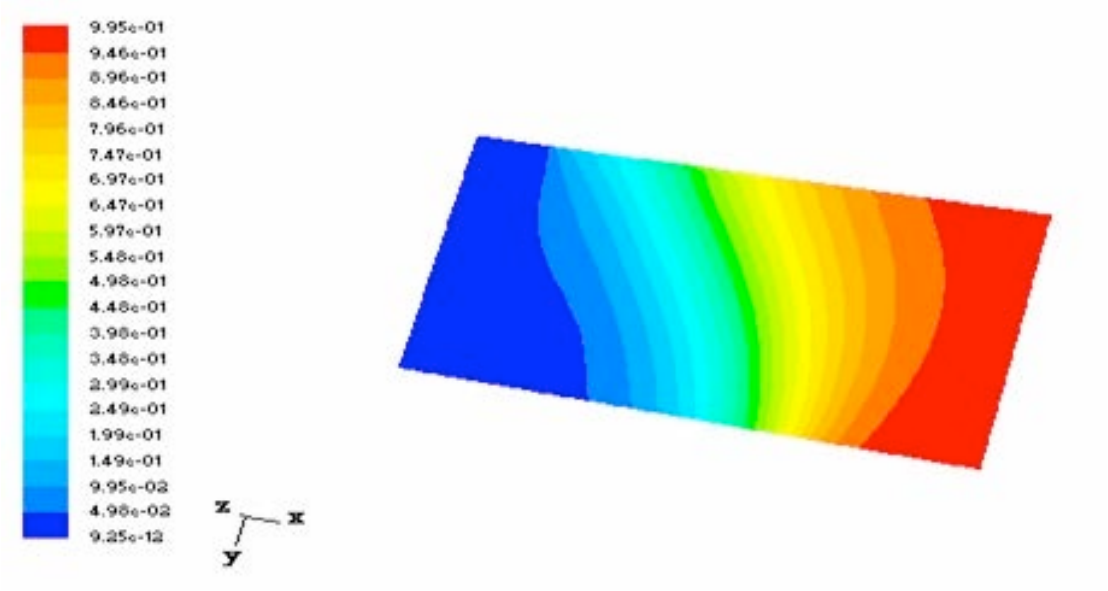

Figure 4.4.10 Cross-section of the gas content distribution in the goaf (Caving zone, Z=15m)

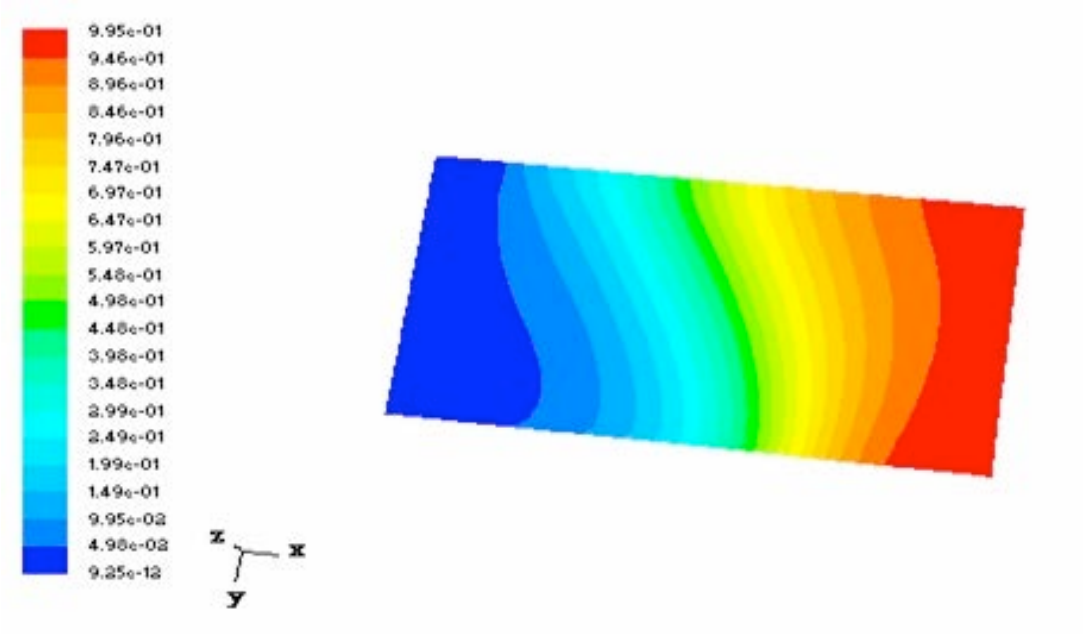

Figure 4.4.11 Cross-section of the gas content distribution in the goaf (Fracture zone, Z=30m)

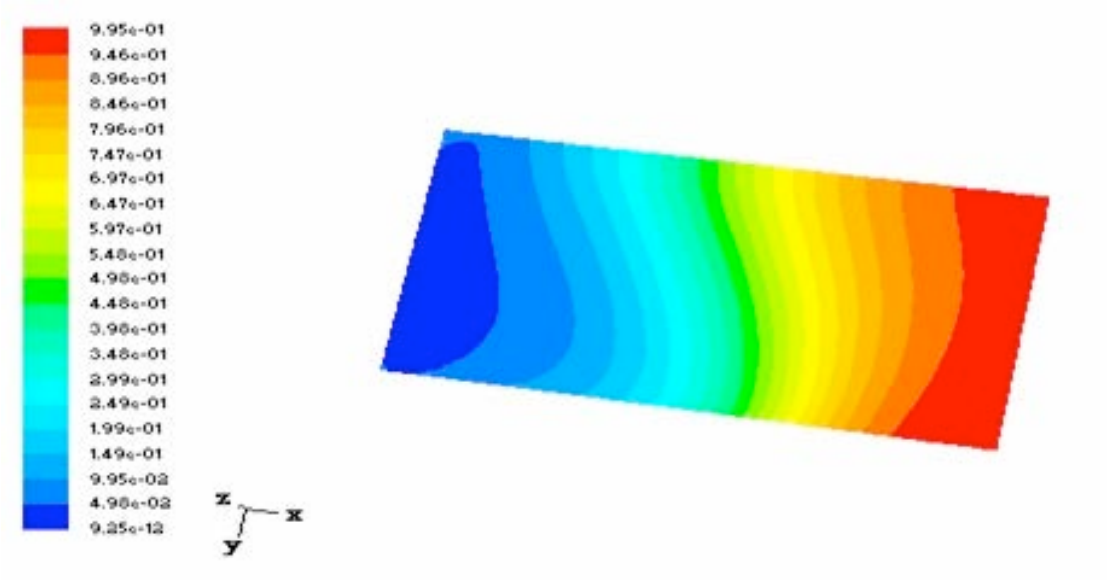

Figure 4.4.12 Cross-section of the gas content distribution in the goaf (Bending Subsidence zone, Z=50m)

It can be seen from these figures that the high concentrated gas moderately moves to the deeper goaf from the upper corner. Along the mining direction, gas content gradually increases from the working face to the deeper goaf, and then tends to be steady after a certain distance. Specifically, the goaf gas content in the range between 0m and 45m basically remains unchanged (lower than 6%) because of the air leakage effect and different pressure between the air inlet and outlet. As is shown in Figure 4.4.13, the goaf gas content dramatically rises from 45m and reaches the peak to approximately 92% at 245m.

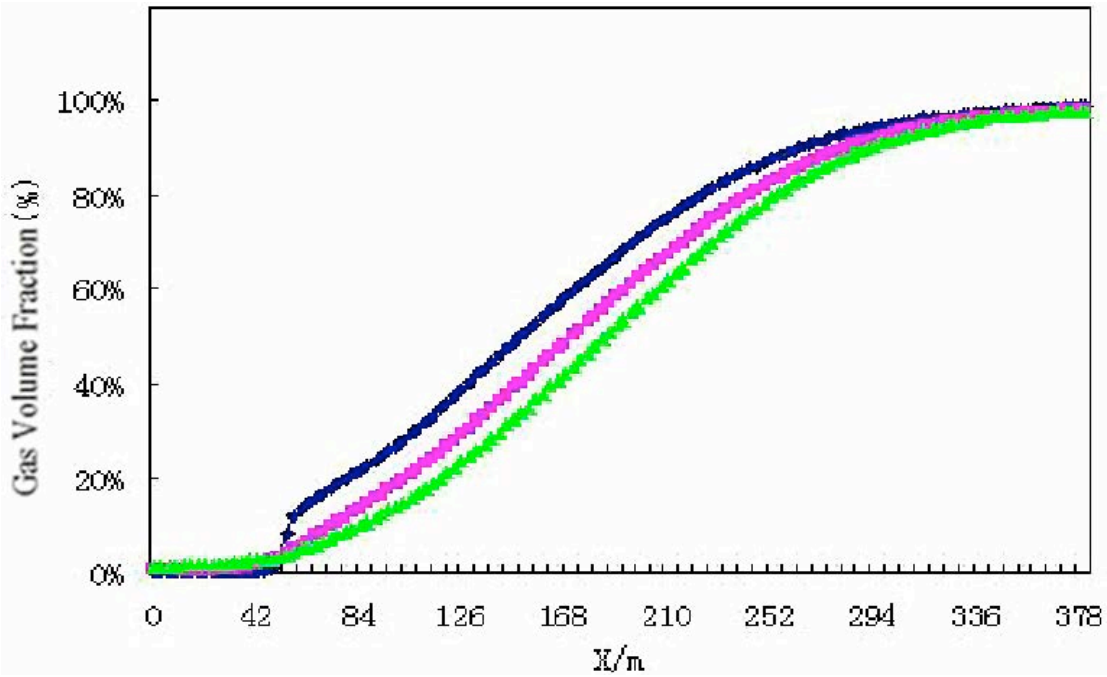

Figure 4.4.13 From Y=0, 30 and 50m section, goaf methane concentration distribution in face forward direction

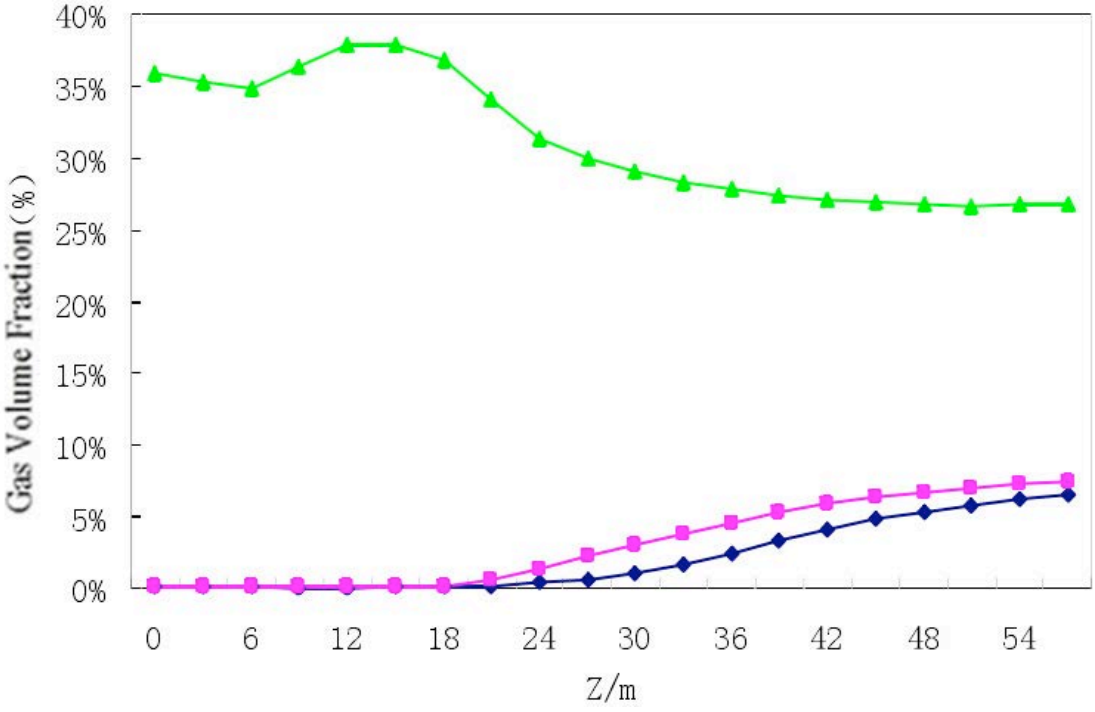

Figure 4.4.14 From X=20, 40 and 120m section, goaf methane concentration distribution in vertically

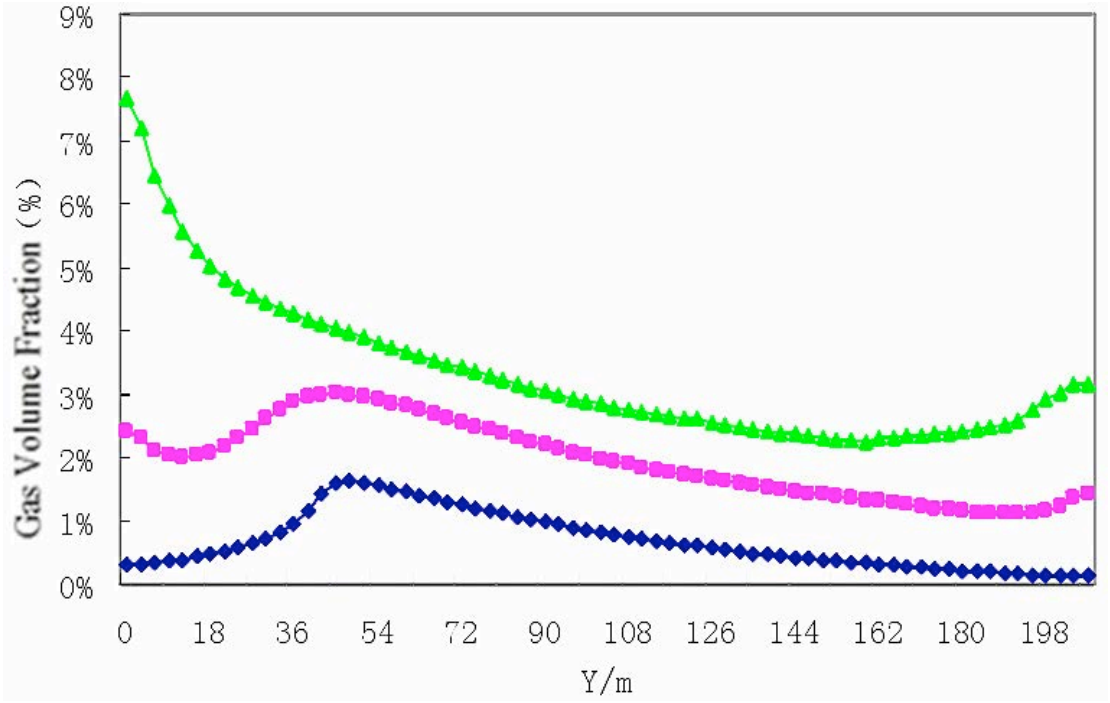

Figure 4.4.15 From Z=20, 35 and 50m section, goaf gas concentration distribution in face width direction

To facilitate the research results, the representative section figures are chosen and discussed, they are Z=10 (the working face floor), Z=13 (the working face roof), Z=20 (the caving zone), Z=30 (fissure zone 1) and Z=50 (fissure zone 2). The variation of goaf concentration is explained by discussing three plans in three dimensions: from goaf to the working face (X direction), from the caving zone to the working face floor (Y direction) and from the air inlet to the air outlet (Z direction)

(1) From goaf to the working face (X direction)

The gas concentration gradually increases from the floor to the caving zones and fracture zones, and it tends to stable after a certain distance. This gas zone is unstable because its concentration is affected by many factors such as the distance to the working face, the air quantity of the air inlet and air outlet. With the mining activities are performed, the transition of the air flow zone is moved forward to the working face continually. Because the air volume and velocity gradually decreases from the top to the bottom, the gas usually accumulates in the upper goaf. Specifically, the variation of goaf gas concentration is not dramatic in the first 40m zone (from the working face to the deep goaf), and it almost below 5%, and the gas concentration of air outlet is only around 0.5%; the zone from 40m to 250m, the gas concentration dramatically increased, and

especially in the side of air outlet; the zone of 250m to deep goaf, the gas concentration is quite stable, and reach at the maximum percent.

(2) From the caving zone to the working face floor (Z direction)

The gas concentration of the working face roof is higher than that of the working face floor, and it gradually increased from the floor to the roof. Specifically, goaf gas content within the vertical range of 10m remains at a lower level while it rapidly increases in caving and fracture zone 1 (from 10m to 40m). The area of 30m to 40m (fracture zone 2) is the area with high and stable gas concentration, and it slightly increased from the bottom to the top. The gas concentration of the zone above 40m tends to stable. The reason of this phenomenon is because the air flow in the top of the working face goaf is very slow, and the gas suspension characteristics made the gas gathered in the top of goaf.

(3) From the air inlet side to the outlet side (Y direction)

The gas content gradually increases from the air inlet side to the outlet side, following the direction inlet-outlet and along all the width. Particularly, it peaks at 42m (4%) from the outlet side rather than the upper corner.

Similar simulation experiments have been performed with the same parameters and boundary conditions, and the air velocity of the inlet changes to 2.0 m/s. The results show that the goaf gas distribution rule is almost the same as before. Besides, with the increase of air velocity, high concentrated gas slightly moves to the deeper goaf. Therefore, it indicates that gas concentration of upper corner can be effectively decreased by slightly increasing the air volume to certain extent.

4.4.3 Results comparison between U-type and U+L-type ventilation systems

The comparison between U-type ventilation systems and U+L-type ventilation system shows that goaf gas distribution rules are similarly applied under both systems. However, in the case of the U-type ventilation system, a large amount of high concentrated gas constantly flows into the upper corner due to the air leakage of goaf, different pressures between the air inlet and outlet. By contrast, U+L-type ventilation system is made up of two air inlets and one outlet, which accelerates the gas emission, diffusion and flow, balances the air pressure of the upper corner, restrains the gas discharge of the upper corner, and compels the high concentrated gas to flow into

the air outlet. Therefore, the gas content in local area is diluted and lowered.

Obviously, the over-limit of gas content in the working face is effectively resolved by changing the ventilation system from U-type to U+L-type. Specifically, the gas content of the upper corner decrease from 10% to around 4%. It can be concluded that the most effective gas extraction spot constantly varies with the area where mining activities are performed. It is mainly located in the area of 40m-250m from the working face (along the horizontal mining direction, coal and rock separation area), 30m-40m from the floor (along the vertically direction, distressed and fracture zone), and approximately 60m-170m from the side of air outlet.

4.5 Chapter conclusion

(1) A brief introduction of numerical simulation theory and the software CFD are performed.

(2) Based on the real condition of working face #14205 of Shaqu coal mine, a numerical simulation model of the goaf is established, and the numerical simulation parameter and boundary conditions are determined.

(3) The numerical simulation experiments are conducted based on both of U-type ventilation system and U+L-type ventilation system, and then the gas distribution and movement rule in goaf (X, Y and Z direction) are obtained.

(4) The comparison between U-type ventilation system and U+L-type ventilation system shows that goaf gas distribution rules are similarly applied under both systems. Obviously, the over-limit of gas content in the working face is effectively resolved by changing the ventilation system from U-type to U+L-type. Specifically, the gas content of the upper corner decrease from 10% to around 4%.

(5) The numerical simulation results show that the most effective gas extraction spot constantly varies with the area where mining activities are performed. It is mainly located in the area of 40m-250m from the working face (along the horizontal mining direction, coal and rock separation area), 30m-40m from the floor (along the vertically direction, distressed and fracture zone), and approximately 40m from the side of air outlet.

5 Laboratorial simulation experiments of ventilation system and gas disaster prevention and control

5.1 Overview

This chapter describes contents concerning the laboratorial modeling used to establish the ventilation system and longwall goaf. The first part provides a brief overview of the application of laboratory simulation technique in mineral industry, analyzes the necessity of numerical simulation, and describes the research goal and contents. The second part offers an introduction to the theoretical basis of laboratorial simulation technique and similarity theory, similarity criterion and similarity theorem. The next part discusses the establishment of the laboratory simulation model of 14205 working face and goaf of Shaqu coal mine. The last part offers the verification of the simulation model based on non-coal mine ventilation system and mine coal ventilation system as well as the analysis of the experimental findings.

5.1.1 The necessity of the application of laboratorial simulation experiments

Working areas in underground mines have become far and deeper from several inlets and exhaust shafts while mining activities are performed (Widodo et al., 2008). Ventilation in any mine features permanently varying air flows under the influence of governor devices or engineering procedures (Yu et al., 2011), and it provides a flow of air to the underground workings of a mine of sufficient volume to dilute and remove noxious gases (typically NO_x, SO_2, methane, CO_2 and CO) (De la Vergne & Jack, 2003). A reasonable ventilation system exerts a long-term effect on mine safety and economic benefits. The analysis and measurements of ventilation system present a crucial element of investigation of the course of ventilation processes in mines (Gao, 2011). As a matter of fact, it is quite difficult to fully observe mine ventilation systems and predict air process behavior under different conditions and constraints in fieldwork. Many scholars use the method of numerical simulation method to simulate mine ventilation system, but it has limitations (Gauti et al., 2012). Therefore, the phase of the ventilation system planning itself may be assisted by the experimental verification of models at laboratory site (Shen

& Wang, 2011).

Moreover, high concentration gas in deep goaf and mining adjacent layers continuously pours into working as the air pressure in different parts of underground mine is imbalanced (Noack, 1998). For example, an outburst ejected over 2000 tones of oil-bearing sandstone with 900,000m^3 of gas at the 554m depth in the air shaft of Haishiwan Colliery in 1995 in China; a gas and dolomite outburst took place in Rudna copper mine in 2009, which was the most serious natural hazards in Polish copper mines (Mirosław & Mariusz, 2013). Strata gas problems have created severe difficulties for the mining industry all over the world, leading to high expenditures and intensity research efforts, and determined attempts to enhance the various ventilation and gas drainage techniques (Leszek and Lunarzewski, 1998; Sander & Connell, 2012). Meanwhile, gas research is thriving in recent years, and gas drainage technology will continue to be a growing industry over the coming decades in many countries (María & González, 2007).

Safety mining technologies including field investigation, numerical simulation and laboratory experiments have also been improved over the past decade (Packham et al., 2012). However, even if the size (height) of the gas emission zone can be estimated globally using various methods or assumptions, it is not uncommon that gas emission predictions may be under- or over-estimated due to the lack of sufficient spatial information defining the quantity and location of the gas sources in the overlying strata (Kurnia, et al., 2014). Therefore, multiple gas control strategies should be developed, including optimizing the ventilation system, preventing goaf spontaneous combustion, enhancing gas risk management, determining the gas emission zone, and implementing a reasonable gas drainage plan.

5.1.2 The research goal and contents of laboratorial simulation experiments

5.1.2.1 Research goals

(1) Teaching purpose

Firstly, the layout and the arrangement of mining roadway, air inlet and outlet, working face, upper corner, ventilation system and goaf can be recognized by establishing this simulation ventilation system model. Secondly, the relationship among the type of ventilation system, the adjustment of air damper and the layout of section roadway can be discovered by controlling the

spherical valves. Thirdly, the measurement method of mine ventilation resistance and usage of its relevant devices can be mastered by conducting the simulation experiments of mine ventilation resistance measurement. Fourthly, the air distribution and migration rule and the way of airflow regulation can be mastered by adjusting the air volume and measuring the air velocity of the simulation model. Lastly, the gas distribution and migration rule and the usage of relevant gas detecting devices can be understood during the simulation experiments are performed.

(2) Research purpose

The establishment of similarity simulation experimental model helps refine the theories about ventilation systems in the working face and goaf including U-type, U+L-type, U+I-type, Y-type and H-type, and has practical significance in the reasonable determination of relevant parameters of production safety. Research on airflow and gas migration of the roadway, working face and goaf is necessary for the integrated survey on parameters of ventilation systems and comparative study of the relevant parameters under different ventilation system conditions. The parameters and findings will play a crucial role in the optimization of the existing mine ventilation system, selection of the new ventilation system and the prevention and control of harmful gases

5.1.2.2 Research contents

The content of laboratory simulation experiment is multiple.

(1) The ventilation parameter can be determined by different part of the simulation system, such as, main air inlet and air outlet, mining roadway, working face and goaf.

(2) The change of air ventilation air resistance causing by the change of air flow can be observed. The impact of air pressure and volume through opening and closing the air door will be discussed.

(3) The rule of air flow can be concluded based on the U-type, U+L-type, Y-type, H-type, U+I-type ventilation system.

(4) The gas distribution rule and migration lay can be discovered by conducting simulation experiments based on multiple ventilation systems.

(5) The comparison among different ventilation systems can be discussed through the research of gas distribution and migration of working face and goaf, and then, the obtained rules

and relevant parameters can be used in the selection of new ventilation system and the optimization of the old ventilation system under the different geological conditions.

(6) The verification of truth that U+L-type ventilation system is more effective than U-type ventilation system in coal mines with high concentrated gas.

(7) The air leakage of goaf have an great influence on the gas distribution and migration rules of working face can be observed discovered and discussed during the experiments are performed based on multiple ventilation systems.

(8) The air volume and pressure have an effect on the gas emission rules can be observed discovered and discussed based on multiple ventilation systems.

(9) The experimental contents mentioned above can be re-performed under the inverted ventilation conditions.

More possible experiments can be conducted in this simulation model.

5.2 Theoretical foundation of simulation model design

Fluid flow phenomenon is very complex and sometimes difficult to prove and describe by mathematical analysis, but only by means of experiments. The theoretical basis of simulation tests is the similarity theory, similarity criterion and similarity law.

5.2.1 Flow condition similarity

If on the corresponding points of the two fluids, the ratio of all the physical quantities that present the flow conditions remains the same, the flow conditions of the two fluids are similar. The necessary and sufficient conditions of flow similarity are geometrical similarity, kinematic similarity and dynamic similarity.

(1) Geometric similarity

Flow similarity of the two fluids requires these two fluids satisfy both geometric similarity and dynamic similarity. Geometric similarity can be defined as two geometrical objects with the same shape; the linear ratio is:

$$L_p / L_m = \delta_l$$

the corresponding angle relationship between the prototype and the model is:

$$\alpha_p = \alpha_m$$

and the area ratio, volume ratio and perimeter ratio are:

$$S_p / S_m = \delta_l^2 ; \ V_p / V_m = \delta_l^3 ; \ U_p / U_m = \delta_l$$

where, m is the model, and p is the prototype.

(2) Kinematic similarity

Kinematics similarity requires that the length and time scales are similar between model and prototype. Obviously, kinematics similarity includes geometrical similarity. The time ratio is:

$$\mathrm{t}_p / t_m = \delta_t$$

By geometric similarity and kinematic similarity criteria, the similarity relation between the velocity of the corresponding points of the substance and the model (V_p and V_m respectively) are:

$$V_p / V_m = \left(L_p / t_p\right) / \left(L_m / t_m\right) = \delta_l / \delta_t = \delta_v$$

The relationship of acceleration ratio between the model and the prototype is:

$$\delta_a = a_p \Big/ a_m = \frac{V_p / t_p}{V_m / t_m} = \delta_l / \delta_t^2$$

(3) Dynamic similarity

Dynamic similarity exists between geometrically and kinematically similar systems and it requires that the ratios of all forces acting on corresponding fluid particles and boundary surfaces in the model and prototype are constant. Its force ratio is:

$$F_p / F_m = \delta_f$$

For different flow movements, fluid particles could be influenced by different effects, e.g. gravity force (F_g), viscous force (T_v), pressure force (P) and inertia force (F_i), but the proportional relationship of the corresponding points in both real fluid and model fluid remain unchanged under the same pressure, and it can be showed as:

$$F_{pg} / F_{mg} = T_{pv} / T_{mv} = P_p / P_m = F_{pi} / P_{mi} = \delta_f \qquad (5\text{-}2\text{-}1)$$

5.2.2 Criterion of flow similarity

Some of the basic similarity criterions can be used to explain the principle of the simulation experiments, including Strouhal similarity criterion ($S_r = 1/v_t$), which means the ratio between time-varying inertia force and space-varying inertia force; Froude similarity criterion ($F_r = v^2/g_l$), which means the ratio between inertia force and gravity force; Euler similarity criterion ($E_u = p/\rho v^2$), which means the ratio between pressure force and inertia force; Reynolds similarity criterion ($\mathrm{Re} = v_1/v = \rho v_1/\mu$), which means the ratio between inertia force and viscous force; Mach similarity criterion ($M_a = v/c$), which means the ratio between elastic force and inertia force.

(1) Newton similarity criterion

According to dynamic similarity formula (5-2-1), we can see that the ratio of inertia force at the corresponding points of the substance and the model is:

$$\begin{aligned}\delta_{fi} &= \frac{F_{pi}}{F_{mi}} = \frac{M_p \cdot a_p}{M_m \cdot a_m} = \frac{\rho_p \cdot V_p \cdot L_p / t_p^2}{\rho_m \cdot V_m \cdot L_m / t_m^2} \\ &= \frac{\rho_p \cdot V_p \cdot L_p \cdot t_m^2}{\rho_m \cdot V_m \cdot L_m \cdot t_p^2} = \frac{\rho_p \cdot V_p \cdot L_p \cdot I_m^2 / V_m^2}{\rho_m \cdot V_m \cdot L_m \cdot I_p^2 / V_p^2} \\ &= \frac{\rho_p \cdot V_p \cdot L_m \cdot V_p^2}{\rho_m \cdot V_m \cdot L_p \cdot V_m^2} = \delta_\rho \cdot \delta_l^2 \cdot \delta_v^2\end{aligned} \tag{5-2-2}$$

where, δ_ρ ——density similarity constant, $\delta_\rho = \rho_p / \rho_m$;

M_p, M_m ——mass of the corresponding points of the substance and the model.

The above formula can be as $\delta_{fi} = F_{pi} / F_{mi} = \left(M_p \cdot L_m \cdot V_p^2\right) / \left(M_m \cdot L_p \cdot V_m^2\right)$

Transpose, then

$$\frac{F_{pi} \cdot L_p}{M_p \cdot V_p^2} = \frac{F_{mi} \cdot L_m}{M_m \cdot V_m^2} = N_e \tag{5-2-3}$$

In the above formula N_e is Newton similarity number, in which if the two flow systems dynamically similar, their Newton similar numbers are certainly the same, and vice versa.

The inertial force is the reactive force to maintain the original motion state of flow. Changes

in the motion state of fluid is the result of interactions of inertial force and various other forces, therefore, the ratio between the various forces is the ratio of inertial force and other various forces.

(2) Reynolds similarity criteria

In the flow if the viscous forces $T = \mu \cdot S \dfrac{du}{dx}$ and the inertial forces both act on the corresponding particles, according to the dynamic similarity,

$$\frac{T_{pv}}{T_{mv}} = \frac{\mu_p \cdot L_p^2 \cdot V_p / L_p}{\mu_m \cdot L_m^2 \cdot V_m / L_m} = \frac{\mu_p \cdot L_p \cdot V_p}{\mu_m \cdot L_m \cdot V_m} = \delta_{tv} \cdot \delta_l \cdot \delta_v \qquad (5\text{-}2\text{-}4)$$

where, δ_{tv}——viscosity similarity constant, $\delta_{tv} = \mu_p / \mu_m$

it is known from formula (5-2-2):

$$F_{pi} / F_{mi} = \delta_\rho \cdot \delta_l^2 \cdot \delta_v^2$$

compare (5-2-2) with (5-2-4), then

$$\frac{F_{pi} \cdot T_{mv}}{F_{mi} \cdot T_{pv}} = \frac{\delta_\rho \cdot \delta_l^2 \cdot \delta_v^2}{\delta_{tv} \cdot \delta_l \cdot \delta_v} = \frac{\delta_\rho}{\delta_{tv}} \cdot \delta_l \cdot \delta_v$$

then

$$\frac{F_{pi}}{F_{mi}} = \frac{T_{pv}}{T_{mv}} \cdot \frac{\delta_\rho}{\delta_{tv}} \cdot \delta_l \cdot \delta_v \qquad (5\text{-}2\text{-}5)$$

substitute formula (5-2-1) in the above formula, then

$$\frac{\delta_\rho}{\delta_{tv}} \cdot \delta_l \cdot \delta_v = 1$$

then

$$\left(\mu_p \cdot \rho_m \cdot L_m \cdot V_m\right) / \left(\mu_m \cdot \rho_p \cdot L_p \cdot V_p\right) = 1$$

or $$\frac{L_p \cdot V_p}{\mu_p / \rho_p} = \frac{L_m \cdot V_m}{\mu_m / \rho_m} = \frac{L \cdot V}{\mu / \rho} = R_e \qquad (5\text{-}2\text{-}6)$$

where: R_e——Reynolds similarity criterion

The equation shows that if the Reynolds similarity criteria of the two flows Reynolds the same, their viscous forces are dynamically similar. Wherein linear dimension L refers to any typical linear dimension, such as pipe diameter and radius; velocity in pipeline can adopt the average flow rate.

(3) Froude similarity criterion

If in the flow phenomenon gravity and inertial force play a leading role, the same deducing method of Reynolds criterion is employed and Froude similarity criterion is obtained as follows:

$$\frac{V^2{}_p}{g_p \cdot L_p} = \frac{V^2{}_m}{g_m \cdot L_m} = \frac{V^2}{g \cdot L} = F_r \tag{5-2-7}$$

where, g ——gravitational acceleration;

V ——flow kinematic velocity;

L ——lineal length;

F ——Froude similarity criterion.

The above equation shows that if the Froude similarity criteria of the two flows are the same, their gravity is dynamically similar.

(4) Euler similarity criterion

If in the flow phenomenon gravity and inertial force play a leading role, the same deducing method of Reynolds criterion is employed and Euler similarity criterion is obtained as follows:

$$\frac{P_p}{\rho_p \cdot V_p^2} = \frac{P_m}{\rho_m \cdot V_m^2} = \frac{P}{\rho \cdot V^2} = E_\mu \tag{5-2-8}$$

where, P ——pressure on flow;

E_μ ——Euler similarity criterion.

The above equation shows that if the Euler similarity criteria of the two flows are the same, their pressures are dynamically similar. When the fluids flow in pipelines, sometimes energy difference of the two points of the fluid ΔP is adopted to substitute the pressure in (5-2-8).

$$\frac{\Delta P}{\rho V^2} = E_\mu$$

5.2.3 Fluid motion differential equation

Fluid motion differential equation are frequently used to describe the relation between fluid motion and stress; model flow and prototype flow, both incompressible, achieve flow similarity on the condition that they satisfy the motion differential equation, which are shown as follows:

$$\frac{\delta_v}{\delta_t} = \frac{\delta_v^2}{\delta_l} = \delta_g = \frac{\delta_p}{\delta_\rho \delta_l} = \frac{\delta_v^2}{\delta_l^2} \tag{5-2-9}$$

Formula (5-2-9) indicates Time-varying inertia force, Space-varying inertia force, Mass force, Pressure and Friction force respectively. It also shows the force polygon of model flow is similar to prototype flow.

Divide Formula (5-2-9) by space-varying inertia force, then,

$$\frac{\delta_l}{\delta_t \delta_v} = 1 = \frac{\delta_l \delta_g}{\delta_v^2} = \frac{\delta_p}{\delta_\rho \delta_v^2} = \frac{1}{\delta_l} \tag{5-2-10}$$

Formula (5-2-10) indicates a certain constraint exists among different ratios when dynamic similarity of model and prototype flow is achieved, and similar standards can be obtained by further analysis. That is: dynamic similarity can be described by similarity criterion. In fact, model and prototype flow cannot become equal flow and fully dynamic similarity; therefore, the main dynamic similarity is a key point of the simulation experiments, which means if the Reynolds of two different flow types are similar, ($\mathrm{Re}_m = \mathrm{Re}_p$), they have dynamic similarity.

5.2.4 Similarity theory

The basis of similarity theory is three similarity theorems. Similarity theorems are used for the guidance of the design and its associated experimental data processing and promotion of the model.

(1) The first similarity theorem

The first similarity theorem can be expressed as: if the process is similar, the similarity criterion is unchanged, and the similarity index is 1.

Based on this theorem, the relations of similarity constants of the corresponding physical quantity within the system are determined, and thus similarity criterion is obtained.

If there are n physical quantities in a phenomenon, its mathematical expression is:

$$\varphi(a_1, a_2 \cdots\cdots, a_n) = 0 \tag{5-2-11}$$

then in n variables, there are k independent variables and m dependent variables, $m = n - k$, and totally it includes i equations:

$$\varphi_1(a_1, a_2 \cdots\cdots, a_n) = 0 \tag{5-2-12}$$

there are j terms in every equation, and the first system can be expressed as:

$$\sum_{j=1}^{Q} \varphi_{ij}\left(a_1', a_2' \cdots\cdots, a_n'\right) = 0 \tag{5-2-13}$$

substitute $a_1' = c_1 a_1''$, $a_2' = c_2 a_2'' \cdots\cdots a_n' = c_n a_n''$ into the above equation, then

$$\sum_{j=1}^{Q} \varphi_{ij}\left(c_1 a_1', c_2 a_2' \cdots\cdots, c_n a_n'\right) = \sum_{j=1}^{Q} \varphi_{ij}\left(c_1, c_2, \cdots\cdots, c_n\right) \varphi_{ij}\left(a_1'', a_2'', \cdots\cdots a_n''\right) = 0 \tag{5-2-14}$$

as the above equation is the homogeneous equation, then

$$\varphi_{i1}(c_1, c_2, \cdots\cdots, c_n) = \varphi_{i2}(c_1, c_2, \cdots\cdots, c_n) = \cdots\cdots \varphi_{ij}(c_1, c_2, \cdots\cdots, c_n) \tag{5-2-15}$$

it can be divided by any term; similarity index equation f_i is obtained and converts to

$$f_j(c_1, c_2, \cdots\cdots, c_n) = \frac{F_j\left(a_1', a_2', \cdots\cdots a_n'\right)}{F_j\left(a_1'', a_2'', \cdots\cdots a_n''\right)} \tag{5-2-16}$$

the above equation is dimensionless number and presented by C

$$\mathrm{C}_j = F_j(a_1, a_2 \cdots\cdots, a_n) = idem \tag{5-2-17}$$

the two processes are similar and their similarity criteria are unchanged

$$\mathrm{C}'_1 = \mathrm{C}''_1, \quad \mathrm{C}'_2 = \mathrm{C}''_2, \cdots\cdots, \mathrm{C}'_m = \mathrm{C}''_m, \cdots \tag{5-2-18}$$

In summary, the first similarity theorem is about similarity criteria, and it shows the physical quantities that should be measured in the experiment.

(2) The second similarity theorem

The second similarity theorem is also known as the C theorem, which states that the basic physics equations that restrain the two similarity phenomena can be converted into similarity judgment equation through dimensional analysis in order to express the new equation, that is converted into the C equation and C equations of two similar systems must be the same.

The equation that expresses a certain physical phenomenon is

$$f(x_1, x_2, x_3, \cdots, x_n) = 0 \tag{5-2-19}$$

where: $x_1, x_2, x_3, \cdots, x_n$——individual physical quantity in the equation can all convert into the non-dimensional equations below;

$$[1] = \phi\left(C_1, C_2, C_3, \cdots C_{(n-m)}\right) \tag{5-2-20}$$

If in an equation there are several physical quantities, which contain m dimensions, the independent similarity criteria C value is $n-m$. The physical equations of the two similar phenomena can be expressed by the relation of the $(n-m)$ non-dimensional physical quantities. Functional relation is among $C_1, C_2, C_3, \cdots C_{(n-m)}$:

$$f\left(C_1, C_2, C_3, \cdots C_{(n-m)}\right) = 0 \tag{5-2-21}$$

the above equation is the mathematical expression of the second theorem.

where,

$$\begin{aligned} C_{1M} &= C_{1H} \\ C_{2M} &= C_{2H} \\ &\mathrm{M} \\ C_{(n-m)M} &= C_{(n-m)H} \end{aligned} \tag{5-2-22}$$

Equation 5-2-14 illustrates that if the result of a phenomenon turns into the corresponding non-dimensional C relational expression, this expression can be applied to other similar phenomena.

The second similarity theorem solves the application of finishing methods and experimental data, and serves guideline of the experiment arrangements.

(3) The second similarity theorem

The second similarity theorem can be expressed as: if the geometry similarity systems have the same text in relational equations, similar single-value conditions and the same similarity criteria consisting of single value, these two phenomena are similar.

The first and second similarity theorems indicate the nature of similar phenomena, but not provide the requirement of the determination of the similarity of the phenomena, and what the proportional relationship is among parameters in simulation experiment.

The third similarity theorem solves these problems that as long as the nature and quantity of the single value is similar, phenomena of the same kind with the same values of stereotype criteria are similar. The third similarity theorem presents the necessary and sufficient conditions of similar phenomena. As a consequence, the above three theorems are the theoretical basis of the similarity simulation experiment.

5.3 Similarity theory and simulation model of ventilation system

5.3.1 The similarity theory in the application of the model design

Air is the flow medium, and its flow state is regarded as pressure steady flows during experiments are performed. The similarity relationship between prototype and model is built according to the similarity criteria such as geometric and dynamic similarity. The ventilation network model is proportional to the tunnel size of designated coal mine. Taking into consideration the experiment feasibility, the establishment of the ventilation model is simplified.

5.3.1.1 The similarity of roadway

The prototype of the model is the working face of inclined longwall coal-mining and caving management in the roof. As the research purpose of this experimental model is to study the gas migration law in goaf, the entire roadway in the ventilation system model mainly refers to the practical situation in Shaqu Mine, and in the model the roadway sections and connection roadway of the working face is designed in strict accordance with the practical roadway of the 14205 working to achieve geometrically similarity. However, in the roadway and main inlet and return airways that have less impact on goaf, the research purpose is on the simplicity of the model production. Standard pipes are used and roadway area approximation is achieved for the research on ventilation resistance measurement and airflow regulation. In order to cushion the airflow so that air velocity distribution becomes stable after a certain distance, the length of roadway segment model is greater than 2m as the stable segment of the geometrical similarity.

Taking the experimental condition, the facility of measurement and other factors into account, the linear scale is determined, $\delta_l = 50$, and the main geometric size of the prototype and the model can be seen in Table 5.3.1.

Table 5.3.1 Geometric similarity of roadway between the prototype and the model

Item	Actual size (m)	Road area (m2)	Size of prototype (m)	Size of model (mm)	comment
Sublevel	3.8×2.8	10.64	3.8×2.8	76×56	Field

roadway					measurement
Mining roadway	4.0×2.8	11.2	4.8×2.3	96×46	Approximately equal
Air inlet and outlet	5.0×3.6	18.0	4.8×3.8	96×76	Approximately equal
Connection roadway	3.3×2.3	7.59	3.3×2.3	66×46	Field measurement
Alternative roadway	—	—	3.3×2.3	66×46	Practical reference

Dynamic similarity requires that stress on corresponding particles of the original object and the model remain the same proportional relation, while flow similarity demands that the force on fluid particles comply with the above guidelines, including inertial force, viscous force, gravity, pressure, elastic force and surface tension, etc.

In fact, due to the restrictions on model structure and experiment conditions, air velocity in the model is difficult to achieve Reynolds similarity criteria. Reynolds similarity criterion requires when the model size is small, the flow velocity is large; while Froude similarity requires when the model size is small, the flow velocity is small, therefore, it is barely impossible to ensure the equality of the two similarities. However, for all the researches on flow phenomena, only one force acts like the main force and rest forces are the minor forces. Besides for every single flow object, its main force is different. Thereby when studying a flow phenomenon, the priority is to identify its main driving force and make it satisfy the corresponding similarity, while the other minor similarity criteria are ignored.

In the similar airflow in coal mine, the main consideration is the viscous force, pressure and inertial forces, and the rest forces can be ignored such as gravity, elastic force and surface tension, hence only Reynolds and Euler criteria are required in coal mine ventilation. It is known in fluid mechanics, when Re is smaller than the first critical value, the flow is in the state of laminar flow, and in the laminar flow range, the flow state and flow velocity distribution of the fluid are similar to each other and unrelated to Re. When Re is larger than the first critical value, the flow is in the

transition zone, and with the increase of Re, the fluid turbulent fluctuation varies greatly at first and then gradually decreases. When Re is larger than the second critical value, the flow state and flow velocity distribution of the fluid no longer change is unrelated to Reynolds. They are similar to each other and enter the resistance square area. If Re in the model is in the resistance square area, their Reynolds are considered equal regardless of what their absolute values are. This phenomenon is called automatic mode that is as long as the object and its model geometrically similar, it is guaranteed dynamic similarity is achieved, and the achievement of geometric similarity and dynamic similarity ensures the satisfaction of kinematic similitude.

5.3.1.2 The similarity of stope

The flow field of the stope in both of the prototype and the model is multiple flow fields of the working face, goaf and adjacent layers, and it is difficult to determine their geometrical boundary and characteristic of flow distribution. Specifically, the air flow in working face is regard as one-dimensional pipe flow, and it is usually in turbulence state. However, the air flow of goaf is regards as three-dimensional porous media flow, and it can be in turbulence state, laminar flow state and transitional flow state.

(1) Geometric similarity of stope

The design of working face length, mining height and other parameters are based on working face 14205 of Shaqu coal mine. Each part of the coal mine prototype is scaled down except the angle, which ensure the prototype and the model meet the requirement of geometric similarity. Taking the experimental condition, the facility of measurement and other factors into account, the linear scale is determined, $\delta_l = 50$, and the main geometric sizes of the prototype and the model of stope are shown in Table 5.3.2.

Table 5.3.2 Geometric similarity of stope between the prototype and the model

Item	Actual size (m)	Model size (m)	Comment
Length of strike	150	4.3	Effect of goaf air flow
Height of mining	2.5	0.05	Height of mining face
Width of mining face	4.5	0.09	Width of mining face

Length of mining face	200	4.0	
Height of roof caving	10	0.2	The air flow law in the caving zone

(2) The similarity criterion of retrieving working face

The airflow of the model and the prototype is in turbulent state. As the size of the working face is small, airflow can be considered as one-dimensional flow along the roadway, therefore, the similarity of its movement can be guaranteed. The pressure drop along the working face is mainly due to the loss of frictional resistance, neglecting other minor external forces. When the two geometrically similar flows achieve mechanical similarity under the influence of frictional resistance, their Froude number and ratio of the hydraulic gradient are equivalent and their resistance coefficient are approximately the same. The relative roughness of the model and the prototype should be the same, but in reality the condition is extremely harsh and the model process is quite costly and even unable to achieve. As a consequence, mechanical similarity in the working face can only be achieved by improving the geometric accuracy in the working face.

The simulation experiment of ventilation fan model is based on the pressure flow phenomenon. In order to ensure dynamic similarity, it must follow the Euler similarity criterion. Euler similarity criterion can be satisfied when $\delta_\rho = 1$ and $\delta_v = 1$, five different points are select in the mining working face model to adjust the air resistance, and ΔP_m of the simulation model and ΔP_0 of the working face measurement points are same

(3) The similarity criterion of goaf

Many research results show that the air flow state of flowing into and out of goaf will be changed from laminar flow state to laminar flow state. Thus, the air flow state in the simulation goaf model can be regard as laminar flow state.

According to fluid motion condition theory, the geometric similarity can lead to kinematic similarity if the air flow can keep in a laminar flow state in flow region.

(4) The similarity criterion of goaf gas migration

The differential equation of goaf gas migration:

$$-\frac{\partial}{\partial x_i}\left(D_{ij}\frac{\partial c}{\partial x_i}\right)+\frac{\partial}{\partial x_i}\left(V_i c\right)=1 \quad (i,j=1,2)$$

where: D_{ij} ——diffusion coefficient, m^2/s;

V_i ——average velocity components, m/s;

c ——gas concentration, g/m^3;

I ——gas emission rate of unit area of goaf roof and floor, $g/m^3 \cdot s$.

Regardless of the fact that some gas flows into goaf by the side, Peclet number (Pe) and Gas flow number (Fq) are derived by integral analogy. The criteria of gas migration in the simulation experiment are Reynolds criterion, Froude criterion, Peclet criterion and Gas flow criterion, among which Froude criterion is excluded because in Froude criterion gravity is the main force, but gravity is supposed to be ignored in forced flow. It is difficult to equal the Reynolds number (Re) in the model and the prototype due to the restriction of the experimental conditions; under the condition of single valued similarity, Re needs to be self-modeling in order to ensure the flow states of fluid in the model and the prototype are similar. Peclet criterion is the ratio of convective gas migration and dynamic dispersion, and it can be achieved when the seepage fields are similar. Gas flow number is the ratio of gas emission volume and the corresponding gas migration volume, and it can be achieved when airflow and gas emission is stable.

5.3.2 The design of experimental facility of the simulation model

5.3.2.1 The proportion determination of the simulation model

This goaf simulation experiment of gas migration mainly focus on the working face 14205 of Shaqu coal mine, the design of simulation model is based on the basic condition of Shaqu coal mine and its parameters. The proportion between the model and the prototype is 1:50, and the specific size can be seen in Table 5.3.1 and Table 5.3.2, and the measured air velocity of the air inlet is 1.5m/s.

The critical velocity of the model in the turbulent state is as follows:

(1) The second critical value of Reynolds number in the general experience model is: 1.0×10^4

~ 1.5×10^5, here when Re=1.0×10^4,

$$V=\frac{\mathrm{Re}Uv}{4s}$$

where: V——the average velocity in the roadway, m/s;

v——dynamic viscosity coefficient of the fluid, related to fluid temperature and pressure, for the ventilation in mine, it usually takes $14.4\times10^{-6}m^2/s$;

U——perimeter of the roadway, m;

S——area of roadway, m^2.

$$V=\frac{10000\times2\times(0.076+0.056)\times14.4\times10^{-6}}{4\times0.076\times0.056}=2.23m/s$$

(2) For simplicity, Reynolds Number (Re) is usually considered as a criterion of flow statement in the tunnel in the practical engineering calculation, namely:

when $\mathrm{Re}\le2300$, it means the flow is in laminar state, and when $\mathrm{R}\ge2300$, it means the flow is in turbulent state.

$$V=\frac{2300\times2\times(0.076+0.056)\times14.4\times10^{-6}}{4\times0.076\times0.056}=0.51m/s$$

For the purpose of making air flow in turbulent flow state in the roadway of the simulation model, the spherical valves are selected.

According to the results of (1) and (2), it can be concluded that the minimum flow velocity for meeting turbulent state in the simulation model of ventilation network must be higher than 0.51m/s. As a matter of fact, the minimum velocity measured in the model reached 3m/s, which means its Reynolds Number (Re) is in the resistance square area. Therefore, its linear scale $\delta_l=50$, density scale $\delta_\rho=1$ and the speed scale $\delta_v=1$ can be decided. Dynamic ssimilarity can be ensured if the flow condition between two fluids satisfies geometric similarity. Similarly, kinematic similarity can be ensured if the flow condition between two fluids satisfies geometric similarity and Dynamic similarity. Thus, the measured parameter can be used as a effective and valid reference for the selection of mine ventilation types and for the optimization of the existing ventilation system.

5.3.2.2 Design of experimental device

Air is the flow medium, and its flow state is regarded as pressure steady flows during experiments are performed. The similarity relationship between the prototype and the model is built according to the similarity criteria including geometric similarity, kinematic similarity and dynamic similarity. The ventilation system model is proportional to the roadway size of Shaqu coal mine. Taking into consideration the experiment feasibility, the plan and the establishment of the ventilation system and goaf model is simplified, and it can be seen in Figure 5.3.1. Figure 5.3.2 shows the effect drawing of the simulation ventilation and goaf model.

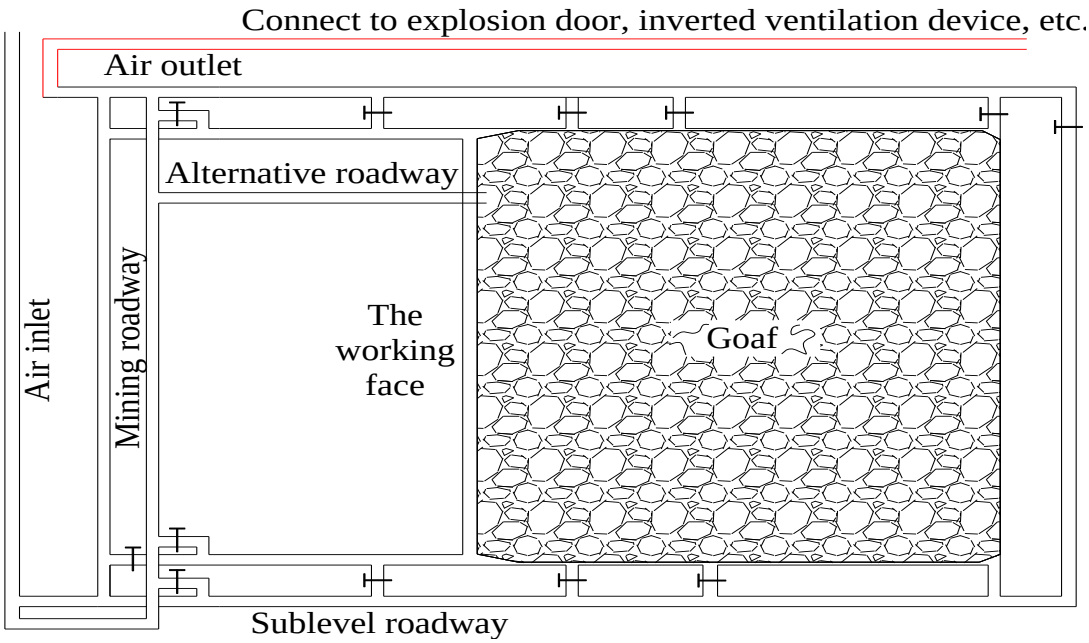

Figure 5.3.1 Plan of simulation model of ventilation system and goaf

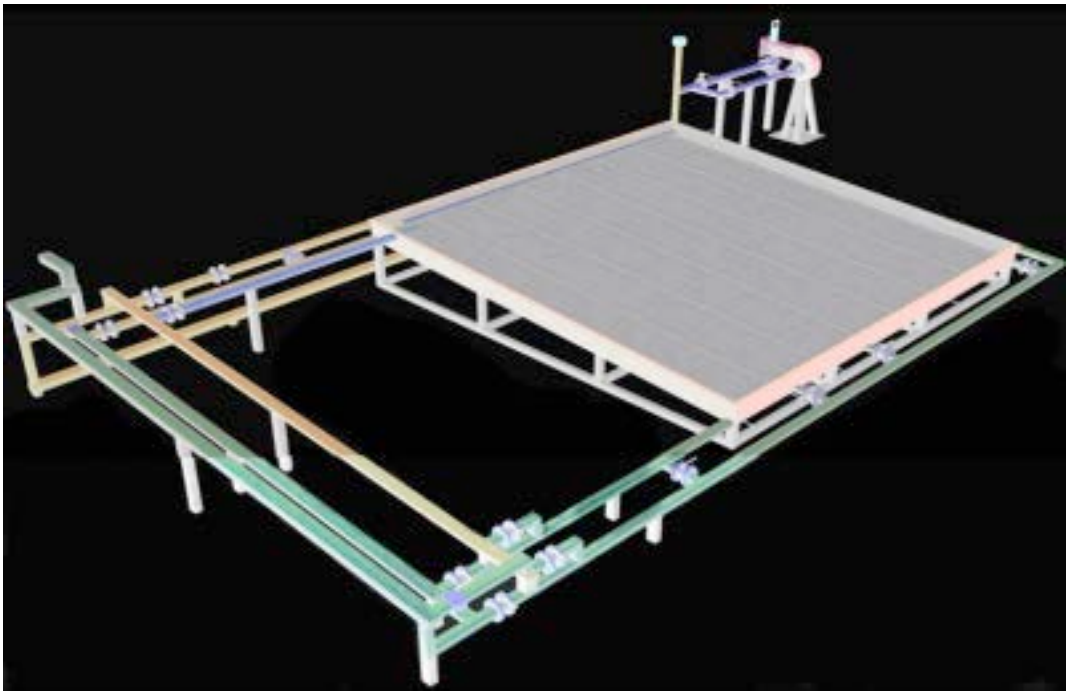

Figure 5.3.2 Effect drawing of simulation ventilation system and goaf

The details of the model establishment are as follows:

The model consists of five parts including model body (roadway, working face and goaf area), fan and its affiliated device, gas drainage system, testing system and collection system. The ratio of the model is 1:50. Specifically in the model, the size of the goaf is 4.32m × 4.16m × 0.2m; the length of the working face is 4.0m; the section is: 0.09m × 0.05m; the angle of face inclination is 8° and the tunnel section is: 0.08m × 0.06m. The measured air velocity in the tunnel of the ventilation model is 3m/s, which means the air flow state is in turbulent flow state. Figure 5.3.3 shows the main body of the model.

Figure 5.3.3 Established simulation model of ventilation system

Spherical valves are selected as the air damper, and the adjustment of air volume and the conversion among different types of ventilation systems can be controlled and switched by opening and closing different spherical valves.

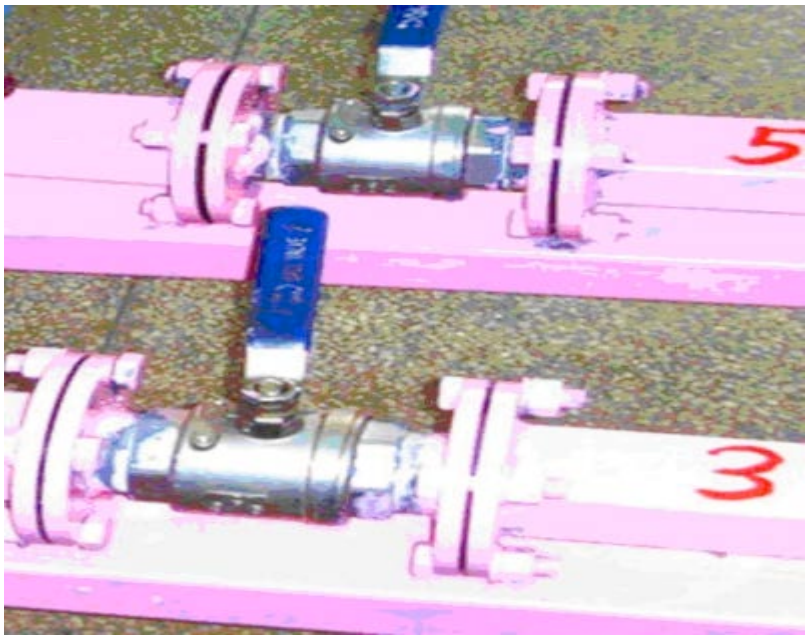

Figure 5.3.4 Spherical valves

Figure 5.3.4 shows the conversion between U-type ventilation system and U+L-type ventilation system can be controlled and switched by opening and closing different spherical valves.

(1) Main part of the simulation model

The model roadway is welded by square and round stainless steel tube, goaf floor and domain boundaries are welded by stainless steel plates, and the model base is made by angle steel. Seams are all welded in order to ensure the robustness and sealability of the box. The roof is covered with 8mm thick polymethyl methacrylate and sealed with glass glue, on which grid square is painted for observation and analysis of flow. In order to fully reflect the lithologic character, the filling materials in goaf are made directly from the wasted coal fragments ranging from 1 ~ 60mm. The pile of rock in goaf is guided by Theory on the critical layer of strata control, and rock in the caving zone is piled by crushed wasted coal. Crushed wasted coals of different compaction characteristics are respectively stacked in the central compaction area and O-ring area of the model, so as to satisfy the permeability characteristics of the caving zone

(2) Selection of ventilation fan

Ventilation fan employs centrifugal fan and extracted ventilation. A number of roadways in the model are installed with ball valves adjusting the air volume and altering ventilation pattern in the working face. Although the model can achieve the conversion of various ventilation systems, for fan type selection, instead of calculating the ventilation resistance for every ventilation system, only the ventilation system with the maximal ventilation resistance is counted. Compared with real coal mines, in the model the single ventilation system is relatively simple and all branches in the ventilation systems are in parallel connection with the mining face, thereby, the research estimates the ventilation resistance in the most difficult situations in the system. Supposedly the air velocity of the main return airway is 15m/s, and the air velocity of the other roadways is 10m/s, local resistance and frictional resistance in the entire model are calculated, and ventilation resistance and motor power of the entire model are estimated as 3300Pa and 9kW respectively, thus centrifugal fan is selected as the ventilation fan.

(3) Ventilation fan and its accessory device

The simulation ventilation fan and its accessory device include explosion door, inverted ventilation device, diffuser, and shock absorber device between ventilation fans and tube, etc

(Figure 5.3.5). Contra flow in the simulation ventilation system can be achieved by opening the special valve on the inverted ventilation roadway.

Figure 5.3.5 Ventilator and its subsidiary unit in-kind photos

(4) System of gas emission source

As is shown in Figure 5.3.6, the gas supply system consists of gas bottles of high content and high pressure, pressure reducing valves, current stabilizer, flow meter, air supply hose and gas release pipeline in goaf. After gas flows from high-pressure gas tank through the pressure valve releasing pressure and enters the current stabilizer, in which the flow is distributed by the flow meter, and then goes through air supply hose and gas release pipeline into goaf.

Figure 5.3.6 Gas container and rubber gas supply tube

Stainless steel tube (Φ=5mm) are selected as the injection and supply of gas emission pipelines, and they are paved at the bottom of simulation goaf (Figure 5.3.7).

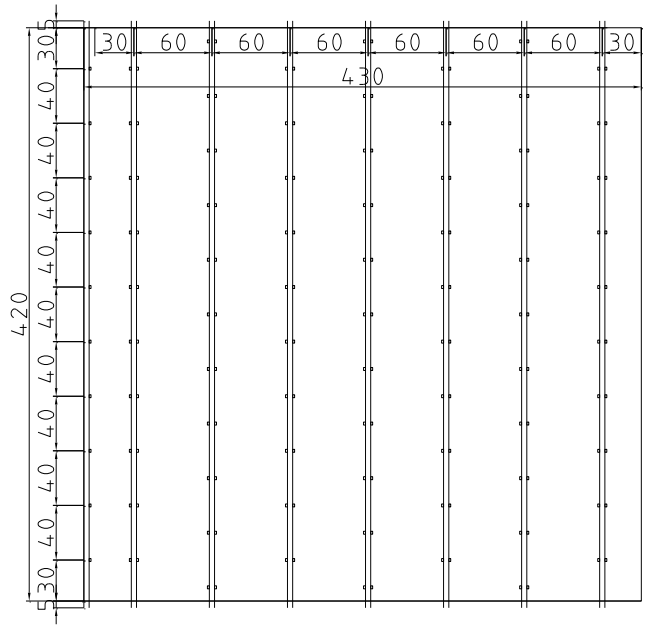

Figure 5.3.7 Layout of gas emission pipeline and emission parameter of emission hole

In order to comply the gas flow into the working face and goaf with the practical situation, holes are punched at a certain distance on both sides of the steel pipe, and the size and distribution of the holes are determined after the smoke test in order to makes characteristics of goaf gas emission in line with the actual situation. The layout of gas emission pipeline in goaf is in Figure 5.3.8.

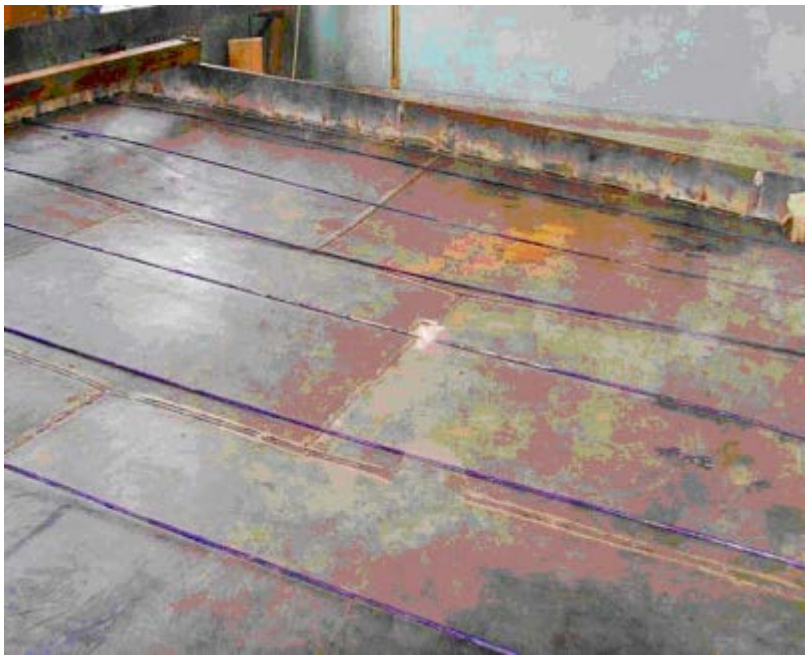

Figure 5.3.8 Gas injection system and layout of gas emission pipeline in goaf

(5) Testing system

The testing system includes JDM9-compensated micro manometer, U-type water barometer, single pipe inclined manometer, and dry-wet ventilated thermometer, QDF-2 hot-bulb anemometer and WY-Single pipe groove mercury barometer. Besides, a pitot-tube is adopted for the purpose of improving the measurement accuracy.

The major testing parameters include gas emission rate, air velocity and static pressure. The gas emission rate can be measured and controlled by flow meter (Figure 5.3.9). The air velocity can be tested by pitot tube and differential pressure gauge. The static pressure can be measured by standard pitot tube and U-type differential pressure gauge.

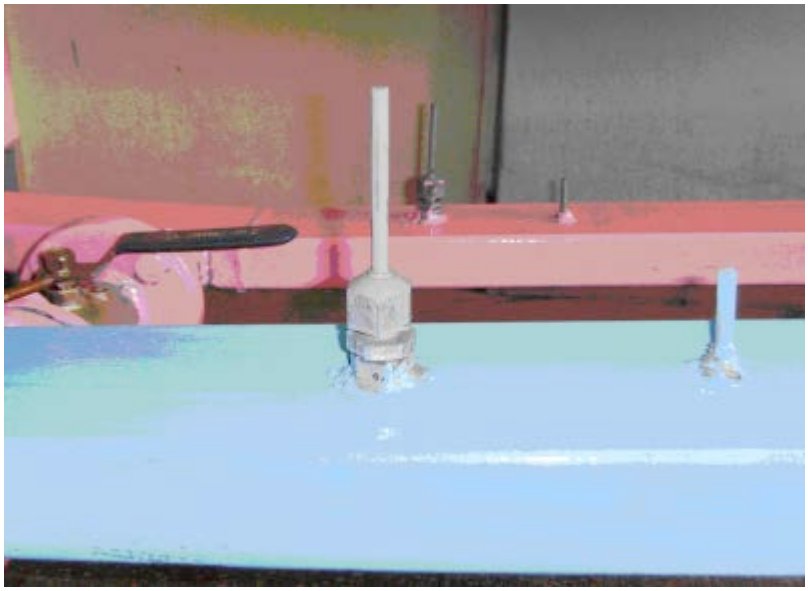

Figure 5.3.9 Static pressure and air velocity tester of roadway

(6) Data collecting system

The top of the simulation goaf area is covered by organic glass with 66 holes (64 normal holes and 2 special holes located in the upper corner and lower corner respectively, and it can be seen in Figure 5.3.10), each of which is plugged by a rubber stopper with a collector inserted in it.

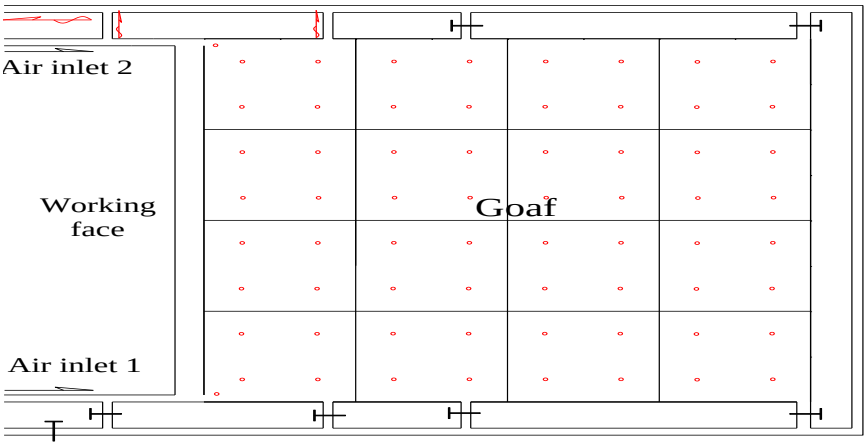

Figure 5.3.10 The monitoring points in goaf area

U+L-type ventilation system with two air inlets and one outlet

Besides, the goaf is also inserted with collectors. The data of gas sample can be detected by gas chromatograph and gas detector (Figure 5.3.11) after the ventilation fan is stably operated and the airflow is stable in the ventilation system and goaf.

Figure 5.3.11 Gas chromatograph and computer group

5.4 Ventilation systems selection and test

Gas from shafts of active mines generates a large number of gas emissions from underground mines; gas concentration in ventilation air is different for each mine not only because of the difference of gas emission volume, but also the different type of ventilation system. This simulation model can significantly help us understand some basic ventilation systems and their characters, and the transformation among different types of ventilation system is controlled by opening or closing the spherical valves.

5.4.1 U-type ventilation system

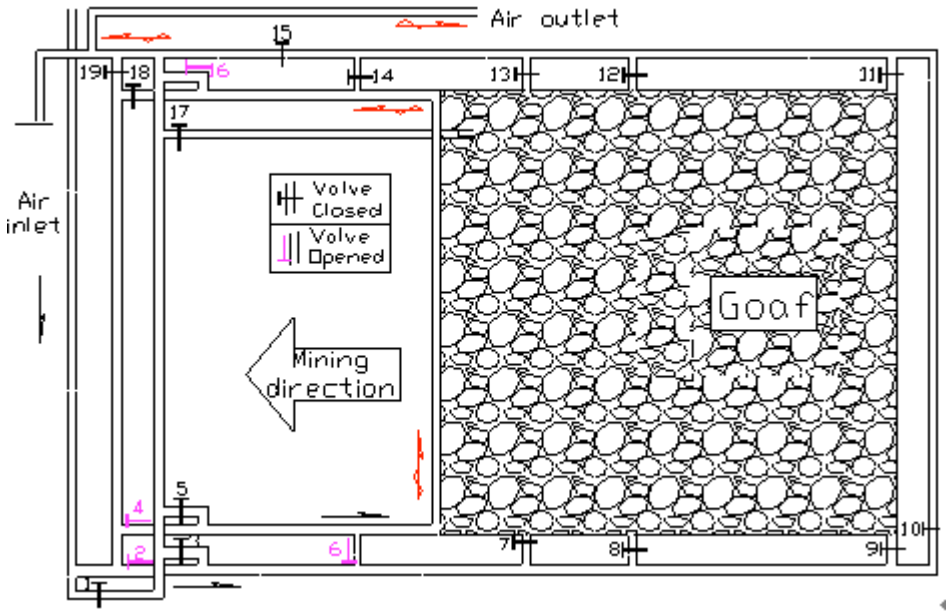

Figure 5.4.1 U-type ventilation system

The spherical valves of No.2, 4, 6 and 16 are opened while others are closed, and it can be seen from Figure 5.4.1, and Figure 5.4.2 shows gas movement in U-type ventilation system.

Figure 5.4.2 Gas movement in U-type ventilation system

The most common and effective method to limit airflow to the goaf in a longwall panel is the U-shaped ventilation system. In this system, the air is brought up the air inlet, across the working face, and down the air outlet. This system is widely used in low gas concentration mine in mining industry around the world because it is economical and easy to design and build. However, when working areas in underground mines have become farther and deeper where more high concentration gas are released, U-shaped ventilation system will not be able to offer enough fresh air for miners, and to dilute the high concentration gas in the working face.

5.4.2 Y-type ventilation system

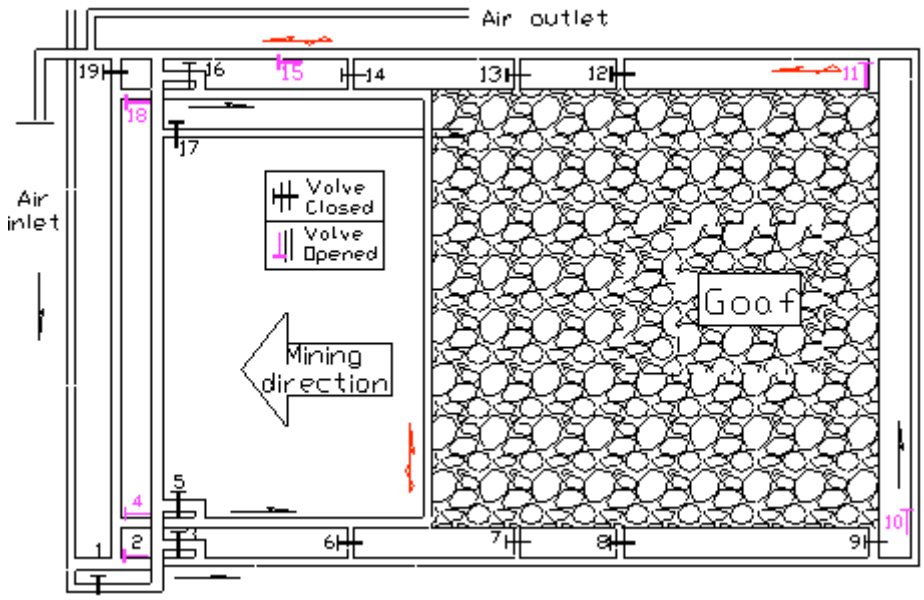

Figure 5.4.3 Y-type ventilation system

The spherical valves of No.2, 4, 10, 11, 13, 15 and 18 are opened while others are closed, and it can be seen from Figure 5.4.3, while Figure 5.4.4 shows gas movement in Y-type ventilation system.

Figure 5.4.4 gas movement in Y-type ventilation system

Y-type ventilation system utilizes multiple air inlets and one tail tunnel. The air is brought up all the air inlets, across the workface and goaf, and removed via the tail tunnel. One advantage of this system is that the working face gas problem can be effectively addressed, and working section recovery can be moderately improved. Another advantage of this system is that the gas-drainage systems are accessible during the life of the panel. The major disadvantages with this system are that conditions exist that contribute to the development of spontaneous combustion in the ventilated portion of the goaf, and there is an absolute reliance on seals between the goaf and the air outlet to prevent air leakage.

5.4.3 U+I-type ventilation system

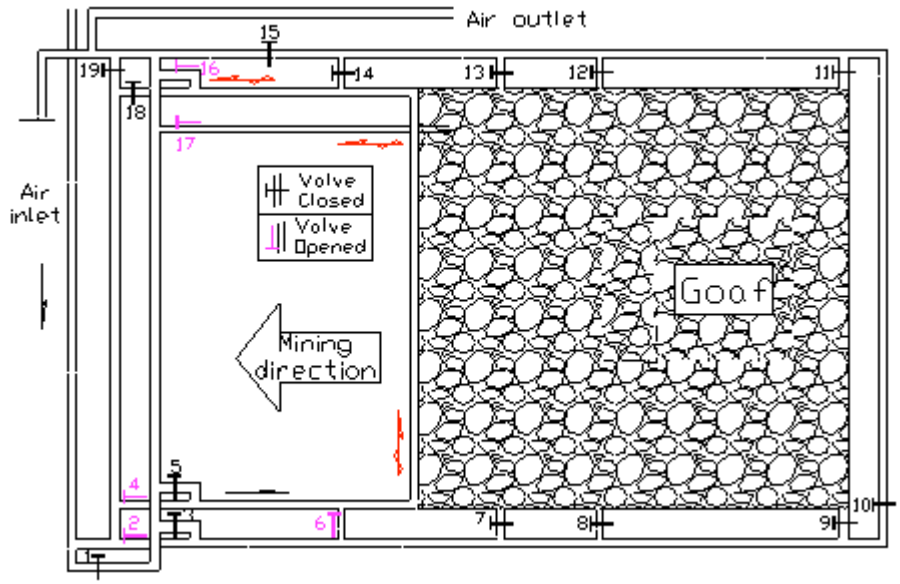

Figure 5.4.5 U+I-type ventilation system

The spherical valves of No.2, 4, 6, 16 and 17 (high level gas drainage tunnel) are opened while others are closed, and it can be seen from Figure 5.4.5, while Figure 5.4.6 shows gas movement in U+I-type ventilation system.

Figure 5.4.6 gas movement in U+I-type ventilation system

U+I-type ventilation system consists of U-type system and a high level gas drainage tunnel. In this system, the air is brought up to the air inlet, across the workface, and down the air outlet. Besides, a high level gas drainage tunnel (above the coal seam) is excavated in the mix zone between the working face and goaf, and then high concentration gas can be extracted from goaf. Therefore, the gas problem of the working face and upper corner can be effectively resolved, and coal spontaneous combustion in goaf can be moderately prevented. However, the major disadvantage with this system is that the cost of the tunnel excavation is too high.

5.4.4 H-type ventilation system

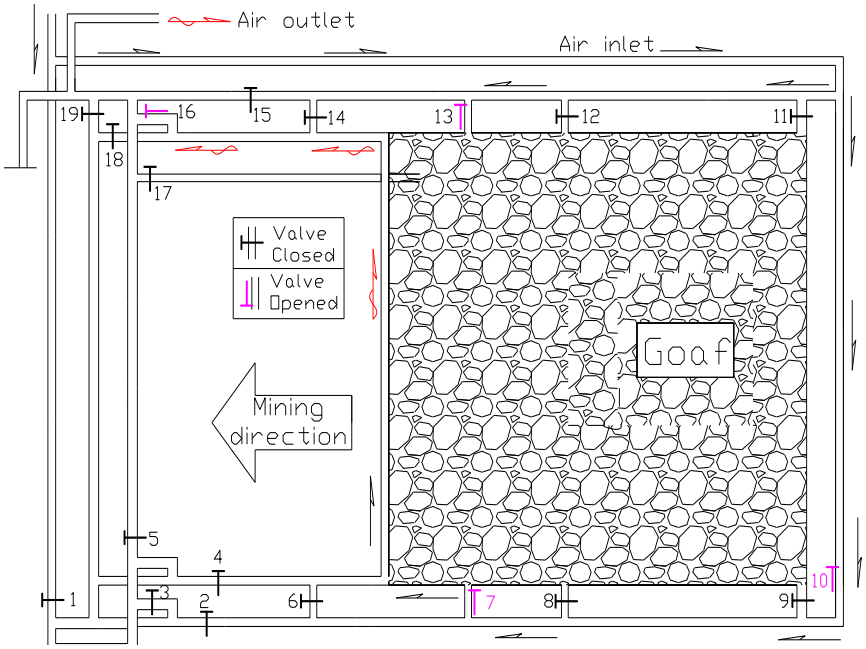

Figure 5.4.7 H-type ventilation system

The spherical valves of No.7, 10, 13, and 16 are opened while others are closed, and it can be seen from Figure 5.4.7, while Figure 5.4.8 shows gas movement in H-type ventilation system.

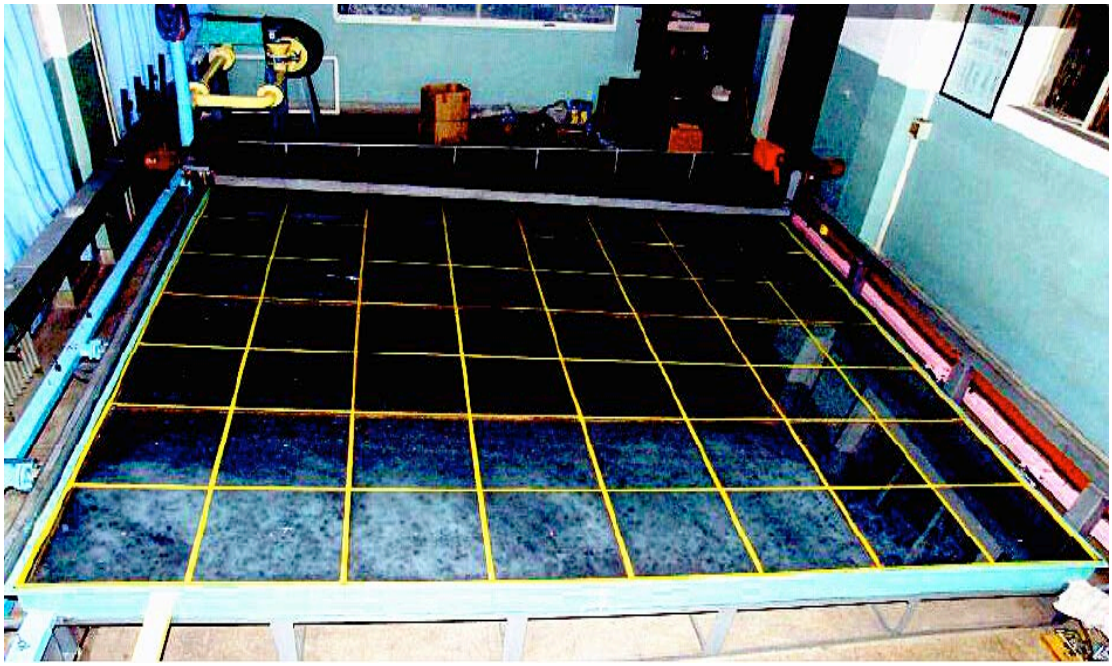

Figure 5.4.8 Gas movement in H-type ventilation system

H-type ventilation system consisted of two air inlets and one air outlet. In this system, the fresh air is brought up to the air inlet, across the workface, and down the air outlet. Where the available airflow is insufficient to dilute the gas emitted from the working face, additional air from valve No.3 can be introduced independently by adopting mine layouts in various configurations such as the “H” system, shown in Figure 5.4.7. This ventilation systems, however, require higher investment such as driving of an additional roadway, roadside dam (pack wall), and strong support of the roadways remaining open behind the longwall in the goaf.

5.4.5 U+L-type ventilation system

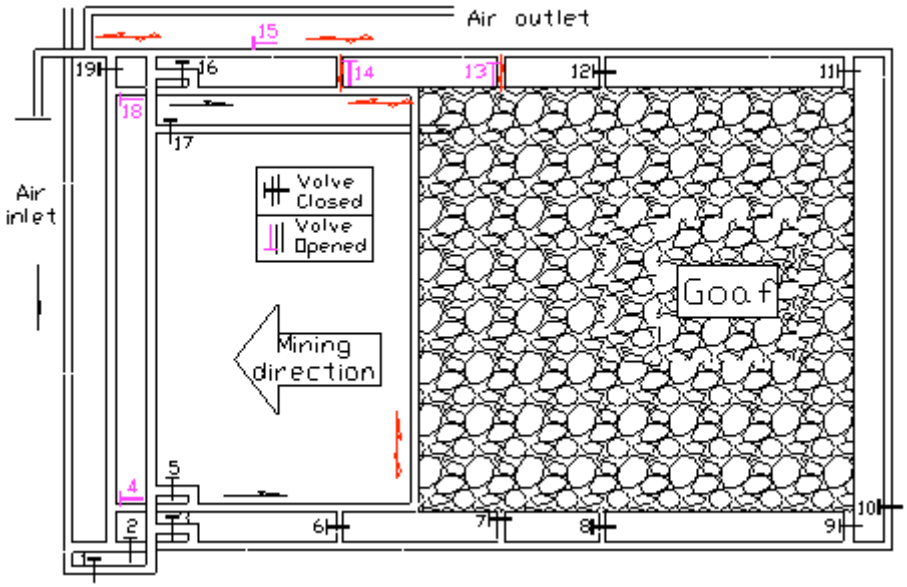

Figure 5.4.9 U+L-type ventilation system

The spherical valves of No.4, 13, 14, 15 and 18 are opened while others are closed, and it can be seen from Figure 5.4.9, while Figure 5.4.10 shows gas movement in U+L-type ventilation system.

Figure 5.4.10 Gas movement in U+L-type ventilation system

U+L-type ventilation network, consisted of two air inlets and one outlet roadway, accelerates the gas emission, diffusion and flow, balances the air pressure of upper corner, restrains the gas emission of upper corner, and compels the high concentration gas and air leakage of goaf to flow over into air outlet, thus, lowers the gas concentration of local areas, aimed to effectively resolve the difficulties of gas over-limit of the working face. In addition, the total air volume in the working face has significantly increased as fresh air is constantly offered from two inlet airways.

5.4.6 Selection of ventilation system

Regardless of whichever system or layout is being used, a sufficient volume of fresh air must arrive at the coal-cutting machine to dilute the coal front gas (arising from the remaining seam gas content after any pre-drainage) to satisfy the local statutory limit. The selected layout should be capable of providing a good standard of ventilation at the most effective methane drainage drilling locations. If this standard is not achieved, it will result in lower drainage efficiency, greater ventilation air demand, and reduced coal production.

Gas control and access for drilling and regulating cross-measure drainage boreholes is simpler on advancing compared with retreating longwall. However, most of the world’s longwall

coal production comes from retreating coalfaces as these are more productive, and ventilation configurations have been developed as attempts to incorporate the advantages of both by ventilating behind the coalface such as “H”, “U+L” and back-return systems.

The ventilation system should incorporate some means of creating a pressure gradient at longwall face-ends to ensure that flammable gas mixtures do not encroach on the working face. This can involve use of regulators (partial obstructions) in roadways and special face-end ventilation arrangements to divert airflow along the waste edge behind the coalface.

Methane layering hazards are a manifestation of inadequate ventilation in the mine. Their presence indicates the need for gas monitoring, an insufficient air velocity to disperse gas layers, and the possible need to improve gas drainage to remove the gas at its source.

5.5 Validation test of the model based on non-coal mine ventilation system

5.5.1 Overview of Vilafruns mine

The potassium deposit in the Catalan basin is currently being exploited by Iberpotash. SA. Iberpotash. SA is the largest mining company in Catalonia (Spain) and the only producer and supplier of potash fertilizers for agriculture and industry uses. The company is located in the comarca of Bages, a county in the center of Catalonia, Figure 5.5.1, in the municipalities of Balsareny, Sallent (Vilafruns) and Suria (Cabanasses). Iberpotash produces over one million tons of red potash for fertilizers and it represents one of Europe's most important potash resources, conveniently located near the major potash consumption areas of the European Union.

Figure 5.5.1 Location of Vilafruns potash mine

5.5.2 Results of airflow distribution measurements

In this simulation experiment, ventilation data from Vilafruns potash mine are used as main parameter reference (Figure 5.5.2).

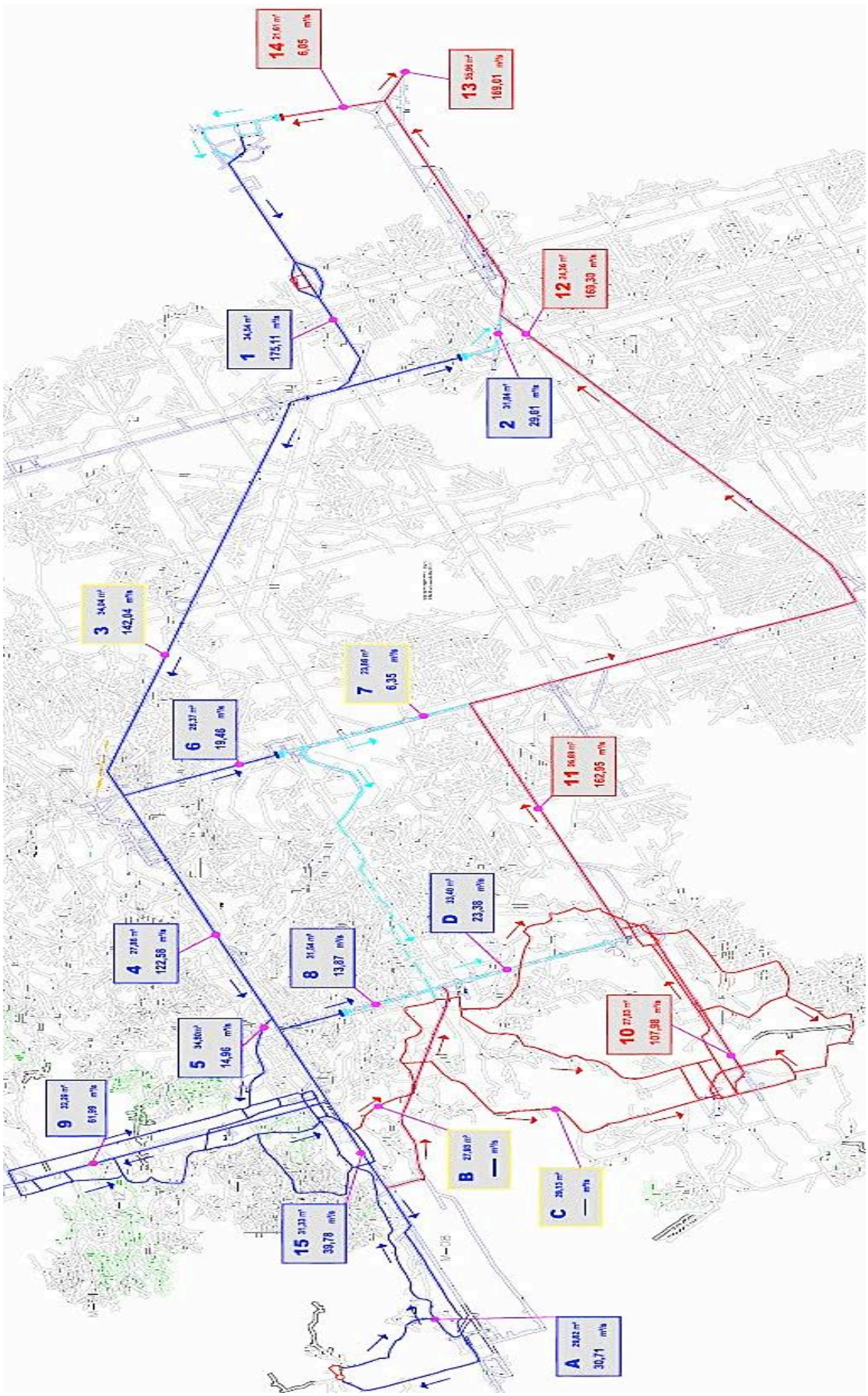

Figure 5.5.2 Ventilation layout of Vilafruns potash mine

First, 14 measuring points in the major air inlet and air outlet are chosen, making it a complete ventilation system, as is shown in Figure 5.5.3.

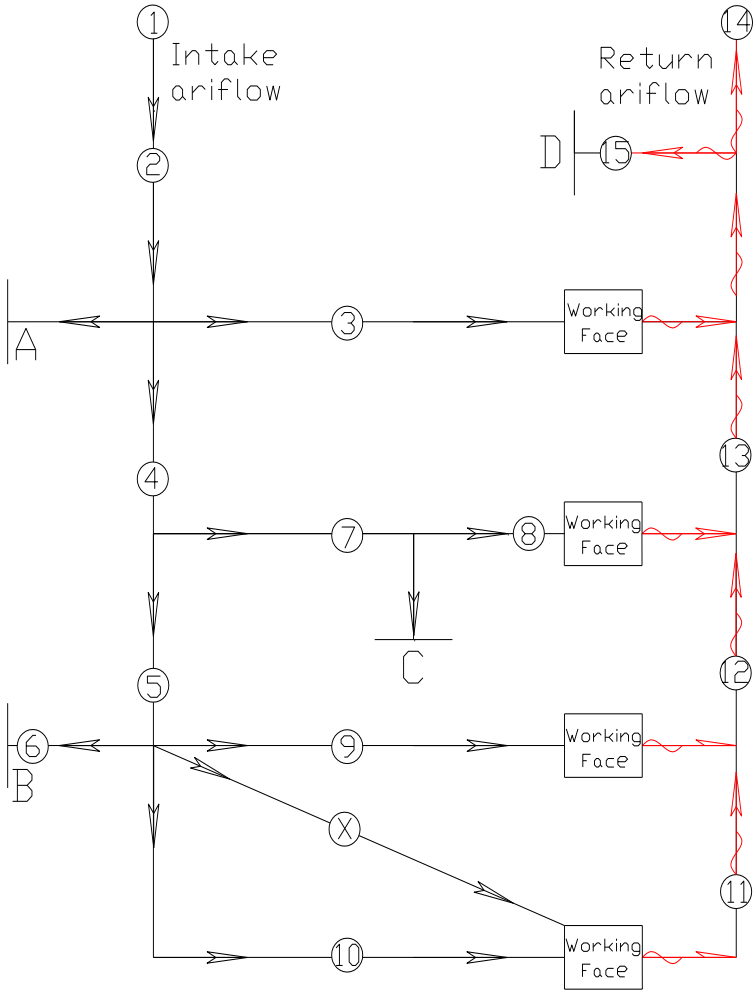

Figure 5.5.3 Simplified ventilation system in Vilafruns potash mine

Due to the significant impacts of season and weather factors on ventilation, data collection in Vilafruns potash mine is made twice both in summer and winter respectively. In the process of air volume measurement, average value is adopted from multiple measurements. The specific results are shown in Table 5.5.1 and Table 5.5.2.

Table 6.5.1 Results of distribution measurements of air quantity in Vilafruns potash mine, July 2011, summer

Points	Air velocity (m/s)	Section (m^2)	Flow rate (m^3/s)	Dry T. (ºC)	Hum. T. (ºC)	Equival.T.(ºC)
1	3.84	39.84	153.00	25	20	19.8

2	4.45	34.34	153.05	29	22	21.7
3	0.71	31.34	22.24	30	23	22.8
4	3.94	33.04	130.05	31	22	22.2
5	3.85	27.56	105.98	31	23	23.1
6	0.41	32.80	13.57	31	23	23.1
7	0.67	27.36	18.26	30	22	22.3
8	0.45	23.86	10.76	32	23	23.2
9	0.41	30.54	12.67	34	24	24.3
10	1.09	31.29	34.20	32	23	23.3
11	3.41	27.36	93.34	39	28	28.6
12	4.60	26.98	124.16	38	27	27.4
13	5.35	24.64	132.06	36	27	27.2
14	4.25	35.06	149.31	35	26	26.1
15	0.19	20.98	3.98	36	27	27.4

Table 5.5.2 Results of distribution of air quantity in Vilafruns potash mine, January 2012, winter

Points	Air velocity (m/s)	Section (m^2)	Flow rate (m^3/s)	Dry T. (ºC)	Hum. T. (ºC)	Equival.T.(ºC)
1	4.41	39.84	175.98	5	10	9.5
2	5.15	34.34	177.04	16	10	10.6
3	0.89	31.34	27.75	22	12	13.0
4	4.60	33.04	151.65	-	-	0.0
5	4.79	27.56	132.21	25	13	14.2
6	0.51	32.80	16.98	26	14	15.2
7	0.69	27.36	18.86	25	13	14.2
8	0.62	23.86	14.78	35	17	18.8
9	0.49	30.54	15.23	31	16	17.5
10	1.93	31.29	60.47	29	15	16.4
11	3.76	27.36	102.76	39	24	25.5

12	6.21	26.98	167.55	38	22	23.6
13	6.82	24.64	168.06	37	22	23.5
14	4.90	35.06	172.02	35	20	21.5
15	0.29	20.98	6.13	35	20	21.5

5.5.3 Results of the simulation experiment

In this case, the air is used as flow medium, and the airflow is regarded as the steady flow. According to the similarity theory, geometric similarity, kinematic similarity and dynamic similarity should be achieved when similarity relations are established between the prototype and the model. In the simulation experiment, the air velocity measurement is used as parameter and reference; different valves in the simulation model are opened and closed, thus it makes the ventilation system as much similar as that in Vilafruns potash mine. The chart of the simulated ventilation system of the adjusted valve is shown below. Similarly, the air velocity measurements in the laboratory are conducted twice, both in summer and winter respectively, and average value is adopted from multi-measurements. The specific results are shown in Table 5.5.3 and Table 5.5.4.

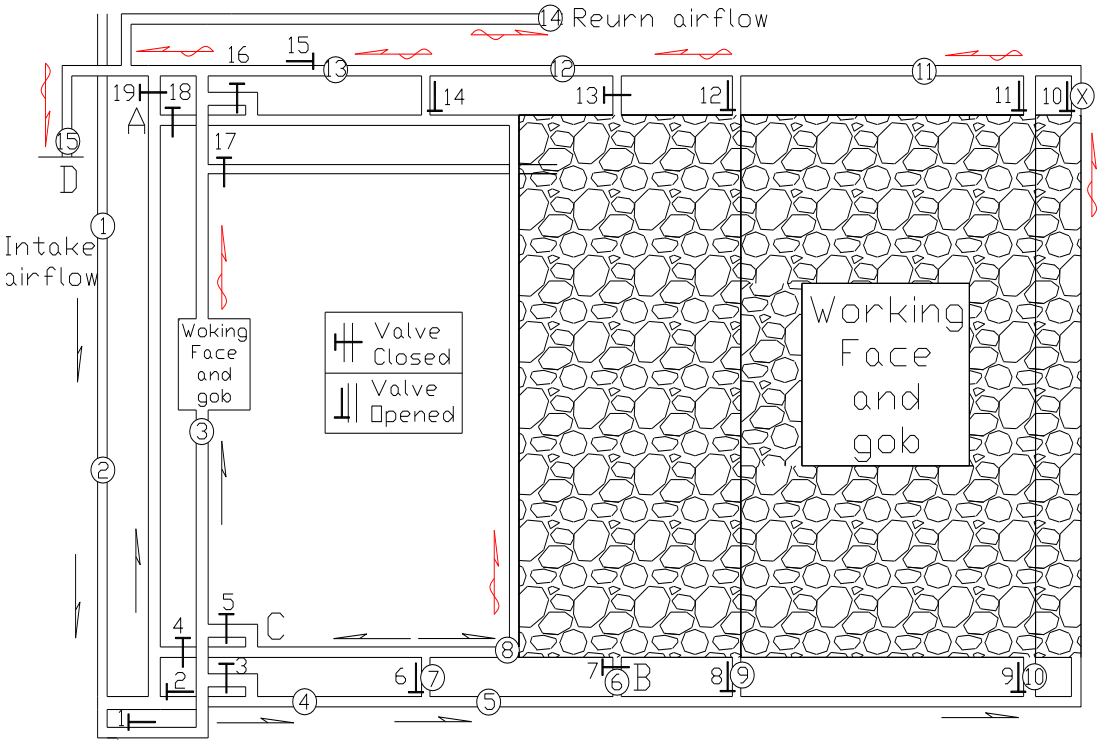

Figure 5.5.4 Model ventilation system and its valve control

Table 5.5.3 Results of air velocity and volume in simulation experiment, summer, June 2011

Points	Section (m^2)	T (ºC)	Velocity (m/s)	Flow (m^3/s)
1	0.0073	25	2.62	0.0168
2	0.0073	25	2.60	0.0167
3	0.0073	25	0.43	0.0028
4	0.0073	25	2.21	0.0141
5	0.0073	25	1.80	0.0115
6	0.0043	25	0.47	0.0030
7	0.0043	25	0.44	0.0028
8	0.0043	25	0.44	0.0028
9	0.0043	25	0.42	0.0027
10	0.0043	25	0.71	0.0045
11	0.0073	25	1.40	0.0090
12	0.0073	25	1.48	0.0095
13	0.0073	25	1.86	0.0119
14	0.0073	25	2.30	0.0147
15	0.0073	25	0.42	0.0027

Table 5.5.4 Results of air velocity and volume in simulation experiment, winter, January 2012

Points	Section (m^2)	T (ºC)	Velocity(m/s)	Flow (m^3/s)
1	0.0073	15	2.95	0.0189
2	0.0073	15	2.97	0.0190
3	0.0073	15	0.52	0.0033
4	0.0073	15	2.49	0.0160
5	0.0073	15	2.26	0.0145

6	0.0043	15	0.56	0.0036
7	0.0043	15	0.46	0.0030
8	0.0043	15	0.45	0.0029
9	0.0043	15	0.42	0.0027
10	0.0043	15	1.00	0.0064
11	0.0073	15	1.39	0.0089
12	0.0073	15	1.91	0.0123
13	0.0073	15	2.42	0.0155
14	0.0073	15	2.73	0.0175
15	0.0073	15	0.42	0.0027

5.5.4 Comparison of the air volume

Figure 5.5.5 and Figure 5.5.6 show the results of air volume measurements in Vilafruns potash mine and the simulation experiment model at different ventilation points in both summer and winter.

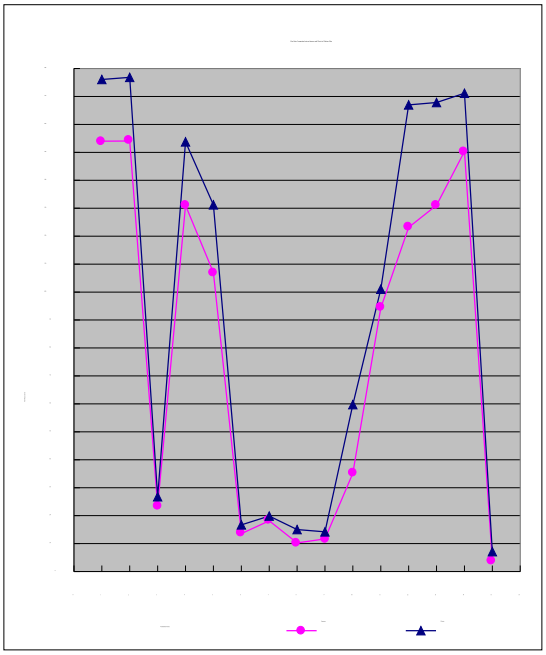

Figure 5.5.5 Distribution diagram of air volume in Vilafruns potash mine

It can be deduced from the Figure 5.5.5 that the air volume in the main roadway of air inlet and air outlet is larger than that in the other sections of the tunnel, being the maximum air flow volume 175m^3/s, and the minimum flow volume less than 10m^3/s. Besides, the air volume in winter is higher than that in summer at the same ventilation point.

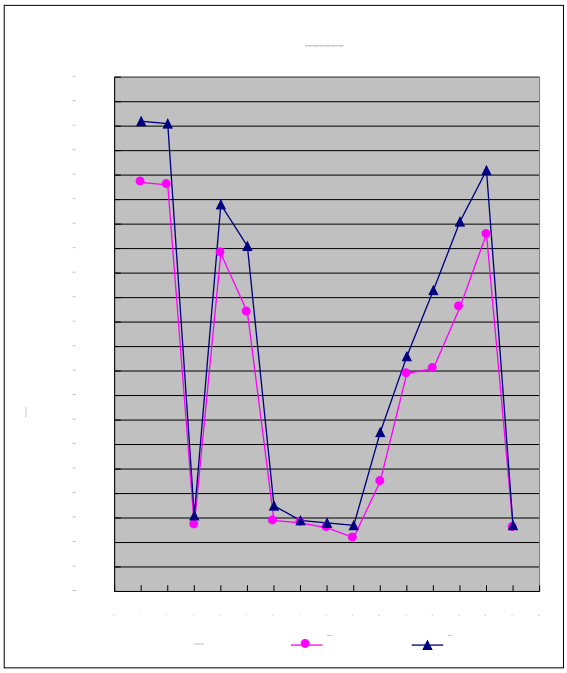

Figure 5.5.6 Distribution diagram of air volume in simulation experiment

Figure 5.5.6 is the result of air volume measurements of the simulation experiment model. It indicates the air volume in main roadway of air inlet and air outlet is higher than that in other sections, and the air volume in winter is higher than that in summer at the same ventilation points.

It can be seen by comparing Figure 5.5.5 and Figure 5.5.6 that the distribution of air volume in the experiment is essentially the same as the one of the mine. The air volume in the main roadway of air inlet and air outlet is higher than that in other sections, and the air volume in winter is higher than that in summer at the same ventilation points in both Vilafruns potash mine and the experiment model as natural air pressure in winter exerts a positive influence on ventilation system.

5.5.5 Air velocity pattern in Vilafruns potash mine

Figure 5.5.7 and Figure 5.5.8 are the results of the air velocity measurements in Vilafruns potash mine and the simulation experiment model at different ventilation points in both summer

and winter.

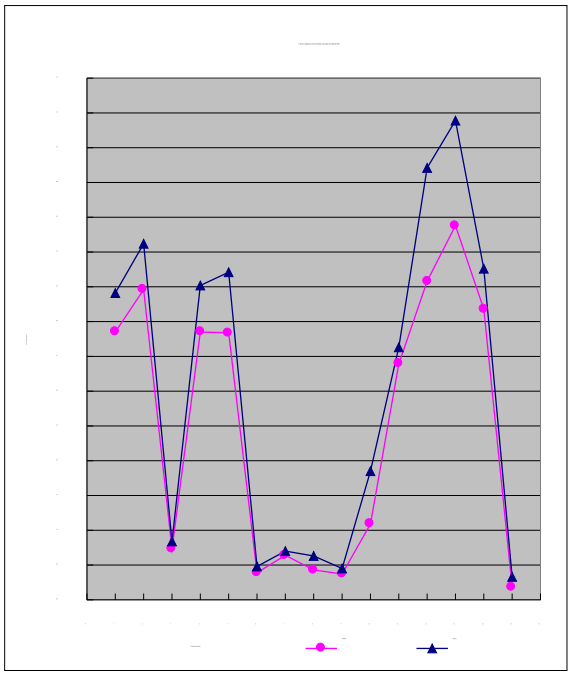

Figure 5.5.7 Air velocity pattern in Vilafruns potash mine

It can be seen from Figure 5.5.7 that in spite of the similarity in air volume between the main road of air inlet and air outlet, the air velocity in air outlet is higher than that in air inlet. This is because the drift sections of air inlet are larger than that of air outlet. Besides, the air velocity in winter is higher than that in summer due to the effect of natural ventilation.

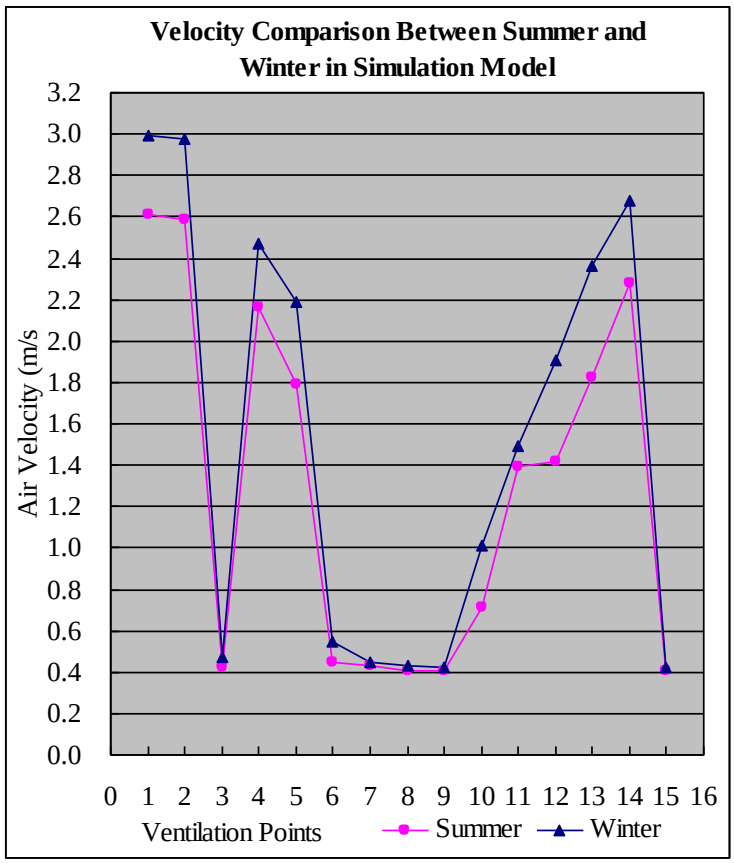

Figure 5.5.8 Air velocity pattern of the simulation experiment

It can be observed from Figure 5.5.8 that the air velocity in winter is higher than that in summer, the minimum air velocity is 0.51m/s, it indicates the airflow in the experiment is in turbulent state, and kinematic and dynamic similarity are achieved. However, under the circumstance where air volume is identical, the air velocity in the air inlet is higher than that in the air outlet. There are two reasons for this: First, most drift sectional areas are the same in each tunnel of the model ($0.0073m^2$ o $0.0043m^2$); second, the fact that many of the drift sections in the simulation model are right-angled and that results into excessive frictional restriction in the tunnels.

If a statistical analysis is performed, the following conclusion can be obtained that the U of Mann-Whitney test has a p-value of 0.1645 and 0.0851for the test between real velocity and velocity of model in summer. Since the p-value is not lower than the chosen confidence level of 0.05, it can be considered that there is insufficient evidence to reject the null hypothesis. Therefore, the comparisons indicate with a confidence level of 0.05 that a difference between air velocities in summer and winter versus the velocities of the model does not exist.

The comparison of Figure 5.5.7 and Figure 5.5.8 indicates that the air velocity in the simulation model is able to basically reflect the air velocity pattern in Vilafruns potash mine, and it also simulates the same situation that the air volume and velocity in winter are higher than that in summer respectively. This means the establishment of the simulation ventilation model is valid and success, it can be used in simulating non-coal mine ventilation system, and the experimental results are accurate and correct.

5.6 Validation test of simulation model based on coal mine ventilation system

5.6.1 Overview of Shaqu coal mine

Liliu mining area, located in Shanxi province, China, contains 15 coal seams with the average thickness of 2.45m (Table.5.6.1). Coal seam #4 in Shaqu coal mine with large gas content (approximately reaches up to 30m^3/t) has created severe difficulties in mine safety and production. The working face length and the strike length of coal seam #4 are 200m and 950m respectively. Extracting method is longwall retreating extraction with U-type ventilation system.

Table 5.6.1 Characteristic of the coal seam

Seam No.	#4
Average coal seam thickness (m)	1.82.-3.08 2..45
Seam spacing (m)	48.55-63.35 55.95
Seam structure	Complicated
Roof	Sand, sandy mud and rock
Floor	Sand, sandy mud and rock
Workability	All minable
Stability	Stable

It is obtained that gas drainage quantity of 14205 working face of coal seam #4 can approximately reach up to 100 m^3/min (Table 5.6.2). A number of gas drainage methods have

been performed by Shaqu coal mine for the purpose of mine safety. However, the results of goaf gas drainage have been far from satisfactory.

Table 5.6.2 Basic gas parameters in Shaqu coal mine

Layer	Gas pressure (MPa)	Gas content (m^3/t)	Emissions (m^3/100m)	Permeability coefficient ($m^2/MPa^2 \cdot d$)	Attenuation coefficient ($100d^{-1}$)
Coal Seam 2#	0.99～1.03	7.92～8.10	4085～4346	1.577～3.999	0.02～0.028
Coal Seam 3#	1.11～1.18	9.70～10.06	4433～5068		0.02～0.025
Coal Seam 4#	1.52～1.57	7.30～17.82	21648～24490		0.01～0.016
Coal Seam 5#	2.20～2.40	10.84～20.15	24350～27180		0.01～0.019

A great deal of gas fails to extract, but has directly flow into the goaf instead, which constantly leads to the overrunning of gas concentration in upper corner (Table 5.6.3). This exerts a negative influence in mine safety and working schedule. Gas emission of Shaqu coal mine involves various physical and human factors including the geological conditions, the degree of strata destruction, permeability of the coal seam, the scale coal occurrence, mine ventilation quantity and method of the mining activities, etc.

Table 5.6.3 Measured results of gas concentration in coal seam #4

Sampling places	Depth (m)	Gas composition (%)				Gas content (m^3/t)
		CH_4	CO_2	N_2	C_2-C_8	
Air outlet tunneling point (10m)	400	50.30	1.59	7.96	0.15	6.08
Between air outlet and air connection tunnel (60m)	450	53.02	3.34	3.43	0.21	7.50
Shaft station 2 and intersection east (18m)	515	56.66	0.87	2.40	0.07	8.20

5.6.2 Gas emission sources

Gas discharge involves various physical factors including the geological conditions, coal occurrence, mining technology and time, etc. The majority sources of coal strata gas, which can be directly discharged into the underground field, are deprived from coal seams (trapped in various surfaces of coal), porous sandstone, fracture networks, joints, faults, and gas pockets (dissociate gas). The amount of gas discharge is greatly influenced by various factors, including the degree of strata destruction, permeability of the coal seam, the scale and method of the mining activities, mine ventilation quantity, etc.

Mining activities disturb existing stress equilibration in the rock mass and create variations to the structural attribute of the affected strata. The fracture process zones are opened and developed by existing and mining-induced fractures. A mass of gas discharge can be expected from the coal mining and strata of loose floor and roof. The specific places where coal seam loose occurred are determined by multiple factors including physical properties of seam system, the geometry of the longwall panel, the volume of the trapped gas sources, and the destructive condition of the relaxed zone. Figure 5.6.1 shows the sources of gas emission from different parts of coal mine.

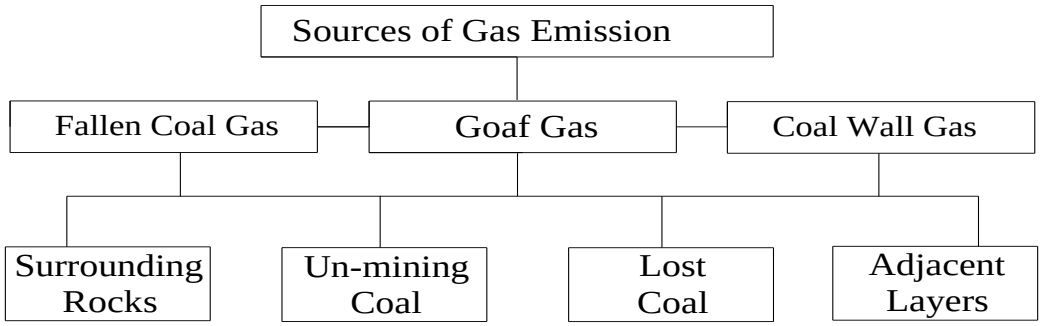

Figure 5.6.1 Sources of gas emission

As a matter of fact, the highest gas emission deprives from working face and goaf since it constantly and alternately destruction and re-compaction. Therefore, the most effective and accurate gas drainage borehole can be expected to pave in this zone. Based on problems mentioned above, multiple research methods will be adopted to determine the most effective gas drainage zone (gas emission zone). The numerical simulation experiments and laboratory method was combined with core data, including thickness, depth and inclination of major coal and

non-coal formations, and obtained from field measure.

Mining strata pressure and movement theory point out that the working face and goaf consists of three parts: coal wall support area, rock separation area and the re-compaction area (Figure 5.6.2).

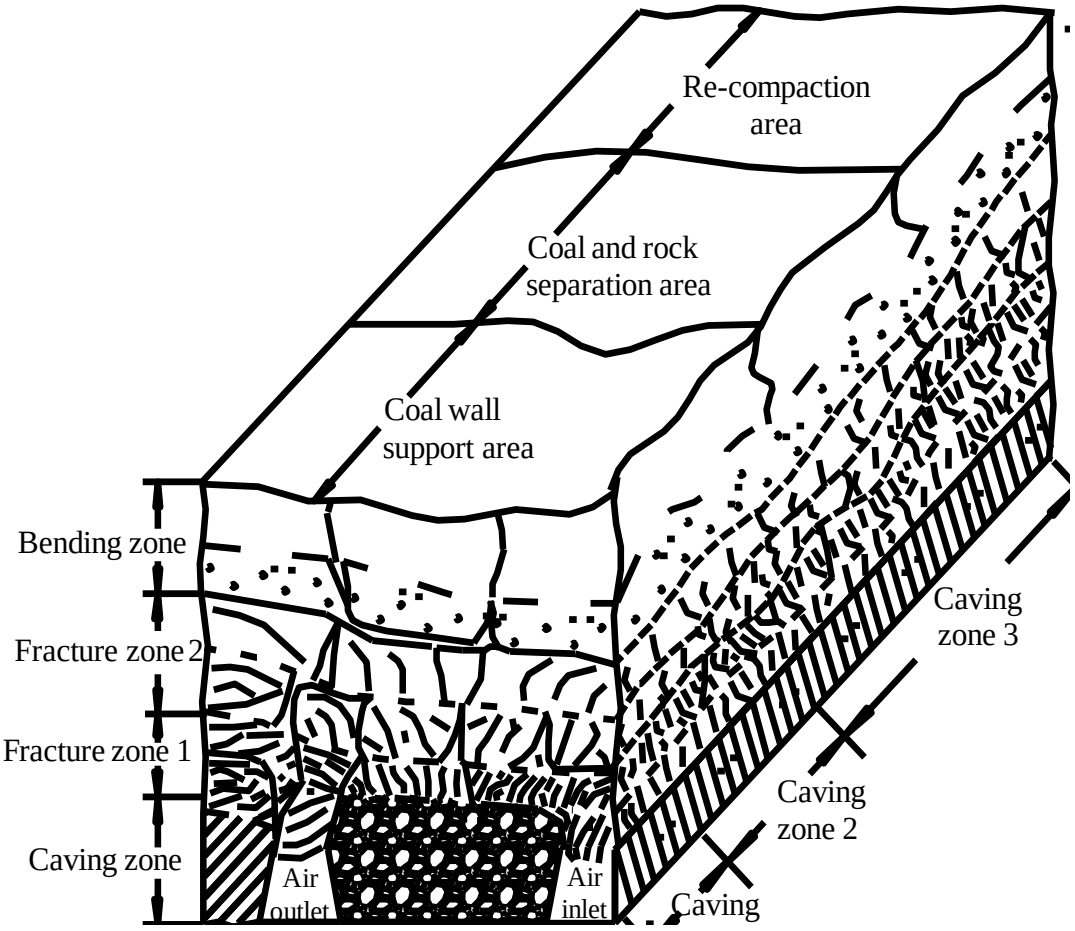

Figure 5.6.2 Cross-section of goaf area

The coal wall support area rapidly changes when the mining activities are performed. The re-compaction area has compacted completely; both of them are not in favor of gas drainage. Rock separation area where exists an amount of fracture space is the ideal and effective gas drainage zone. Similarly, rock stratum from top to bottom is divided into 3 parts: caving zone, fracture zone and bending subsidence zone (Figure 5.6.2). As a matter of fact, it is extremely difficult to excavate gas drainage borehole in both caving zone and bending subsidence zone. Fracture zone where exists a mass of fissuring area obviously is the more reasonable and effective gas drainage zone.

5.6.3 Simulation experimental results of U-type ventilation system

The most common and effective method to control air flow to the goaf area in a longwall panel is the U-type ventilation system (Figure 5.6.3). In this system, the air is brought up to the air inlet, across the working face, and down the air outlet. This system is widely used in mines with low-concentrated gas in mining industry around the world because it is economical and easy to design and build. However, when working areas in underground mines become farther and deeper where more high-concentrated gas is released, U-type ventilation system will not be able to offer enough fresh air for miners and to dilute the high-concentrated gas in the working face.

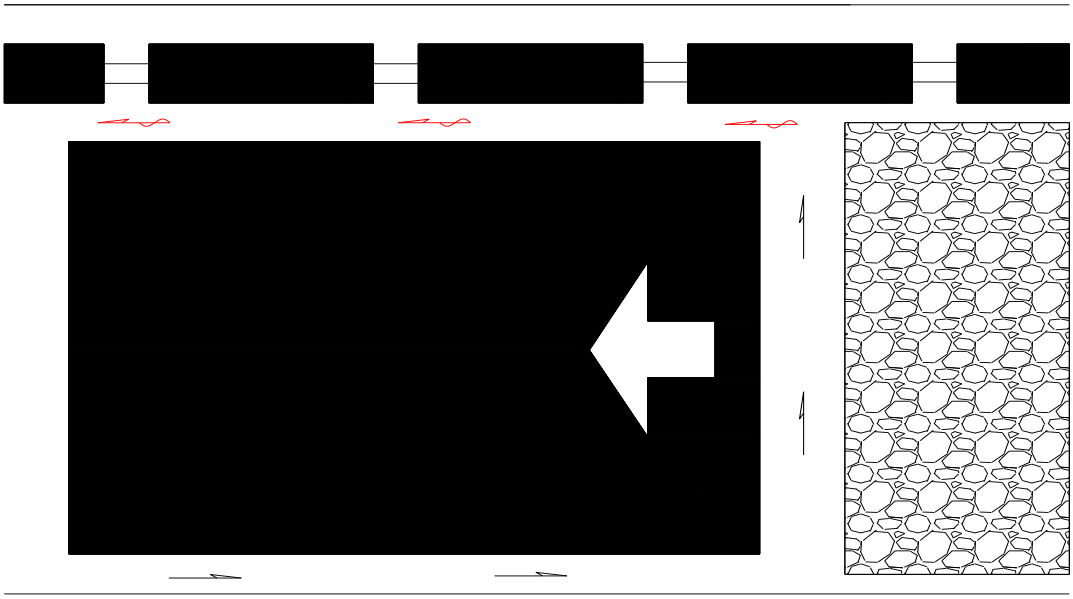

Figure 5.6.3 U-type ventilation system (one air inlet and one air outlet)

The variation and flow process of trace gas in U-type ventilation system is recorded in the simulation model, as is shown in the Figure 5.6.4 - Figure 5.6.8. The air velocity of air inlet is 1.5 m/s, and the pressure of air outlet is 90kPa.

Figure 5.6.4 Goaf gas flow process of U-type ventilation system

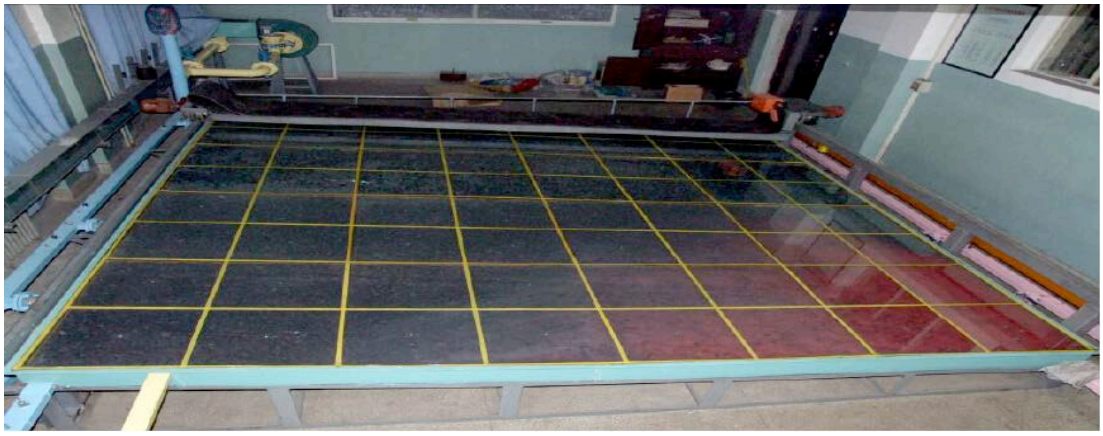

Figure 5.6.5 Goaf gas flow process of U-type ventilation system

Figure 5.6.6 Goaf gas flow process of U-type ventilation system

Figure 5.6.7 Goaf gas flow process of U-type ventilation system

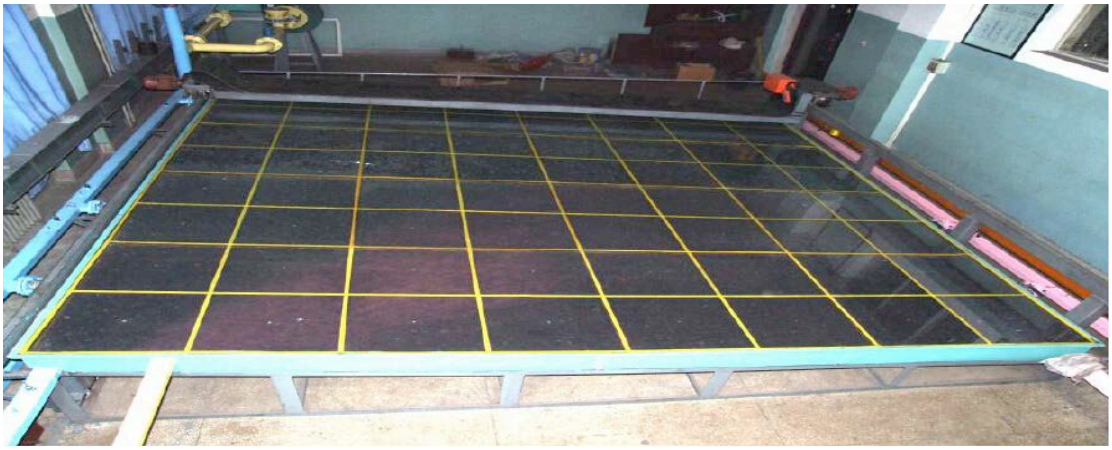

Figure 5.6.8 Goaf gas flow process of U-type ventilation system

It can be seen from these figures that high-concentrated gas is mainly gathered in the upper corner of the working face. It sharply increases from the working face to the deeper goaf area and then tends to be steady. The gas concentration gradually augments from the working face floor to the roof. Moreover, the gas concentration of the air outlet side is higher than that of the air inlet side due to factors such as air leakage and air pressure difference.

The average gas concentration in 64 different points of goaf area is obtained from multiple measurements during the experiments. The results are shown in Table 5.6.4.

Table 5.6.4 Results of gas concentration (%) in the simulation goaf (U-type ventilation system)

	Distance from the working face/cm							
From air outlet/cm	27	81	135	189	243	297	351	405

26	6.39	9.88	38.44	43.44	63.45	67.75	68.88	70.02
78	10.77	15.76	41.76	56.58	64.15	65.21	66.62	69.63
130	14.37	14.89	37.65	54.59	62.01	63.54	65.65	64.92
182	12.82	12.39	33.82	52.92	60.13	62.89	63.95	63.53
234	10.45	11.69	30.47	50.12	58.86	61.87	62.96	61.98
286	7.78	11.38	27.72	42.51	55.98	61.09	61.53	61.12
338	4.15	10.83	25.98	35.33	51.24	55.68	58.83	60.23
390	3.09	9.98	22.87	34.94	48.72	52.65	56.32	59.73

Table 5.6.4 shows that the gas concentration of the air inlet (3.09%) is lower than that of the air outlet (6.39%), with the difference of 3.3%. This demonstrates that high-concentrated gas mainly gathers in the working face, and the U-shaped ventilation system is not able to offer enough fresh air to dilute it. Figure 5.6.9 indicates the variation and the rule of gas flow and gas concentration in the U-type ventilation system model. Specifically, the average gas concentration is around 8.73% (27cm from the working face and the upper corner), and it rapidly increases to 32.34% when the measuring point is 135cm from the working face, then hovers at 58.07% from 243cm to 405cm.

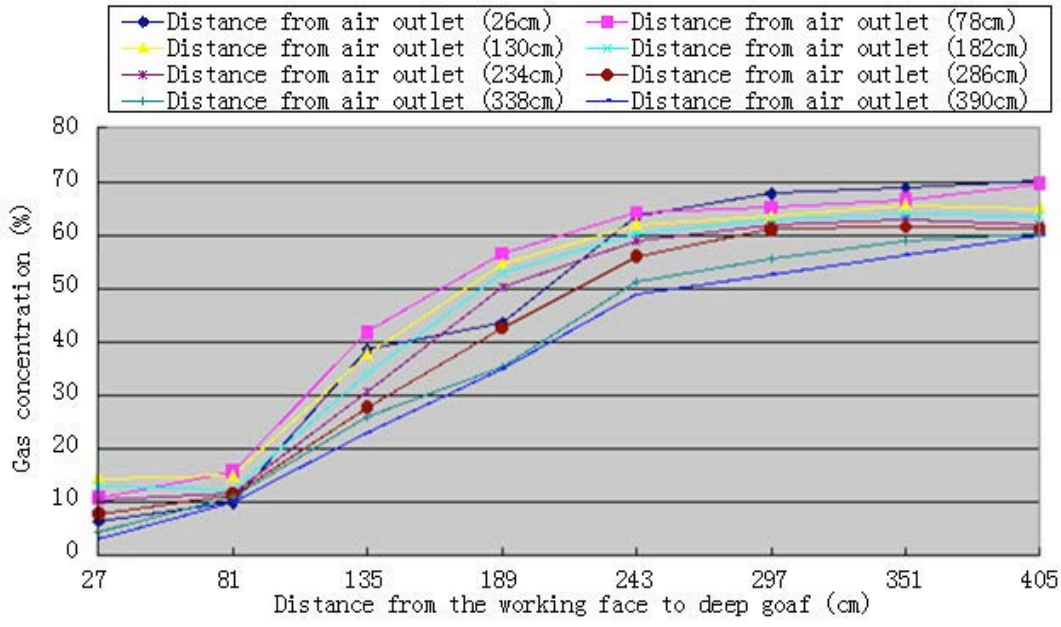

Figure 5.6.9 Measured results of goaf gas distribution rule with U-type ventilation system

Another simulation experiment is conducted by increasing the velocity of the air inlet to 2.0 m/s. The measured result manifests that the high-concentrated gas slightly moves from the working face to the deeper goaf. However, the problem of over-limit gas at working face and the upper corner cannot be totally resolved by greatly increasing the air volume and accelerating the air velocity. Instead, it should be incorporated with manifold technological means of gas control and prevention. Therefore, U+L-type ventilation system with two air inlets and one outlet could be an effective solution.

5.6.4 Simulation experimental results of U+L-type ventilation system

U+L-type ventilation system, consisting of two air inlets and one air outlet (Figure 5.6.10), accelerates the gas emission, diffusion and flow, balances the air pressure of upper corner, restrains the gas emission of upper corner, and compels the high-concentrated gas to flow over into the air outlet. Finally, it lowers the gas concentration of local areas, and effectively resolves the difficulties of gas over-limit of the working face. In addition, the total air volume in the working face has significantly increased as the fresh air is constantly offered from two air inlets.

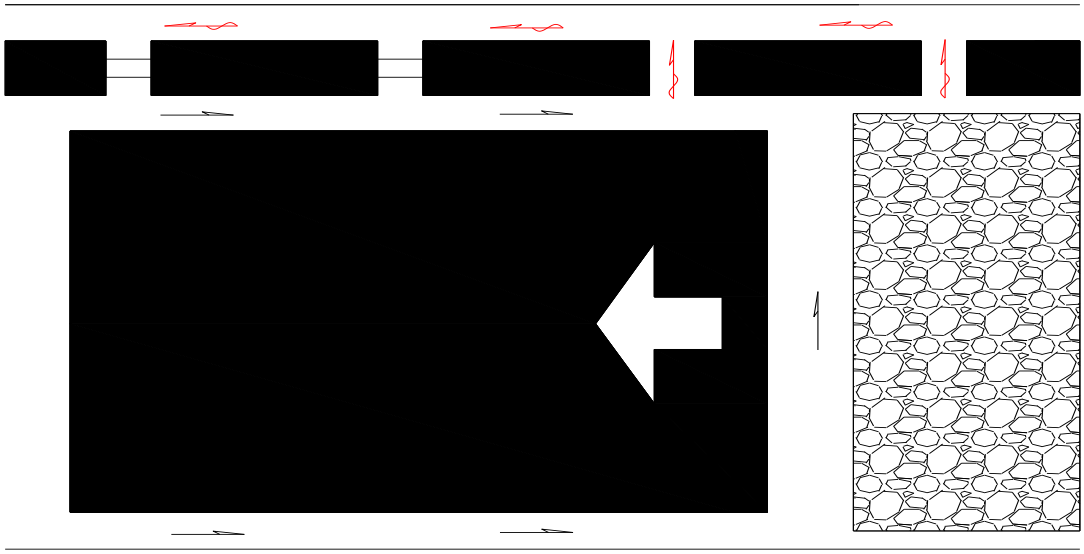

Figure 5.6.10 U+L-type ventilation system (two air inlets and one air outlet)

The flow process of gas in U+L-type ventilation system is recorded in the simulation model,

as is shown in Figure 5.6.11 - Figure 5.6.15. The air velocity of inlet is 1.5 m/s, and the pressure of outlet is 90kPa.

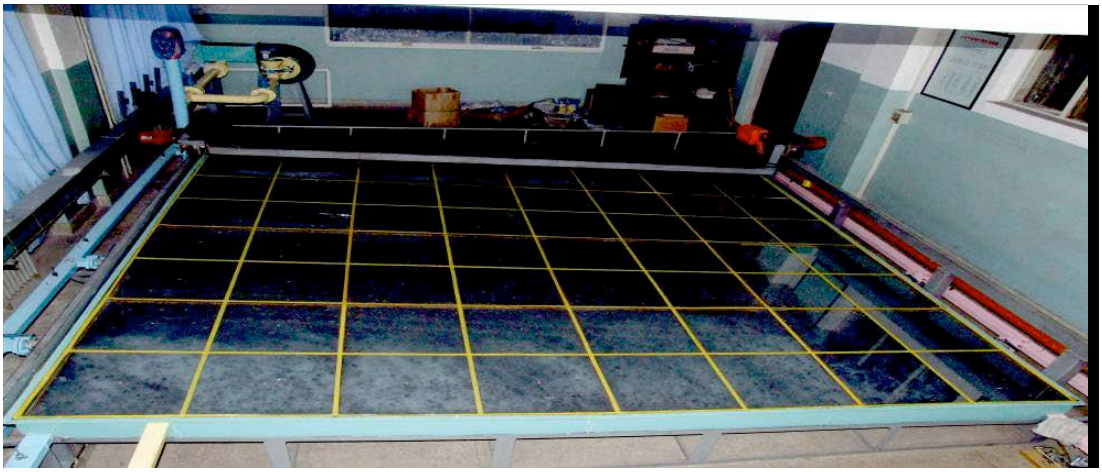

Figure 5.6.11 Goaf gas flow process of U+L-type ventilation system

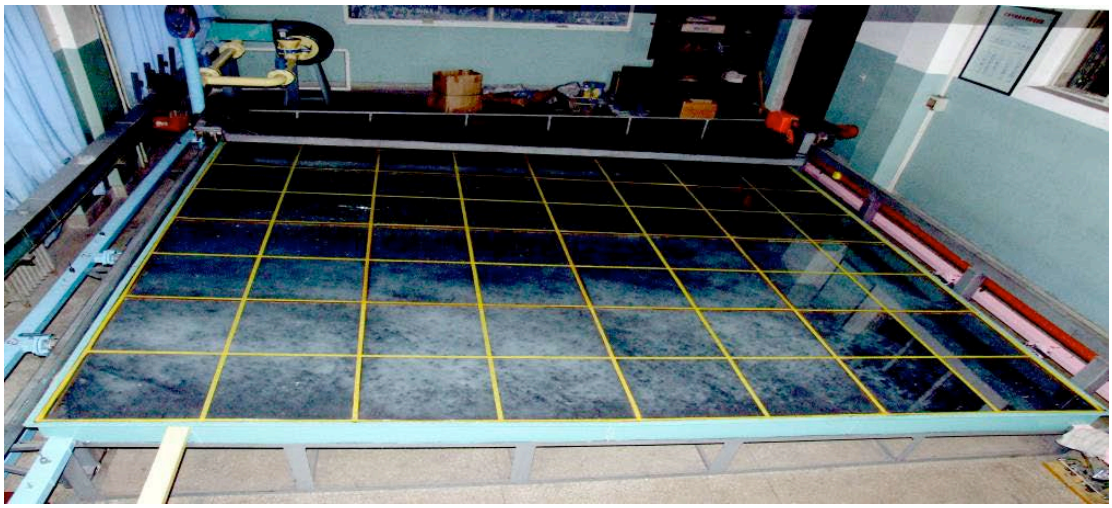

Figure 5.6.12 Goaf gas flow process of U+L-type ventilation system

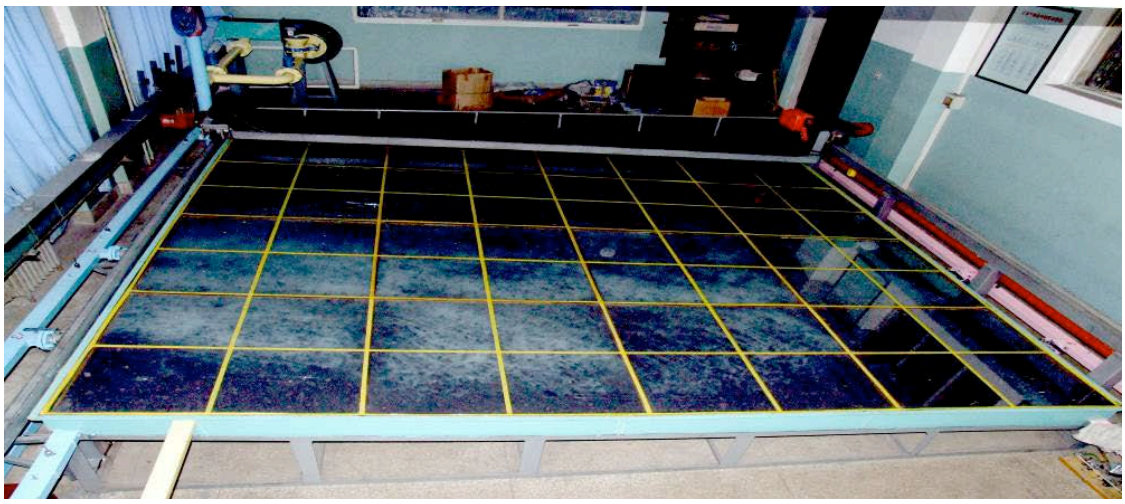

Figure 5.6.13 Goaf gas flow process of U+L-type ventilation system

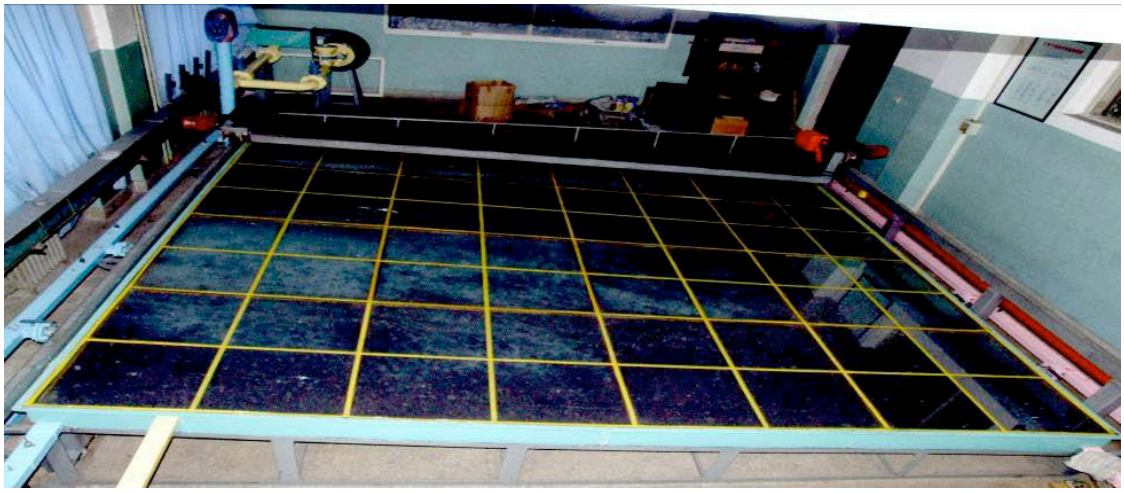

Figure 5.6.14 Goaf gas flow process of U+L-type ventilation system

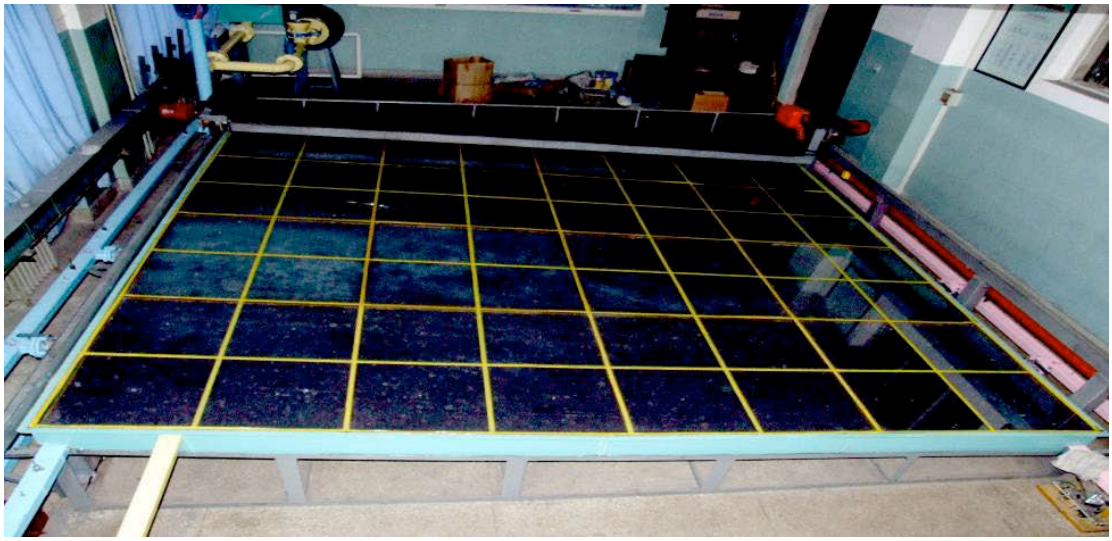

Figure 5.6.15 Goaf gas flow process of U+L-type ventilation system

From these figures we can see that the high-concentrated gas moderately moves to the deeper goaf rather than gathering in the working face and upper corner. Average value is obtained from multiple measurements and the results are shown in Table 5.6.5.

Table 5.6.5 Average gas concentration (%) in simulation goaf (U+L-type ventilation system)

	Distance from the working face/cm							
From air outlet/cm	27	81	135	189	243	297	351	405
26	4.24	6.16	33.39	42.16	64.12	66.53	68.26	69.52
78	9.16	12.67	36.93	57.84	63.87	64.76	67.14	68.61
130	11.25	11.81	32.11	52.38	61.89	63.22	64.15	65.08
182	10.19	10.76	27.39	51.91	59.15	62.35	63.71	63.17
234	8.34	10.31	33.67	55.99	57.62	62.68	62.96	62.15
286	5.97	10.12	29.88	41.38	54.78	60.61	61.33	61.07
338	3.13	10.94	27.46	36.22	50.87	54.91	57.76	59.39
390	2.99	9.52	24.39	35.87	49.38	53.19	57.16	58.84

Table 5.6.5 shows that the gas concentration of the air inlet (2.99%) is lower than that of the air outlet (4.24%). This is because the air leakage and the pressure difference, and the difference between the two of them is only 1.23%, which is less than that of U-type ventilation system (3.3%). This indicates that high-concentrated gas not only gathers in the upper corner, but moves to the deeper goaf area as well, and it is able to be diluted by offering more fresh air from the two air inlets of U+L-type ventilation system. Besides, the gas concentration also gradually augments from the working face floor to the roof. Figure 5.6.16 demonstrates the variation and the rule of gas flow and gas concentration in the U+L-type ventilation system model. To be specific, the average gas concentration is around 6.91% (27cm from the working face and the upper corner), and it also rapidly rises to 30.65% when the measuring point is 135cm from the working face, then hovers at approximately 57.71% from 243cm 405cm.

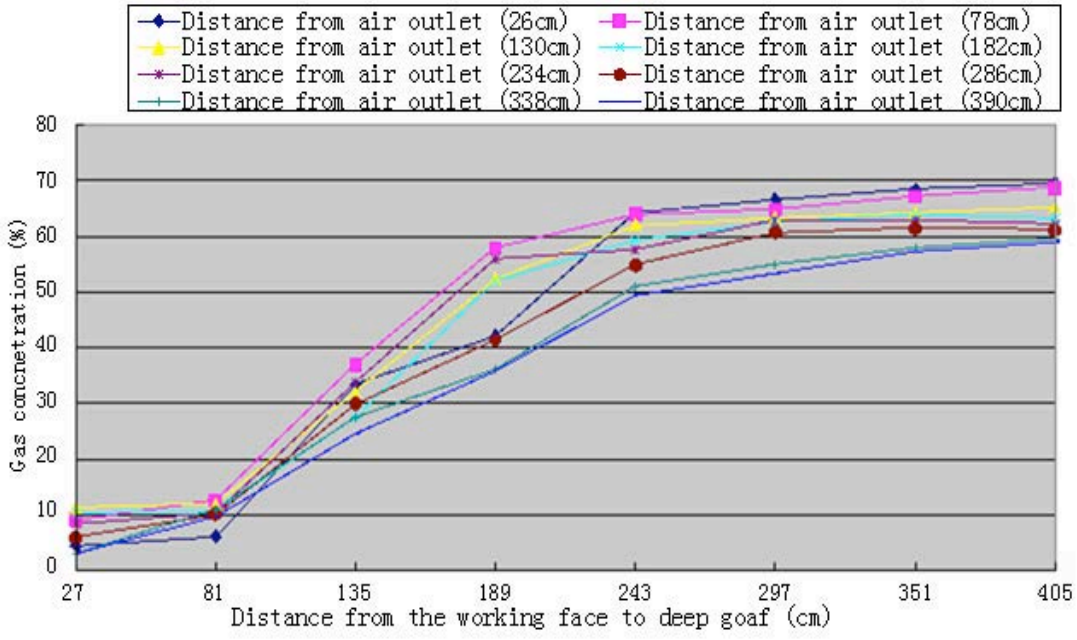

Figure 5.6.16 Measured results of goaf gas distribution rule with U+L-type ventilation system

Another simulation experiment has been conducted by increasing the velocity of the air inlet to 2.0 m/s. The measured result manifests that the average gas concentrations of the three main measured lines of goaf are approximately 6.74% (27cm from the working face), 30.29% (135cm from the working face) and 57.65% (243cm from the working face) respectively. Therefore, the gas concentration of the working face and goaf area declines by increasing the velocity of the air inlet and changing from the U-type ventilation system to U+L-type ventilation system.

5.6.5 Comparison between U-type and U+L-type ventilation system

The comparisons of the simulation results demonstrate the goaf gas distribution and movement rules are similar in both U-type ventilation system and U+L-type ventilation system. However, in the case of the U-type ventilation system, a large amount of high-concentrated gas constantly flows into the upper corner due to the air leakage, air pressure difference and other factors. By contrast, U+L-type ventilation system is made up of two air inlets and one outlet; it accelerates the gas emission, diffusion and flow, balances the air pressure of the upper corner, restrains the gas discharge of the working face and compels the high-concentrated gas to flow into the air outlet. Therefore, the gas concentration in the working face, upper corner and other local areas are diluted and lowered.

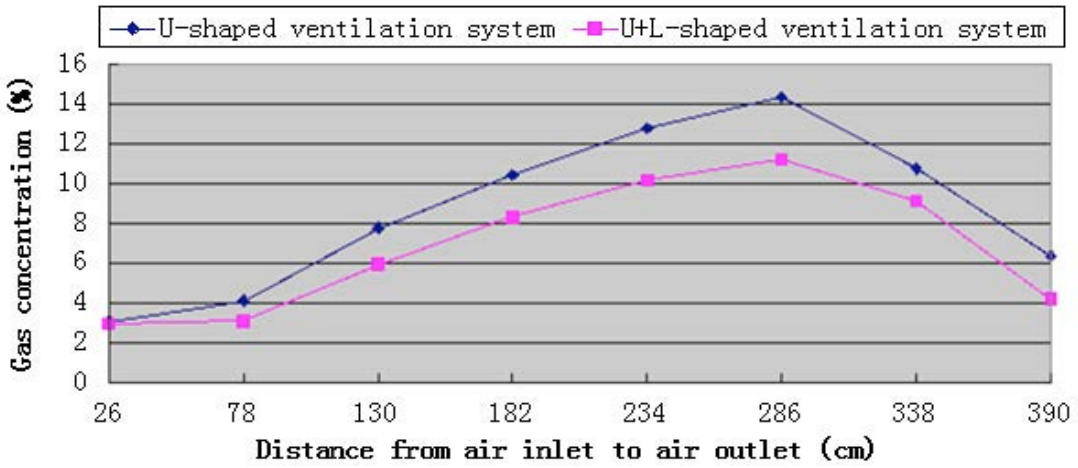

Figure 5.6.17 Comparison of goaf gas concentration between U-type ventilation system and U+L-type ventilation system (27cm from the working face)

It can be clearly seen from Figure 5.6.17 that the gas concentration of U-shaped ventilation system (8.73% on average) is higher than that of U+L-type ventilation system (6.74%) when the measure line is 27cm from the working face. Besides, the gas concentration has dropped by 1.99% after increasing the velocity of the air inlet and changing the ventilation network. To be specific, in the case of U-type ventilation system, the lowest measured gas concentration point lies in the air inlet, then it gradually increases and peaks at the point that is 130cm from the air outlet (14.37%). Finally it decreases to 6.39% at the measured point of air outlet. In the case of U+L-type ventilation system, the lowest measured gas concentration point also lies in the air inlet, and then it reaches the highest point that is 130cm from the air outlet (11.25%). Finally it decreases to 4.24% at the measured point of air outlet.

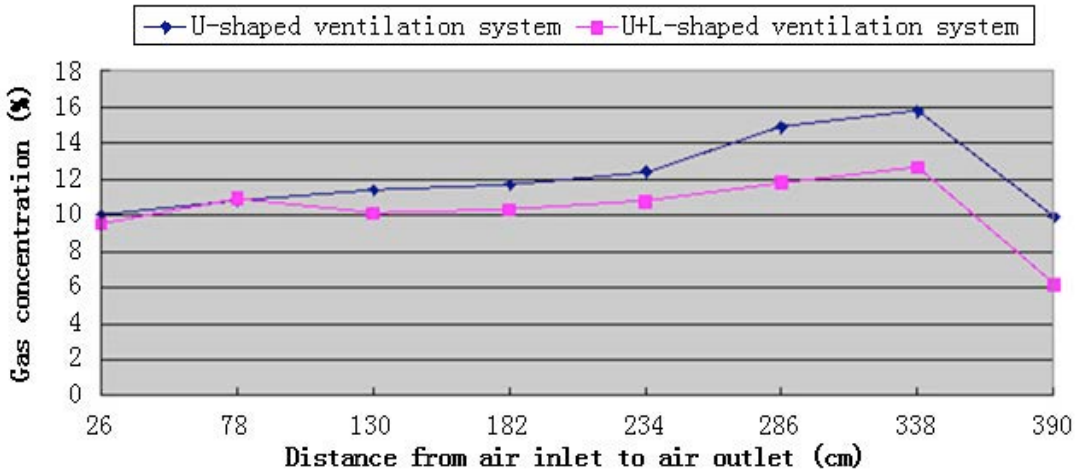

Figure 5.6.18 Comparison of goaf gas concentration between U-type ventilation system and U+L-type ventilation system (81cm from the working face)

Figure 5.6.18 shows that the gas concentration of U-type ventilation system (12.1% on average) is higher than that of U+L-type ventilation system (10.29%) when the measure line is 81cm from the working face. This indicates the gas concentration has dropped by 1.81% after increasing the velocity of the air inlet and changing the ventilation network. Specifically, in the case of U-type ventilation system, the lowest measured gas concentration point lies in the air inlet, then it rises and reaches the highest point that is 78cm from the air outlet (15.76%). Finally it decreases to 9.88% at the measured point of air outlet. In the case of U+L-type ventilation system, the lowest measured gas concentration point locates in the air outlet (6.16%), and then it peaks at the point that is 78cm from the air outlet (12.67%). Finally it drops to 9.52% at the measured point of air inlet.

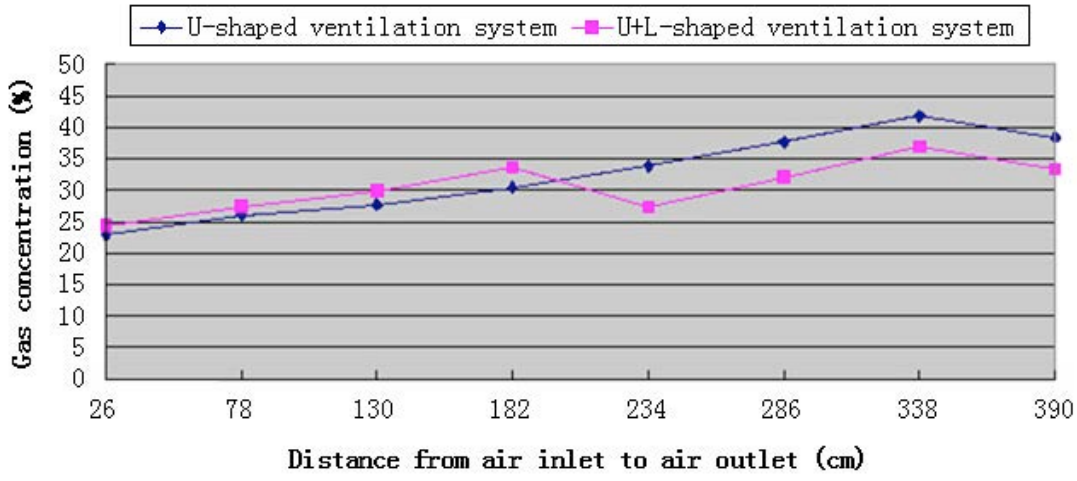

Figure 5.6.19 Comparison of goaf gas concentration between U-type ventilation system and U+L-type ventilation system (135cm from the working face)

It can be seen from Figure 5.6.19 that the gas concentration of U-type ventilation system (32.34% on average) is higher than that of U+L-type ventilation system (30.65%) when the measure points are 135cm from the working face. This indicates that the gas concentration has dropped by 1.69% after increasing the velocity of the air inlet and changing the ventilation network. Specifically, in the case of U-type ventilation system, the lowest measured gas concentration point lies in the air inlet, and then it gradually increases and peaks at the point that is 78cm from the air outlet (41.76%). Finally it decreases to 22.87% at the measured point of air inlet. In the case of U+L-type ventilation system, the lowest measured gas concentration point lies in the air inlet, and then it reaches the highest point that is 78cm from the air outlet (36.93%). Finally it decreases to 24.39% at the measured point of air outlet. It also can be clearly seen from Figure 5.6.19 that the gas concentration of U+L-type ventilation system is higher than that of U-type ventilation system within 190cm from the air outlet. This is because one of the gas outlet gates lies in that area and the fresh air coming from the special air inlet also pushes the high-concentrated gas into that area.

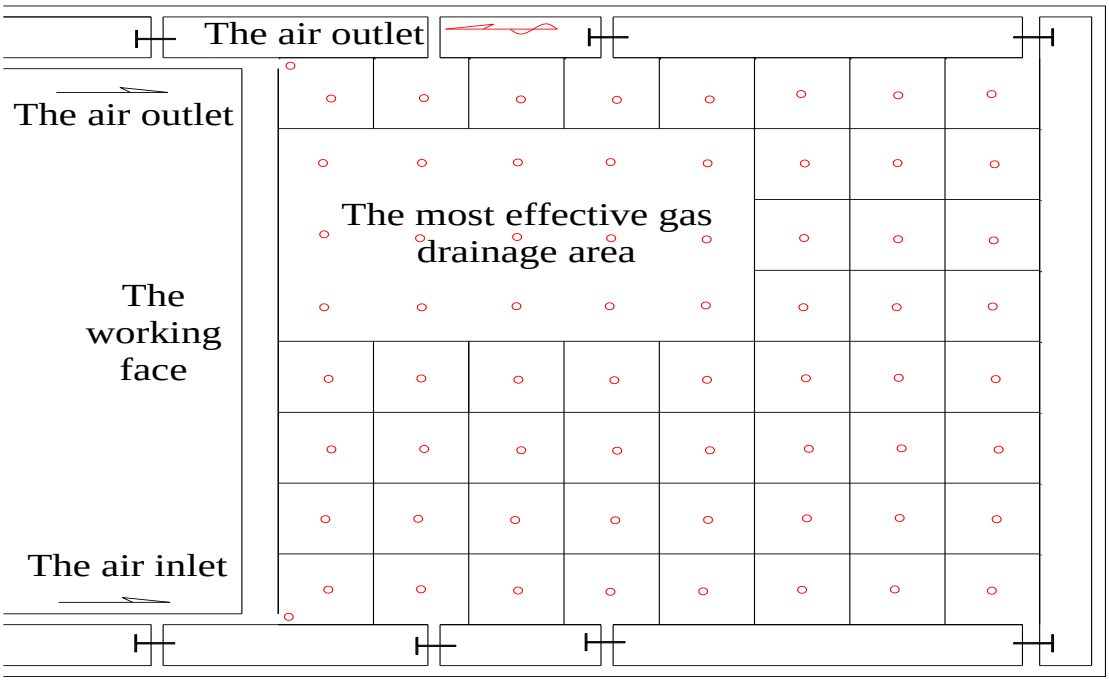

Figure 5.6.20 The most effective gas extraction spots

Obviously, the over-limit of gas in the working face and goaf area of the simulation model is effectively controlled by increasing the velocity of the air inlet and changing the ventilation system from U-type to U+L-type. The gas concentration of the upper corner has declined from 6.39% to 4.24%. Combined with Figure 5.6.11 - Figure 5.6.15 and Table 5.6.5, it can be concluded that the most effective gas extraction spot constantly varies with the area where mining activities are performed. As is shown in Figure 5.6.20, it mainly locates in coal and rock separation area of 27cm - 243cm (between working face and deep goaf), 28cm - 42cm (between the working face floor to the roof) and 78cm - 182cm (between air inlet and air outlet).

5.7 Results comparison between numerical simulation and laboratory simulation

In order to verify the validity of establishment of the simulation models (both numerical one and laboratory one) and the reliability of the simulation experiments, the results between numerical experiments and laboratory experiments are compared, discussed and concluded.

Numerical simulation experimental comparison results between U-type ventilation system and U+L-type ventilation systems indicate that goaf gas distribution rules are similarly applied under both systems. Moreover, the over-limit of gas content in the working face, upper corner and goaf is effectively resolved by changing the ventilation system from U-type to U+L-type. Particularly, the gas content of the upper corner decrease from 10% to around 4%. On the other hand, the same similar results can be found in the laboratory simulation experiments. The gas concentration of the upper corner has declined from 6.39% to 4.24% after the ventilation system has been changed from U-type to U+L-type.

Under the circumstances of numerical simulation experiments, the results demonstrate that the most effective gas extraction spot constantly varies with the area where mining activities are performed. It is mainly located in the area of 40m - 250m (between working face and deep goaf), 30m - 40m from the working face floor (along the vertically direction, distressed and fracture zone), and approximately 60m - 170m (between air inlet and air outlet). On the other hand, laboratory simulation experiments indicate the similar conclusion that the most effective gas extraction spot constantly varies with the area where mining activities are performed, and it

mainly locates in coal and rock separation area of 27cm - 243cm (between working face and deep goaf), 28cm - 42cm (between the working face floor to the roof) and 78cm - 182cm (between air inlet and air outlet).

It can be conclude that the similar gas distribution rule and migration law of numerical simulation experiments are found in laboratory simulation experiments.

5.8 Chapter conclusion

(1) A brief introduction of similarity theories is presented.

(2) Based on the real condition of working face #14205 of coal seam #4 of Shaqu coal mine, a laboratory simulation model of ventilation system and goaf is established, the simulation experimental devices are selected, and the relevant parameter and boundary conditions are determined.

(3) The laboratory simulation experiments are conducted based on both of U-type ventilation system and U+L-type ventilation system, and then the gas distribution rule and migration law of working face and goaf are obtained.

(4) The comparison between U-type ventilation system and U+L-type ventilation system shows that goaf gas distribution rules are similarly applied under both systems. Obviously, the over-limit of gas content in the working face is effectively resolved by changing the ventilation system from U-type ventilation system to U+L-type ventilation system. Specifically, the gas concentration of the upper corner has declined from 6.39% to 4.24%.

(5) The laboratory simulation experimental results show that the most effective gas extraction spot constantly varies with the area where mining activities are performed. It is mainly located in the area of 40m - 250m (between working face and deep goaf), 30m - 40m from the working face floor (along the vertically direction, distressed and fracture zone), and approximately 60m - 170m (between air inlet and air outlet).

(6) The similar gas distribution law and migration rule of numerical simulation experiments are found in laboratory simulation experiments.

6 Gas distribution, migration, drainage design and field measured

6.1 Overview

This chapter describes contents concerning the field gas distribution and migration measurement, gas drainage design and measured results of gas drainage rate in the working field. The first part discusses gas concentration distribution rule of Shaqu coal mine, and provides a measured results of actual gas concentration in 25 different measuring points in the working face. The second part provides an introduction to the gas migration rule of working face and goaf, and analysis field measured results of gas concentration of Shaqu coal mine. The next part offers an analysis of the necessity and feasibility of gas drainage of Shaqu coal mine. The fourth part provides the gas drainage design project, layout and technical parameters based on the simulation results of numerical experiments and laboratorial experiments. The last part offers gas drainage rate of special gas drainage tunnels, the upper corner and the air inlet based on U-shape ventilation system and U+L-shape ventilation system as well as the analysis of gas drainage rate and results.

6.1.1 Gas drainage challenges

The fundamental purpose of gas drainage is to capture high-purity gas at its source before it can enter mine airways. For regulatory purposes, the quantity of gas released into the air flow must not exceed the capacity of the ventilation air used to dilute gaseous pollutants to mandated safety levels; however, there is a strong case for maximizing gas capture to achieve enhanced safety, environmental mitigation, and energy recovery (United Nations, 2010).

Many gas capture methods are applied around the world. Taking unsuitable methods or poor implementation of those methods will result in low gas drainage capture efficiencies and excessive ingress of air-producing flows of low-concentration gas. When these gases are in or near the explosive range during release, transport and use, they will create hazards (United Nations, 2010).

6.1.2 Worldwide gas drainage practices

Differing geological and mining conditions in the coal basins around the world have resulted

in the development of different gas drainage techniques. Gas drainage methods are conventionally classified as involving either pre-drainage or post-drainage techniques (SukSang et al., 2013). Pre-drainage involves capturing gas from the coal seam o adjacent layers to be worked before mining activities, while post-drainage involves removing all types of hazardous gases released from coal seam or surrounding seams as a result of the strata movement, relaxation, and increased permeability induced by mining activities (United Nations, 2010).

(1) Pre-drainage Basics

Pre-drainage is an important means of removing gas flow directly from the coal working face and seam, and it can be significant when the coal seam being retrieved is the dominant gas emission source. Besides, pre-drainage is necessary for controlling, preventing and reducing gas outburst hazards in many gassy coal mine all over the world. Due to the gas drainage is performed before mining activities, the gas collection networks are not likely to be affected and disturbed by ground strata movement, and then if feasible, relatively high purities of gas can easily be retrieved (Liu et al., 2011). Gas drainage from blocks of coal ahead of mining usually creates continuous gas flows of high concentration, offered that the permeability and gas concentrations of the coal bed and coal seam are sufficient to allow important gas flow. Essential gas flows into virgin headings are indicative of medium-to high-fracture permeability and present potential for both effective pre-drainage and gas utilization (United Nations, 2010).

Coal permeability directly affects the time required to sufficiently drain the coal seam. The lower the coal's permeability, the more time is needed to drain gas to reduce coal seam gas content to a required average value. Alternately, the lower permeability coals require a greater number of boreholes needed to achieve the desired methane levels in advance of mining. The available time for degassing and the cost of the drilling operation determines the ultimate feasibility of pre-mine degasification under site-specific conditions (United Nations, 2010).

(2) Post-drainage Basics

Many coal basins around the world, with the low permeability of the coal bed and seams (<0.1 mD) and geologic characteristics of the seams (e.g., soft coals, faulting) are not conducive to pre-drainage techniques. As shallow reserves are mined out and mining moves to deeper seams in many mining countries, this become even more common (Zhou et al., 2014). Any effective gas drainage in these coal basins relies on the fracturing and permeability enhancement caused by the

caving of the strata as the coal is progressively mined. Post-drainage methods involve intercepting gas released by activities of mining disturbance before it can access to a mine airway and obtaining enter the zone of disturbance above, and also sometimes below, the worked coal bed and seam (United Nations, 2010).

Where there are one or more coal seams above or below the worked seam, gas emissions from these sources can significantly exceed emissions limit from the worked seam depending primarily on net coal thickness and gas content of these seams (Sang et al., 2010). Therefore, much higher quantity gas flows can often be drained using post-drainage techniques compared to pre-drainage methods. Ensuring sufficiently high gas concentrations for efficient drainage and safe utilization requires careful design and management of the drainage networks. The greater the incidence of coal in the gassy working coal seam roof and floor, the more significant post-drainage becomes (United Nations, 2010; Karacan, 2014). There are three wide-used post-drainage methods.

The first one is Guided Horizontal Boreholes. Drilled from a air way or specially prepared drilling galleries. Boreholes can be drilled into surrounding strata that will relax as the working face retreats. The relaxing adjacent layers produce gas into areas acting as pathways and collection points for gas as it migrates upward (United Nations, 2010; Karacan, 2014).

The second one is Cross-measure Boreholes. Drilled in various configurations and designed to drain roof and floor rock strata as it relaxes in response to de-stressing caused by coal mining. One set is drilled before the retreating longwall face into the overlying roof rock behind the coalface. This type tends to perform better than those drilled before performing mining activities, as they invariably suffer damage as the face passes strata after the working face has already formed (United Nations, 2010). In general, cross-measure boreholes drilled behind the longwall working face achieve higher capture efficiencies and maintain higher gas concentration than those drilled in front of the coal face. However it is imperative to maintain the entry behind the face by building pack walls, and in some cases to also form a seal against the goaf. Seals on the goaf side of the open air way behind the face serve to enhance roadway support and isolate the goaf from air ingress to minimize the spontaneous combustion risk (Karacan, 2014).

The last one is Surface Goaf Boreholes. It drilled from the surface into the upper limits of the goaf, and it usually in advance of mining activities. These boreholes are drilled so that the lower

portion of the hole drains gas that migrates upward from underlying relaxed and broken strata. The boreholes are usually operated under a partial vacuum. Care must be taken that the suction is not excessive as to draw in large amounts of mine air and dilute the gas purity below 30%. When the purity drops below 25% to 30%, these goaf holes must be shut in (United Nations, 2010; Karacan, 2014).

6.1.3 Design considerations for gas drainage systems

The capacity of a gas drainage network should be designed to accommodate the maximum expected captured gas mixture (methane and air) flows from all sources in the mine, including working faces, exhausted faces from which material and equipment are removed, dumped zones and goaf area.

The expected quantity of produced gas can be estimated using a gas prediction method. The highest flow that has to be transported through the piping system is given by the highest expected captured gas flow with the lowest gas concentrations likely to arise during normal operations. The resulting flow rate should be within the network's planned capacity when all the pumps are operating (Krishna et al., 2014).

Gas quality is a design feature of the gas drainage network, not an inherent or natural characteristic. Gas concentration of less than 30% methane in air should be considered unacceptable for both safety requirements and efficiency reasons. The maintenance of gas concentration in underground gas drainage systems rely on the quality of borehole sealing, including proper installation of standpipes, the systematic regulation of individual boreholes, and the suction pressure applied at the surface extraction plant. Increasing suction in an effort to increase gas flow will introduce more air and hence reduce the gas concentration (United Nations, 2010; Karacan, 2014). Conversely, reducing suction will reduce the total mixture flow but improve gas concentration. Most importantly, suction and flow at the surface plant should only be adjusted with a full knowledge of the underground status and while maintaining communication with the longwall ventilation supervisors.

When planning, implementing, and managing a gas drainage system, many factors should be taken into account (United Nations, 2010; Karacan, 2014):

- Safety of enter for drilling, controlling and regulation.
- Ground stability and essential support systems to stabilize boreholes.
- Gas drainage borehole configurations, with consideration given to differences between the expected performance of roof and floor post-drainage boreholes.
- Drainage capacity, pipe diameters, extraction pump, and infrastructure requirements.
- Location, installation, and commissioning of the drainage pipe network.
- Water traps and dewatering facilities.
- Operational control and maintenance of the drainage system and infrastructure.
- Monitoring of boreholes, pipe networks, and the surface extraction plant.
- Protection of gas drainage pipes from crushing behind longwall retreat faces.

6.1.4 Underground gas pipeline infrastructure

GRP pipelines are relatively brittle and should not be used in coal-production districts; however, their ease of handling and installation, compared with steel pipe, makes them the preferred material for the main trunk lines (United Nations, 2010).

Where space is restricted and the line might be vulnerable to physical damage (e.g., from roadway deformation or free-steered vehicles), steel pipe should be used and connected using proprietary flexible joints to allow movement (Honegger and Wijewickreme, 2013).

PE pipe is used in some mining countries, but high temperature fusion of these pipe joints or segments underground should be avoided. Safety regulators in some mining countries allow this practice in well ventilated areas under supervision of qualified mine safety personnel, whereas in other countries, it is deemed unacceptable. In addition, a conductive medium is essential to reduce risk of static discharge (Ye et al., 2012).

Regardless of material choice and positioning, underground pipe systems are vulnerable to damage even in the most regulated mines. The principal potential source of damage is mining materials and equipment, including mineral conveyors, rope haulage systems, locomotives and their loads, and blasting activities (Karacan, 2014).

There is also the potential for damage from strata movement and roof collapse. The gas drainage system should therefore be designed and operated with the premise that there is a finite

risk of integrity failure.

6.1.5 Monitoring of gas drainage systems

Manual or intelligent remote monitoring systems should be used to determine the effectiveness of the gas drainage system. Controlling and monitoring quality depends on the sensors' reliability, positioning, maintenance, calibration, and use (Thomas et al., 2012).

Measurements are needed at individual boreholes, in gas drainage pipe-work, and at the surface gas extraction plant that houses the pumps that draw the drained gas out of the mine. Parameters to be monitored include mixture flow, gas concentration, gauge pressure, and temperature (Karacan, 2014). Barometric pressure should also be recorded to facilitate standardization of flow data. In some cases, gas being drained or emitted into the mine workings may contain other components such as moisture, sulphur compounds, or heavier gaseous hydrocarbons (e.g., ethane or propane) that may cause inaccurate measurement of gas. Care should be taken to design a monitoring and measurement program capable of correcting for any additional constituents so that accurate measurements are ensured. Monitoring should be used to assess the actual performance of the installed system against the original design concept (United Nations, 2010).

6.2 Gas distribution rule of working face and field measurement results

6.2.1 Layout of measuring points in the working face

In order to fully understand the gas emission law in the working face and goaf, present the scientific and representation of the test findings and truly reflect the practical situation of gas in the working face, observation stations are set every 45 meters along the working face, with 5 measuring points evenly arrange between the coal wall to goaf (along the working face) in each station. A total of 25 measuring points are set, and 2 measuring points are respectively set 15 meters from the air inlet to air outlet. The arrangement of the measuring points is shown in Figure 6.2.1. When measuring the concentration distribution of gas in the working face, time is selected when the coal cutter cuts the coal the first time (coal cutter at air inlet) and when maintenance shift is on duty, as at that point the working face is relatively stable and not affected by coal cutting.

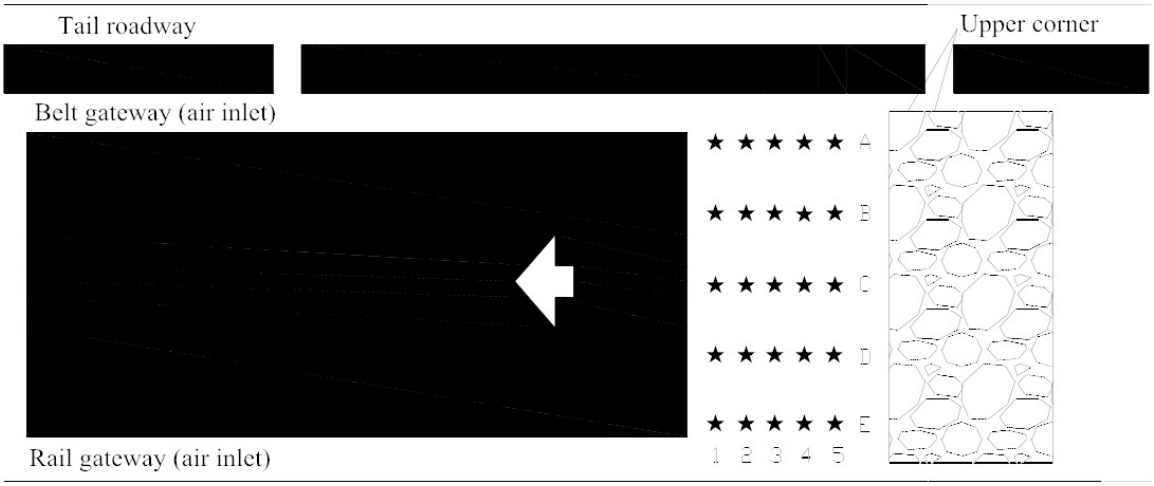

Figure 6.2.1 Layout of measuring points in the 14205 working face of Shaqu coal mine

6.2.2 Gas concentration distribution along the working face

According to gas measurements data Table 6.2.1 and Table 6.2.2 of production shift and maintenance shift of the 14205 working face, gas concentration distribution pattern along the working face is drawn as in Figure 6.2.2 and Figure 6.2.3.

Table 6.2.1 Measurements of gas concentration distribution of the 14205 working face on production shift

Test position (hydraulic support)	Point 1 Gas concentration (%)	Point 2 Gas concentration (%)	Point 3 Gas concentration (%)	Point 4 Gas concentration (%)	Point 5 Gas concentration (%)
Support 10	0.81	0.76	0.75	0.8	0.88
Support 40	0.63	0.58	0.55	0.57	0.67
Support 70	0.40	0.36	0.32	0.34	0.39
Support 100	0.25	0.22	0.19	0.19	0.20
Support 130	0.15	0.13	0.11	0.10	0.11
Air inlet	0.06				
Air outlet	0.78				

Table 6.2.2 Measurements of gas concentration distribution of the 14205 working face on maintenance shift

Test position (hydraulic support)	Point 1 Gas concentration (%)	Point 2 Gas concentration (%)	Point 3 Gas concentration (%)	Point 4 Gas concentration (%)	Point 5 Gas concentration (%)
Support 10	0.76	0.69	0.68	0.73	0.79
Support 40	0.56	0.53	0.50	0.54	0.60
Support 70	0.45	0.39	0.37	0.40	0.42
Support 100	0.33	0.30	0.28	0.28	0.29
Support 130	0.24	0.23	0.21	0.20	0.21
Air inlet	0.04				
Air outlet	0.72				

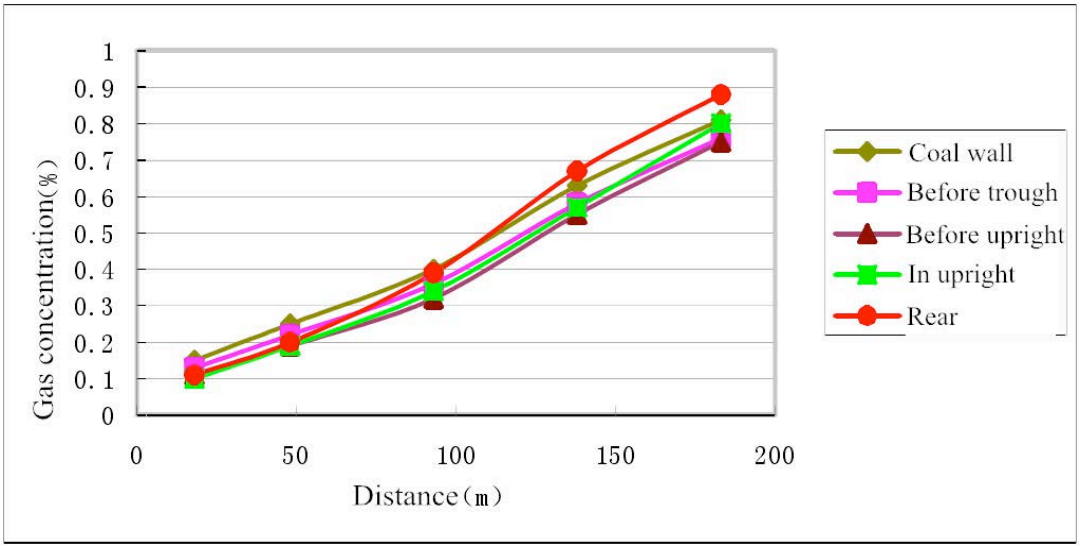

Figure 6.2.2 Gas concentration distribution along 14205 working face on production shift

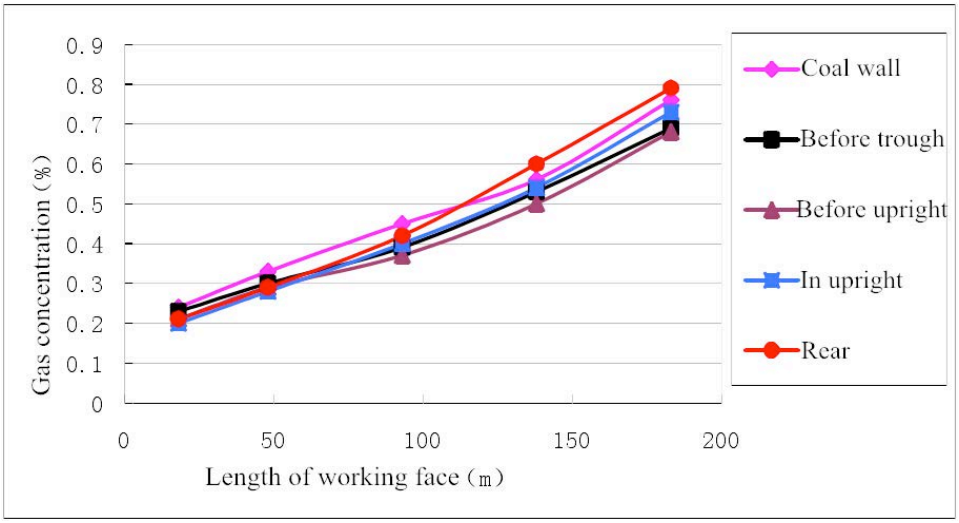

Figure 6.2.3 Gas concentration distribution along 14205 working face on maintenance shift

Studies suggest that gas concentration in the mining face increases from inlet airway to return airway. The range of variation of gas concentration decreases from inlet airway to the central section of the mining face, while gas concentration increases rapidly from the central section of the mining face to the upper corner of the return airway, and gas concentration reaches the highest at 30m from the return airway. The reason is that when airflow goes through the stope from the inlet side, a part of it leaks into goaf from the central section of the mining face, and then comes back to the working face with high-concentrated gas in goaf, which increases the gas concentration in the working face. It is indicated in practical researches that the reason of gas at upper corner exceeding limit easily is when airflow goes back from goaf, a great deal of gas is brought to the return corner and thus the gas concentration at the upper corner increases.

6.2.3 Distribution of gas concentration in vertical direction of coal wall

Distribution diagrams of gas concentration in vertical direction of coal wall are made based on the gas measurements in the 14205 working face on production shift and maintenance shift, as shown in Figure 6.2.4 and Figure 6.2.5.

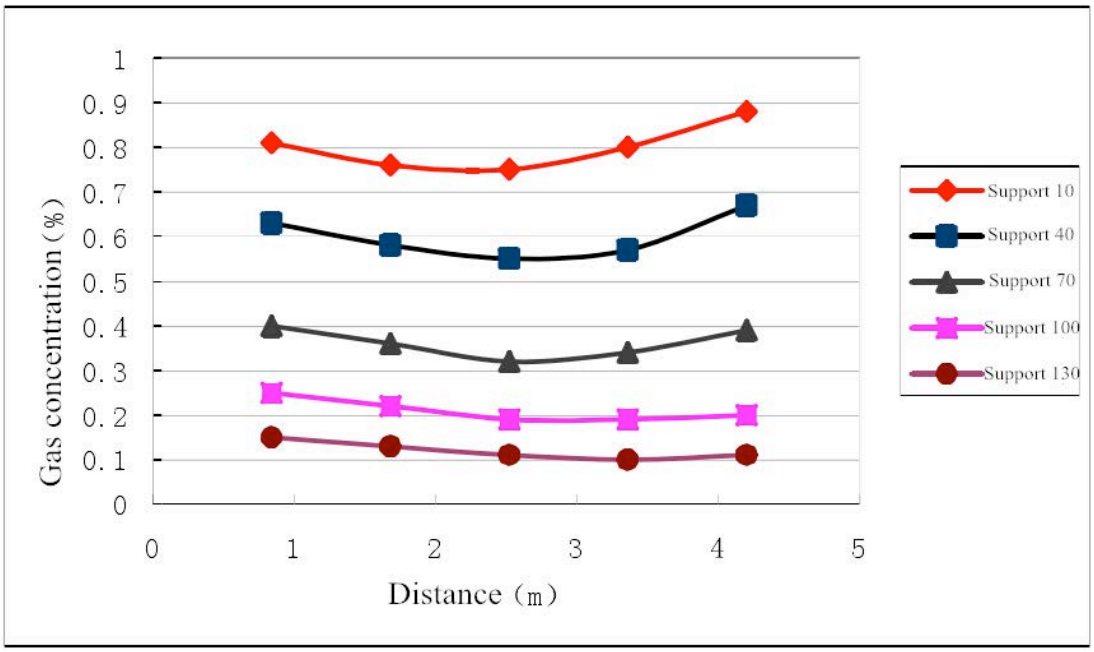

Figure 6.2.4 Distribution of gas concentration in 14205 working face in vertical direction of coal wall on production shift

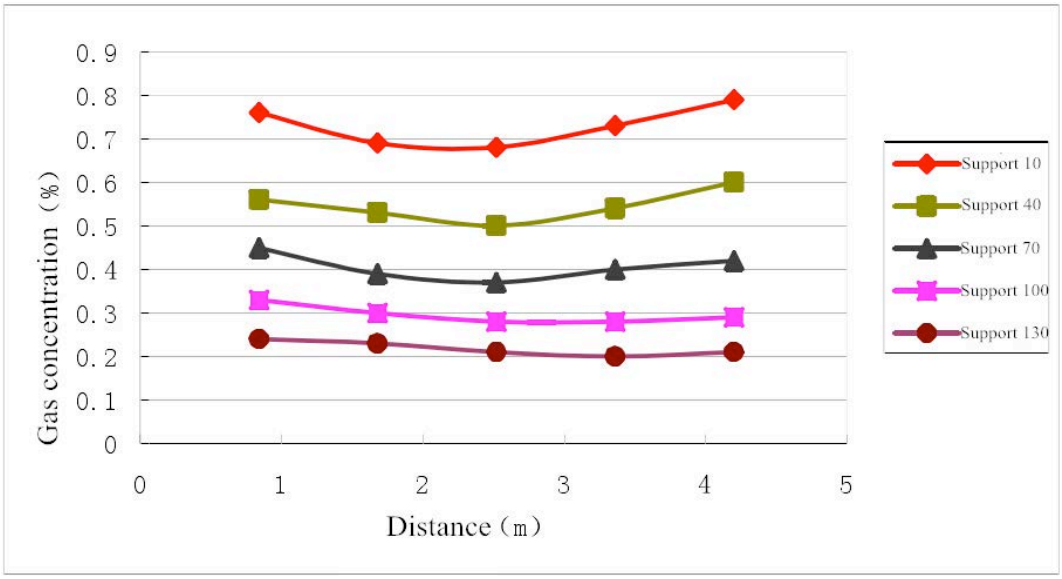

Figure 6.2.5 Distribution of gas concentration in 14205 working face in vertical direction of coal wall on maintenance shift

Research shows that gas concentration appears to be high, relatively high, low, relatively high, and high respectively from coal wall to goaf (stand tail), that is, between the coal wall and goaf there is a spot where gas concentration is the lowest, and it locates differently in the mining face in different situations. In U-type ventilation the high-low-high situation is more obvious

whereas it is less obvious in U+L-type ventilation.

It is believed that in the high-low-high situation, the spot where the gas concentration is the lowest is the demarcation point of gas emission of coal wall and goaf. According to the experimental and observational data, in U+L-type ventilation, gas emission volume from goaf to the working face is smaller that that in U-type ventilation. The reason is gas emission from goaf is split by “L” lane. It can also be seen that gas at the upper corner has higher concentration and it is the main channel through which gas flows into the mining face from goaf. Therefore, the emphasis on gas governance in the working face is the prevention of gas overrun at the upper corner.

6.2.4 Vertical distribution of gas concentration in the 14205 working face

Based on the gas spatial measurements of the 14205 working face on production shift and maintenance shift Table 6.2.3 and Table 6.2.4, spatial distribution of gas concentration is made in Figure 6.2.6 and Figure 6.2.7.

Table 6.2.3 Data sheet of spatial distribution of gas concentration in the 14205 working face on production shift

Test position (hydraulic support)		Point 1 Gas concentration (%)	Point 2 Gas concentration (%)	Point 3 Gas concentration (%)	Point 4 Gas concentration (%)	Point 5 Gas concentration (%)
Support 5	Top	0.75	0.74	0.72	0.75	0.83
	Middle	0.73	0.71	0.70	0.74	0.80
	Bottom	0.74	0.72	0.7	0.73	0.79
Support 65	Top	0.40	0.38	0.35	0.38	0.41
	Middle	0.39	0.38	0.36	0.38	0.40
	Bottom	0.41	0.39	0.37	0.38	0.42
Support 125	Top	0.16	0.13	0.11	0.12	0.12
	Middle	0.15	0.14	0.12	0.11	0.13

	Bottom	0.14	0.13	0.11	0.12	0.13

Table 6.2.4 Data sheet of spatial distribution of gas concentration in the 14205 working face on maintenance shift

Test position (hydraulic support)		Point 1 Gas concentration (%)	Point 2 Gas concentration (%)	Point 3 Gas concentration (%)	Point 4 Gas concentration (%)	Point 5 Gas concentration (%)
Support 5	Top	0.73	0.67	0.69	0.73	0.79
	Middle	0.74	0.68	0.69	0.73	0.76
	Bottom	0.72	0.64	0.66	0.71	0.75
Support 65	Top	0.51	0.47	0.44	0.47	0.49
	Middle	0.52	0.45	0.44	0.47	0.49
	Bottom	0.53	0.45	0.43	0.46	0.48
Support 125	Top	0.27	0.24	0.23	0.22	0.24
	Middle	0.28	0.25	0.22	0.22	0.23
	Bottom	0.25	0.23	0.21	0.22	0.22

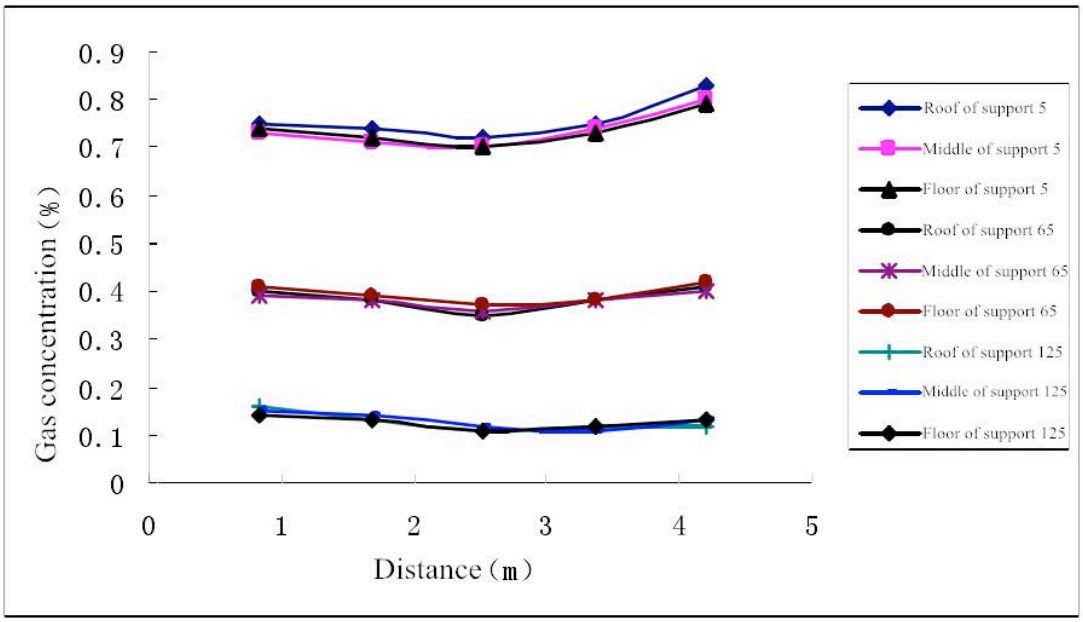

Figure 6.2.6 Spatial distribution diagram of gas concentration in the 14205 working face on

production shift

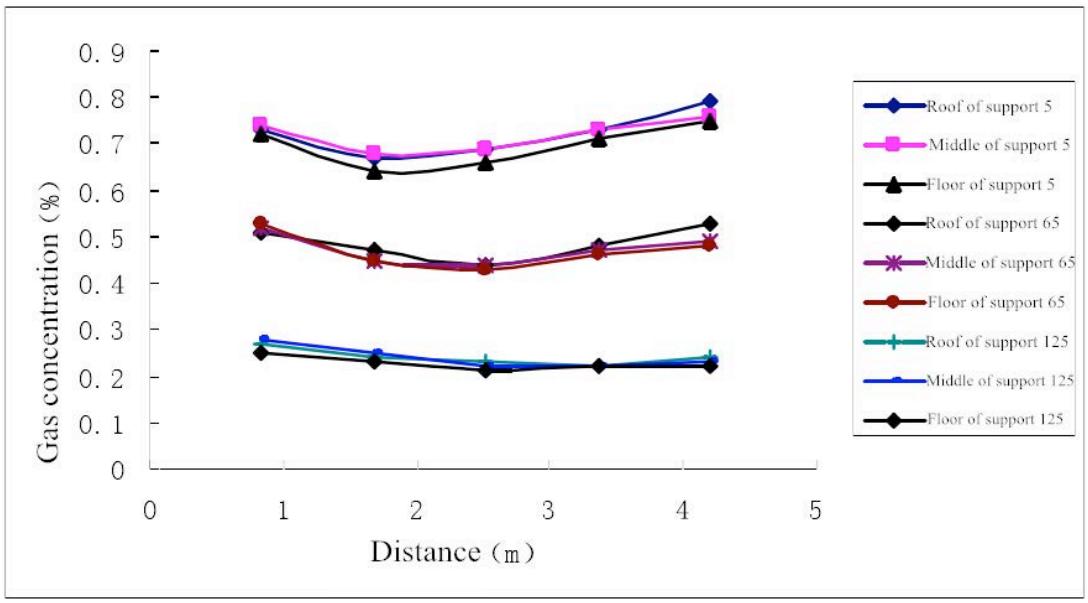

Figure 6.2.7 Spatial distribution diagram of gas concentration in the 14205 working face on maintenance shift

Studies indicate that the variation of gas concentration distribution gets smaller from upper airway to the central section whereas the variation is large at tail gateway. It is mainly because when airflow goes through the stope from the inlet side, a part of it leaks into goaf from the central section of the mining face, and then comes back to the working face with high-concentrated gas in goaf, which increases the gas concentration in the working face and results in the huge variation of the gas concentration in spatial distribution. It is indicated in both theory and practice that when airflow goes back from goaf, a great deal of gas is brought to the return corner, which results in the increase of the gas concentration at the upper corner and difference of gas spatial distribution.

6.2.5 Imbalance of gas emission in the mining face

The gas concentration distribution in the mining face mentioned above is measured in relatively stable conditions. When the shearer cuts coal, gas distribution in the mining face is generally in compliance with the above rules, but gas emission is more uneven. Through the measurements on measuring points with the shearer at different locations, it is found that as

position of the shearer keeps changing due to the coal cutting; the gas distribution in the mining face is greatly affected. During the coal cutting from inlet airway to the working face, gas mainly emits from coal wall and fallen coals, and a part of it leaks into goaf with the wind flow. In this situation the gas emission volume in the mining face is small. On the contrary when the coal cutting is from the central section to return airway, gas flown into goaf gradually comes back to the working face with gas and leads to the increase of the gas emission volume. It is testified in both theoretical analysis and practical works that under negative pressure, most gas gathers within 30m of the return airway, where plenty of high-concentrated gas stays behind the stand. The coal cutting, propeller and mobile support of the shelter in this section reduces the cross-section of the working face and increases the resistance. Part of the airflow leaks into goaf again through the inter-frame channel. Due to the leakage area is small, the airflow goes back to the working face in a short period of time with the high-concentrated gas behind the stand, and the sharp increase in gas causes the gas rapid emission in the working face. Observations show that the gas overrun in the working face is generally caused during this period of time.

6.3 Gas migration law of working face and goaf and filed measurement

6.3.1 Layout of measuring points in the working face

The working face is divided into several sections along the strike (from the stand to the coal wall), with one section taken as an example in Figure 6.3.1. Gas emission volume and gas concentration at the cross-section are measured respectively in each section, and gas emission volume of each emission source and gas concentration distribution of the working face are obtained through accumulative composite analysis. This is called gas segmentation measurement.

Within each section, several measuring points are set evenly from coal wall to goaf (based on the actual situation).

As in Figure 6.3.2, gas concentration of each measuring point c_1, c_1, c_1, c_1, c_1 and inlet air volume C_{in} and outlet air volume C_{out} in the section are measured.

Gas balance equation and air volume balance equation applied to all sections:

$$\begin{cases} Q_{in} \pm Q_{goaf} - Q_{out} = 0 \\ q_{goaf} = Q_{goaf} c_{goaf} \\ q_{face} = Q_{out} c_{out} - Q_{in} c_{in} - q_{goaf} \end{cases} \quad (6\text{-}3\text{-}1)$$

where: Q_{in}——airflow volume into in the section, m/min;

Q_{out}——airflow volume out of the section, m^3/min;

Q_{goaf}——airflow from goaf to the section, m^3/min;

q_{goaf}——gas volume from goaf to the section, m^3/min;

q_{face}——gas emission volume from coal wall, roof, floor and fallen coal in the section, m^3/min;

C_{goaf}——gas concentration of leaking airflow in goaf, %;

C_{in}——gas concentration of air inflow of the section, %;

C_{out}——gas concentration of air outflow of the section, %.

Thus from the above equations, volume of air leakage in goaf, gas emission volume in goaf, coal wall, roof and floor, and fallen coal are obtained.

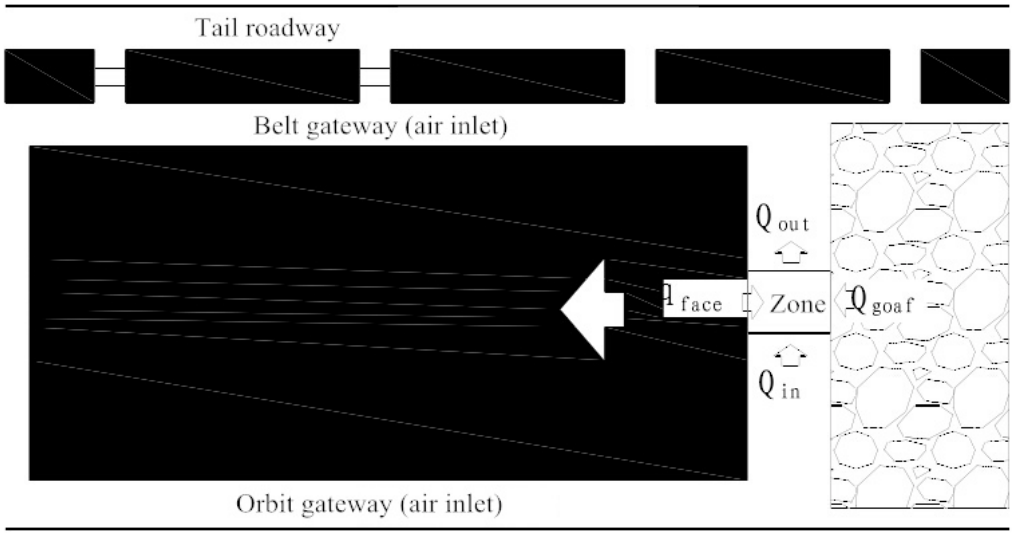

Figure 6.3.1 Section division plan of the working face

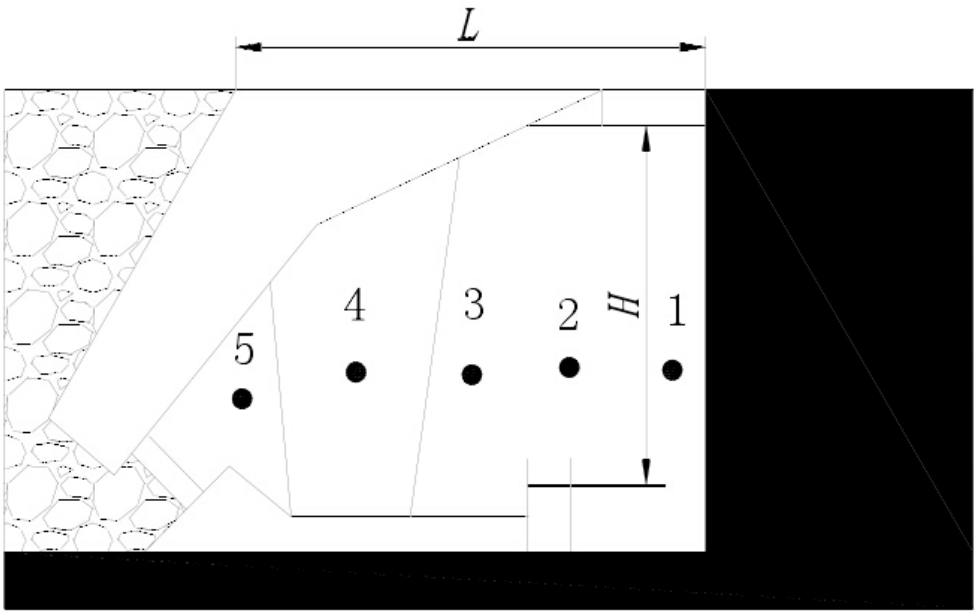

Figure 6.3.2 Layout of measuring points

6.3.2 Procedure of segmentation measurement on gas emission

According to segmentation measurement principals, the measurement of gas distribution in the working face can take the following steps:

(1) The working face is divided into 8~12 sections (8 sections in this research) based on the length of incline section. The most commonly used equipment is used for the measurements of gas concentration and air velocity.

(2) Air inlet volume and outlet volume are measured in each section.

(3) Gas concentration of measuring points from coal wall to goaf is measured at both air inlet and return cross-sections of each section.

(4) Volume of air leakage in goaf, and gas emission volume in goaf, coal wall and fallen coal are obtained based on gas balance equation and air volume balance equation.

6.3.3 Findings and analysis of segmentation measurement

According to the above procedure, repeat measurements are made on gas concentration and air velocity of the 14205 working face on non-production shift, and findings are shown in Table 6.3.1. The calculation of gas emission volume is in Table 6.3.2.

Table 6.3.1 Findings of segmentation measurement in the 14205 working face

Test position (hydraulic support)	Unite number	Gas concentration (%)					Section (m^2)	Quantity (m^3/min)
		Point 1	Point 2	Point 3	Point 4	Point 5		
Support 0	8	0.90	0.89	0.89	0.96	0.98	8.45	1180
Support 10	7	0.87	0.87	0.86	0.90	0.92	8.82	1050
Support 30	6	0.88	8.85	0.85	0.86	0.88	8.20	910
Support 60	5	0.89	0.76	0.75	0.77	0.77	7.50	770
Support 70	4	0.67	0.65	0.64	0.67	0.65	6.70	680
Support 90	3	0.51	0.51	0.50	0.52	0.53	6.70	620
Support 110	2	0.35	0.33	0.37	0.37	0.37	8.78	730
Support 120	1	0.25	0.25	0.24	0.25	0.28	8.34	900
Support 130		0.22	0.22	0.22	0.21	0.20		1720

The data of above measurements indicate that:

(1) In terms of gas concentration in goaf, in the working face gas concentration increases from inlet airway to return airway. In units near the inlet airway, gas concentration of measuring points 4 and 5 is the same as that of measuring point 3 on the cross-section, which indicates there is airflow leakage in goaf and no gas in goaf flows into the working face. In units near the return airway, gas concentration of measuring point 5 is apparently higher than that of measuring point 3, and it shows there is air leakage from goaf and gas in goaf flows into the working face.

(2) In terms of measurements on air volume, in units near the inlet airway air volume gradually decreases in the working face and airflow leaks into goaf. In units near the return airway, air volume in the working face increases and air leaks out of goaf.

(3) In terms of measurements on gas concentration of coal wall, gas concentration is lower at upside and downside of the working face, but is higher on coal wall of unit 5 and 6 inclined to return airway. It suggests that in units inclined to the return airway, more gas is reserved in coal and less is released, and during the exploitation gas emission volume is large and there is likely to be coal and gas outburst.

Table 6.3.2 Data sheet of gas emission of the 14205 working face

Unit number	Q_{in}	C_{in}	Q_{out}	C_{out}	Q_{goaf}	q_{face}	C_{goaf}	q_{goaf}
1	1720	0.2	900	0.28	-820	1.048	0.24	-1.968
2	900	0.28	730	0.37	-170	0.734	0.33	-0.561
3	730	0.37	620	0.53	-110	1.08	0.45	-0.495
4	620	0.53	680	0.65	60	0.78	0.59	0.354
5	680	0.65	770	0.77	90	0.87	0.71	0.639
6	770	0.77	910	0.88	140	0.924	0.83	1.162
7	910	0.88	1050	0.92	140	0.392	0.90	1.260
8	1050	0.92	1180	0.98	130	0.669	0.95	1.235
Amount	-	-	-	-	-	6.497	-	4.650
Proportion (%)	-	-	-	-	-	58.3	-	41.7

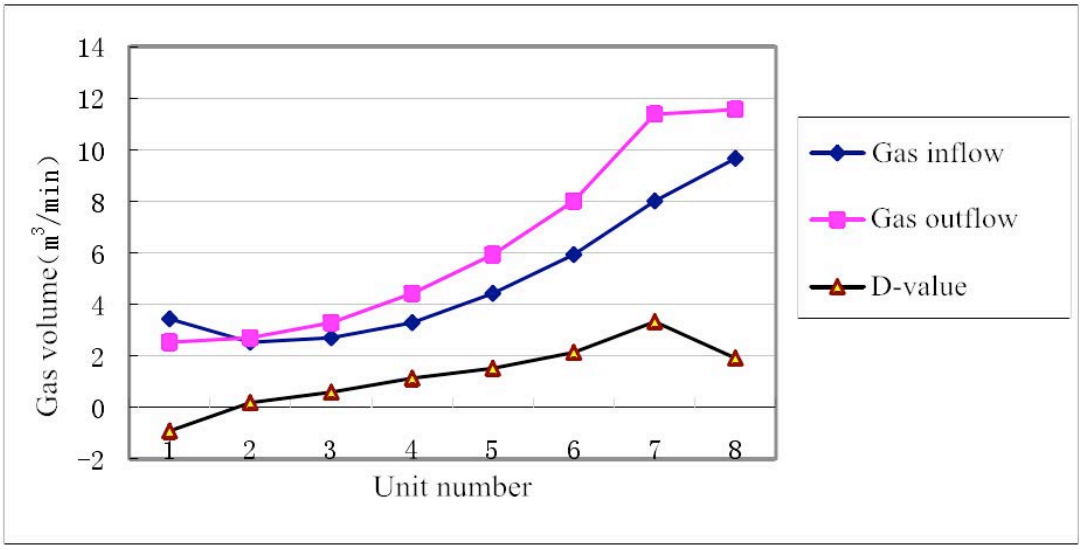

Figure 6.3.3 Dynamic analysis on gas of the 14205 working face

Dynamic analysis on gas of the 14205 working face is obtained through segmentation measurement. Findings are as follows:

(1) Gas emission volume in goaf accounts for 58.3% of the total amount, while the

percentage of gas emission in coal wall is 41.7%. This is in general accordance with the proportion of gas emission of goaf and coal wall from actual measurements above.

(2) From the inlet airway to the return airway of the entire working face, gas volume into each segment maintains increase along the way and gas concentration gradually increases due to the gas migration affected by airflow leakage in goaf. However, as leakage at inlet airway is serious and gas flows into goaf, gas volume keeps reducing from the first section to the second section.

(3) In the front half of the working face, that it the side closer to the inlet airway, there is no significant variation in the increase of gas. Besides, the total amount of gas emission from coal wall and fallen coal is slightly bigger than the gas volume brought from goaf. As a result, the volumes of inflow and outflow are in balance.

(4) In the central section of the working face, leakage gradually weakens and gas volume in each section increases sharply, therefore the gas volume remained in the working face increases.

(5) In the rear half of the working face, the net inflow of gas volume increases significantly, indicating that part of air Leakage in goaf backflows into the working face with high-concentrated gas in goaf. It results in the substantial increase of the gas concentration in the working face.

(6) At return airway of the working face, net inflow of gas volume reaches the top and then keeps decreasing, which means that under the effect of inlet ventilation pressure and converging hole of gas tail way, airflow in the working face leaks into goaf again and takes part of gas away into the tail gateway， which as a result partially alleviates the problem of gas overrun at the upper corner of the working face.

6.4 The necessity and feasibility of gas drainage

6.4.1 Analysis of the necessity of gas drainage

According to Article 145 of <*Coal Mine Safety Regulations enacted*> in 2009 by China Coal Mine Safety Supervision Bureau, long-term or temporary gas drainage system must be established in mines with one of the following situations.

(1) Gas emission volume in a mining working face is greater than $5m^3$/min or gas emission volume in an excavating working face is greater than $3m^3$/min; ventilation solution of the gas

problem is unreasonable.

(2) Absolute gas emission volume fulfills the following requirements:

(2.1) is greater than or equal to 40 m^3/ min;

(2.2) is greater than 30 m^3 / min for mines with annual output of 1.0Mt to 1.5Mt;

(2.3) is greater than 25 m^3 / min for mines with annual output of 0.6Mt to 1.0Mt;

(2.4) is greater than 20 m^3 / min for mines with annual output of 0.4Mt to 0.6Mt;

(2.5) is greater than 15 m^3 / min for mines with annual output of 0.4Mt or less;

(3) Working seam bears danger of coal and gas outburst.

From the perspective of production status, the result of coal mine gas rank appraisal in 2011 is: coal seam gas relative emission volume is 52.12 m^3/t and the absolute emission volume is 225.15 m^3/min. From the perspective of gas emission situation, the #4 coal seam of Shaqu coal mine as the first working seam relies only on ventilation to dilute gas in the working face which is difficult and unreasonable. Instead, according to draining while mining rule, gas drainage should be immediately implemented. Therefore based on the current gas emission situation, it is quite necessary to establish the gas drainage system.

6.4.2 Analysis of feasibility of gas drainage

The classification of complexity of coal gas drainage can be seen in Table 6.4.1

.

Table 6.4.1 Classification of complexity of coal gas drainage

Complexity and Index	Attenuation coefficient of flow rate of gas drainage borehole, α (d^{-1})	Permeability coefficient of coal seam, λ ($m^2/MPa^2 \cdot d$)
Easy to drainage	＜0.003	＞10
Can drainage	0.003～0.05	10～0.1
Difficult to drainage	＞0.05	＜0.1

In the coal seam #4 of Shaqu caol mine, attenuation coefficient of gas flow rate of 1000 meters gas drainage borehole is 0.042d^{-1}, and seam permeability coefficient is 0.511$m^2/MPa^2 \cdot d$. It can be concluded from the comprehensive analysis of the above data that coal seam of Shaqu coal

mine is suitable for gas drainage and the establishment of long-term gas drainage systems.

6.5 Gas drainage scheme of Shaqu coal mine

6.5.1 Selection principle of gas drainage scheme

The selection of gas drainage method is mainly based on comprehensive consideration of gas sources in mine (working face and goaf), coal seam occurrence, mining layout, mining program and mining geology conditions. Currently the main methods of gas drainage are: gas drainage in mining layer, in adjacent layer and in goaf. Gas drainage method should be chosen specifically by the following principles:

(1) The selected gas drainage method should comply with coal seam occurrence, mining roadway layout, geological conditions and mining conditions;

(2) The selection should be based on methane emission sources and emission formation, and integrated gas drainage method is usually adopted to improve gas drainage;

(3) The selection should help reduce the underground construction work and achieve the combination of mining roadway and drainage roadway;

(4) The selected gas drainage method should help facilitate and maintain the drainage roadway, improve the effectiveness and reduce the drainage costs;

(5) The selected gas drainage method should help facilitate drainage construction, drainage pipes layout and increase the drainage time.

6.5.2 Gas drainage parameters and drainage layout

According to the principles of drainage selection and taking into account the coal seam occurrences and gas sources of Shaqu coal mine, and the required drainage volume in the working face, a reasonable drainage method for Shaqu coal mine is proposed as is shown in Table 6.5.1.

Table 6.5.1 Drainage scheme selection

Type	Drainage method	Reason	Comment
Coal	In front of the working	High concentrated gas in coal	Gas drainage

seam	face, pre-drainage or mining while drainage	seam with low air permeability coefficient,	borehole in the air outlet
	In excavating working face, excavating while drainage	High gas emission volume in excavation working face	Next to the gate roadway
Goaf area	Gas drainage pipe in the upper corner	A large amount of high concentrated gas constantly flows into the upper corner	Gas drainage pipe in the upper corner
	Special gas drainage borehole in the fracture zone above the goaf	High concentrated gas come from the old closed goaf, adjacent layers, mined coal and lost coal	Gas drainage borehole in the closed goaf

(1) The gas drainage layout of the working face of excavating tunnel

It is impossible to solve the gas over-limit problem only by optimizing the ventilation system because a large amount of high concentrated gas constantly emit from the working face of excavating tunnel of coal seam #4 of Shaqu coal mine. Increasing high concentrated gas continually emit from the working face when the excavating tunnel is further and deeper. The gas drainage method of excavating while drainage should be adopted as soon as possible and its design can be seen in Figure 6.5.1.

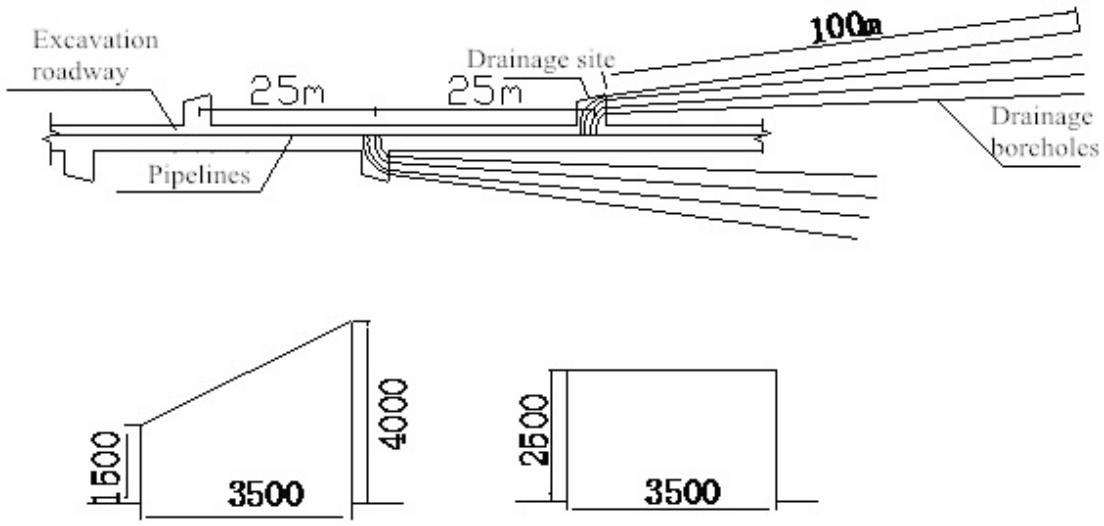

Figure 6.5.1 Excavating while drainage in the working face of excavating tunnel

Gas drainage size of length, width and height in the excavating tunnel are 3.5m, 4m and 2.5m respectively. Tunnel support should be installed after the drainage tunnel is drilled, with a space of 25m. The drainage method and technical parameters can be seen in Figure 6.5.1 and Table 6.5.2.

Table 6.5.2 Gas drainage borehole parameters of excavating while drainage

Type of drainage borehole	Included angle between borehole and tunnel (°)				Elevation of borehole (°)	Depth (m)	Diameter (mm)
Excavating while drainage	β_1 5°	β_2 10°	β_3 15°	β_4 20	Inclination in the coal seam	100	94

For the purpose of gas drainage productivity, the gas drainage site is selected in an undisturbed area (where the gas drainage tunnels and pipes is easy to seal) rather than the geological structural belt. The best option is the excavated tunnels or well-prepared to be excavated tunnels. The connection method between the gas drainage boreholes and pipes can be seen in Figure 6.5.2.

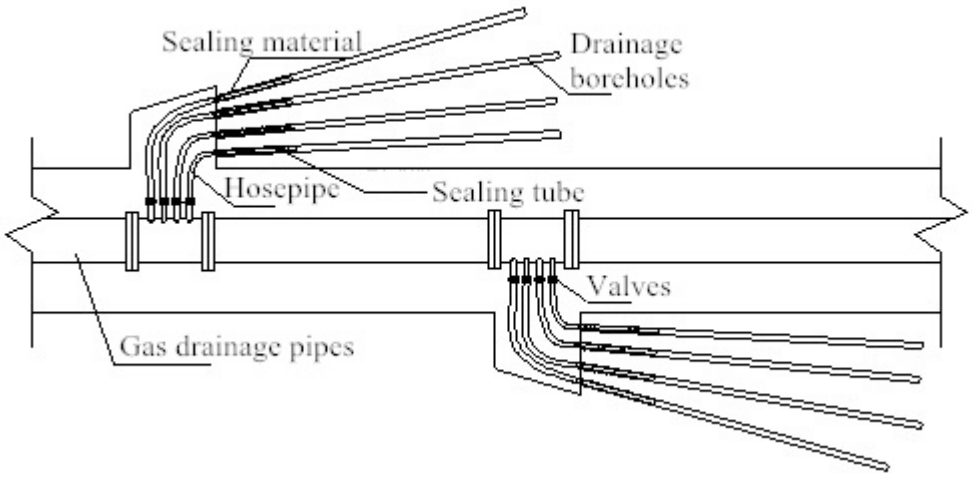

Figure 6.5.2 Connection method between the gas drainage boreholes and pipes

The gas drainage boreholes are sealed by polyurethane (PU), the depth of borehole sealing is 5m-9m, and the length of sealed borehole section is 1m. Anti-flaming and antistatic PE (Φ= 50mm) are selected as the sealed tube. Armored hoses connect to the branch pipes, and the branch pipes connect to the main pipes, finally the main pipes connect to the ground. The internal structure of polyurethane sealing borehole and gas drainage borehole can be seen in Figure 6.5.3.

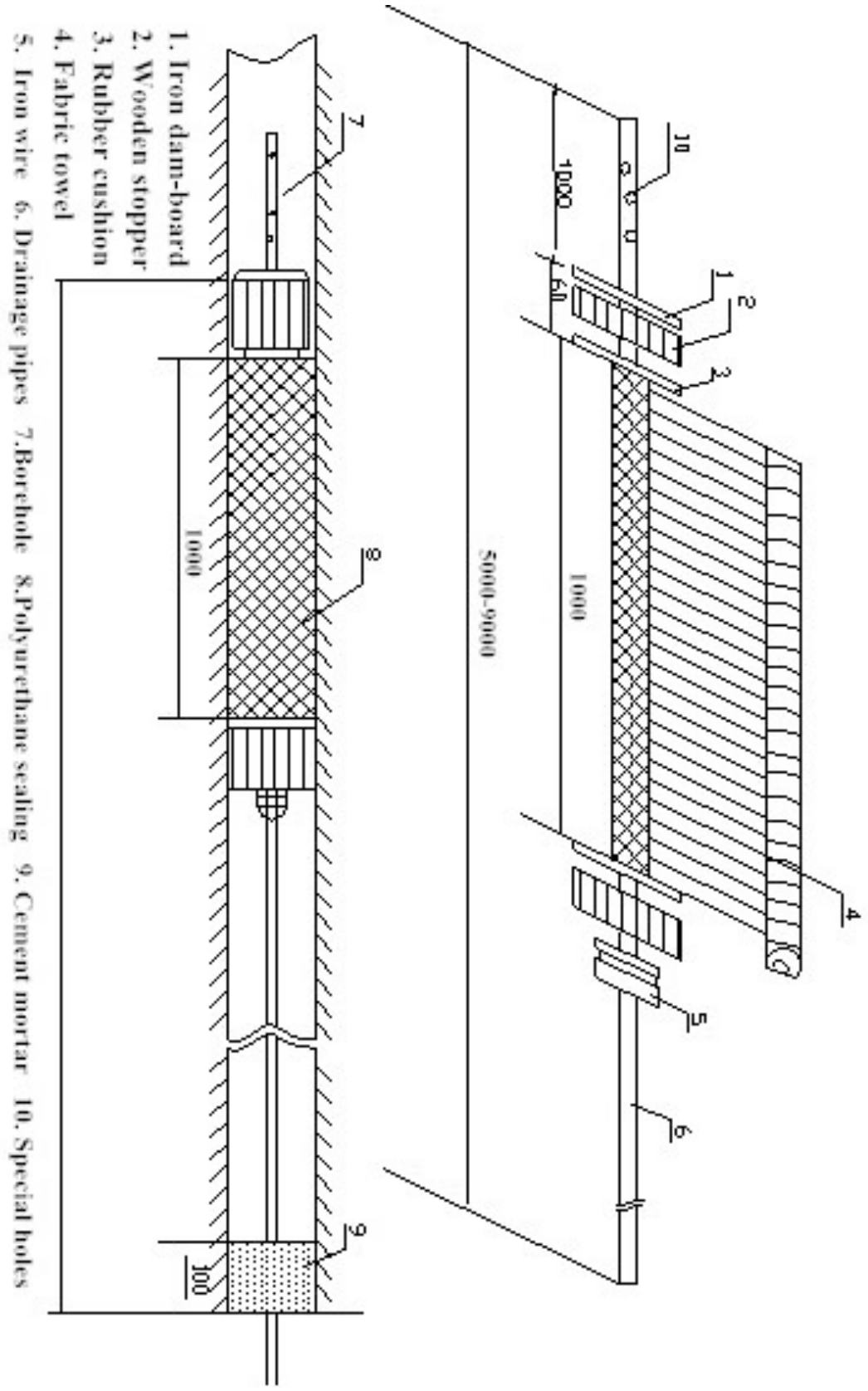

Figure 6.5.3 Method of polyurethane sealing borehole and the internal structure of sealed borehole

(2) The gas drainage layout of the coal mining working face

The gas drainage boreholes are drilled through the air outlet of the coal mining working face, and the pressure of the coal seam and rock stratum is released. Table 6.5.3 shows the layout and the technical parameters of the gas drainage boreholes.

Table 6.5.3 The technical parameters of the gas drainage boreholes

Type of borehole	The included angle between boreholes and roadway (°)	The included angle between boreholes and horizontal plane (°)	Depth of boreholes (m)	Diameter of boreholes (mm)	Pitch of boreholes (m)
Slanting borehole	60	The same as coal seal pitch	120	94	5

The layout of gas drainage boreholes can be seen in Figure 6.5.4, and the borehole sealing techniques is the same as techniques of the excavating working face.

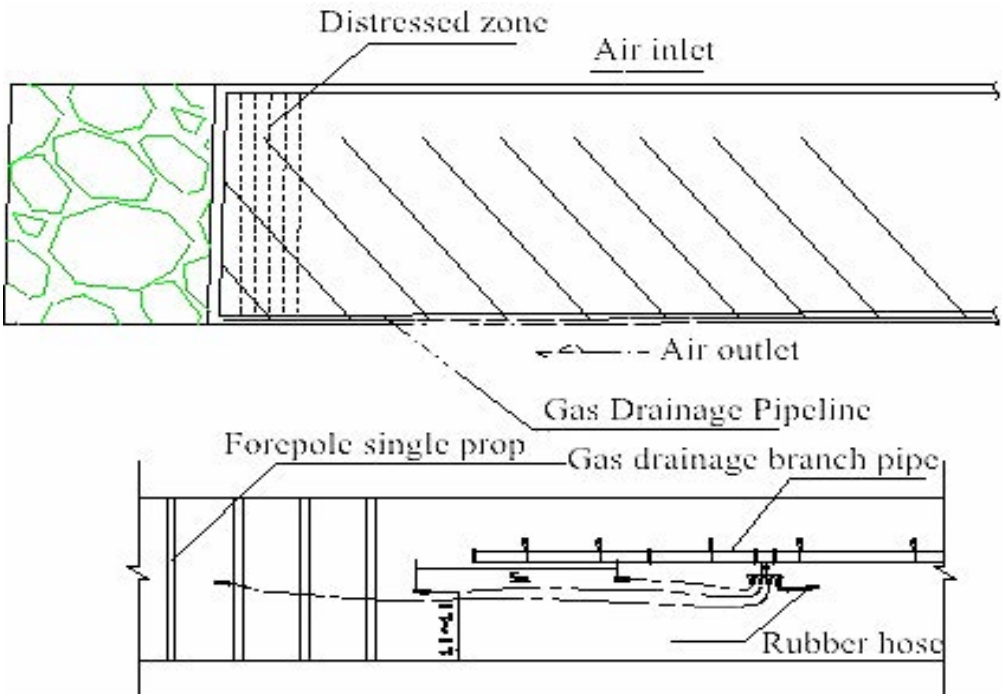

Figure 6.5.4 Layout of gas drainage borehole in the coal mining working face

(3) The gas drainage layout in the upper corner

A negative pressure zone is formed when the gas drainage tubes are installed and the gas is extracted from the upper corner. Then the problem of air flow blocking, gas over-limit and air leak in some parts of the upper corner and goaf can be effectively solved. Figure 6.5.5 indicates the gas drainage layout in the upper corner.

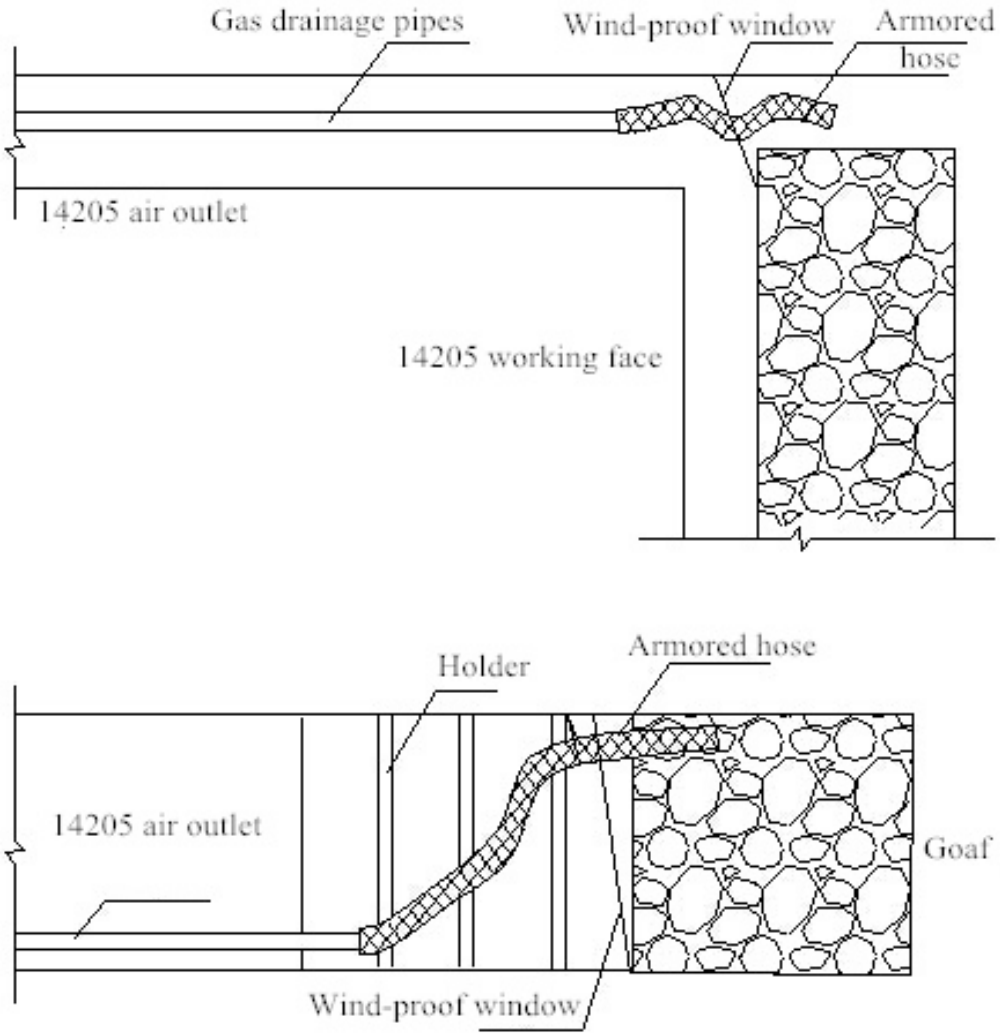

Figure 6.5.5 Gas drainage layout in the working face and upper corner

In general, the nature of adjacent coal seams and rock stratums are different, and the conditions of caving zones are different. Therefore, the selection of the negative pressure zone has a great influence on the gas drainage effect and rate. For the purpose of exactly determining the suitable gas drainage position on the upper corner, 4 more branch gas drainage rubber hoses with the length of 4 inch are selected, and installed, and it can be seen in Figure 6.5.6.

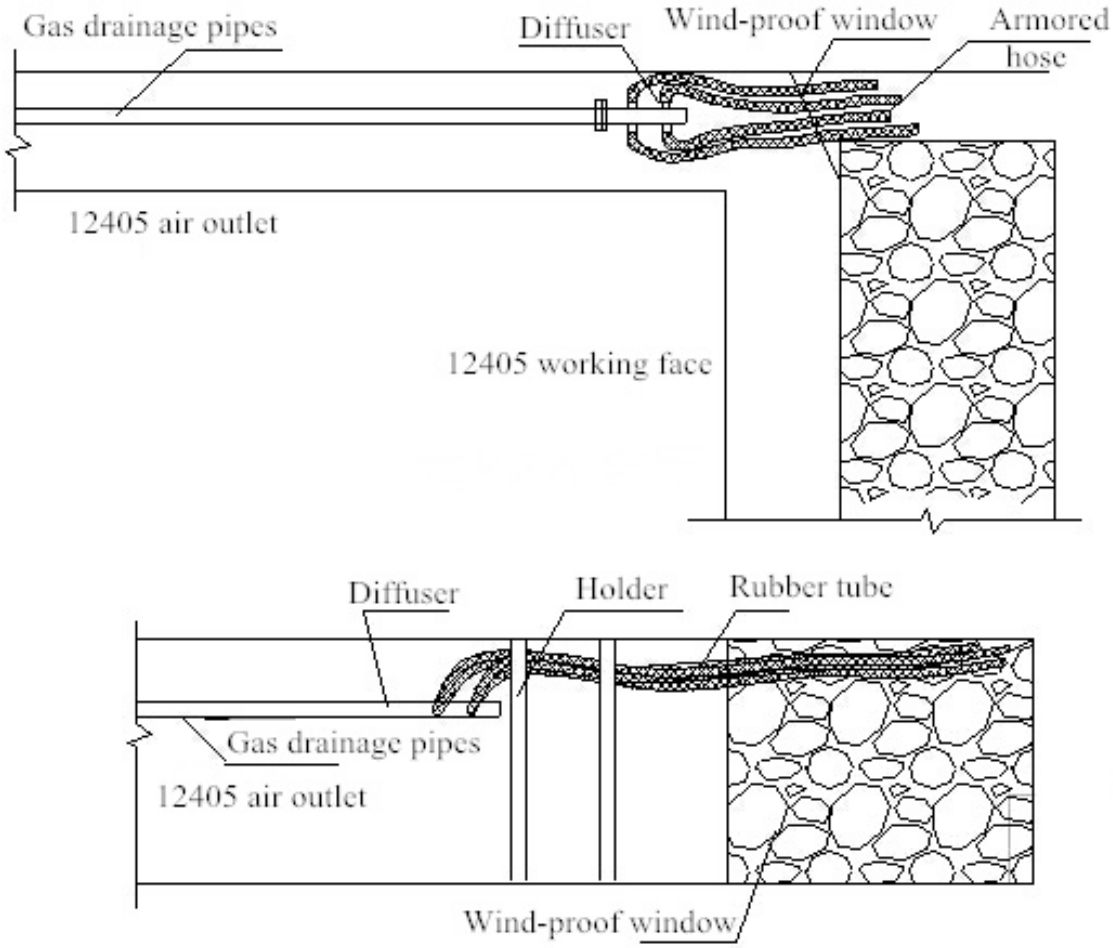

Figure 6.5.6 Multiple gas drainage rubber hoses in the working face and goaf

(4) The gas drainage layout in the adjacent coal seam, rock stratums and goaf

The special gas drainage boreholes and tunnels are arranged in the adjacent coal seam, rock stratums and goaf. The technique of special gas drainage boreholes and tunnels mainly targets hazardous gassy coal mine. Horizontal directional gas drainage boreholes are drilled along the mining coal seam.

The coal mine goaf area can be horizontally or vertically divided into three zones. To be specific, the coal mine goaf area horizontally consists of three parts: coal wall support area, rock separation area and the re-compaction area. The coal wall support area rapidly changes when the mining activities are performed. The re-compaction area has the compact completely; both of them are not easy for gas drainage. By contrast, the rock separation area has an amount of fracture space, and it is ideal and effective gas drainage area. On the other hand, rock strata from top to

bottom are vertically made up of three parts: caving zone, fracture zone and bending subsidence zone. It is well known that excavating gas drainage hole in both caving zone and bending subsidence zone is an extremely difficult project. However, fracture zone has a mass of fissuring area, which is the most reasonable and effective gas drainage zone.

According to the theories mentioned above, the gas drainage layout in the laboratorial simulation model can be seen in Figure 6.5.7 and Figure 6.5.8.

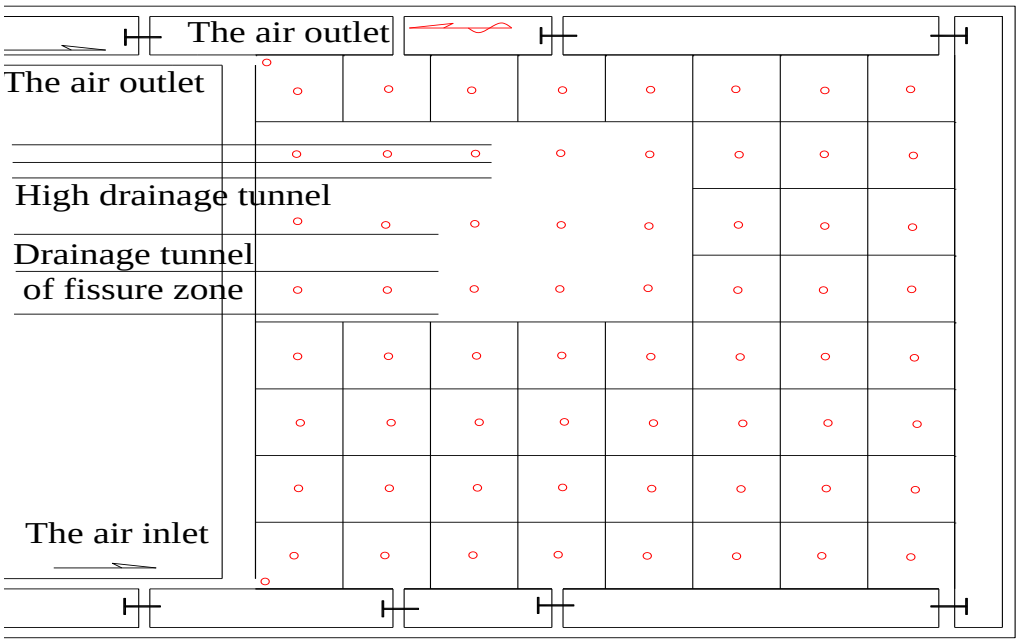

Figure 6.5.7 gas drainage arrangement in the laboratorial simulation model

To be specific, a tail roadway (15m from the mining seam) is drilled, and three high-position gas drainage tunnels are selected and evenly situated 20m from the working face floor, and 40m from the side of air outlet.

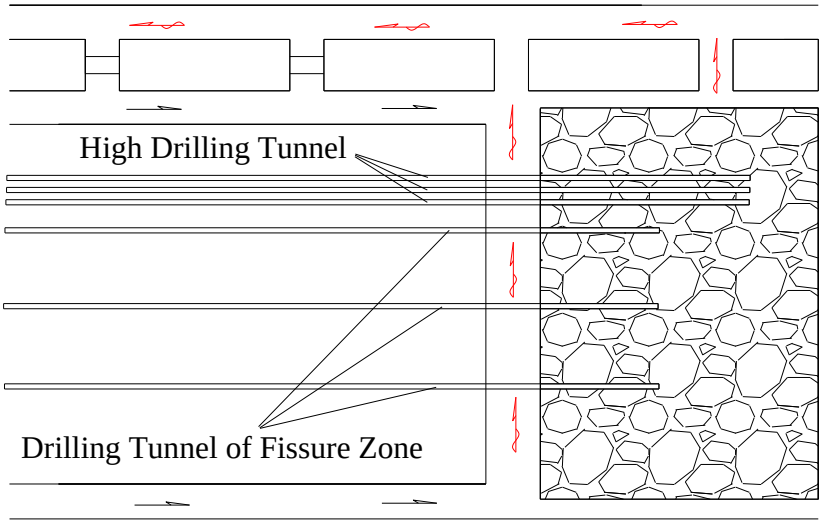

Figure 6.5.8 The gas drainage arrangement in goaf

Besides, another three special gas drainage tunnels in fissure zone are selected and vertically placed in the zone of 24m - 32m from the working face floor, horizontally in the same level with 45m among each other.

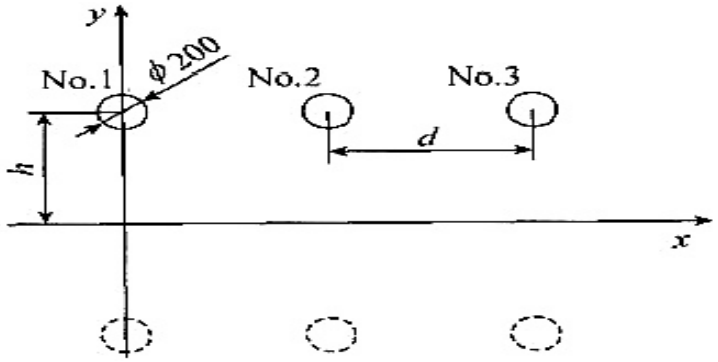

Figure 6.5.9 Kilometer gas drainage borehole and their mirror hole

The arrangement of the gas drainage hole (Φ=200mm) is settled based on field measurements and previous laboratory simulated results, as is shown in Figure 6.5.9.

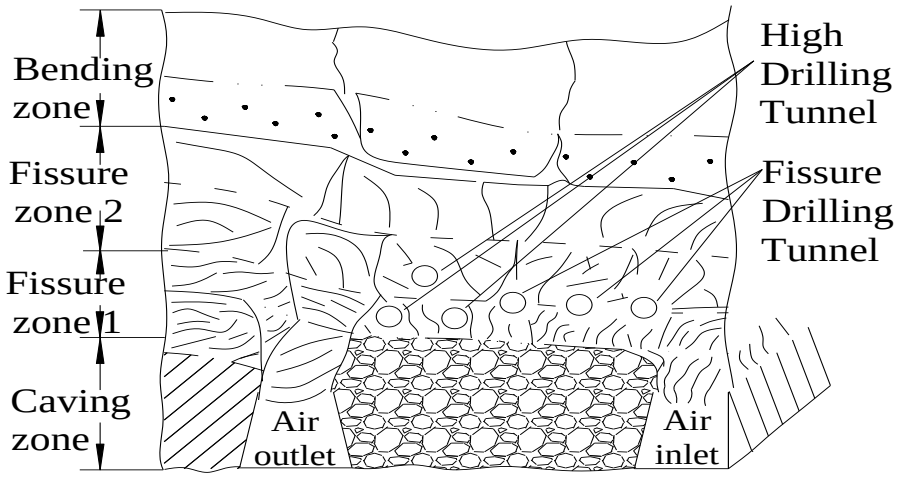

Figure 6.5.10 Section of the gas drainage boreholes layout and arrangement

The gas drainage arrangement in the adjacent coal seam, rock stratums and goaf of Shaqu coal mine can be seen in Figure 6.5.10 and Figure 6.5.11.

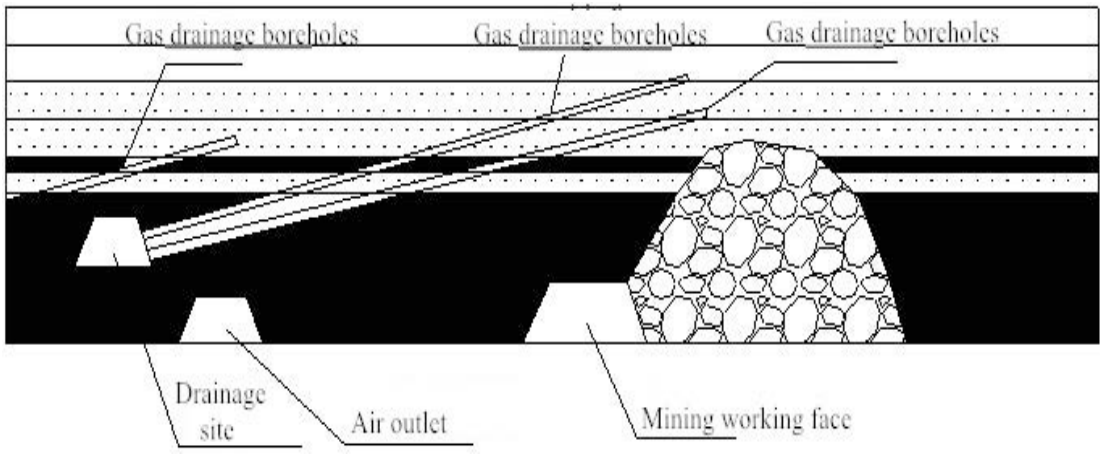

Figure 6.5.11 Section of the gas drainage boreholes layout and arrangement

6.6 Field measured results of gas concentration and drainage rate

In order to verify actual gas drainage effects, a series of measure points are selected in the air outlet, upper corner and tail tunnel respectively. The results reveal that the average gas concentrations in each point of U+L-type ventilation system are lower than that of U-type ventilation system while the gas drainage rate of U+L-type ventilation system is higher than that of U-type ventilation system

6.6.1 U-type ventilation system drainage rate

It can be obviously seen from Figure 6.6.1 that the average gas concentration of tail airway, the upper corner and the return airway are 1.88%, 0.85% and 0.61% respectively in the U-type ventilation system of Shaqu coal mine.

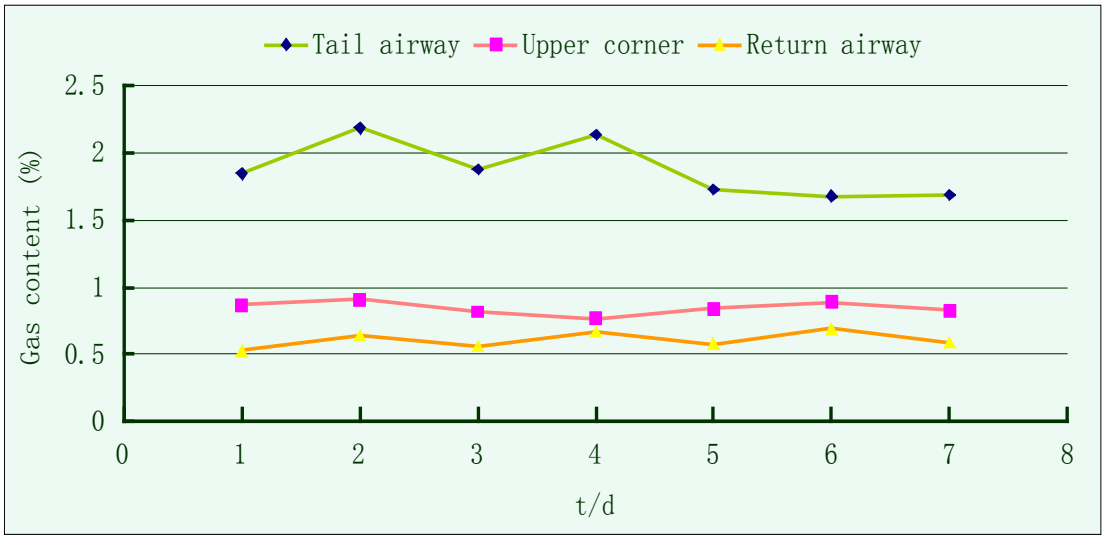

Figure 6.6.1 Measured result of gas content in different tunnels in U-type ventilation system

As is shown in Table 6.6.1 the average gas concentration of the upper corner is around 0.85% and the average gas drainage rate of high drainage tunnels is around 39.6 $m^3 \cdot min^{-1}$ in the U-type ventilation system of Shaqu coal mine.

Table 6.6.1 Data of gas concentration in the coal seam #4 of the U-type ventilation system

Observation date	Gas concentration of the upper corner (%)	Range of gas drainage concentration	Gas drainage concentration of the high drilling ($m^3 \cdot min^{-1}$)
03-10-2012	0.79	43-44	38.9
21-11-2012	0.89	44-45	39.5
27-12-2012	0.87	42-43	40.4
18-04-2013	0.77	44-45	40.1
19-05-2013	0.87	42-44	39.9
22-06-2013	0.91	41-44	38.8

6.6.2 U+L-type ventilation system drainage rate

It can be clearly seen from Figure 6.6.2 that the average gas concentration of the tail airway, upper corner and return airway decrease to 1.69%, 0.75% and 0.55% from 1.88%, 0.85% and 0.61% respectively in U+L-type ventilation system of Shaqu coal mine.

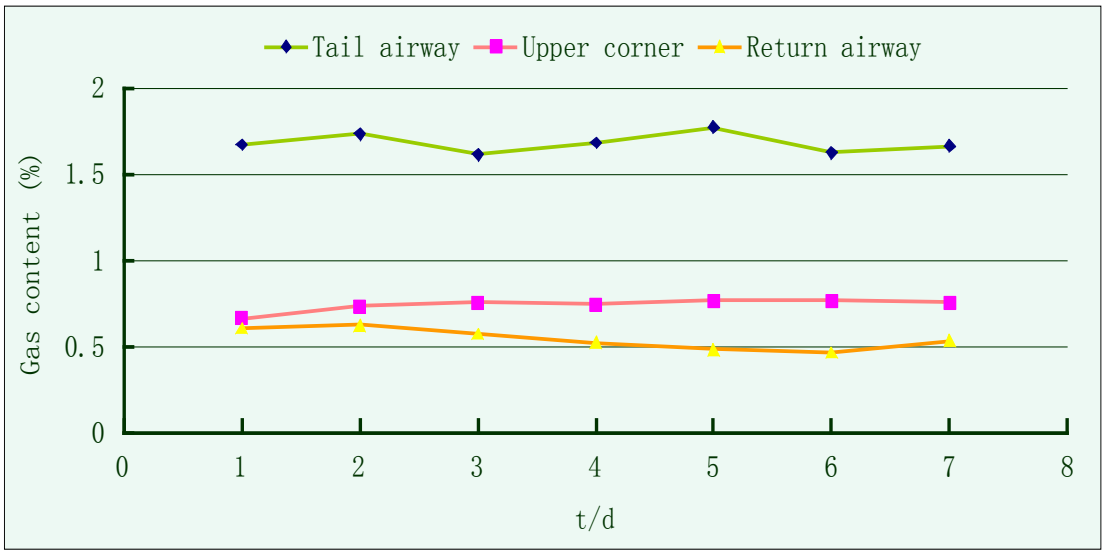

Figure 6.6.2 Measured results of gas content in different gas drainage borehole

Figure 6.6.2 also demonstrates that more gas flows into special gas drainage tunnels and as a consequence the gas concentration of upper corner in the working field moderately decreases from a hazardous situation.

Table 6.6.2 Data of gas concentration in coal seam #4 of U+L-type ventilation system

Observation date	Gas concentration of the upper corner (%)	Range of gas drainage concentration	Gas drainage concentration of the high drilling ($m^3 \cdot min^{-1}$)
05-10-2013	0.68	58-89	50.1
22-11-2013	0.79	55-84	49.2
28-12-2013	0.78	59-86	47.4
19-04-2014	0.75	56-81	48.0
18-05-2014	0.73	60-82	47.7

23-06-2014	0.78	65-87	50.9

Table 6.6.2 shows the average gas concentration of the upper corner decreases to 0.75% from 0.85% while the average gas drainage rate of high drainage tunnel increases to approximately 48.9 $m^3 \cdot min^{-1}$ from 39.6 $m^3 \cdot min^{-1}$ in U+L-type ventilation system of Shaqu coal mine.

7 Conclusion and future work

7.1 Conclusion

Mine gas disaster have created severe difficulties for the mining industry all over the world, leading to expensive expenditures and intensity research efforts, and determined attempts to enhance the various ventilation and gas drainage techniques. Meanwhile, gas drainage and usage research is thriving in the last decade, and it will continue to be a growing dominant industry over the coming decades in many mining countries and areas.

The objective of this dissertation was to analysis, discuss and discover a multiple and effective strategy for the purpose of preventing, controlling and reducing gas-related disasters. First of all, the basic theories of gas emission, distribution and migration are discussed. Then a numerical prediction model based on a specific coal mine is established to predict its gas emission volume. The next two parts offer the establishment of the numerical simulation model (CFD) and laboratorial experimental model for the purpose of discussing the gas distribution and migration rule and determining the most effective gas drainage zones in the working face and goaf. The last part of this dissertation provides a field study (25 gas measuring points are selected and measured in both of production shift and maintenance shift.) in order to obtain the gas distribution and migration rule in the working face and goaf. Some conclusions can be made through the studies mentioned above.

(1) A numerical gas emission prediction model used to establish the Shaqu coal mine gas emission of working face 14205. Main gas emission sources (gas of coal seam and wall, gas of fallen or mined coal and goaf gas) are determined and predicted. The result shows that the prediction measurement of gas emission in the working face is quite close to the actual measurement and owns high accuracy (less than 10%). Taking into account the uneven factor of gas emission in the working face always reaches 20%, it is considered that the prediction accuracy can totally meet the design and production requirements, and also indicates that the method is fully credible and feasible for the prediction of gas emission in the working face of Shaqu coal mine.

(2) A numerical simulation model for the purpose of discussing the gas distribution and

migration rule and determining the most effective gas drainage zones in the working face and goaf. The numerical simulation experiments are performed based on U-type ventilation system and U+L-type ventilation system respectively. The comparison between U-type ventilation system and U+L-type ventilation system shows that goaf gas distribution rules are similarly applied under both systems. However, in the case of the U-type ventilation system, a large amount of high concentrated gas constantly flows into the upper corner due to the air leakage of goaf, different pressures between the air inlet and outlet. By contrast, U+L-type ventilation system is made up of two air inlets and one outlet, which accelerates the gas emission, diffusion and flow, balances the air pressure of the upper corner, restrains the gas discharge of the upper corner, and compels the high concentrated gas to flow into the air outlet. Therefore, the gas content in local area is diluted and lowered.

Obviously, the over-limit problem of gas concentration in the working face can be effectively resolved by changing the ventilation system from U-type to U+L-type. Specifically, the gas concentration of the upper corner decrease from 10% to around 4%. It can be concluded that the most effective gas extraction spot constantly varies with the area where mining activities are performed. It is mainly located in the area of 40m-250m from the working face (along the horizontal mining direction, coal and rock separation area), 30m-40m from the floor (along the vertically direction, distressed and fracture zone), and approximately 60m-170m from the side of air outlet.

(3) A U+L-type similarity ventilation system model is built in a special simulation laboratory. Based on similarity criteria, the model has a scale ratio of l: 50 of full-mechanized mining ventilation system. The distributing characteristics of trace gas and its distribution and migration rule are gained from the laboratorial simulation experiments (under both U-type ventilation system and U+L-type ventilation system). The laboratorial simulation experimental results are similar to the numerical simulation results. It indicate that the over-limit of gas in the working face and goaf area of the simulation model is effectively controlled by increasing the velocity of the air inlet and changing the ventilation system from U-type to U+L-type. It also demonstrates that that the most effective gas extraction spot constantly varies with the area where mining activities are performed. It mainly locates in coal and rock separation area of 27cm-243cm (between working face and deep goaf), 28cm-42cm (between the working face floor to the roof) and 78cm-182cm (between air

inlet and air outlet).

(4) In order to verify the validity of establishment of the simulation models (both numerical one and laboratory one) and the reliability of the simulation experiments, the results between numerical experiments and laboratory experiments are compared, discussed and concluded.

Numerical simulation experimental comparison results between U-type ventilation system and U+L-type ventilation systems indicate that goaf gas distribution rules are similarly applied under both systems. Moreover, the over-limit of gas content in the working face, upper corner and goaf is effectively resolved by changing the ventilation system from U-type to U+L-type. Particularly, the gas concentration of the upper corner decrease from 10% to around 4%. On the other hand, the same similar results can be found in the laboratory simulation experiments. The gas concentration of the upper corner has declined from 6.39% to 4.24%.

Under the circumstances of numerical simulation experiments, the results demonstrate that the most effective gas extraction spot constantly varies with the area where mining activities are performed. It is mainly located in the area of 40m-250m (between working face and deep goaf), 30m-40m from the working face floor (along the vertically direction, distressed and fracture zone), and approximately 60m-170m (between air inlet and air outlet). On the other hand, laboratorial simulation experiments indicate the similar conclusion that the most effective gas extraction spot constantly varies with the area where mining activities are performed, and it mainly locates in coal and rock separation area of 27cm-243cm (between working face and deep goaf), 28cm-42cm (between the working face floor to the roof) and 78cm-182cm (between air inlet and air outlet). This indicates that the similar gas distribution rule and migration law of numerical simulation experiments are found in laboratory simulation experiments.

(5) A field study is conducted in order to obtain the gas distribution and migration rule in the working face and goaf. 25 gas measuring point are selected and measured in both of production shift and maintenance shift. The field measured results are similar with the results of numerical simulation and laboratorial simulation experiments. Moreover, one entire gas drainage system is established based on all obtained results (numerical simulation, laboratorial experiments and field measurement), and the gas drainage rate is measured as well. The field measured results show the average gas drainage rate increase to approximately 48.9 $m^3 \cdot min^{-1}$ (U+L-type ventilation system) from 39.6 $m^3 \cdot min^{-1}$ (U-type ventilation system) while the gas concentration of the special drainage

tunnel, upper corner and air outlet decrease to 1.69%, 0.75% and 0.55% (U+L-type ventilation system) from 1.88%, 0.85% and 0.61% (U-type ventilation system) respectively. These results indicate the layout of the gas drainage boreholes is rational and effective; the gas drainage quantity is reliable. Therefore, it is feasible and reliable to arrange the layout of gas drainage tunnels based on the experimental results of numerical simulations and laboratorial tests.

The experiments provide benefits for Shaqu coal mine because the simulation models can be first adjusted before adjusting the real ventilation system. Then the decision of whether or not to apply it to the real ventilation system in Shaqu coal mine can be made based on the experimental results of the models. It can also provide experimental evidences on the selection of the ventilation system in on-site production and the optimization of the existing ventilation systems in other mines.

7.2 Recommendation for future work

Combining the findings of the literature survey with the research conducted during the course of preparing this dissertation, leads to the following recommendations for future work.

(1) Numerical gas emission prediction method will be increased the accuracy. The error between the prediction data and actual measured data should be lowered below 5%.

(2) Numerical simulation model will be conducted with more actual and complicated boundary conditions. Scale modeling of the goaf environment could lead to fresh insight into the problem that would lead to better modeling in CFD. The inhospitable nature of the goaf prevents direct study, so scale modeling would be the next logical course to take.

(3) The laboratorial simulation model will be refined regularly according to the real mines. For example, the many tunnel sectional areas are the same in the laboratorial simulation model, it should be designed based on all the tunnels as much as possible; many sections of the ventilation model are right-angled and that results in excessive frictional restriction in the tunnels. Therefore, different cross-section of mine tunnels will be simulated and optimized, and arc-shaped section instead of the right-angled one will be used. The experiments of control and prevention of goaf gas and spontaneous combustion will be performed in the near future.

(4) Field studies will be performed continually; more gas measuring points will be selected; the gas concentration of the special drainage tunnel, upper corner and air outlet will be lowered

while gas drainage rate will be increased.

Reference

Agricola, G. (1556). De Re Metallica. Translated from Latin by H.C. Hoover and L.H. Hoover. Modern publication by Dover Pub., Inc., New York (1950).

Alireza Salmachi, Mohammad Reza Bonyadi, Mohammad Sayyafzadeh, Manouchehr Haghighi. Identification of potential locations for well placement in developed coalbed methane reservoirs, International Journal of Coal Geology, Volume 131, 1 September 2014, Pages 250-262

All Mining Fatalities By State U.S. Department of Labor, Mine Safety and Health Administration, 15 January 2007

Andrei D. Polyanin, Alexei I. Zhurov. Exact solutions of non-linear differential-difference equations of a viscous fluid with finite relaxation time. International Journal of Non-Linear Mechanics, Volume 57, December 2013, Pages 116-122

ANSYS. 2010. ANSYS FLUENT Theory Guide. 13.0 edn. Canonsburg, PA: SAS IP, Inc.

Arif Widiatmojo, Kyuro Sasaki, Nuhindro Priagung Widodo, Yuichi Sugai, Johannes Sinaga, Haris Yusuf. Numerical simulation to evaluate gas diffusion of turbulent flow in mine ventilation system, International Journal of Mining Science and Technology, Volume 23, Issue 3, May 2013, Pages 349-355

Arnab Chatterjee, Lijun Zhang, Xiaohua Xia. Optimization of mine ventilation fan speeds according to ventilation on demand and time of use tariff, Applied Energy, Volume 146, 15 May 2015, Pages 65-73

Aziz, N I, 2006. Rank of coal seam, Coal Mining Science and Technology Website, University of Wollongong [online]. Available from: http://www.uow.edu.au/eng/outburst/html/rank.html [Accessed: May 2010].

Aziz, N, Srinivasa, R B and Baafi, E, 1993. Application of computational fluid dynamics codes to develop effective gas/dust control measures in underground coal mines, The Australian Coal Journal, 42:19-27.

Bartłomiej Jura, Jacek Skiba, Krystian Wierzbinski. Applicability of surface directional wells for upper Silesia Basin coal seams' drainage ahead of mining, International Journal of Mining Science and Technology, Volume 24, Issue 3, May 2014, Pages 353-362

Bertard, C, Bruyet, B and Gunther, J, 1970. Determination of desorbable gas concentration of coal (direct method), International Journal of Rock Mechanical and Mining Sciences and Geomechanics, Volume 7, Issue 1, pp 43-65.

Boleslav Taraba, Zdeněk Michalec. Effect of longwall face advance rate on spontaneous heating process in the gob area - CFD modelling, Fuel, Volume 90, Issue 8, August 2011, Pages 2790-2797

B. Plante, B. Bussière, M. Benzaazoua. Lab to field scale effects on contaminated neutral drainage prediction from the Tio mine waste rocks, Journal of Geochemical Exploration, Volume 137, February 2014, Pages 37-47

Brune, J., & Sapko, M. 2012. A Modeling Study on Longwall Tailgate Ventilation. In: Calizaya, F, & Nelson, Michael (eds), 14th United States/North American Mine Ventilation Symposium. Salt Lake City: University of Utah, Dept. of Mining Engineering.

CEC (1988). Investigation of firedamp and its emissions in coal seams. Final Report on ECSC. Contract 7220-AC/819, Report EUR 1147, Commission of the European Communities.

Charlee Boger, James S. Marshall, Raymond C. Pilcher. Chapter 18 - Worldwide Coal Mine Methane and Coalbed Methane Activities. Coal Bed Methane, 2014, Pages 351-407

CHENG Jiatang, ZHANG Hui, XU Xiaokun. Combination Forecast of Gas Emission in Coal Mine Based on Evidence Theory, Safety Science Journal, 2012, 22(1): 106-111.

"China coal mine gas explosion kills 19 miners and traps dozens". The Guardian (London). 2012-08-30. Retrieved 2012-09-03

China sees coal mine deaths fall, but outlook grim 11 January 2007, Reuters

China takes steps to halt coal mine disasters Embassy of the People's Republic of China in the U.S.A., 02 February 2005

Chu Ting-xiang, Zhou Shi-xuan, Xu Yong-liang, Zhao Zhi-jun. Research on the Coupling Effects Between Stereo Gas Extraction and Coal Spontaneous Combustion. Procedia Engineering, Volume 26, 2011, Pages 218-227

Claus Kohfahl, Torsten Graupner, Christian Fetzer, Asaf Pekdeger. The impact of cemented layers and hardpans on oxygen diffusivity in mining waste heaps, A field study of the Halsbrücke lead–zinc mine tailings (Germany), Science of The Total Environment, Volume 408, Issue

23, 1 November 2010, Pages 5932-5939

Close, J C and Erwin, T M, 1989. Significance and determination of gas content data as related to coalbed methane reservoir evaluation and production implications, in Proceedings of the 1989 International Coalbed Methane Symposium, University of Alabama, Tuscaloosa, 17-20 April, pp 37-55.

Coal Fatalities By State U.S. Department of Labor, Mine Safety and Health Administration, 15 January 2007

Coal mining: Most deadly job in China Zhao Xiaohui & Jiang Xueli, Xinhua News Agency, Updated: 2004-11-13 15:01

Corin, John (1992). Levant, A Champion Cornish Mine. The Trevithick Society. pp. 40-44. ISBN 0-904040-37-2.

Creedy, D P. and Clarke, R D C, 1992. Minimizing firedamp risks on high production coalfaces: a computational modeling approach, in Proceedings International Symposium: Safety, Hygiene and Health in Mining, pp 192-203 (The Institution of Mining Engineers).

Creedy, D.P. and Kershaw S. (1988). Firedamp prediction - a pocket calculator solution. The Mining Engineer. Inst of Mining Engineers, Vol. 147, No. 317, Feb., pp.377-379.

Creedy, D.P. & Phillips, H.R. (1997, July). Methane Layering in Bord−and−Pillar Workings. Safety in Mines. Research Advisory Committee (SIMRAC) Final Report. Project COL 409. Johannesburg, South Africa: Safety in Mines Research Advisory Committee.

Currie, J A N, 1994. Measurement and control of diesel particulate emissions in underground coal mines, The Mining Engineer, 154(396):58-62.

Danell, R E, Saghafi, A, Williams, R J and Wood, J, 2003. Reproducibility of gas content measurements using the fast desorption technique, Australian Coal Association Research Program, Project Report C8024.

Darshit Parmar, Teresa Wu, Jennifer Blackhurst. MMR: An algorithm for clustering categorical data using Rough Set Theory, Data & Knowledge Engineering, Volume 63, Issue 3, December 2007, Pages 879-893

David A. Kirchgessner, Stephen D. Piccot, J.David Winkler. Estimate of global methane emissions from coal mines, Chemosphere, Volume 26, Issues 1–4, January–February 1993, Pages 453-472

De la Vergne, Jack, 2003. Hard Rock Miner's Handbook. Tempe/North Bay: McIntosh Engineering. pp. 157. ISBN 0-968006-1-6.

Diamond, W P, Murrie, G W and McCulloch, C M, 1976. Methane gas content of the Mary Lee group of coalbeds, Jefferson, Tuscaloosa, and Walker Counties, Ala., United States Department of the Interior, Bureau of Mines Report of Investigations RI8117, 13p. [online]. Available from: http://www.cdc.gov/niosh/mining/pubs/pdfs/ri8117.pdf [Accessed: November 2010].

Diamond, W P and Schatzel, S J, 1998. Measuring the gas content of coal: a review, International Journal of Coal Geology, Volume 35, pp 311-331.

Diamond, W.P., Schatzel, S.J., & Garcia, F. 1999. Characterization of gas flow in longwall gobs: Pittsburgh Coalbed, PA. Pages 233-244 of: Proceedings of the International Coalbed Methane Symposium.

Diamond, W.P., Ulery, J.P., & Kravits, S.J. 1992. Determining the Source of Longwall Gob Gas: Lower Kittanning Coalbed, Carnbria County, PA. NIOSH, 21.

Dingqi Li, Yuanping Cheng, Lei Wang, Haifeng Wang, Liang Wang, Hongxing Zhou. Prediction method for risks of coal and gas outbursts based on spatial chaos theory using gas desorption index of drill cuttings, Mining Science and Technology (China), Volume 21, Issue 3, May 2011, Pages 439-443

Dziurzynski, W., & Wasilewski, S. 2012. Model and experimental studies in the longwall goaf under methane inflow conditions. Pages 111-120 of: Calizaya, F, & Nelson, M. (eds), 14th United States/North American Mine Ventilation Symposium. Salt Lake City: University of Utah.

Esterhuizen, G.S., & Karacan C.Ö., 2005. Development of Numerical Models to Investigate Permeability Changes and Gas Emission around Longwall Mining Panel. In: Alaska Rocks 2005, The 40th US Symposium on Rock Mechanics.

Esterhuizen, G. S.; Karacan, C. A methodology for determining gob permeability distributions and its application to reservoir modeling of coal mine longwalls. In 2007 SME Annual Meeting, Denver, CO; 2007.

E.K. Stefopoulos, D.G. Damigos. Design of emergency ventilation system for an underground storage facility, Tunneling and Underground Space Technology, Volume 22, Issue 3, May

2007, Pages 293-302

Evangelos Gidarakos, Kalliopi Anastasiadou, Emmanuil Koumantakis, Stappas Nikolaos. Investigative studies for the use of an inactive asbestos mine as a disposal site for asbestos wastes, Journal of Hazardous Materials, Volume 153, Issue 3, 30 May 2008, Pages 955-965

Faiz, M M, 1993. Thermal history and geological controls on the distribution of coal seam gases in the southern Sydney basin, Australia, PhD Thesis, Department of Geology, University of Wollongong.

Fletcher, C A J, Jancar, T, Matthews, B, Guzman, M M de and Tu, J Y, 1995. Computational simulation for mineral processing, in Proceedings APCOM XXV 1995, pp 361-370 (The Australasian Institute of Mining and Metallurgy: Melbourne).

Forster, I.; Enever, J. R. Hydrogeological response of overburden strata to underground mining, Central Coast, New South Wales; Office of Energy: Sydney, 1992.

F.Talay Akyildiz, Hamid Bellout, K Vajravelu. Exact solutions of nonlinear differential equations arising in third grade fluid flows. International Journal of Non-Linear Mechanics, Volume 39, Issue 10, December 2004, Pages 1571-1578

Galvin, J. M. Surface subsidence mechanisms–theory and practice. Part I - Theory. Coal J (16) 1987, 31-41.

Gang Wang, Weimin Cheng, Jun Xie. Field Test Research on Two-dimensional Gas Concentration and Temperature Distribution in the Goaf of Fully Mechanized Caving Face, Procedia Engineering, Volume 43, 2012, Pages 478-483

Gao Wei, 2011. Optimization of Mine Ventilation System Based on Bionics Algorithm. Procedia Engineering, Volume 26, Pages 1614-1619

Gauti A., Erik H., Magnus E., 2012. Modeling and dynamic simulation of gradual performance deterioration of a crushing circuit - Including time dependence and wear. Minerals Engineering, Volume 33, June, Pages 13-19

G Bruneau, M.R Hudyma, J Hadjigeorgiou, Y Potvin. Influence of faulting on a mine shaft—a case study: part II - Numerical modelling, International Journal of Rock Mechanics and Mining Sciences, Volume 40, Issue 1, January 2003, Pages 113-125

Ginting J. Kusuma, Hideki Shimada, Candra Nugraha, Akihiro Hamanaka, Takashi Sasaoka, Kikuo Matsui, Rudy S. Gautama, Budi Sulistianto. Study on Co-placement of Coal

Combustion Ash-coal Waste Rock for Minimizing Acid Mine Drainage Generation: A Preliminary Result of Field Column Test Experiment, Procedia Earth and Planetary Science, Volume 6, 2013, Pages 251-261

Green, M. S.; Flanegan, K. C.; Gilcrease, P. C. Characterization of a methanogenic consortium enriched from a coalbed methane well in the Powder River Basin, U.S.A. International Journal of Coal Geology 2008, 76, 34-45.

Grubb, J.W. 2008. Preventative Measures for Spontaneous Combustion in Underground Coal Mines. Ph.D. thesis, Colorado School of Mines.

Guang Xu, Edmund C. Joni, Kray D. Luxbacher, Saar A. Ragab, Michael E. Karmis. Remote characterization of ventilation systems using tracer gas and CFD in an underground mine Safety Science, Volume 74, April 2015, Pages 140-149

Guo, H.; Adhikary, D. P.; Craig, M. S. Simulation of mine water inflow and gas emission during longwall mining. Rock Mechanics and Rock Engineering 2008, 42, 25–51.

HAO. Tian-xuan, JIN. Zhi-chao, LI Feng. Optimization of Goaf Gas Drainage Parameters Based on Numerical Simulation Studying Fracture in Overlying Strata, Procedia Engineering, Volume 43, 2012, Pages 269-275

Haoran Zhang, Yaojiang Zhao, Shengrong Xie. Similarity simulation experimental study on gas drainage from goaf in Shaqu Coal Mine. China Coal, Volume 37 (3), August, 2011.

Hartman, H. L, Mutmansky, J.M., Ramani, R.V., & Wang, Y.J. 1997. Mine Ventilation and Air Conditioning. Third edit edn. John Wiley & Sons, Inc.

Heather N. Dougherty, C. Özgen Karacan. A new methane control and prediction software suite for longwall mines, Computers & Geosciences, Volume 37, Issue 9, September 2011, Pages 1490-1500

HE Jun, PAN Jienan, NIE Baisheng. Research on Fractal Prediction of Severity of Gas Emission, China Safety Science Journal, 2006, 16(5): 22–25.

Hinsley, F.B. (1967). The control of atmospheric conditions in mines. 11th Cadman Memorial Lecture. Mining Engineer No. 77, pp 289.

Historical Data on Mine Disasters in the United States U.S. Department of Labor

Hwang C.C., Edwards J.C. The critical ventilation velocity in tunnel fires - a computer simulation, Fire Safety Journal, Volume 40, Issue 3, April 2005, Pages 213-244

"International News | World News - ABC News". abcnews.go.com. Retrieved2014-01-28.

Jana Kandarachevová, Lenka Sedláčková, Lada Hýlová, Jakub Jirásek, Martin Sivek. Lateral development of coalification in the Czech part of the Upper Silesian Coal Basin and its connection with gas deposits, International Journal of Coal Geology, Volume 78, Issue 3, 1 May 2009, Pages 225-232

Javier Fernández, Pablo Marín, Fernando V. Díez, Salvador Ordóñez. Coal mine ventilation air methane combustion in a catalytic reverse flow reactor: Influence of emission humidity Fuel Processing Technology, Volume 133, May 2015, Pages 202-209

Jazbec M., Fletcher D.F., Haynes B.S. Simulation of the ignition of lean methane mixtures using CFD modeling and a reduced chemistry mechanism, Applied Mathematical Modeling, Volume 24, Issues 8-9, July 2000, Pages 689-696

J. Banks, J. Carson, B. Nelson, D. Nicol, 2001. Discrete-Event System Simulation. Prentice Hall. p. 3. ISBN 0-13-088702-1.

Jeenu Kim, Jysoo Lee, Koo-Chul Lee. Nonlinear correction to Darcy's law for a flow through periodic arrays of elliptic cylinders. Physica A: Statistical Mechanics and its Applications, Volume 293, Issues 1-2, 1 April 2001, Pages 13-20

Jing Guo-xun, Xu Sheng-ming, Heng Xian-wei, Li Chuang-qi. Research on the Prediction of Gas Emission Quantity in Coal Mine Based on Grey System and Linear Regression for One Element, Procedia Engineering, Volume 26, 2011, Pages 1585-1590

Joaquim A. Macedo-Sousa, Almut Gerhardt, Christopher M.A. Brett, António J.A. Nogueira, Amadeu M.V.M. Soares. Behavioural responses of indigenous benthic invertebrates (Echinogammarus meridionalis, Hydropsyche pellucidula andChoroterpes picteti) to a pulse of Acid Mine Drainage: A laboratorial study, Environmental Pollution, Volume 156, Issue 3, December 2008, Pages 966-973

Johanna Nyquist, Maria Greger. A field study of constructed wetlands for preventing and treating acid mine drainage, Ecological Engineering, Volume 35, Issue 5, May 2009, Pages 630-642

Joseph H. S., Amy M. Cummings. Safety in the mining industry and the unfinished legacy of mining accidents: Safety levers and defense-in-depth for addressing mining hazards, Safety Science, Volume 49, Issue 6, July 2011, Pages 764–777

Jundika C. Kurnia, Agus P. Sasmito, Wai Yap Wong, Arun S. Mujumdar. Prediction and

innovative control strategies for oxygen and hazardous gases from diesel emission in underground mines. Science of The Total Environment, Volume 481, 15 May 2014, Pages 317-334

J.W. Molson, O. Fala, M. Aubertin, B. Bussière. Numerical simulations of pyrite oxidation and acid mine drainage in unsaturated waste rock piles, Journal of Contaminant Hydrology, Volume 78, Issue 4, August 2005, Pages 343-371

Kapp, W. A.; Williams, R. C. Extraction of coal in the Sydney Basin from beneath large bodies of water. In Proceedings of the Aust IMM Conference. Newcastle; 1972; pp. 77-88.

Karacan C. Özgen, (2007). Modeling and prediction of ventilation methane emissions of U.S. longwall mines using supervised artificial neural networks. International Journal of Coal Geology, doi:10.1016/j.coal.2007.09.003.

Karacan C. Özgen. 2009a. Degasification System Selection for US Longwall Mines Using an Expert Classification System. Computers & Geosciences, 35(3), 515-526.

Karacan C. Özgen. 2009b. Reconciling Longwall Gob Gas Reservoirs and Venthole Production Performances Using Multiple Rate Drawdown Well Test Analysis. International Journal of Coal Geology, 80(3-4), 181-195.

Karacan C Özgen., E Okandan. Assessment of energetic heterogeneity of coals for gas adsorption and its effect on mixture predictions for coalbed methane studies, Fuel, Volume 79, Issue 15, December 2000, Pages 1963-1974

Karacan C. Özgen, Esterhuizen G.S., Schatzel S.J., Diamond W.P. Reservoir simulation-based modeling for characterizing longwall methane emissions and gob gas venthole production, International Journal of Coal Geology, Volume 71, Issues 2-3, 2 July 2007, Pages 225-245

Karacan C. Özgen, Felicia A. Ruiz, Michael Cotè, Sally Phipps. Coal mine methane: A review of capture and utilization practices with benefits to mining safety and to greenhouse gas reduction, International Journal of Coal Geology, Volume 86, Issues 2-3, 1 May 2011, Pages 121-156

Karacan C. Özgen, Ricardo A. Olea, Gerrit Goodman. Geostatistical modeling of the gas emission zone and its in-place gas content for Pittsburgh-seam mines using sequential Gaussian simulation. International Journal of Coal Geology, Volumes 90-91, 1 February 2012, Pages 50-71

Kawabata, Tai, "Film mines rich seams of history", Japan Times, 14 August 2011, p. 8.

Kee, R.J., Coltrin, Michael E., & Glarborg, Peter. 2003. Chemically Reacting Flow: Theory and Practice. Hoboken, New Jersey: John Wiley & Sons, Inc.

Kim, A G, 1977. Estimating methane content of bituminous coalbeds from adsorption data, United States Department of the Interior, Bureau of Mines Report of Investigations RI8245.

Kissell, F. N. Handbook for methane control in mining; Dept. of Health and Human Services, Public Health Service, Centers for Disease Control and Prevention, National Institute for Occupational Safety and Health, Pittsburgh Research Laboratory: Pittsburgh, PA, 2006.

"14 killed in Chinese coal mine blast". The Independent (London). 2012-09-03. Retrieved 2012-09-03.

Lafraniere, Sharon (2009-04-11). "Graft in China Covers Up Toll of Coal Mines". The New York Times. Retrieved 2010-05-12.

Lama, R D and Bartosiewicz, H, 1982. Determination of gas content of coal seams, in Proceedings of the Symposium on Seam Gas Drainage with Particular Reference to the Working Seam, (ed: A J Hargraves), Australasian Institute of Mining and Metallurgy - I llawarra Branch, University of Wollongong, Wollongong, Australia, 11-14 May, pp 36-52.

Lei Wang, Yuan-Ping Cheng. Drainage and utilization of Chinese coal mine methane with a coal–methane co-exploitation model: Analysis and projections, Resources Policy, Volume 37, Issue 3, September 2012, Pages 315-321

Leszek (Les) W. Lunarzewski. Gas emission prediction and recovery in underground coal mines, International Journal of Coal Geology, Volume 35, Issues 1-4, February 1998, Pages 117-145

Levine, J. R. Coalification: the evolution of coal as source rock and reservoir rock for oil and gas. Hydrocarbons from coal: AAPG Studies in Geology 1993, 38, 39-77.

Li Dingqi, Cheng Yuanping, Wang Lei, Wang Haifeng. Wang Liang. Zhou Hongxing. Prediction method for risks of coal and gas outbursts based on spatial chaos theory using gas desorption index of drill cuttings, Mining Science and Technology (China), 21 (2011) 439-443

Liming Yuan, Alex C. Smith. Numerical study on effects of coal properties on spontaneous heating in longwall gob areas. Fuel, Volume 87, Issues 15-16, November 2008, Pages 3409-3419

Liu Ying-ke, Zhou Fu-bao, Liu Lang, Liu Chun, Hu Shen-yong. An experimental and numerical investigation on the deformation of overlying coal seams above double-seam extraction for controlling coal mine methane emissions, International Journal of Coal Geology, Volume 87, Issue 2, 1 August 2011, Pages 139-149

Lolon, S. 2008. Computational Fluid Dynamics Simulation Study on Hot Spot Location in a Longwall Mine Gob. Ph.D. thesis, University of Utah.

L. Preziosi, A. Farina. On Darcy's law for growing porous media. International Journal of Non-Linear Mechanics, Volume 37, Issue 3, April 2002, Pages 485-491

Lunarzewski, L. (1998). Gas emission prediction and recovery in underground coal mines. International Journal of Coal Geology 35, pp. 117-145.

Malcolm J. McPherson, of Blacksburg, VA, passed away on Nov., 12, 2008 at the age of 71.

Manoj Khanal, Deepak Adhikary, Rao Balusu. Numerical analysis and geotechnical assessment of mine scale model, International Journal of Mining Science and Technology, Volume 22, Issue 5, September 2012, Pages 693-698

María B. Díaz Aguado, C. González Nicieza. Control and prevention of gas outbursts in coal mines, Riosa-Olloniego coalfield, International Journal of Coal Geology, Volume 69 (2007), Pages 253–266

Masayuki Itoh, Shigeto Sudo, Shizuka Mori, Hiroshi Saito, Takahiro Yoshida, Yutaka Shiratori, Shinobu Suga, Nanako Yoshikawa, Yasufumi Suzue, Hiroyuki Mizukami, Toshiyuki Mochida, Kazuyuki Yagi. Mitigation of methane emissions from paddy fields by prolonging midseason drainage, Agriculture, Ecosystems & Environment, Volume 141, Issues 3-4, May 2011, Pages 359-372

Mavor, M J, Close, J C and Pratt, T J, 1992. Review of recent US coalbed natural gas reservoir research, in Proceedings of the Symposium on Coalbed Methane Research and Development in Australia, Coalseam Gas Research Institute - James Cook University, Townsville, November 19-21, Volume 2, pp 109-152.

McAteer, Davitt (December 6, 2007). Monongah: The Tragic Story of the 1907 Monongah Mine Disaster, the Worst Industrial Accident in US History. West Virginia University Press. p. 332. ISBN 1-933202-29-7.

McCulloch, C M, Levine, J R, Kissell, F N and Deul, M, 1975. Measuring the methane content of

bituminous coalbeds, United States Department of the Interior, Bureau of Mines Report of Investigations RI8043, 25p.

Mirosław Wierzbicki, Mariusz Młynarczuk. Structural aspects of gas and dolomite outburst in Rudna copper mine, Poland, International Journal of Rock Mechanics and Mining Sciences Volume 57, January 2013, Pages 113-118

M. Jafari, Z. Mansoori, M. Saffar Avval, G. Ahmadi. The effects of wall roughness on erosion rate in gas–solid turbulent annular pipe flow. Powder Technology, Volume 271, February 2015, Pages 248-254

M.J. McPherson. Chapter 1: Mine Ventilation - An Overview. Background to subsurface ventilation and environmental engineering, "1993

M Ohba, I Lun. Overview of natural cross-ventilation studies and the latest simulation design tools used in building ventilation-related research. Advances in Building Energy Research, 2010

Moore, T. A. Coalbed methane: A review. International Journal of Coal Geology 2012, 101, 36–81.

MSHA - Statistics - Fatal Charts http://www.msha.gov/stats/charts/chartshome.htm (accessed Nov 14, 2012).

M.T. Parra, J.M. Villafruela, F. Castro, C. Méndez. Numerical and experimental analysis of different ventilation systems in deep mines, Building and Environment, Volume 41, Issue 2, February 2006, Pages 87-93

Nicholas P. Wallerstein, Carlos V. Alonso, Sean J. Bennett, Colin R. Thorne, 2001. Earth Surface Processes and Landforms, Volume 26, Issue 12,pages 1265-1283, November

Ni Wenyao, Liu Baokuan, Gai Wenmei. The Research on Integrated Visual Information Management System of the Mine Ventilation and Safety, Procedia Engineering, Volume 26, 2011, Pages 2070-2074

Noack, K., 1998. Control of gas emissions in underground coal mines. International Journal of Coal Geology 35, 57 – 82.

Noim Uddin, Mascha Blommerde, Ros Taplin, David Laurence. Sustainable development outcomes of coal mine methane clean development mechanism Projects in China, Renewable and Sustainable Energy Reviews, Volume 45, May 2015, Pages 1-9

N. Szlązak, D. Obracaj, J. Swolkień. Methane drainage from roof strata using an

overlying drainage gallery, International Journal of Coal Geology, Volume 136, 15 December 2014, Pages 99-115

N. P. Widodo, K. Sasaki, R. S. Gautama & Risono, 2008. Mine ventilation measurements with tracer gas method and evaluations of turbulent diffusion coefficient. International Journal of Mining, Reclamation and Environment, Volume 22, Issue 1, Pages 60-69

N. Szlązak, D. Obracaj, J. Swolkień. Methane drainage from roof strata using an overlying drainage gallery, International Journal of Coal Geology, Volume 136, 15 December 2014, Pages 99-115

Ramurthy, M.K., Young, G.B.C., Daves, S.B., & Witsell, F. 2003. Case History: Reservoir Analysis of the Fruitland Coals Results in Optimizing Coalbed Methane Completions in the Tiffany Area of the San Juan Basin. Pages 1-9 of: SPE Annual Technical Conference and Exhibition. Denver, Co: Society of Petroleum Engineers.

Reid, P.; McNally, G. H.; Ward, C. R. Effects of mining on the permeability of rock strata in the Southern Coalfield. In Proceedings of the Symposium on Geology in Longwall Mining; 1996; pp. 273–280.

René Lefebvre, Daryl Hockley, Jason Smolensky, Ann Lamontagne. Multiphase transfer processes in waste rock piles producing acid mine drainage: 2. Applications of numerical simulation, Journal of Contaminant Hydrology, Volume 52, Issues 1-4, November 2001, Pages 165-186

Ren, T. X.; Balusu, R. CFD Modelling of Goaf Gas Migration to Improve the Control of Spontaneous Combustion in Longwalls 2005.

Ren, T. X.; Edwards, J. S. Three-dimensional computational fluid dynamics modeling of methane flow through permeable strata around a longwall face. Mining Technology 2000, 109, 41-48.

Rice, D. Composition and Origins of Coalbed Gas: Chapter 7. 1993, 180, 159-184.R. Sander, L.D. Connell. Methodology for the economic assessment of enhanced coal mine methane drainage (ECMM) as a fugitive emissions reduction strategy. International Journal of Greenhouse Gas Control, Volume 8, May 2012, Pages 34-44

Romeo M. Flores. Chapter 4 - Coalification, Gasification, and Gas Storage, Coal and Coalbed Gas, 2014, Pages 167-233

R. Sander, L.D. Connell. Methodology for the economic assessment of enhanced coal mine

methane drainage (ECMM) as a fugitive emissions reduction strategy. International Journal of Greenhouse Gas Control, Volume 8, May 2012, Pages 34-44

R. Sander, L.D. Connell. A probabilistic assessment of enhanced coal mine methane drainage (ECMM) as a fugitive emission reduction strategy for open cut coal mines, International Journal of Coal Geology, Volume 131, 1 September 2014, Pages 288-303

Russell Packham, Luke Connell, Yildiray Cinar, Roy Moreby. Observations from an enhanced gas recovery field trial for coal mine gas management. International Journal of Coal Geology, Volume 100, 1 October 2012, Pages 82-92

Russell Packham, Yildiray Cinar, Roy Moreby. Simulation of an enhanced gas recovery field trial for coal mine gas management. International Journal of Coal Geology, Volume 85, Issues 3–4, 1 March 2011, Pages 247-256

Saghafi, A, Roberts, D, Fry, R, Quintanar, A, Day, S, Lange, T, Hoarau, P, Dokumcu, C and Carras, J, 2008. Evaluating a tier 3 method for estimating fugitive emissions from open cut coal mining, Australian Coal Association Research Program, Project Report C15076.

Saghafi, A, Williams, D J and Battino, S, 1998. Accuracy of measurement of gas content of coal using rapid crushing techniques [online], in Proceedings of the 1st Australasian Coal Operators' Conference COAL98, University of Wollongong, 18-20 February, pp 551-559.

Sanna Ala-Mantila, Jukka Heinonen, Seppo Junnila. Relationship between urbanization, direct and indirect greenhouse gas emissions, and expenditures: A multivariate analysis Ecological Economics, Volume 104, August 2014, Pages 129-139

Schatzel, J and Garcia, F, 1999. Apparatus for measuring the gas content of coal or rock core samples [online], National Institute for Occupational Safety and Health, NIOSH Technology News No.478. Available from: http://www.cdc.gov/niosh/mining//pubs/pdfs/tn478.pdf [Accessed: November 2008].

Schatzel, S.J., Krog, R.B., Garcia, F., Marshall, J.K., & Trackemas, J. 2006. Prediction of longwall methane emissions and the associated consequences of increasing longwall face lengths: a case study in the Pittsburgh Coalbed. Pages 375-382 of: Proceedings of 11th US/North American Mine Ventilation Symposium.

Şenel, İ. G.; Gürüz, A. G.; Yücel, H.; Kandas, A. W.; Sarofim, A. F. Characterization of Pore

Structure of Turkish Coals. Energy Fuels 2001, 15, 331-338.

Shao Hao, Jiang Shuguang, Wang Lanyun, Wu Zhengyan. Bulking factor of the strata overlying the gob and a three-dimensional numerical simulation of the air leakage flow field. Mining Science and Technology (China), Volume 21, Issue 2, March 2011, Pages 261-266

Shen Yun, Wang Hai-ning, 2011. Study and Application on Simulation and Optimization System for the Mine Ventilation Network. Procedia Engineering, Volume 26, Pages 236-242

Shi Shiliang, Song Yi, He Liwen, et al. Research on determination of chaotic characteristics of gas gush based on time series in excavation working face of coal mine, Journal of China Coal Society, 2006, 31(6): 58–62.

"Sichuan coal mine blast death toll rises to 43". Xinhuanet news. 2012-09-01. Retrieved 2012-09-03.

Singh, M.; Kendorsky, F. Strata disturbance prediction for mining beneath surface water and waste impoundments Proc 1st conference on ground control in mining, Morgantown, 2729 July 1981, P7689. Publ Morgantown: West Virginia University, 1981. International Journal of Rock Mechanics and Mining Sciences & Geomechanics Abstracts International Journal of Rock Mechanics and Mining Sciences & Geomechanics Abstracts 1983, 20, A13-A13.

Society of American Archivists, USA, 1999

Sokolowski, J.A., Banks, C.M., 2009. Principles of Modeling and Simulation. Hoboken, NJ: Wiley. p. 6. ISBN 978-0-470-28943-3.

Steven A. Keim, Kramer D. Luxbacher, Michael Karmis. A numerical study on optimization of multilateral horizontal wellbore patterns for coalbed methane production in Southern Shanxi Province, China, International Journal of Coal Geology, Volume 86, Issue 4, 1 June 2011, Pages 306-317

Stéphane Lafortune, Francis Adelise, Gaëtan Bentivegna, Christophe Didier, Régis Farret, Philippe Gombert, Candice Lagny, Zbigniew Pokryszka, Noel Canto Toimil. An Experimental Approach to Adsorption of CO_2 + CH_4 Gas Mixtures Onto Coal (European RFCS CARBOLAB Research Project), Energy Procedia, Volume 63, 2014, Pages 5870-5878

Strapoc D; Schimmelmann A; Mastalerz M; Drobniak A; Hedges S Variability of geochemical properties in a microbially dominated coalbed gas system from the eastern margin of the Illinois Basin, USA. Int. J. Coal Geol. International Journal of Coal Geology 2008, 76,

98-110.

Sullivan, P and Heerden, J V, 1993. The simulation of environmental conditions in continuous miner developments using Computational Fluid Dynamics, Journal of the Mine Ventilation Society of South Africa, January, pp 2-11.

Susana Torno, Javier Toraño, Marcos Ulecia, Cristina Allende. Conventional and numerical models of blasting gas behaviour in auxiliary ventilation of mining headings, Tunneling and Underground Space Technology, Volume 34, February 2013, Pages 73-81

Tauziede, C, Mouilleau, Y and Bouet, R, 1993. Modelling of gas flows in the goaf of retreating faces, in Proceedings 25th International Conference on Safety in Mines Research Institutes, Pretoria, SA.

T. Chevalier, C. Chevalier, X. Clain, J.C. Dupla, J. Canou, S. Rodts, P. Coussot. Darcy's law for yield stress fluid flowing through a porous medium. Journal of Non-Newtonian Fluid Mechanics, Volume 195, May 2013, Pages 57-66

"Tibet mine landslide: Rescue workers recover more bodies". BBC News. 1 April 2013. Retrieved 2014-01-28

Ting Xiang Ren, Rao Balusu. Proactive goaf inertisation for controlling longwall goaf heatings, Procedia Earth and Planetary Science, Volume 1, Issue 1, September 2009, Pages 309-315

Tobias Strömgren, Geert Brethouwer, Gustav Amberg, Arne V. Johansson. Modelling of turbulent gas-particle flows with focus on two-way coupling effects on turbophoresis. Powder Technology, Volume 224, July 2012, Pages 36-45

Urbina, Ian (9 April 2010). "The New York Times". nytimes.com. Retrieved2014-01-28.Volta, Alessandro (1777) Lettere del Signor Don Alessandro Volta … Sull' Aria Inflammabile Nativa delle Paludi [Letters of Signor Don Alessandro Volta … on the flammable native air of the marshes], Milan, Italy: Guiseppe Marelli.

Van Kirk, C. 2010. PEGN 515: Reservoir Engineering Principles Course Notes. Golden, CO: Colorado School of Mines.

Vivian, John (1970). "The Wheal Agar Skip Disaster". Tales of the Cornish Miners. St. Austell: H. E. Warne Ltd. pp. 22-24.

Vivian, John (1970). "When the Bottom of Dolcoath Fell In". Tales of the Cornish Miners. St. Austell: H. E. Warne Ltd. pp. 38-40.

Wala, A.M., Vytla, S., & Taylor, C.D. 2007. Mine face ventilation: a comparison of CFD results against benchmark experiments for the CFD code validation. Mining Engineering, 59 (10), 49-55.

Wachel, E.W. 2012. Establishing Longwall Gob Porosity from Compaction in Western Coal Mines. Ph.D. thesis, Colorado School of Mines.

Ward, C R, 1984. Coal geology and coal technology, Blackwell Scientific Publications, Carlton, Victoria, Australia.

Widodo N. P., Sasaki K., Gautama & Risono R..S., 2008. Mine ventilation measurements with tracer gas method and evaluations of turbulent diffusion coefficient. International Journal of Mining Reclamation and Environment, Volume 22, Issue 1, Pages 60-69

William P Diamond, Steven J Schatzel. Measuring the gas content of coal: A review, International Journal of Coal Geology, Volume 35, Issues 1-4, February 1998, Pages 311-331

Williams, R J, 2002. Gas content testing for outburst management compliance, in Proceedings of the 3rd Australasian Coal Operators' Conference COAL2002, Australasian Institute of Mining and Metallurgy, Wollongong, 6-8 February, pp 47-52 [online]. Available from: http://www.uow.edu.au/eng/outburst/presentations_publications/coal_2002-3/Williams%20 2002.pdf [Accessed: November 2010].

Woodburn P.J., Britter R.E.. CFD simulations of a tunnel fire - Part I, Fire Safety Journal, Volume 26, Issue 1, February 1996, Pages 35-62

Xiaodong Cao. Differential Harnack estimates for backward heat equations with potentials under the Ricci flow. Journal of Functional Analysis, Volume 255, Issue 4, 15 August 2008, Pages 1024-1038

Xuan Tang, Jinchuan Zhang, Yansheng Shan, Jinyu Xiong. Upper Paleozoic coal measures and unconventional natural gas systems of the Ordos Basin, China, Geoscience Frontiers, Volume 3, Issue 6, November 2012, Pages 863-873

Xue Qiang, Liang Bing, Wang Hui-yun, Liu Lei. Numerical simulation of trace element transport on subsurface environment pollution in coal mine spoil, Journal of Trace Elements in Medicine and Biology, Volume 20, Issue 2, 12 July 2006, Pages 97-104

Yasin Tunckaya, Etem Koklukaya. Comparative analysis and prediction study for effluent gas emissions in a coal-fired thermal power plant using artificial intelligence and statistical tools,

Journal of the Energy Institute, In Press, Corrected Proof, Available online 7 August 2014

Yu. V.K., Levin L.Y., Zaitsev A.V., 2011. Calculation Method for the Unsteady Air Supply in Mine Ventilation Networks. Journal of Mining Science, Vol. 47, No. 5, pp. 651-659

Yuan, L. 2009. CFD modeling of spontaneous heating in a large-scale coal chamber. Journal of Loss Prevention in the Process Industries, 22(4), 426-433.

Yuan, L, & Smith, A C. 2008. Effects of ventilation and gob characteristics on spontaneous heating in longwall gob areas. Pages 141-147 of: Proceedings of the 12th US/North American Mine Ventilation Symposium, vol. 322. Society for Mining, Metallurgy, and Exploration.

Yuan, Liming, Smith, Alex C, & Brune, Jürgen F. 2006. Computational Fluid Dynamics Study on the Ventilation Flow Paths in Longwall Gobs. Pages 591-598 of: 11th US North American Mine Ventilation Symposium.

Yunan Hu, Olga I. Koroleva, Miroslav Krstić. Nonlinear control of mine ventilation networks, Systems & Control Letters, Volume 49, Issue 4, 23 July 2003, Pages 239-254

Zhang Haoran, Lluis Sanmiquel Pera, Yaojiang Zhao, Carla Vintro Sanchez. Researches and applications on geostatistical simulation and laboratory modeling of mine ventilation network and gas drainage zone, Process Safety and Environmental Protection, Volume 94, March 2015, Pages 55-64

Zhang Ruilin, Ian S. Lowndes. The application of a coupled artificial neural network and fault tree analysis model to predict coal and gas outbursts, International Journal of Coal Geology, Volume 84, Issue 2, 1 November 2010, Pages 141-152

Zofia Majewska, Grażyna Ceglarska-Stefańska, Stanisław Majewski, Jerzy Ziętek. Binary gas sorption/desorption experiments on a bituminous coal: Simultaneous measurements on sorption kinetics, volumetric strain and acoustic emission, International Journal of Coal Geology, Volume 77, Issues 1-2, 7 January 2009, Pages 90-102